Quantum chemical study of reactions forming a first aromatic ring in hydrocarbon flames

Xavier Lories

January 2011

This thesis is now over. It is time to thank those without whom this work and these past five years would not have been the same.

First of all, I would like to thank professor Daniel Peeters for his availability, his advice, and all his supervising work during this thesis. I also want to thank him for letting me carry out this research almost as freely as I wanted to.

I am grateful to professor Jacques Vandooren for allowing me to carry out part of this thesis in the combustion laboratory and to take part in the life of this laboratory. I am also grateful for his full support in a work that I suspect turned out to be globally more theoretical than he first expected.

Many thanks to Véronique Dias for everything, from small talk to the Région Wallonne business and her help with the combustion modeling part of this work.

Thanks to everyone in the combustion and quantum chemistry laboratories: Catherine, Valéry, Nicolas, Thomas, Pino and Thomas.

I would also like to thank all those people who played their part in these past five years: Christiane, professor Van Tiggelen, professor Tom Leyssens, Eliot, Laurent, Fanny and Geraldine.

Last and not least, thanks to my wife, Aude, for her support and to my mother and father for their continuous help. All this would not have been possible without them. And finally, I cannot forget my children: Julien, Guillaume and the one to come, who also all had their part in this work. Those parts are however not clearly defined.

Thanks also to all those who deserve it and that I may have forgotten.

This work would not have been possible without the financial support
of the Ministère de la Région Wallonne.

Abstract

In this work, quantum chemical methods are used to determine thermodynamic properties (heats of formation, heat capacities and entropies) and rate constants for combustion modeling. Combining those methods with statistical thermodynamics and transition state theory allows the determination of data, experimentally difficult, or impossible to obtain. In the thermodynamic section of this work, the accent is put on the determination of standard heats of formation through the use of isodesmic processes. This leads to the determination of Ring Conserving Isodesmic Reactions to account for the ring strain in certain hydrocarbons, to the definition of an extrapolation procedure for the heats of formation of open-shell systems, allowing the removal of spin contamination effects, and to the proposal of an isodesmicity index, which can be used for the evaluation of the error conservation within a given bond conserving process. The kinetic part of the work starts with the determination of potential mechanisms from the analysis of energy surfaces (C_6H_5, C_6H_7 for a first aromatic ring, $C_{10}H_7$ and $C_{14}H_9$ for the further growth of Polycyclic Aromatic Hydrocarbons). From these analyses, new mechanisms are proposed, leading to new product distributions. The data concerning the formation of the first aromatic ring is introduced into a combustion kinetic model to evaluate its impact. This shows no unrealistic results, and highlights potential incompleteness in the initial mechanism, and therefore provides leads for future improvements of the combustion model.

Jury members

Prof. Jean-François Pauwels

Université Lille1, France

Prof. Shaun Carl

Katholiek Universiteit Leuven, Belgium

Prof. Joseph Delhalle

Facultés Universitaires Notre dame de la Paix, Belgium

Prof. Tom Leyssens

Université catholique de Louvain, Belgium

Prof. Jean-François Gohy (president of the jury)

Université catholique de Louvain, Belgium

Prof. Jacques Vandooren (supervisor)

Université catholique de Louvain, Belgium

Prof. Daniel Peeters (supervisor)

Université catholique de Louvain, Belgium

Publications associated to this work

Journal articles and letters

- Xavier Lories, Jacques Vandooren, Daniel Peeters, Theoretical calculation of the heat of formation of fulvene, *Chemical Physics Letters*, 452 (2008) 29-32
- Xavier Lories, Jacques Vandooren, Daniel Peeters, Cycle formation from acetylene addition on C_4H_3 radicals, *Physical Chemistry Chemical Physics*, 12 (2010) 3762-3771
- Xavier Lories, Jacques Vandooren, Daniel Peeters, Definition of an isodesmicity index from G3B3 energy components, accepted for publication in the *International Journal of Quantum Chemistry* on December the 13^{th} 2010
- Xavier Lories, Jacques Vandooren, Daniel Peeters, Theoretical study of the isomerization of 6-dehydro fulvene radicals to the phenyl radical and application to the growth of Polycyclic Aromatic Hydrocarbons, *submitted to Physical Chemistry Chemical Physics*
- Xavier Lories, Jacques Vandooren, Daniel Peeters, Heats of formation and hydrogenation of fused bicyclic benzene isomers: the use of Ring Conserving Isodesmic Reactions, *in writing*
- Xavier Lories, Jacques Vandooren, Daniel Peeters, Theoretical study of the dehydrofulvene $+H_2 \rightarrow$ fulvene$+$ H reactions, *in writing*

Conference proceedings

- Xavier Lories, Jacques Vandooren, Daniel Peeters, Computation of Heats of Formation of Precursors of the First Aromatic Ring, *Proceedings of the Third European Combustion Meeting*, 2007
- Xavier Lories, Jacques Vandooren, Daniel Peeters, Theoretical Determination of Thermodynamic Data of Precursors of the First Aromatic Ring In Flames, *Proceedings of the 29th Task Leaders Meeting of the International Energy Agency Implementing Agreement on Energy Conservation and Emissions Reduction in Combustion.* 2007
- Xavier Lories, Jacques Vandooren, Daniel Peeters, Theoretical Study of the C_6H_7 Energy Surface, *Proceedings of the Fourth European Combustion Meeting*, 2009

Table of acronyms

AO	Atomic Orbital
AR	Atomization Reaction
BDE	Bond Dissociation Energy
BSR	Bond Separation Reaction
CBS	Complete Basis Set
CC	Coupled Cluster
CGTO	Contracted Gaussian Type Orbitals
CI	Configuration Interaction
CID	CI with Double excitations
CIS	CI with Single excitations
CISD	CI with Single and Double excitations
CombR	Combustion Reaction
DFT	Density Functional Theory
FC	Frozen Core
GTO	Gaussian Type Orbitals
HACA	Hydrogen Abstraction C_2H_2 Addition
HF	Hartree-Fock
HLC	Higher Level Correction
HTR	Hydrogen Transfer Reaction
HyR	Hydrogenation Reaction
i.i.	isodesmicity index
JPCRD	Journal of Physical and Chemical Reference Data
KS	Kohn and Sham
LCAO-MO	Linear Combinaison of Atomic Orbitals-Molecular Orbitals
MO	Molecular Orbital

(Continued on next page)

(Continuing from previous page)

MP	Møller-Plesset
NIST	National Institute of Standard and Technology
PAC	Phenyl Addition Cyclization
PAH	Polycyclic Aromatic Hydrocarbon
PES	Potential Energy Surface
QCISD	Quadratic CISD
QCISD(T)	QCISD with non-iterative Triple excitations
RBSR	Radical Bond Separation Reaction
RCIR	Ring Conserved Isodesmic Reaction
RHF	Restricted Hartree-Fock
ROHF	Restricted Open-shell Hartree-Fock
RRKM	Rice Ramsperer Kassel Marcus
SC	Spin Contamination
SD	Slater Determinant
SPC	Single Point Calculation
STO	Slater Type Orbital
TAE	Total Atomization Energy
TST	Transition State Theory
UHF	Unrestricted Hartree Fock
ZPE	Zero-Point Energy

Contents

Chapter 1

Introduction

1.1 Hydrocarbon combustion

The combustion of hydrocarbons remains an important source of energy. It is used for transportation, heating and electricity production. The combustion of those fossil fuels causes the emissions of pollutants and/or greenhouse gases such as carbon oxides, nitrous and sulfur oxides and soot. The incomplete combustion of hydrocarbons is responsible for the formation of polyynes and Polycyclic Aromatic Hydrocarbons (PAH). The size of the latter may increase to form soot.

1.1.1 Polycyclic aromatic hydrocarbons and soot

The formation of soot is an unwanted phenomenon as it causes several different types of issues. Here we briefly discuss some of those issues.

Effects on health

The effects of PAH and soot on human health has been the subjects of numerous studies and are now well recognized [1, 2, 3]. Historically, soot induced skin cancer is the first discovered cancer cause (Sir Percival Pott, 1775 [4]). Important exposure to PAH and soot may cause lung cancer (by inhalation) and skin cancer (by contact) cancers. It can also be the source of other pulmonary afflictions (such as chronic bronchitis, pulmonary oedema, asthma ...) and of decrease of the cardiac functions.

Effects on climate

The effect of soot and PAH on climate is also a recognized fact. It is now quite clear that the particulate matter in the atmosphere contributes to global warming and the ice meltdown. The soot absorbs solar radiations and warms the atmosphere. To this may possibly be added a reduction of cloudiness. Furthermore, deposited particulate matter blackens the snow and reduces its ability to reflect incoming radiation. It is also stated that soot may be the primary cause of ice meltdown (more important than carbon dioxide)[5, 6, 7]. Globally, the effects of soot on global climate are believed to be quite important. As soot has a shorter lifetime in air, and as it is more easily filtered, the effect of targeting soot to limit global warming and ice meltdown could be noticed faster than the ones induced by the reduction of carbon dioxide emissions.

1.2 Combustion modeling

It is clear that the understanding of soot production during combustion processes is an important field of combustion chemistry. For many years, combustion scientists have established models in order to be able to predict the formation of pollutants in flames. Such modeling is carried out at the Université catholique de Louvain. (For recent experimental and modeling studies, see references [8, 9, 10, 11, 12, 13, 14, 15]). A description of a combustion model is given in chapter 4.3. The good modeling of the formation of PAH needs chemical mechanisms for their growth from intermediates of combustion processes. Different hypotheses have been presented and are shortly described in the following sections.

Formation of PAH

Different pathways for PAH growth have been suggested. The most accepted one is the Hydrogen Abstraction C_2H_2 Addition path, known as the HACA path (see Figure 1.1). This mechanism has recently been reviewed by Kislov and coworkers [16], who provided a more complete analysis of the different possible reaction pathways. Quite recently, Mebel and coworkers have described a mechanism, involving ethynyl radicals rather than acetylene, which could be responsible for the low temperature formation of PAH in the atmosphere of Titan [17]. Another mechanism is the so-called biphenyl path (See Figure 1.2), which involves, as a first step, the formation of biphenyl. This may be due to the addition of a phenyl radical on benzene followed by hydrogen elimination or by the recombination of phenyl radicals. Similarly to the HACA path, the growth of the PAH is ensured by acetylene. Using bicyclopentadiene as

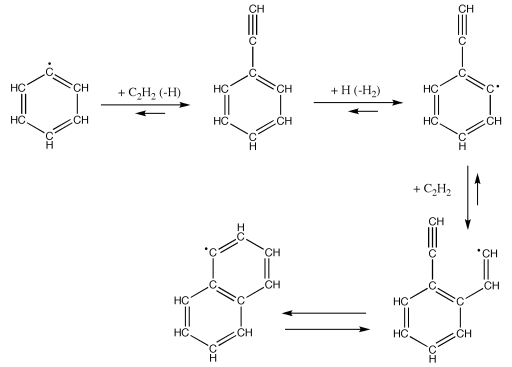

Figure 1.1: Major path of the HACA mechanism, as presented by Frenklach and coworkers [18].

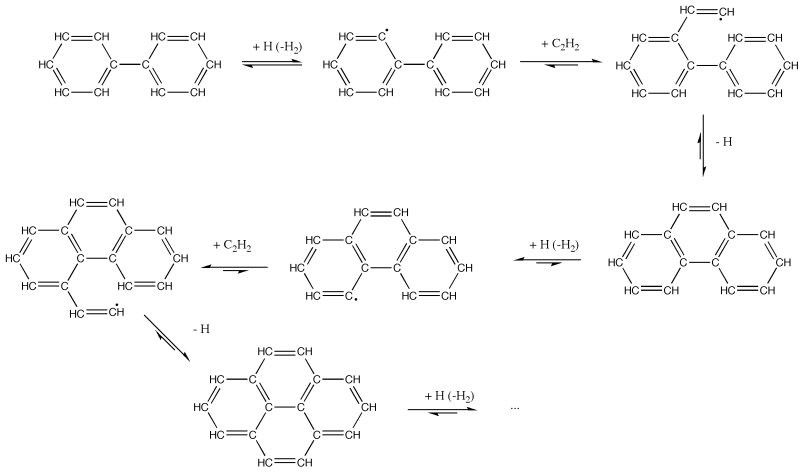

Figure 1.2: Major path of the biphenyl mechanism, such as presented by Frenklach and coworkers [19].

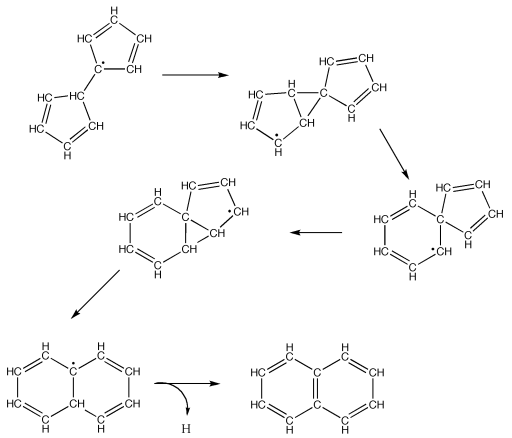

Figure 1.3: Bicyclopentadiene path for PAH growth (Melius and coworkers [20]).

a starting point has also been considered by Melius and coworkers [20] for the formation of polycyclic systems (See Figure 1.3). Recently, another mechanism from a similar starting point has been studied by Mebel and Kislov [21](See Figure 1.4). This mechanism however presents important activation barriers, making it an unlikely path for PAH growth. In a more recent work, Shukla and coworkers [22] have suggested a Phenyl Addition Cyclization (PAC) path for the growth of PAH. An illustration of PAH growth from benzene using the latter path is given on Figure 1.5.

1.2.1 Formation of a first aromatic ring

Figures 1.1 and 1.2 suggest that the growth of PAH needs a first aromatic ring. It is indeed a commonly accepted fact that the formation of a first aromatic ring is the rate limiting step to the formation of PAH. There has also therefore been an important number of hypotheses on the mechanisms of formation of a first aromatic ring from intermediates

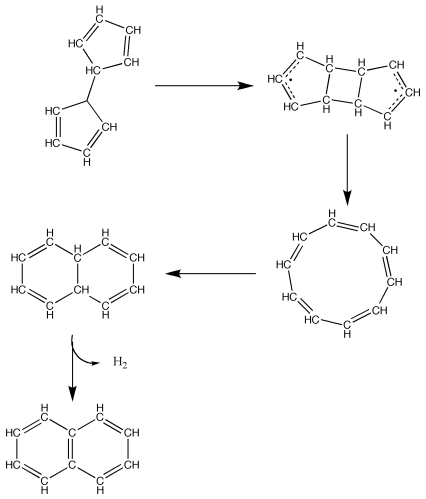

Figure 1.4: Bicyclopentadiene path for PAH growth (Mebel and Kislov [21]).

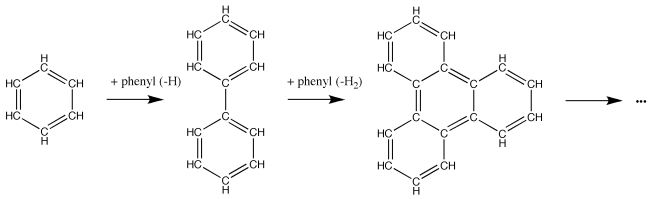

Figure 1.5: Growth of PAH by the PAC path of Shukla and coworkers [22].

of combustion processes. The different suggested mechanisms are commonly divided in two categories, the odd paths, involving the reaction between species having an odd number of carbons and the even paths, involving species having an even number of carbon atoms. The relative weight of each of those paths are dependent on the nature of the flame, and therefore, their relative importance must be discussed for a given burning condition.

Odd carbon pathways

The two categories of odd pathways include $C_3 + C_3$ reactions, and the $C_5 + C_1$ reactions.

$C_3 + C_3$ reaction The propargyl radical recombination is the main $C_3 + C_3$ path. The reaction mechanism has been described in detail by Miller and Klippenstein [23]. It is commonly considered to be the most important path for the formation of a first aromatic ring in most combustion conditions.

$C_5 + C_1$ reactions Those paths are generally considered as negligible. However, the dissociation of benzene to $C_5H_3 + CH_3$ has been described by Mebel and coworkers [24]. Recently, the addition of methyl to cyclopentadienyl radical has also been considered. These reactions may yield fulvene or fulvene related radicals, which may isomerize to produce benzene.

Even carbon pathways

Even carbon pathways generally involve acetylene and a four-carbon radical. Most commonly *n*- or *i*-C_4H_3 or *n*- or *i*-C_4H_5. Those paths have been the subjects of numerous discussions concerning their relative importance, based on the relative stability of the *n*- and *i*- form of the radical reactant. A detailed discussion is given in chapter 7. The even-carbon paths are among the oldest considered pathways [25, 26] and have also been the subject of numerous studies, both experimental and theoretical. The interest in those paths diminished as the consideration of the propargyl radical recombination gained popularity. There is now a regain of interest for even carbon pathways [27, 28, 29, 30].

1.2.2 Data for combustion modeling

The different models established to describe combustion phenomena need thermodynamic and transport data concerning the reactants, intermediates and products that are involved in the different kinetic schemes. Rate constants are also needed for every reaction included in the model.

Thermodynamic data

The thermodynamic properties needed for combustion modeling are: heats of formation, entropies and heat capacities. As experimental properties exist and are quite accurate for relatively simple and stable compounds such as ethane, ethylene, acetylene or benzene, the values for less common systems may be quite inaccurate or poorly defined, especially when the size of the hydrocarbon increases (see cyclopentadiene). As is shown in this work, if the compounds are highly unstable, the heats

of formation may be quite inaccurate. Concerning open-shell systems, the available experimental data may cover an important range of values. Examples are the propargyl and cyclopentadienyl radicals, for which experimental data range from 79 to 86 kcal.mol^{-1} [31] and from 57.8 to 64.7 kcal.mol^{-1} [32]. If no accurate experimental heat of formation is available, the data may be obtained following different methods:

- A first method is the group additivity of Benson and coworkers [33]. This method is highly parametrized. The accuracy of the results depends on how close the system is from the system used in the parametrization, and how accurate the data used for the parametrization were (as is presented in section 5.2 , this method for cylopropene derivatives is probably inaccurate).

- A second possibility, for radical systems, is to use analogy with similar data. For instance, Wu and Kern [34] established the standard heat of formation of propen-1-yl using the heat of formation of allene and the bond dissociation energy of ethylene. As is discussed in section 6.1.1 , their result is inaccurate.

- Finally, a common alternative to experimental measurements for the determination of heats of formation is the use of quantum chemical methods. These methods may be more accurate than experiment for very unstable species for which experimental measurements are difficult, or even impossible to carry out. This however depends on the quality of the quantum chemistry method used.

This last method is the one used for the determination of the standard heats of formation of several systems in this thesis.

Kinetic data

As mentioned earlier, accurate experimental kinetic data, for the systems under investigation and in combustion conditions, only exists for very few reactions. Most commonly, even for quite simple reactions, experimental data may vary greatly. Alternatives to experimental data also exist. As can be done for heats of formation, analogy with similar reactions is an important source of data for combustion modelists. As is noted in section 8.1, this method can provide accurate rate constants. In using this method, it is important that the reaction used for the analogy is similar to the reaction under investigation. Results from quantum chemistry can also be used for the determination of rate constants, through the identification of transition states. In this work, this is done using transition state theory (see section 3.3).

1.3 Objectives of the thesis

The objective is to develop and test a reaction sub-mechanism leading to the formation of a first aromatic ring in hydrocarbon flames. This testing is done by introducing the data in a combustion modeling software to evaluate its impact on the results. The use of the modeling software requires the knowledge of different thermodynamic data concerning the different intermediates of the sub-mechanism. Those data are the heats of formation, the constant pressure heat capacities and the entropies. From a kinetic point of view, the software also requires the rate constant for every reaction introduced, under the form of the Arrhenius equation parameters or the modified Arrhenius equation parameters. Most of the compounds that are to be studied are unstable and in the

gas phase, this makes quantum chemistry the most practical tool for accurate estimation of the thermodynamic and kinetic data.

- The first part of this work consists in evaluating the performances of a quantum chemistry method on the determination of the thermodynamic data of hydrocarbons. This is done through a series of comparisons with experimental data. This allows defining the best method for each category of system (radicals, bicyclic, ...).

- The next step consists in defining reaction mechanisms by searching stationary points on chosen potential energy surfaces. Those stationary points are either minima or first-order saddle points. The former are the intermediates for which the thermodynamic data have to be calculated, and the latter are transition states, which allow the calculation of rate constants based on transition state theory. In this work, this part is called the surface analysis. The results from the surface analyses may provide an important number of elementary reactions and intermediates.

- This number has to be reduced for practical combustion modeling. A part of the work is dedicated to the simplification of the obtained mechanism, and to the obtention of global rate constants.

- Once all the data is obtained, it is gathered into a reaction submechanism and introduced in the combustion modeling software.

- Finally, it has to be mentioned that it is not the aim of this work to provide a combustion mechanism which correctly describes the formation of soot precursor. The combustion modeling part of this work is used to test the validity of theoretically obtained thermodynamic and kinetic data.

1.4 Results presentation

The presentation of the results is divided into three main parts.

- The first is the thermodynamic part, itself subdivided into two chapters, one concerning the closed-shell systems, and the other the open-shell ones.
- The second part is the kinetic part, which contains the surface analyses and the determination of reaction mechanisms and elementary and global rate constants.
- Finally, in a third part, the results are included in the combustion model. Comparisons are made with and experimental data and with results from the original model.

The chart presented on Figure 1.6 shows those different parts and their main subdivisions. The thermodynamic results include, as main points, the highlight of strain as a source of error, the development of Ring Conserving Isodesmic Reactions and of an isodesmicity index. There also is the development of a new extrapolation method to remove the spin contamination error from Møller-Plesset heats of formation. In the kinetic part, two surfaces are studied, the C_6H_5 and C_6H_7 energy surfaces. Mechanisms and rate constants are obtained from those analyses. The combustion modeling part presents the results obtained by including the determined sub-mechanism into an already existing and validated model. Finally, a last chapter deals with the ring closing reactions in the growth of a second and third aromatic cycle. This last chapter includes reaction mechanisms, rate constants for elementary reactions as well as the determination of global rate constants.

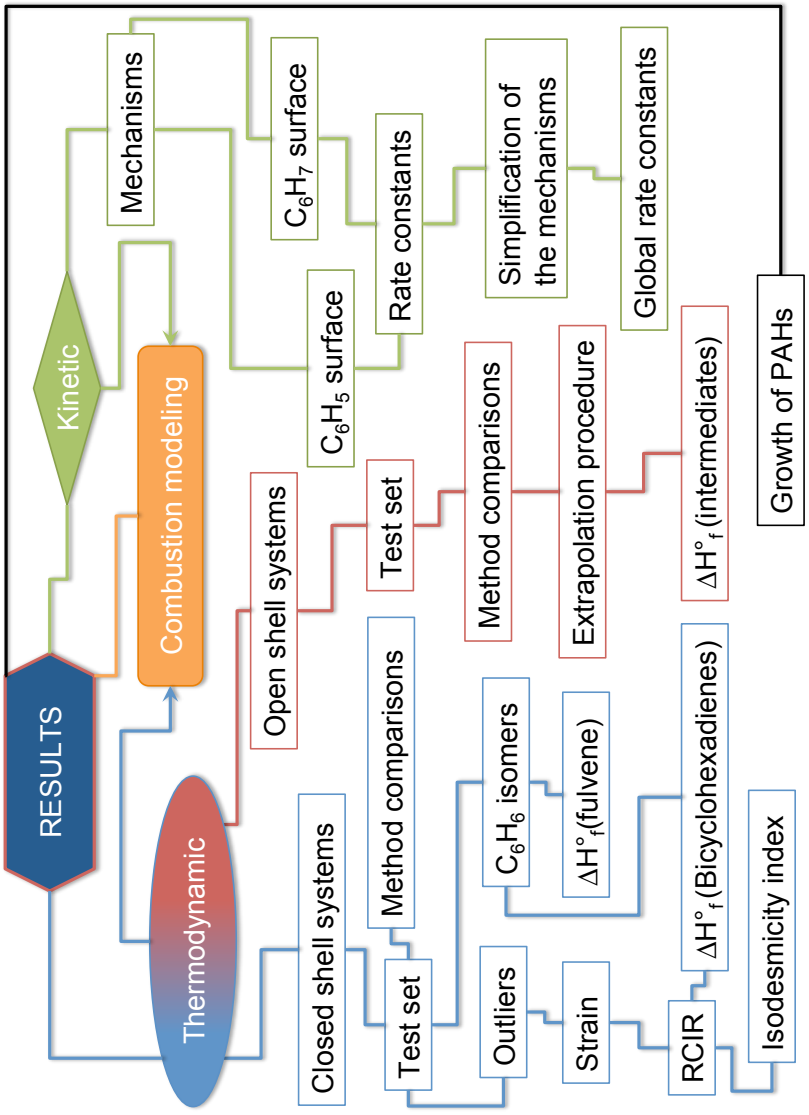

Figure 1.6: Overall organization of the presentation of the results.

Part I

Theoretical background

Chapter 2

Quantum chemistry

In this chapter, the various methods of quantum chemistry used in this thesis are described. Most of the descriptions have been taken from the work of Jensen [35] or the one of Widmark [36].

2.1 Schrödinger equation

In quantum chemistry one tries to solve the Schrödinger equation

$$\hat{H}\Psi_k = E_k\Psi_k \tag{2.1}$$

In which E_k is the energy spectrum of the system, Ψ_k is the set of wave function solutions of $\hat{H}$ the Hamiltonian energy operator.

$$\begin{aligned}\hat{H} = &-\sum_A^N \frac{1}{2m_A}\nabla_A^2 - \sum_i^n \frac{1}{2}\nabla_i^2 - \sum_A^N\sum_i^n \frac{Z_A}{|r_i - R_A|} \\ &+ \sum_i^n\sum_{j<i}^n \frac{1}{|r_i - r_j|} + \sum_A^N\sum_{B<A}^N \frac{Z_A Z_B}{|R_A - R_B|}\end{aligned} \tag{2.2}$$

This operator may be divided into two parts. First a kinetic part ($\hat{T}$), which includes the kinetic energy of the nuclei ($\hat{T}_N$) and the kinetic

energy of the electrons ($\hat{T}_e$). The second part of the Hamiltonian is the potential term $\hat{V}$, which decomposes in three contributions, $\hat{V}_{Ne}$, the interactions between nuclei and electrons, V_{ee}, the electron-electron interactions, and $\hat{V}_{NN}$, the nuclei-nuclei interactions. The Hamiltonian operator can be rewritten in a more compact way.

$$\hat{H} = \hat{T}_N + \hat{T}_e + \hat{V}_{Ne} + \hat{V}_{ee} + \hat{V}_{NN} \tag{2.3}$$

The $\hat{H}$ operator does not contain any time-dependent variable. We are therefore dealing with the time-independent Schrödinger equation. One of the most common approximations used to solve this equation is the Born-Oppenheimer approximation. The latter approximation is based on the fact that, due to the mass difference, the nuclei may be considered as immobile with respect to the electronic motion. Variables in equation 2.3 can therefore be separated and the wave function split into form an electronic equation and a nuclear equation.

$$(\hat{T}_e(r) + \hat{V}_{Ne}(r) + \hat{V}_{ee}(r))\Psi_{el}(r;R) = E_{el}(R)\Psi_{el}(r;R) \tag{2.4}$$

$$(\hat{T}_N(R) + \hat{V}_{NN}(R) + E_{el}(R))\Psi_{nucl}(R) = E_{nucl}\Psi_{nucl}(R) \tag{2.5}$$

with $\Psi = \Psi_{el}(r;R)\Psi_{nucl}(R)$. Chemists are mostly interested in the solutions of the electronic equation. For the remainder of this theoretical description $\hat{H}_{el}$ and Ψ_{el} and E_{el} will be denoted $\hat{H}$, Ψ, and E.

2.2 Wave function and Slater determinants

To solve the Schrödinger equation, one needs an expression of the wave function Ψ. A first possibility is to describe the n-particle wave function as a product of n one-particle wave functions.

$$\Psi = \varphi_1(1)\varphi_2(2)\varphi_3(3)...\varphi_n(n) = \prod_i^n \varphi_i(i) \tag{2.6}$$

In which all φ_i describe a single electron, and are called Atomic Orbitals (AOs) in the case of atomic systems and Molecular Orbitals (MOs) for the molecular systems. The wave function such as approximated in equation 2.6 does not respect Pauli's exclusion principle and must be anti-symmetrized with respect to the permutation of any two electrons. To do so, the wave function is expressed as a Slater determinant (SD).

$$\Psi^{SD} = \frac{1}{(n!)^{\frac{1}{2}}} \begin{vmatrix} \varphi_1(1) & \varphi_2(1) & \dots & \varphi_n(1) \\ \varphi_1(2) & \varphi_2(2) & \dots & \varphi_n(2) \\ \vdots & \vdots & \ddots & \vdots \\ \varphi_1(n) & \varphi_2(n) & \dots & \varphi_n(n) \end{vmatrix} \tag{2.7}$$

The energy associated to the approximated wave function is

$$E = \frac{\langle \Psi^{SD} | \hat{H} | \Psi^{SD} \rangle}{\langle \Psi^{SD} | \Psi^{SD} \rangle} = \langle \Psi^{SD} | \hat{H} | \Psi^{SD} \rangle \tag{2.8}$$

which may also be written as

$$\begin{aligned} E = \sum_i^n \langle \varphi_i | \hat{h} | \varphi_i \rangle + \frac{1}{2} \sum_{i,j}^n \langle \varphi_i \varphi_j | \frac{1}{|r_\mu - r_\nu|} | \varphi_i \varphi_j \rangle \\ - \frac{1}{2} \sum_{i,j}^n \langle \varphi_i \varphi_j | \frac{1}{|r_\mu - r_\nu|} | \varphi_j \varphi_i \rangle \end{aligned} \tag{2.9}$$

In which

$$\hat{h} = -\frac{1}{2}\nabla^2 - \sum_A^N \frac{Z_A}{|r - R_A|} \tag{2.10}$$

defines the mono-electronic operator. The remaining part of equation defines the classical Coulomb operators ($\hat{J}$)

$$\hat{J} = \sum_j \hat{J}_j, \qquad \hat{J}_j f(\mu) = [\int \frac{\varphi_j^*(\nu)\varphi_j(\nu)}{|r_\nu - r_\mu|} d\tau] f(\mu) \tag{2.11}$$

and the exchange operators ($\hat{K}$)

$$\hat{K} = \sum_j \hat{K}_j, \qquad \hat{K}_j f(\mu) = [\int \frac{\varphi_j^*(\nu) f(\nu)}{|r_\nu - r_\mu|} d\tau] \varphi_j(\mu) \tag{2.12}$$

2.3 Hartree-Fock Method

The orbitals defining the SD have to be determined. To do so, the variational principle is applied. According to this principle, any approximated wave function leads to an energy superior or equal to the energy obtained with the correct wave function. The assumption is made that the best orbitals are the ones providing the lowest energy. Application of this principle leads to the Hartree-Fock equation in its canonical form (see equation 2.13).

$$\hat{F}\varphi_i = \varepsilon_i \varphi_i \tag{2.13}$$

with the Fock operator defined as

$$\hat{F} = \hat{h} + \hat{J} - \hat{K} \tag{2.14}$$

The φ_i orbitals of equation 2.13 are known as canonical Hartree-Fock orbitals and the eigenvalues ε_i are the orbital energies. The total energy is obtained by

$$E = \sum_i^n \varepsilon_i - \frac{1}{2} \sum_i \langle \varphi_i | \hat{J} - \hat{K} | \varphi_i \rangle \tag{2.15}$$

2.3.1 Restricted and unrestricted Hartree-Fock theories

Up to this point, the spin properties of the electrons have been neglected. In order to introduce electron spin, we have to let the MOs depend on the spin and become spin-orbitals, of α or β type.

$$\varphi_i^\alpha = \varphi_i^\alpha(r)\alpha(\omega) \tag{2.16}$$

$$\varphi_i^\beta = \varphi_i^\beta(r)\beta(\omega) \tag{2.17}$$

If those new orbitals are used, the energy may be redefined

$$\begin{aligned} E &= \sum_{i}^{n} \langle \varphi_i | \hat{h} | \varphi_i \rangle \\ &+ \frac{1}{2} \sum_{i^\alpha, j^\alpha}^{n} [\langle \varphi_i \varphi_j | \frac{1}{|r_\mu - r_\nu|} | \varphi_i \varphi_j \rangle - \langle \varphi_i \varphi_j | \frac{1}{|r_\mu - r_\nu|} \varphi_j \varphi_i \rangle] \\ &+ \frac{1}{2} \sum_{i^\beta, j^\beta}^{n} [\langle \varphi_i \varphi_j | \frac{1}{|r_\mu - r_\nu|} | \varphi_i \varphi_j \rangle - \langle \varphi_i \varphi_j | \frac{1}{|r_\mu - r_\nu|} | \varphi_j \varphi_i \rangle] \\ &+ \sum_{i^\alpha, j^\beta}^{n} [\langle \varphi_i \varphi_j | \frac{1}{|r_\mu - r_\nu|} | \varphi_i \varphi_j \rangle \end{aligned} \tag{2.18}$$

As exchange only occurs between electrons of the same spin, the Fock operator may be defined for α or β electrons

$$\hat{F}^\alpha = \hat{h} + \hat{J} - \hat{K}^\alpha \tag{2.19}$$

and

$$\hat{F}^\beta = \hat{h} + \hat{J} - \hat{K}^\beta \tag{2.20}$$

with

$$\hat{K}^\alpha = \sum_{j^\alpha} \hat{K}_j \tag{2.21}$$

and

$$\hat{K}^\beta = \sum_{j^\beta} \hat{K}_j \tag{2.22}$$

Unrestricted Hartree-Fock (UHF) theory is the straightforward implementation of this duplication of orbitals. In this case, the UHF wave function is not necessarily an eigenfunction of the $\hat{S}^2$ spin operator. This latter issue is known as spin contamination and will be discussed in a further section. In the case of closed-shell systems (even number of electrons, singlet state), it is possible to require that the spin-orbitals have the same spatial functions. This is known as the Restricted Hartree-Fock (RHF) theory. A similar spin constraint may be used for open-shell systems (odd number of electrons) by considering doubly-occupied

space orbitals for the paired electrons and spin-orbital(s) for the unpaired electron(s). This last method is called the Restricted Open-Shell Hartree-Fock (ROHF).

2.3.2 LCAO-MO

The Linear Combination of Atomic Orbitals (LCAO) method is commonly used to obtain the molecular orbitals. This method defines the molecular orbital φ_i as a linear combination of known, atom centered orbitals χ_p.

$$\varphi_i = \sum_{p=1}^{\infty} C_{ip}\chi_p \simeq \sum_{p=1}^{N} C_{ip}\chi_p \tag{2.23}$$

In this case deriving equation 2.13 requires the minimization of the energy with respect to the C_{ip} coefficients which define the MOs. The HF equation can be written

$$\langle\varphi_a|\hat{F}|\varphi_i\rangle = \sum_{p,q} C^*_{pa}F_{pq}C_{qi} \tag{2.24}$$

with

$$F_{pq} = \langle\chi_p|\hat{F}|\chi_q\rangle \tag{2.25}$$

The Fock operator must be constructed via the actual MOs in their LCAO form. The equation has to be solved under the orthonormality constraint

$$C^\dagger SC = 1 \tag{2.26}$$

with

$$S_{pq} = \langle\chi_p|\chi_q\rangle \tag{2.27}$$

Simultaneous solution of 2.24 and 2.26 is achieved and leads to the Rothaan-Hall equation

$$FC = SC\varepsilon \tag{2.28}$$

where ε is the diagonal matrix of orbital energies. This equation is a generalized matrix eigenvalue equation, in order to solve it, it is convenient to turn it into a conventional matrix eigenvalue form, without the S matrix. This can be achieved if we express the orbitals in an orthonormal basis of atomic orbitals. By a transformation, usually a Lowdin orthogonalisation, the original basis set is transformed into an orthonormal set, for which equations 2.28 may be written as

$$\tilde{F}\tilde{C}_i = \tilde{C}_i\varepsilon_i \tag{2.29}$$

where $\tilde{C}_i$ denotes the i-th column vector of $\tilde{C}$. Using the LCAO-MO expansion, one can also express the total energy and the Fock matrices using the density matrices (D) constructed from the orbital coefficients

$$D^{\alpha}_{rs} = \sum_{i^{\alpha}} C^{\alpha}_{ri} C^{\alpha}_{si} \tag{2.30}$$

$$D^{\beta}_{rs} = \sum_{i^{\beta}} C^{\beta}_{ri} C^{\beta}_{si}. \tag{2.31}$$

This leads to a new expression of equation 2.18.

$$\begin{aligned} E &= \sum_{p,q}[D^{\alpha}_{pq} \\ &+ D^{\beta}_{pq}]h_{pq} + \frac{1}{2}\sum_{p,q,r,s} D^{\alpha}_{pq}D^{\alpha}_{rs}[\langle\chi_p\chi_r|\chi_q\chi_s\rangle - \langle\chi_p\chi_r|\chi_s\chi_q\rangle \\ &+ \frac{1}{2}\sum_{p,q,r,s} D^{\beta}_{pq}D^{\beta}_{rs}[\langle\chi_p\chi_r|\chi_q\chi_s\rangle - \langle\chi_p\chi_r|\chi_s\chi_q\rangle \\ &+ \sum_{p,q,r,s} D^{\alpha}_{pq}D^{\beta}_{rs}[\langle\chi_p\chi_r|\chi_q\chi_s\rangle \end{aligned} \tag{2.32}$$

The two Fock matrices of equations 2.19 and 2.20 become

$$F^{\alpha}_{pq} = h_{pq} + \sum_{rs}\{[D^{\alpha}_{rs} + D^{\beta}_{rs}]\langle\chi_p\chi_r|\chi_q\chi_s\rangle - D^{\alpha}_{rs}\langle\chi_p\chi_r|\chi_s\chi_q\rangle\} \tag{2.33}$$

$$F^{\beta}_{pq} = h_{pq} + \sum_{rs}\{[D^{\beta}_{rs} + D^{\beta}_{rs}]\langle\chi_p\chi_r|\chi_q\chi_s\rangle - D^{\beta}_{rs}\langle\chi_p\chi_r|\chi_s\chi_q\rangle\} \tag{2.34}$$

with

$$h_{pq} = \langle \chi_p | \hat{h} | \chi_q \rangle \tag{2.35}$$

the Fock operators are constructed from the molecular orbitals. We therefore have to know the solutions of the HF equation before being able to define the operators needed to obtain these equations. To solve this problem, the method used is the Self Consistent Field method (SCF). It consists in

1. Make an initial guess of molecular orbitals and construct a trial density matrix. (Or directly guess the density matrix.)
2. Determine an orthonormal set of functions within the basis set used.
3. Construct the Fock Matrix.
4. Transform the Fock matrix to the orthonormal basis and diagonalize it to obtain an improved set of orbitals.
5. If new orbitals obtained are equal to the initial set, convergence is reached. If not, construct a new density matrix and repeat from point 3.

2.3.3 Basis sets

The LCAO-MO expansion of molecular orbitals has been introduced in section 2.3.2. It is now time to open a small parenthesis to explain what atomic basis sets are. It is quite obvious from equation 2.23 that the results of the calculation grow more accurate as the basis set grows larger. Due to atomic symmetry, atomic orbitals have the form of

$$\chi(r) = R(r) Y_{lm}(\Theta, \phi) \tag{2.36}$$

In which $R(r)$ and $Y_{lm}(\Theta, \phi)$ are respectively describing the radial and angular part of the wave function. The form of those orbitals can only be obtained analytically for one electron atoms. For which the wave function decays exponentially with increasing distance to the nucleus. It would therefore seem reasonable to use exponential wave functions as basis functions, especially since they are known to be exact solutions for atomic systems. The first basis used are the Slater Type Orbitals (STO) characterized by a exponential factor in the radial part.

$$\chi^{STO}(r) = P(r)e^{-\zeta r}Y_{lm}(\Theta, \phi) \tag{2.37}$$

where *P(r)* is a polynomial in the radial coordinate, which can take several different forms. Gaussian basis functions were introduced to remedy the difficulties associated with evaluating multi-center integrals with STOs. They can be written in a similar form

$$\chi^{GTO}(r) = P(r)e^{-\alpha r^2}Y_{lm}(\Theta, \phi) \tag{2.38}$$

With, usually, a different polynomial *P(r)*, but will preferentially be expressed using cartesian coordinates:

$$\chi^{GTO}(r) = (x - A_x)^k(y - A_y)^l(z - A_z)^k e^{-\alpha r^2} \tag{2.39}$$

The GTO is entirely defined by its center A, the orbital exponent α and the k, l, m powers. A single Gaussian has a qualitatively wrong behavior both at the nuclei and in the asymptotic limit for a Hamiltonian with point charge nuclei and Coulomb interaction. Nevertheless, the cusp behavior represents an idealized point nucleus and for more realistic nuclei of finite extension, the Gaussian behavior is acceptable. Although the gaussian basis does not represent the correct asymptotic behavior, this does not lead to important errors. Indeed, if accurate solutions for

a point charge model Hamiltonian are desired, they can be obtained at any desired accuracy by expanding the basis functions in a sufficiently large number of Gaussians to ensure their correct behavior. In almost all *ab initio* calculations today, basis sets of contracted GTO are used. Those are linear combination, or contraction, of GTO, and reproduce quite well the STOs

$$\chi^{STO} \approx \chi_p^{CGTO} = \sum_a C_{ap} \chi_a^{GTO} \tag{2.40}$$

The use of such CGTO reduces the number of basis functions to consider in the SCF procedure and facilitates calculations. The aim is to describe the MOs as accurately as possible with a reduced number of atomic-like basis functions, and thus rectify the shortcoming of GTO. In a molecule, it is likely that an atom experiences the field from all others, the electrons on that atom may thus shift away from the center of the nucleus, causing a displacement of the electron density, which is no longer symmetrically centered on the nucleus. If this situation is to be described accurately, we need to supply basis functions with higher L-quantum numbers than the original ones (polarization functions). Most of the time is is sufficient to augment the basis by a few or just one polarization function. If the molecule studied presents a charge distribution much more diffuse than in neutral atoms (anion, polar systems), it will be necessary to still augment the basis set by adding diffuse functions.

Pople basis sets

Pople and coworkers have designed a series of basis sets of the following nomenclature: k-nlmG. The k indicates how many GTOs are used in the description of the core orbitals. The nlm after the dash indicates

both how many functions the valence orbitals are split into, and how many GTO are used for their representation. Two values (nl) indicate a split valence and three values (nlm) indicate a triple split valence. The values before the G indicate s and p functions in the basis set. For instance:

- 6-31G is a split valence basis where the core orbitals are a contraction of 6 GTOs, the inner part of the valence orbitals is described by a contraction of three GTOs and the outer part is described by a single GTO.
- 6-311G is a triple split valence where core orbitals are a contraction of six GTOs and the valence split into three functions, represented by three, one, and one GTO respectively.

To those bases may be added diffuse and or polarization functions. Diffuse functions are usually s- and p- functions and consequently come before the G. They are denoted by a + or ++, with the second + indicating that a diffuse s- function is added to hydrogen. Polarization functions are noted after the G with a separate designation for heavy atoms and light ones. The 6-31G(d) basis is the 6-31G basis set with d functions added to heavy atoms. The 6-31G(d,p) basis is the 6-31G(d) basis with p functions added on hydrogen. The largest basis set of this type is 6-311++G(3df,3pd), and is not used in this work.

Correlation consistent basis sets

From a series of calculations using Pople style basis sets of increasing size, it is not obvious whether the properties of interest are converged. To this end, correlation consistent basis sets have been developed. The

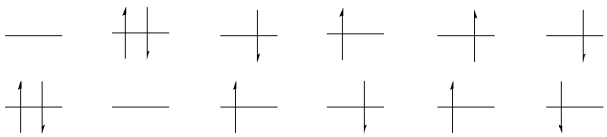

Figure 2.1: Six possible states (Φ_0 to Φ_5 from left to right) constructed from the RHF Slater determinant.

systematic nature of those basis sets allows the determination of formulas permitting the extrapolation of the energies to the infinite basis set. Several extrapolation formulas exist and are extensively used in model chemistries (as we shall see later on in section 2.6).

2.3.4 Spin contamination

As mentioned earlier, spin contamination is an issue that arises when unrestricted wave functions are used. To illustrate the nature of this issue, let us consider the H_2 system, and let us describe this system with a minimal basis set. Within RHF, two orbitals are created.

$$\phi_1(\nu) = (\chi_A(\nu) + \chi_B(\nu)) \tag{2.41}$$

$$\phi_2(\nu) = (\chi_A(\nu) - \chi_B(\nu)) \tag{2.42}$$

The RHF approach indicates that ϕ_1 and ϕ_2 may be doubly occupied. The ground state Slater determinant is defined by

$$\Phi_0 = \frac{1}{\sqrt{2}} \begin{vmatrix} \phi_1(1) & \bar{\phi}_1(1) \\ \phi_1(2) & \bar{\phi}_1(2) \end{vmatrix} \tag{2.43}$$

In which , the $^-$ notation indicates the β spin of the occupying electron.

Five excited configurations may be created (see Figure 2.1).

$$\Phi_1 = \frac{1}{\sqrt{2}} \begin{vmatrix} \phi_2(1) & \bar{\phi}_2(1) \\ \phi_2(2) & \bar{\phi}_2(2) \end{vmatrix} \tag{2.44}$$

$$\Phi_2 = \frac{1}{\sqrt{2}} \begin{vmatrix} \phi_1(1) & \bar{\phi}_2(1) \\ \phi_1(2) & \bar{\phi}_2(2) \end{vmatrix} \tag{2.45}$$

$$\Phi_3 = \frac{1}{\sqrt{2}} \begin{vmatrix} \bar{\phi}_1(1) & \phi_2(1) \\ \bar{\phi}_1(2) & \phi_2(2) \end{vmatrix} \tag{2.46}$$

$$\Phi_4 = \frac{1}{\sqrt{2}} \begin{vmatrix} \phi_1(1) & \phi_2(1) \\ \phi_1(2) & \phi_2(2) \end{vmatrix} \tag{2.47}$$

$$\Phi_5 = \frac{1}{\sqrt{2}} \begin{vmatrix} \bar{\phi}_1(1) & \bar{\phi}_2(1) \\ \bar{\phi}_1(2) & \bar{\phi}_2(2) \end{vmatrix} \tag{2.48}$$

Now, let us consider the UHF ground state. In this case, spin orbitals must be used.

$$\phi_1(\nu) = (\chi_A(\nu) + c\chi_B(\nu))\alpha \tag{2.49}$$

$$\bar{\phi}_1(\nu) = (c\chi_A(\nu) + \chi_B(\nu))\beta \tag{2.50}$$

The ground state SD is

$$\Phi_0^{UHF} = \frac{1}{\sqrt{2}} \begin{vmatrix} \phi_1(1) & \bar{\phi}_1(1) \\ \phi_1(2) & \bar{\phi}_1(2) \end{vmatrix} \tag{2.51}$$

This determinant may be written as

$$\begin{aligned} \Phi_0^{UHF} = [c(\chi_A\chi_A + \chi_B\chi_B) + (\chi_A\chi_B + \chi_B\chi_A)](\alpha\beta - \beta\alpha) \\ + (1 - c^2)[\chi_A\chi_B\beta\alpha - \chi_B\chi_A\alpha\beta] \end{aligned} \tag{2.52}$$

In this notation, electrons have been omitted, for instance, $\chi_A\chi_B\beta\alpha - \chi_B\chi_A\alpha\beta$ stands for $\chi_A(1)\chi_B(2)\beta(1)\alpha(2) - \chi_B(1)\chi_A(2)\alpha(1)\beta(2)$. The first term of this last equation may be written as a linear combination

of pure singlet states, namely, states 0 and 1 of the RHF determinants. The second part of this determinant is however common with the triplet combination (2)+(3) of RHF determinant. The UHF determinant contains therefore a singlet and a triplet term. This feature is called spin contamination. The amount of spin contamination is given by the $\langle S^2 \rangle$ value. The theoretical value for a pure spin state (no spin contamination) is $S(S+1)$. In this work, beside singlets, we only encounter doublet open-shell systems, which expected $\langle S^2 \rangle$ value is 0.75. The $< S^2 >$value of an UHF wave function is calculated from the spatial overlap between pairs of α and β spin-orbitals [35], and turns out to be

$$\langle S^2 \rangle = S_z(S_z+1) + N_\beta - \sum_{ij}^{OM} \langle \phi_i^\alpha | \phi_j^\beta \rangle^2 \tag{2.53}$$

2.3.5 Correlation energy

The energy obtained at Hartree-Fock level is higher than the energy of a system. This is mainly due to the approximate description of the electron-electron interactions within this theory. The difference between the HF energy and the exact energy is called the correlation energy.

2.4 Post Hartree-Fock methods

2.4.1 Configuration interaction

The simplest way to deal with the correlation energy is the Configuration Interaction (CI) method. In this method, the wave function is expressed as a linear combination of determinants. The coefficients of this linear

combination are variationally optimized. In general, the CI wave function contains the HF determinant as well as other excited configuration obtained from this determinant.

$$\Psi_{CI} = a_0\Phi_{HF} + \sum_S a_S\Phi_S + \sum_D a_D\Phi_D + \sum_T a_T\Phi_T \ldots = \sum_{i=0} a_i\Phi_i \quad (2.54)$$

Subscripts S, D, T,... indicate determinants that are Singly, Doubly, Triply,... excited relative to the HF configuration. The wave function including all possible determinants (Full CI) would provide the best non-relativistic energy within a given basis set, and the exact energy is at the complete basis set limit. However those calculations are not feasible due to the computational cost of such a procedure. Most common simplification is the truncation of the linear combination to only single excitations, only double excitations or only single and double excitations. The truncation to CIS does not provide significant improvement to the HF results as singly excited states do not interact with the HF wave function. The lowest truncation that brings an improvement is the truncation to CID, including double excitation but not single ones. CISD is also used, single excitation do not interact with the ground state but do interact with the doubly excited determinants. This latter method suffers from size inconsistency and inextensivity, meaning that the energy of non interacting fragment is not equal to the sum of the energy of the two fragment taken separately. The main cause is the lack of triple and quadruple excitations. This latter deficiency is often corrected by using the QCISD(T) method developed by Pople and coworkers [37]. This method introduces Quadratic Configuration Interaction (QCI) with Single and Double excitations (SD) and Triple excitation (T) taken from Møller-Plesset calculations. This correction guarantees the size consistency of the method.

2.4.2 Perturbation and Møller-Plesset theories

Perturbation theory is based on the idea that the problem only slightly differs from an already solved problem. The solution to the given problem should therefore be close to that of the already solved problem.

$$H = H_0 + \lambda H' \tag{2.55}$$

This is described by dividing the Hamiltonian operator into two parts. The first is the reference (H_0) and the second part is the perturbation (H'). Perturbation methods can be used in quantum mechanics to add corrections to solutions that uses an independant particle model approximation, and the theory is then called Many Body Perturbation Theory. We assume that the Schrödinger equation is solved for the unperturbed Hamiltonian

$$H_0\Phi_i = E_i\Phi_i \qquad i = 0, 1, 2, \ldots, \infty \tag{2.56}$$

The solutions for the unperturbed Hamiltonian operator form a complete set which can be chosen to be orthonormal, and λ is a variable parameter determining the strength of the perturbation. The perturbed Schrödinger equation is given by

$$H\Psi = W\Psi \tag{2.57}$$

If $\lambda = 0$, then $\hat{H} = \hat{H}_0$, $\Psi = \Phi_0$ and $W = E_0$. As the perturbation increases from zero to 1, the new energy and the new wave function must also change continuously. Those energies and wave functions can be expressed as a Taylor expansion in powers of the perturbation parameter λ.

$$W = \lambda^0 W_0 + \lambda^1 W_1 + \lambda^2 W_2 + \lambda^3 W_3 + \ldots \tag{2.58}$$

$$\Psi = \lambda^0 \Psi_0 + \lambda^1 \Psi_1 + \lambda^2 \Psi_2 + \lambda^3 \Psi_3 + \ldots \tag{2.59}$$

The zeroth-order, or unperturbed wave function corresponds to $\lambda = 0$, $H = H_0$, $\Psi = \Phi_0$ and $W = E_0$. The following Ψ_i and W_i terms correspond to the i-th order corrections. It is convenient to choose the perturbed wave function to be intermediately normalized, *i.e.* the overlap with the unperturbed wave function should be one. This has the consequences that all correction terms are orthogonal to the reference wave function. With the expansion, the Schrödinger equation becomes

$$\begin{aligned}(H_0+\lambda H')(\lambda^0\Psi_0+\lambda^1\Psi_1+\lambda^2\Psi_2+\lambda^3\Psi_3+\ldots) = (\lambda^0 W_0+\lambda^1 W_1+\lambda^2 W_2 \\ + \lambda^3 W_3+\ldots)(\lambda^0\Psi_0+\lambda^1\Psi_1+\lambda^2\Psi_2+\lambda^3\Psi_3+\ldots)\end{aligned} \quad (2.60)$$

The terms with the same λ power values may be put together:

$$\begin{aligned} H_0\Psi_0 &= W_0\Psi_0 \\ H_0\Psi_1 + H'\Psi_0 &= W_0\Psi_1 + W_1\Psi_0 \\ H_0\Psi_2 + H'\Psi_1 &= W_0\Psi_2 + W_1\Psi_1 + W_2\Psi_0 \\ H_0\Psi_n + H'\Psi_{n-1} &= \sum_{i=0}^{n} W_i\Psi_{n-i} \end{aligned} \quad (2.61)$$

The zeroth-order equation is the Schrödinger equation for the unperturbed problem. The first-order equation contains two unknowns, which are the first-order correction to energy, W_1, and the first-order correction to the wave function, Ψ_1. If the unperturbed Hamiltonian is chosen to be a sum of Fock operators, the theory becomes the Møller-Plesset perturbation theory. As the sum of Fock operators counts twice the average electron-electron repulsion, the perturbation is the exact electron-electron repulsion operator $\hat{V}_{ee}$ minus twice the average repulsion operator $\langle\hat{V}_{ee}\rangle$. The unperturbed Hamiltonian is written

$$H_0 = \sum_{i=1}^{n} F_i = \sum_{i=1}^{n}(h_i + \sum_{j=1}^{n}(J_j - K_j)) = \sum_{i=1}^{n} h_i + 2\langle\hat{V}_{ee}\rangle \quad (2.62)$$

The perturbation operator is

$$H' = H - H_0 = \sum_{i=1}^{n}\sum_{j>i}^{n}\frac{1}{|r_\nu - r_\mu|} - \sum_{i=1}^{n}\sum_{j>i}^{n}\langle\frac{1}{|r_\nu - r_\mu|}\rangle \tag{2.63}$$

The zeroth order wave function is the HF determinant and the corresponding energy is the sum of the MO energies. The first-order energy correction is the average of the perturbation operator over the zeroth order wave function.

$$W_1 = \langle\Phi_0|H'|\Phi_0\rangle = \langle\hat{V}_{ee}\rangle - 2\langle\hat{V}_{ee}\rangle = -\langle\hat{V}_{ee}\rangle \tag{2.64}$$

This indicates that the first-order energy $(W_0 + W_1)$ is the Hartree-Fock energy. From now on, $E(MPn)$ is used to express the n-th order energy correction and MPn is used to indicate the energy sum up to order n. As we have seen, introduction of correlation starts at order 2. This first contribution to the correlation energy involves a sum over doubly excited determinants, generated from promoting two electrons from occupied i and j orbitals to virtual orbitals a and b.

$$W_2 = \sum_{i>j}^{occ}\sum_{a>b}^{virt}\frac{\langle\Phi_0|H'|\Phi_{ij}^{ab}\rangle\langle\Phi_{ij}^{ab}|H'|\Phi_0\rangle}{E_0 - E_{ij}^{ab}} \tag{2.65}$$

the second-order energy correction is given by

$$E(MP2) = \sum_{i>j}^{occ}\sum_{a>b}^{virt}\frac{\langle\phi_i\phi_j|\phi_a\phi_b\rangle - \langle\phi_i\phi_j|\phi_b\phi_a\rangle}{\varepsilon_i + \varepsilon_j - \varepsilon_a - \varepsilon_b} \tag{2.66}$$

MP2 is considered as introducing $80 - 90\%$ of the correlation energy. The full fourth-order Møller-Plesset energies introduce about $95 - 98\%$. There is very little work with MPn beyond MP4. Practically, the MP2 energies are often too low (overestimation of the correlation effect) and the MP3 ones too high. The correct energy is most commonly between MP3 and MP4. Møller-Plesset methods are not variational. As those

methods are based on HF wave function, they are also submitted to spin contamination issues. Formulas have been derived for removing all spin contaminants from UMP2 energies and the first few states for UMP3 and UMP4. Those methods are preferred as RMPn presents stability issues when bonds get larger. The projected UMPn methods are however more time consuming as there are twice as many orbitals.

2.5 Density functional theory

Density Functional Theory (DFT) has become a widely used tool to describe ground state systems. This is mainly due to the fact that this method introduces part of the electron correlation, which makes it superior to HF and similar to MP2 results. DFT does not look for wave functions but rather for the electron density ρ(r).

2.5.1 Hohenberg-Kohn theorems

Density functional theory is based on the two Hohenberg-Kohn theorems. The first one states that the external potential ν(r) is determined, within a trivial additive constant, by the electron density ρ(r). Since ρ(r) determines the number of electrons N, it follows that ρ(r) also determines the ground state wave function and many electronic properties of the system. The energy can then be written as

$$E(\rho) = T(\rho) + V_{ne}(\rho) + V_{ee}(\rho) \tag{2.67}$$

In which $T(\rho)$ is the kinetic energy, $V_{ne}(\rho)$ is the electron nucleus interaction, which can be written

$$V_{ne}(\rho) = \int \rho(r)\nu(r)dr \tag{2.68}$$

ν (r) being the external potential due to the position of the nuclei. $V_{ee}(\rho)$ describes the electron electron interaction and is given by a classical Coulomb repulsion term J(ρ) (see Equation 2.69) and a non-classical term called exchange correlation energy. This last term is discussed in more details later on.

$$J(\rho) = \frac{1}{2}\int\int \frac{1}{r_{12}}\rho(r_1)\rho(r_2)dr_1dr_2 \tag{2.69}$$

The second Hohenberg-Kohn theorem makes DFT a variational method. For any trial density $\tilde{\rho} \geq 0$ and $\int \tilde{\rho}dr = N$,

$$E(\tilde{\rho}) \geq E(\rho) \tag{2.70}$$

In which ρ(r) is the exact ground state electron density. This allows us to write the condition that the energy is stationary with respect to changes in the electron density, subject to the constraint $\int \rho(r)dr = N$:

$$\delta E(\rho) - \mu\delta(\int \rho(r)dr - N) = 0 \tag{2.71}$$

for which the Euler Lagrange equation is, in terms of functional derivatives:

$$\mu = \nu(r) + \frac{\delta T(\rho)}{\delta\rho(r)} + \frac{\delta V_{ee}(\rho)}{\delta\rho(r)} \tag{2.72}$$

the Lagrange multiplier μ being named the chemical potential. This last equation would be exact for ρ(r) if the functional forms of $T(\rho)$ and V_{ee} were exactly known. As this is not the case, one has to use an alternative approach. This alternative approach is Kohn and Sham theory.

2.5.2 Kohn and Sham orbitals

Kohn and Sham proposed introducing orbitals into the problem in such a way that the kinetic energy can be computed simply to good accuracy, leaving a small residual correction handled separately. For a determinantal wave function, describing exactly N non-interacting electrons, in N orbitals ψ_i. The representation of the exact kinetic energy and density are given respectively by

$$T_s(\rho) = \sum_i^N \langle\psi_i| - \frac{1}{2}\nabla^2|\psi_i\rangle \tag{2.73}$$

$$\rho(r) = \sum_i^N |\psi_i(r)|^2 \tag{2.74}$$

Where the orbitals for the system of non-interacting electrons moving in the external potential $\nu(r)$ obey an equation of the form

$$[-\frac{1}{2}\nabla^2 + \nu_s(r)]\psi_i = \varepsilon_i\psi_i \tag{2.75}$$

The energy written as a functional of density may be rewritten

$$\begin{aligned} E(\rho) &= \int \rho(r)\nu(r)dr + T(\rho) + V_{ee}(\rho) \\ &= \int \rho(r)\nu(r)dr + T_s(\rho) + J(\rho) + [T(\rho) - T_s(\rho)] \\ &\quad +[V_{ee}(\rho) - J(\rho)] \\ &= \int \rho(r)\nu(r)dr + T_s(\rho) + J(\rho) + E_{xc}(\rho) \end{aligned} \tag{2.76}$$

The $E_{xc}(\rho)$ term is called the exchange correlation energy. It contains the difference between T an T_s and the non-classical part of $V_{ee}(\rho)$. The chemical potential becomes

$$\mu = \nu_{eff}(r) + \frac{\delta T_s(\rho)}{\delta\rho(r)} \tag{2.77}$$

In which ν_{eff} is the effective Kohn and Sham potential defined by

$$\begin{aligned} \nu_{eff}(r) &= \nu(r) + \frac{\delta J(\rho)}{\delta\rho(r)} + \frac{\delta E_{xc}(\rho)}{\delta\rho(r)} \\ &= \nu(r) + \int \frac{\rho(r')}{|r-r'|} dr' + \nu_{xc}(r) \end{aligned} \tag{2.78}$$

This defines the exchange correlation potential ν_{xc}. Equation 2.77 with the constraint $\int \rho(r)dr = N$ is precisely the same one obtains from conventional DFT when one applies it to a system of non-interacting electrons moving in the external potential $\nu_s(r) = \nu_{eff}(r)$. Therefore, for a given $\nu_{eff}(r)$ one can obtain $\rho(r)$ that satisfies equation 2.77 by solving the N one-electron equations

$$[-\frac{1}{2}\nabla^2 + \nu_{eff}(r)]\psi_i = \varepsilon_i\psi_i \tag{2.79}$$

Those last two equations are Kohn and Sham (KS) equations for the Kohn and Sham orbitals ψ_i, which gives the exact density once the exact exchange correlation functional is known. The effective potential depends on the electron density, therefore, those equation have to be solved self consistently. One begins with a guessed electron density from which the effective potential is obtained, then finds the ψ_i orbitals and so on until self consistency is reached. As the orbitals in HF development, the KS orbitals were approximated by a LCAO-MO development. Different expressions for the exchange-correlation potential have been proposed, each carrying a certain number of parameters. Historically, the first exchange correlation functionals depended solely on $\rho(r)$ and are called Local Density Approximation (LDA). Improvement came from Generalized Gradient Approximation (GGA) , which depended both on $\rho(r)$ and on its gradient. Meta-GGA functionals include higher order derivatives of the electron density. In most of recent literature, the hybrid functionals are used. Those functionals include a part of the exact

HF exchange. In this thesis, the functional used is an hybrid functional called B3LYP, defined as:

$$\begin{aligned} E_{xc}(B3LYP) &= AE_x^{Dirac} + (1-A)E_x^{HF} + B\Delta E_x^{Becke88} \\ &\quad +(1-C)E_C^{VWN} + CE_c^{LYP} \end{aligned} \tag{2.80}$$

introducing the Dirac exchange, the exact HF exchange and Becke gradient exchange correction and the Vosko, Wilk and Nussair as well as the Lee, Yang and Parr correlation functional. A, B and C are fitting parameters which are respectively 0.8, 0.72 and 0.81.

2.6 Model chemistries

Ab initio (HF and post-HF methods) and DFT methods to obtain energies have been described. The accuracy of the energies resulting from those calculations is limited by three main factors. The first of these is the limitation of the size of the basis set used in the LCAO-MO expansion. The second limitation is the limited description of electron correlation. Finally, the last one is the single determinant limitation. In this work, we only used single reference methods. In this context, the quality of our energies is therefore only limited by the quality of the electron-electron interaction description and by the size of the basis set (See Figure 2.2). Despite being in constant growth, the computational capacities are not sufficient to carry out calculations with methods including important part of electron correlation combined with very large basis set. In the early 90's, those computational capacities were more limited. This led to the development of what we call model chemistries. In this part of the work we describe the three main categories of model chemistries. Those are the Gaussian family of model chemistries, the

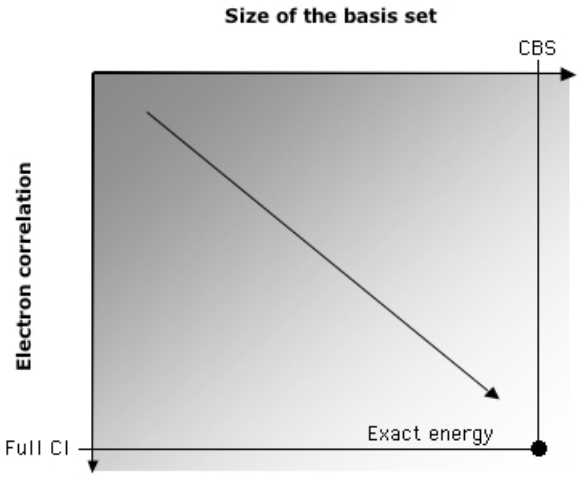

Figure 2.2: Variation of the quality of the energies with the levels of theory used (within the single determinant approach).

Complete Basis Set family and finally the Weizmann one. All those methods rely on an energy correction additivity assumption. The latter assumption is only confirmed *a posteriori* by the quality of the results obtained.

2.6.1 Gaussian model chemistries

The first Gaussian model (G1) appeared in 1989 [38]. Since then, an important number of variation have been developed such as G2 [39], G2(MP2, rcc), G3 [40], G3(MP2), G3B3 (this method will be described in details hereafter). All those methods rely on additive schemes and follow similar procedures that include the determination of geometries and frequencies at a relatively low level of theory (HF, MP2 or DFT in most cases), a series of single point calculations (SPC) to account for various effects, such as electron correlation (at QCISD(T) or CCSD(T)

levels), or basis set effects (using extended basis sets with diffuse and/or polarization functions). Most of the total energies also include an empirical correction based on the number of α and β valence electrons in the system. Whether calculations are carried out using restricted or unrestricted wave functions depends on the method used, however, most commonly, unrestricted wave functions are used. The latest versions of Gaussian model chemistry are G4 [41], G4(MP3) and G4(MP2) [42]. Those methods include an extrapolation to the infinite basis set, which was not the case of the earlier versions of Gaussian model chemistries.

G3B3

This section describes in detail the G3B3 model. This model has been extensively used in this work. Most information in this description comes from the reference G3B3 article [43]. Unlike previous Gaussian methods, (G1, G2, G3) the G3B3 geometry and frequencies are obtained using a DFT method, more precisely, B3LYP with the 6-31G(d) basis set (the G3B3 name comes from the modification of the **G3** method with **B3**LYP geometries and frequencies). This modification was applied as DFT shows better agreement with experiment at the 6-31G(d) level than MP2 (method used in previous Gn model chemistries). The frequencies are then scaled by a factor of 0.96 to fit as well as possible theoretical data to experimental results. In the G3B3 case, energy corrections are obtained by carrying out several SPC at the B3LYP/6-31G(d) geometry. The results of those calculations are then used to calculate the energy corrections. The preliminary SPC provides the starting point energy, it is a MP4SDTQ/6-31G(d) calculation within the frozen core approximation (FC). The energy corrections are added to this energy.

- A first calculation is carried out at the QCISD(T, FC)/6-31G(d) level and provides a first energy correction. This correction accounts for electron correlation and is obtained through:

$$\begin{aligned}\Delta(QCI) &= E[QCISD(T,FC)/6-31G(d)] \\ &\quad -E[MP4(FC)/6-31G(d)] \end{aligned} \tag{2.81}$$

- The second correction is used to correct the energy for the effects of diffuse function in the basis set. This is done through a MP4SDTQ(FC)/6-31+G(d) basis set SPC and the correction is obtained through:

$$\begin{aligned}\Delta(+) &= E[MP4(FC)/6-31+G(d)] \\ &\quad -E[MP4(FC)/6-31G(d)] \end{aligned} \tag{2.82}$$

- Polarization of the basis set is also accounted for through the Δ(2df,p) correction. The SPC consists in an MP4SDTQ(FC)/6-31G(2df,p). Similarly to $\Delta(+)$, the Δ(2df,p) correction is obtained through:

$$\begin{aligned}\Delta(2df,p) &= E[MP4(FC)/6-31G(2df,p)] \\ &\quad -E[MP4(FC)/6-31G(d)] \end{aligned} \tag{2.83}$$

- A correction for larger basis set effects, core correlation and for non-additivity caused by the assumption of separate basis set extension for diffuse and polarization functions is obtained by a MP2(FU)/GTLarge calculation. FU indicates full electron correlation and is to be opposed to FC.

Table 2.1: Parameters of the Δ(HLC) correction (mhartree).

Parameter	Atoms	Molecules
A	6.786	6.760
B	1.269	3.233

The GTLarge basis set is sometimes referred to as GTL and consists in a 6-311+G(3d2f, 2p) for the second row atoms and 6-311+G(2df, 2p) for the first row ones.

$$\begin{aligned}\Delta(GTL) &= E[MP2(FU)/GTLarge] \\ &\quad -E[MP2(FC)/6-31G(2df,p)] \\ &\quad -(E[MP4(FC)/6-31+G(d)] \\ &\quad -E[MP4(FC)/6-31G(d)]) \end{aligned} \tag{2.84}$$

- A Higher Level Correction corrects remaining deficiencies in the energy calculation. This Δ(HLC) is a parameterized empirical correction function of the number of α and β valence electrons

$$\Delta(HLC) = -An_\beta - B(n_\alpha - n_\beta) \tag{2.85}$$

Parameters A and B (see Table 2.1) have been optimized to give the smallest average absolute deviation from experiment for the G2/97 test set [44]. Separate corrections are used for atomic and molecular species. For atomic species, a spin-orbit correction is added to the energies.

2.6.2 Complete Basis set Model chemistries

A year before G1; Petersson and coworkers presented their first Complete Basis Set (CBS) model chemistry. There are also a wide variety of

CBS methods (CBS-Q, CBS-QB3, CBS-4M, CBS-APNO, CBS-q, CBS-RAD,...) first developed by Petersson, which include an energy correction coming from a complete basis set extrapolation of MP2 energies. Those also include energy correction similar to those included in Gn models. Among all CBS methods, we note the presence of a spin contamination correction in the CBS-Q and CBS-QB3 methods [45]. The method considered being the most accurate is CBS-APNO [46]. This method has been used in this thesis and is described hereafter.

CBS-APNO

The CBS-APNO (Complete Basis Set - Atomic Pair Natural Orbital) method is a seven step model chemistry, quite computationally demanding. The first step is a HF/6-311G(d,p) geometry optimization followed by a frequency calculation at that same level. The frequencies obtained are then scaled by a factor of 0.9251 to fit as well as possible theoretical to experimental data. The geometry is then refined at the QCISD(T) 6-311G(d,p) level to obtain the geometry at which SPC are carried out. The first is a QCISD(T) 6-311++G(2df,p) calculation for higher order correlation energy corrections. The final three calculations use HF, MP2(FU) and MP2(FC) with CBS methods specific basis sets to extrapolate the MP2 energies to the complete basis set. Those extrapolations provide energy corrections for truncation of the basis set. Finally, an empirical correction is also added to yield the final CBS-APNO energy. Due to its computational cost and the relatively poor accuracy of the heats of formations obtained from CBS-APNO energies, the method was not extensively used.

2.6.3 Weizmann theories

Weizmann theories (W1, W2 [47], W3 [48], W4 [49],...) have been developed by J. M. L. Martin and coworkers. This last type of model chemistries is often much more accurate than experimental data itself as it aims at the 1 J accuracy. These methods imply several complete basis set extrapolations (other extrapolation than in CBS methods) which allow the calculation of infinite basis set energy corrections, relativistic effects,... The accuracy of the result is an attractive aspect of those methods, however they are hardly applicable to relatively large compounds due to their computational costs. As this method was not used in this thesis, only a short description is given.

W1

The W1 model is the first of the Wn developped by J. L. M. Martin and coworkers. As implemented into Gaussian03, it involves a geometry optimization at the B3LYP/cc-pvTZ + d level of theory followed by a harmonic frequency calculation. A series of SPCs are then carried out at that geometry. First CCSD(T FC)/augh-cc-pVDZ +2df and CCSD(T FC)/augh-cc-pVTZ +2df are carried out. Then the CCSD(FC)/augh-cc-pVDZ +2df energy is computed. Energies resulting from those calculations are used in extrapolation formulas to obtain SCF energy at the complete basis set, correlation contribution of CCSD at infinite basis set and the contribution of the connected triples at infinite basis set. Finally, two supplementary SPCs are carried out to account for relativistic effects and core correlation. Those are CCSD(T, FC)/MTSmall and CCSD(T, Full)/MTSmall with Douglas-Kroll-Hess relativistic cor-

rection. It has to be mentioned that despite being named "small", the MTSmall basis set is larger than the GTLarge basis set in the G3B3 method.

2.7 Structures and energy surfaces

2.7.1 Energy surface

The Born-Oppenheimer approximation leads to the separation of the motion of the nuclei and electrons. There is therefore one electronic energy for each possible nuclear geometry. Once the electronic Schrödinger equation has been solved for an important number of those geometries, the Potential Energy Surface (PES) of the system is known. For an N nuclei system, the PES has 3N-6 dimensions (3N-5 for linear compounds).

Stationary points

The determination of the complete energy surface of a system is an almost impossible task. Luckily, the description of a chemical reaction does not need the complete PES. The only points of importance are stationary points; minima and first-order saddle points, representing stable structures and transition states respectively (see Figure 2.3). A stationary point $\mathbf{x}$ on a n dimension energy surface f may be characterized in terms of the derivatives of f at point $\mathbf{x}$.

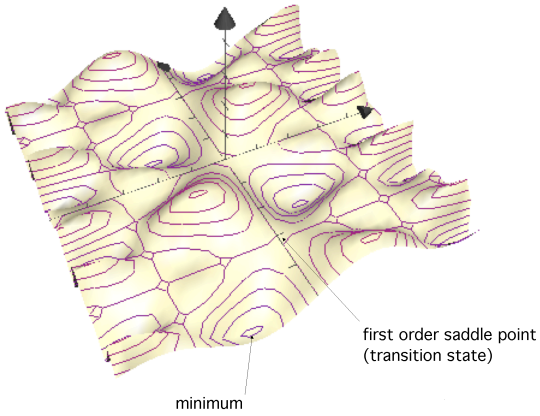

Figure 2.3: Minima and saddle points on a 2-dimensional surface.

The gradient vector and Hessian matrix at that point are given by

$$\nabla f(\mathbf{x}) = \begin{bmatrix} \frac{\delta E}{\delta x_1} \\ \vdots \\ \frac{\delta E}{\delta x_n} \end{bmatrix}, \quad \nabla^{\mathbf{2}} f(\mathbf{x}) = \begin{bmatrix} \frac{\delta^2 E}{\delta x_1 x_1} & \cdots & \frac{\delta^2 E}{\delta x_1 x_n} \\ \vdots & \ddots & \vdots \\ \frac{\delta^2 E}{\delta x_n x_1} & \cdots & \frac{\delta^2 E}{\delta x_n x_n} \end{bmatrix} \tag{2.86}$$

In order to have a stationary point at $\mathbf{x}$, it is required that

$$\nabla f(\mathbf{x}) = \mathbf{0} \tag{2.87}$$

If the Hessian matrix is positive definite (positive curvature in all direction), the stationary point is a minimum. If the Hessian matrix presents a negative eigenvalue, the stationary point is a first-order saddle point. In extension, if the Hessian matrix has k negative eigenvalues, the stationary point is a k^{th} order saddle point.

Minimum energy path

The minimum energy path of a given reaction is the lowest energy path on the potential energy surface connecting the reactants to the products. This path has its maximum at the transition state of the reaction. It is the most likely path to be followed when the reaction takes place.

Optimization of stationary points

To obtain the energy of a stationary point, one has to know its geometry. Using the harmonic approximation to locally describe the PES, one has

$$E(x) = E^0 + \Delta x^T \nabla E + \frac{1}{2}\Delta x^T \nabla\nabla E \Delta x \tag{2.88}$$

in which ∇E is the molecular gradient containing the negative molecular forces acting on the nuclei, and $\nabla\nabla E$ is the molecular Hessian containing the quadratic force constants.

$$\nabla E = \frac{\delta E}{\delta x} = -F \quad and \quad \nabla\nabla E = \frac{\delta^2 E}{\delta x^2} \tag{2.89}$$

Considering this harmonic PES, the localization of a stationary point requires

$$\nabla E = \frac{\delta E}{\delta x} = 0 \tag{2.90}$$

from the quadratic model,

$$FG^{-1} = \Delta x \tag{2.91}$$

With Δx being the displacement vector leading to the stationary point and Δx^T the transposed vector. If the exact Hessian is used, the Δx step is called the Newton step, if an approximate Hessian is used, the step is called the quasi-newton step. The quadratic description of the

PES remains an approximation and the quadratic expression has to be re-evaluated at the new geometry, and a new displacement is commonly calculated. This leads to a stepwise procedure towards the stationary point. Optimization of a minimum often starts with an estimated Hessian, as analytical evaluation of the Hessian is a large, time demanding computation effort, which can be updated at each step of the procedure, based on the forces in the previous step. The determination of the structure of a transition state calls for a good approximation of the starting Hessian, which is therefore often calculated analytically. In the search of the transition state, the energy is increased in the direction of the negative force constant, and minimized in all other directions. For this procedure to succeed, one has to have a good initial idea of the structure of the transition state, for instance, a structure already having one negative force constant. It is not always easy to obtain the initial guess of the transition state structure. To that end , some methods to guess starting geometries have been developed. The Synchronous Transit Quasi Newton Methods [50, 51] determine a starting geometry from the structures of the reactants and the one of the products (QST2) or from the structures of the reactant, products and a first estimate of the transition state structure input by the user (QST3). Ideally, once a transition structure is obtained, one should verify the connectivity of this saddle point to make sure it connects the considered reactants and products. This can be done through Intrinsic Reaction coordinate calculations [52, 53]. Those calculations start at the transition state and follow the negative force constant downhill to the connected minima.

Chapter 3

Obtention of thermodynamic and kinetic data

Ab initio computational methods provide detailed molecular information such as the geometry or the molecular energy. Further calculations are needed to generate gas properties, such as entropies and heat capacities. The link between the molecular (microscopic) level and the molar (macroscopic) level is made by the use of statistical thermodynamics. The first part of this chapter gives the necessary information for practical calculation of the needed thermodynamic quantities. In a second section, we define different methods used to obtain heats of formation from the energies obtained by *ab initio* calculations and the thermal energy correction from statistical thermodynamics. Finally, we provide a description of transition state theory, which is used in this work to obtain rate constants.

Table 3.1: Thermodynamic properties expressed as a function of the partition function.

Property	Relation to the partition function Q
Internal energy	$U = kT^2[\frac{\delta(lnQ)}{\delta T}]_{N,V}$
Enthalpy	$H = kT(T[\frac{\delta(lnQ)}{\delta T}]_{N,V} + V[\frac{\delta(lnQ)}{\delta V}]_{N,T})$
C_v	$C_v = [\frac{\delta U}{\delta T}]_{N,V} = 2kT[\frac{\delta(lnQ)}{\delta T}]_{N,V} + kT^2[\frac{\delta^2(lnQ)}{\delta T^2}]_{N,V}$
Entropy	$S = kT[\frac{\delta(lnQ)}{\delta T}]_{N,V} + kln(Q) = \frac{U}{T} + kln(Q)$

3.1 Statistical Thermodynamics

3.1.1 Partition function

The partition function Q (see equation 3.1) allows the determination of thermodynamic quantities such as thermal corrections to energy, entropies and heat capacities (see Table 3.1).

$$Q_{(N,V,T)} = \sum_j exp(\frac{-E_j}{kT}) \tag{3.1}$$

in which N is the number of particles, V is the volume, T the temperature and E_j is the energy of the system in state j. This partition function may be written in term of the individual atomic or molecular partition function *q(V,T)*.

$$Q_{(N,V,T)} = \frac{q^N_{(V,T)}}{N!} \tag{3.2}$$

The molecular energy levels,ϵ_i , are used to compute the molecular partition function noted *q(V,T)*.

$$q_{(V,T)} = \sum_i exp(\frac{-\epsilon_i}{kT}) \tag{3.3}$$

3.1.2 Practical calculations

Using the complete set of molecular energy levels is almost never possible. To simplify the problem, one generally adopts a model in which translation, rotation, vibration and electronic excitations are uncoupled. This leads to the separability of the partition function in four factors corresponding to four partition functions (translation, rotation, vibration and electronic excitation).

$$q_{(V,T)} = q^{trans}_{(V,T)} . q^{rot}_{(T)} . q^{vib}_{(T)} . q^{elec}_{(T)} \tag{3.4}$$

Thermodynamic molar functions can be derived from the molecular partition function. Using the uncoupled partition function allows the determination of the contribution of each partition function to the different thermodynamic data.

Translational partition function

The translational partition function q_{trans} is calculated from a sum over all energy levels.

$$q^{trans}_{(V,T)} = [\sum_{n=1}^{\infty} exp(-\frac{h^2 n^2}{kT8ma^2}]^3 \tag{3.5}$$

As the translational energy levels are close to each other, the sum is approximated by an integral. The resulting expression for the partition function is

$$q^{trans}_{(V,T)} = \frac{(2\pi mkT)^{\frac{3}{2}}}{h^3} V \tag{3.6}$$

This partition function leads to the expression of the different contribution to the thermodynamic functions

$$U^{trans} = \frac{3}{2}RT \tag{3.7}$$

$$C_v^{trans} = \frac{3}{2}R \tag{3.8}$$

$$S^{trans} = R(\frac{5}{2} + \frac{3}{2}[ln(T) + ln(m) + ln(\frac{2\pi k}{h^2}] + ln(\frac{V}{N})) \tag{3.9}$$

Rotational partition function

The free rotation of a molecule is also quantized. The rotational energy levels are therefore also restricted to certain discrete levels.

$$\varepsilon_i = \frac{\hbar^2 J(J+1)}{2I} \tag{3.10}$$

In which I is the moment of inertia. The rotation partition function therefore becomes

$$q_{(T)}^{rot} = \sum_{J=0}^{\infty}(2J+1)exp(-\frac{\hbar^2 J(J+1)}{2IkT}) \tag{3.11}$$

At high enough temperatures, the sum over all levels may be replaced by an integral, as was done for the translation partition function. We define here the partition function for the general case and for the linear systems.

$$q_{(T)}^{rot} = \frac{\sqrt{\pi}}{\sigma}(\frac{T}{\Theta_A})^{\frac{1}{2}}(\frac{T}{\Theta_B})^{\frac{1}{2}}(\frac{T}{\Theta_C})^{\frac{1}{2}} \quad with \quad \Theta_N = \frac{\hbar^2}{2I_N k} \tag{3.12}$$

$$q_{rot,linear} = \frac{1}{\sigma}\frac{T}{\Theta_A} \tag{3.13}$$

In which I_N is the moment of inertia and σ is the rotational symmetry number.

The contribution of rotation to the various thermodynamic functions are

$$\begin{aligned} U^{rot} &= \frac{3}{2}RT \\ U^{rot}_{linear} &= RT \\ C^{rot}_{v} &= \frac{3}{2}R \\ C^{rot}_{v,linear} &= R \\ S^{rot} &= R[\frac{3}{2} + \frac{1}{2}ln\pi + \frac{3}{2}ln(T) - \frac{1}{2}ln(\Theta_A\Theta_B\Theta_C) - ln(\sigma)] \\ S^{rot}_{linear} &= R[ln(T) - ln(\Theta) - ln(\sigma) + 1] \end{aligned}$$

Vibrational partition function

If the vibrational energy levels are measured relative to the bottom of the internuclear potential well, the energies are given by

$$\varepsilon_\nu = (\nu + \frac{1}{2})h\nu \tag{3.14}$$

The vibrational partition function is given by equation 3.15.

$$q^{vib}_{(T)} = \sum_{\nu=0}^{\infty} exp(-\frac{(\nu + \frac{1}{2})h\nu}{kT}) \tag{3.15}$$

Once the sum is evaluated , the vibrational partition function becomes

$$q^{vib} = \frac{exp(\frac{-\Theta_\nu}{2T})}{1 - exp(\frac{-\Theta_\nu}{T})} \quad with \quad \Theta_\nu = \frac{h\nu}{k} \tag{3.16}$$

In a polyatomic molecule having N atoms, there are 3N-6 normal modes (or 3N-5 for linear molecules). The partition function becomes a product of the partition functions of the individual vibrators.

$$q^{vib}_{(T)} = \prod_{i=1}^{vib.\ modes} q^{vib}_i \tag{3.17}$$

The participations of each vibration mode to the thermodynamic functions are given by the following equations.

$$U^{vib} = R\Theta_{v_i}[\frac{1}{2} + \frac{1}{exp(\frac{\Theta_{v_i}}{T}) - 1}] \quad (3.18)$$

$$C_v^{vib} = R(\frac{\Theta_{v_i}}{T})^2 \frac{exp(\frac{\Theta_{v_i}}{T})}{[exp(\frac{\Theta_{v_i}}{T}) - 1]^2} \quad (3.19)$$

$$S^{vib} = R[(\frac{\Theta_{v_i}}{T}) \frac{1}{exp(\frac{\Theta_{v_i}}{T})} - ln(1 - exp(\frac{\Theta_{v_i}}{T}))] \quad (3.20)$$

Electronic partition function

The electronic partition function is given by

$$q_{elec} = \sum_{i=0}^{nb\ levels} g_i exp(\frac{-\varepsilon_i}{kT}) \quad (3.21)$$

In this equation, g_0 and ε_0 correspond to the degeneracy and the energy of the ground state respectively. This energy is set to zero. All energies of excited states are measured relative to this ground state. If there are no low lying excited states the partition function becomes a constant, which is the degeneracy of the ground state. The electronic partition function being constant, it only has an effect on entropies (see Table 3.1). In the case of doublet systems, the entropy is increased by Rln(2). If there are low lying electronic states, the partition function must be developed using the number of significant electronic states. The electronic contribution to the various thermodynamic functions are then obtained by applying the relations given in Table 3.1 to the electronic partition function.

Internal rotations

Internal rotation refers mostly to torsional motion. There are three ways of dealing with such a rotor. If the rotation barrier is much greater than kT, the motion can be treated as an harmonic oscillator. The second way is to treat the motion as a free rotor. This is usually done if the barrier is much smaller than kT. The third way, when the torsional barrier (V_{max}) is comparable to kT, is the hindered rotor treatment. If the torsional potential is assumed to have a simple sinusoidal form (see equation 3.22), then the tables of Pitzer and Gwinn [54] are used to compute the contribution of the hindered rotor to the thermodynamic functions.

$$V(\phi) = \frac{V_{max}}{2}(1 - \cos(\sigma_{int}\phi)) \tag{3.22}$$

In the *ab initio* software package used (Gaussian03), all normal modes are treated as vibrations. If one mode has to be treated as a free rotor or a hindered one, the contribution of this mode has to be removed and replaced by the contribution of the corresponding rotor.

3.2 From energies to heats of formation

The *ab initio*, as all methods described previously, only provides total energies at 0 K (fixed nuclei). Those energies may be corrected for thermal effects through the use of computed normal mode frequencies and statistical thermodynamics to obtain the total energies at a given temperature. Those energies still have to be converted into heats of formation. According to the definition, the standard heat of formation of a compound is the heat exchanged when the compound is formed from its elements in their standard state.

In the case of a C_nH_m hydrocarbon this reaction should be

$$nC_{s,gr} + \frac{n}{2}H_{2,g} \longrightarrow C_nH_m \tag{3.23}$$

This definition can however not be used to compute heats of formation as *ab initio* calculations on condensed phase elements are not available. This section describes the methods used in this work to deduce heats of formation of hydrocarbons from total energies or enthalpies. Two different cases appear: the closed-shell systems (molecules) and the open-shell ones (radicals). Apart from the atomization reaction method, the methods used to obtain the heat of formation of closed and open-shell systems are different. They are therefore presented in different sections.

Atomization Reactions (AR)

The first method, uses atomization reactions. According to this scheme, the standard heat of formation for a C_nH_m hydrocarbon is obtained by equations.

$$\Delta H_f^\circ(C_nH_m, 0K) = n\Delta H_f^\circ(C, 0K) + m\Delta H_f^\circ(H, 0K) - \sum D_0 \tag{3.24}$$

$\sum D_0$ are the calculated molar atomization energies

$$\sum D_0 = nE(C, 0K) + mE(H, 0K) - E(C_nHm, 0K) \tag{3.25}$$

Atomic heats of formation are taken from literature and are respectively for carbon and hydrogen 169.98 and 51.63 kcal.mol^{-1}. The next step corrects the value at 0 K to obtain the heat of formation at 298.15 K. The enthalpy corrections for carbon and hydrogen atoms are respectively 0.25 and 1.01 kcal.mol^{-1} [55].

$$\begin{aligned}\Delta H_f^\circ(C_nH_m, 298.15K) &= \Delta H_f^\circ(C_nH_m, 0K) \\ &+[H(C_nH_m, 298.15K) - H(C_nH_m, 0K)] \\ &-n[H(C, 298.15) - H(C, 0K)] \\ &-m[H(H, 298.15) - H(H, 0K)] \qquad (3.26)\end{aligned}$$

3.2.1 Methods applied to closed-shell systems

Apart from the atomization reactions, three methods were applied to closed-shell systems. Those are the hydrogenation, combustion and isodesmic reactions.

Hydrogenation reaction (HyR)

In this method the compound is completely hydrogenated into methane. Contrarily to the atomization scheme, this method is isogyric, meaning that it offers conservation of the number of electron pairs. It also conserves the number of radicals and their multiplicity, however, those reactions are not applied to open-shell systems in this work. The reaction for a C_nH_m hydrocarbon is

$$C_nH_m + (\frac{4n-m}{2})H_2 \longrightarrow nCH_4 \qquad (3.27)$$

The standard heat of formation is then obtained from the heat of reaction using the experimental value for the heat of formation of methane at 298.15 K. From a theoretical point of view, this method should be more accurate than the atomization scheme [23].

Combustion reactions

Combustion reactions are also considered. Those are interesting because experimental data is available for the heats of reaction. This allows analysis of the error on the heat of combustion, and on the final heat of formation, therefore separating the error from the energies from the error on the experimental references. As is seen later on, most of the error on the resulting heats of formation comes from the energies.

Isodesmic reactions

Isodesmic reactions have been introduced by Hehre and coworkers [56]. As defined in their work, this term is used to describe reactions in which all the formal bonds between heavy atoms are separated into the simplest molecules with the same type of bonds. Methane is used to ensure stoichiometry. Later, George and coworkers [57] introduced homodesmotic reactions, which conserve the number of carbon atoms in their various states of hybridation and the number of carbon atoms with one, two or three hydrogen attached. With time, various other names were used, such as homodesmic reactions, bond separation reactions, hypohomodesmotic reactions, semihomodesmotic reactions, ... The important number of names for the different types of reactions makes the discussion uneasy. In this work, the term Bond Separation Reaction is used to describe the isodesmic reactions as defined by Herhe. Those are used extensively. Very recently, bond separation reactions have been the subject of a classification by Wheeler and coworkers [58]. This classification is shortly described here, as it is discussed in section 5.5.

Hierarchy in homodesmotic reactions The highest level in this hierarchy is occupied by the hyperhomodesmotic reactions. Those reactions conserve the number of carbon-carbon bond types (H_3C-CH_2, H_3C-CH, H_2C-CH_2, H_3C-C, H_2C-C, HC-CH, HC-C, C-C, H_2C=CH, HC=CH, H_2C=C, HC=C, C=C, HC≡C, and C≡C). They also conserve the number and type of carbon atom with zero, one, two and three hydrogens attached in reactants and products. The second level is the homodesmotic one in which there is an equal number of carbon-carbon bond type (sp^3-sp^3, sp^3-sp^2, sp^3,sp, sp^2-sp^2, sp^2-sp, sp-sp, sp^2=sp^2, sp^2=sp, sp=sp, sp≡sp) and an equal number of each type of carbon atom with zero, one, two or three hydrogens attached in reactants and products. Hypohomodesmotic reactions conserve the number of carbon in their various states of hybridation and the number of carbon atoms with zero, one, two or three hydrogens attached. The bond separation reactions as defined by Raghavachari and coworkers are now simply called isodesmic reactions. They retain the number and type of carbon-carbon bond and carbon hydrogen bonds. This type of reaction is used extensively in this work, as the number of references remains limited, and thermodynamic data on those are accurately known. The acronym BSR for those reactions is maintained throughout this work. Finally, the fifth and lowest level of their hierarchy is occupied by the isogyric reactions we have previously called HyR. As defined by Wheeler and coworkers, all those reactions are isodesmic bond separation reactions, apart from the isogyric level. They show the advantage of being uniquely defined. There can however be a limitless number of bond conserving reactions for a given system. Figure 3.1 shows the different possible isodesmic bond separation reactions for 2-methylhexa-1,3-diene-5-yne.

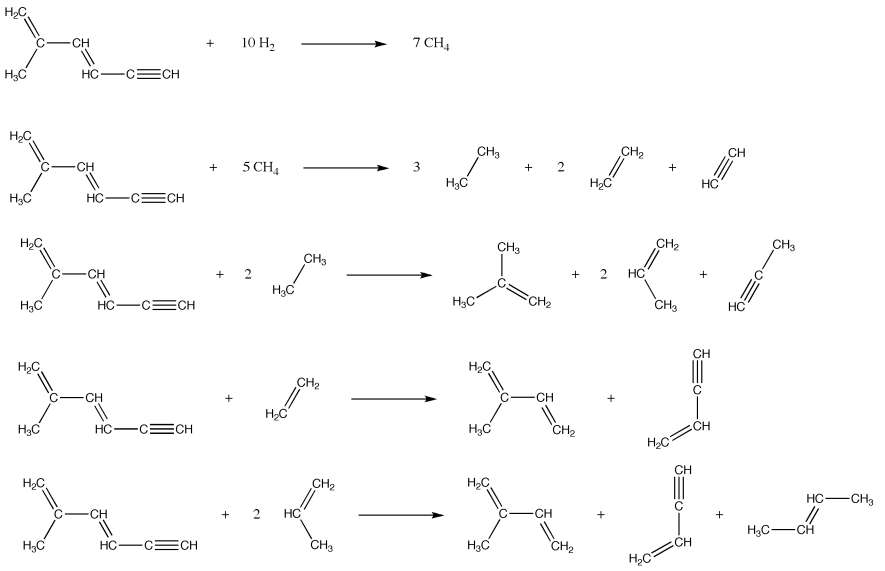

Figure 3.1: Illustration of hierarchy in bond separation isodesmic reaction, from isogyric (top) to hyperhomodesmotic (bottom) reactions.

3.2.2 Methods applied to open-shell systems

The open-shell systems are treated using unrestricted wave functions, which involves having to deal with spin contamination.

Hydrogen transfer reactions (HTR)

An example of such a reaction for the determination of the heat of formation of the phenyl radical is given on Figure 3.2. This method consist in considering hydrogen transfer reaction from a closed-shell system (benzene in the example) to a open-shell one (the methyl radical in the example). The heat of formation of the radical under investigation (the phenyl radical in the example) is obtained from the heat of the hydrogen transfer reaction and the experimental heats of formation of the open and closed-shell references (the methyl radical, methane and ben-

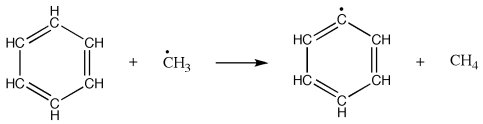

Figure 3.2: Hydrogen Transfer Reaction for the phenyl radical.

zene). From an isodesmicity point of view, this method retains almost completely the electronic environment and should therefore provide very accurate data. There are however two main drawbacks to that method. The first is the need to compute the energy of the corresponding closed-shell systems for each radical to be studied. This significantly increases the computational cost of the determination of a heat of formation. Furthermore, for unusual systems, the experimental heat of formation of the closed-shell system may not be available. Further work is, in those cases, needed to establish the heat of formation of that system. Secondly, if the open-shell system is studied using unrestricted wave function, an important spin contamination may cause a significant overestimation of the heat of formation [59].

Radical Bond separation Reaction (RBSR)

To avoid the practical drawbacks of the HTR method, we introduced open-shell references into the BSR test set. Those references are C_2H, C_2H_3, and C_2H_5 and have to be used in a way that best reflects the electronic environment of the radical site (see Figure 3.3). This method has well defined references and eliminates the first drawback of the hydrogen transfer method at the expense of a diminution of the conservation of electronic environment. By introducing open-shell systems in the reference set, we also introduce spin contaminated systems.

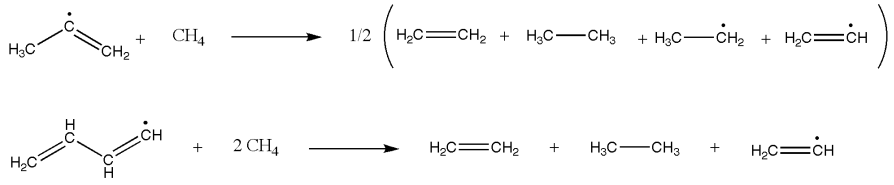

Figure 3.3: Radical bond separation reactions for the propene-2-yl and 1,3-butadiene-4-yl radicals

By doing so, we hope to partially cancel the error linked to spin contamination in the radical under investigation.

Notations Different methods have been described to obtain heats of formation. Each calculated heat of formation is therefore obtained combining the energy from an *ab initio* method and one of the presented methods to turn this energy into a standard heat of formation at 298.15 K. A heat of formation obtained using an energy E and a method M will be noted noted E/M. For instance, a heat of formation obtained with G3B3 energies and the hydrogenation method is noted G3B3/HyR. This notation is maintained throughout this work.

3.3 Transition state theory

Transition state theory views a reaction between A and B to form product P to proceed via de formation of a transition state $C^{\neq}$. The transition state then decomposes unimolecularly to the product P.

$$A + B \rightleftarrows C^{\neq} \rightarrow P \tag{3.28}$$

Using this scheme, one can establish Eyring's equation (equation 3.30), providing the bimolecular rate constant k_2 (for reaction A + B $\rightarrow$ P).

The rate of that reaction is defined as the rate of formation of the product P, or the rate of consumption of any of the two reactants.

$$\frac{d[P]}{dt} = -\frac{d[A]}{dt} = \frac{d[B]}{dt} = k_2[A][B] \tag{3.29}$$

Eyring's equation defines the rate constant k_2:

$$k_2 = \kappa \frac{RT}{p} \frac{kT}{h} K^{\neq} \tag{3.30}$$

In which $K^{\neq}$ is the equilibrium constant for the $A+B \rightleftarrows C^{\neq}$ equilibrium, and κ is the transmission coefficient. The latter classically has a value between 0 and 1. If κ=0, all the systems reaching the transition state go back to the reactants, if κ=1, all systems reaching the transition state continue to form the products. Generally, κ is set to 1. As the equilibrium constant may be expressed as a function of the Gibbs free energy, equation 3.30 may be rewritten:

$$k_2 = \kappa \frac{RT}{p} \frac{kT}{h} e^{(\frac{-\Delta G^{\neq}}{RT})} \tag{3.31}$$

In which $\Delta G^{\neq}$ is the activation free energy, namely, the difference in Gibbs free energy between the transition state and the reactants. The latter expression can also be developed to define the Arrhenius parameters as a function of the activation entropy ($\Delta S^{\neq}$) and activation enthalpy ($\Delta H^{\neq}$). This development leads to the general expression of the rate constant k for unimolecular or bimolecular reactions.

$$k = \kappa \frac{kT}{h} e^{(1-\Delta n^{\neq})} (\frac{RT}{p})^{-\Delta n^{\neq}} e^{(\frac{\Delta S^{\neq}}{R})} e^{(\frac{-E_a}{RT})} \tag{3.32}$$

In which $E_a = \Delta H^{\neq} + (1 - \Delta n^{\neq})RT$ is the activation energy. The remainder of the expression defines the pre-exponential term.

3.3.1 Tunneling

Tunneling is the process by which a particle or a set of particles crosses a barrier on its potential energy surface without having the energy required to surmount this barrier. In the theoretical determination of a rate constant, not accounting for this tunneling may lead to an underestimation of the rate constant. The easiest way to correct the rate constant for tunneling effect is to use Wigner's formula (see equation 3.33), which provides a corrected transmission coefficient.

$$\kappa(T) = 1 + \frac{1}{24}(\frac{hIm(\nu^{\neq})}{kT})^2 \tag{3.33}$$

This method is quite widely used as it only requires the value of the imaginary frequency ($\nu^{\neq}$) of the transition state. The Eckart method takes into account, not only the imaginary frequency of the transition states, but also the barrier height and the energies of the two minima connected by the transition state (details may be found in the work of Vandeputte and coworkers [60]). The Eckart method is the one used in this thesis.

3.3.2 Practical calculation of a rate constant

The practical determination of a rate constant involves both the quantum chemical methods described in chapter 2 and the statistical thermodynamic ones presented earlier in this chapter. Quantum chemical methods allow the determination of (among others) the geometries, energies (at 0 K, without residual vibrational energy), moments of inertia and vibrational frequencies of the reactants (minima) and transition state (first-order saddle points). The statistical thermodynamic formulas presented in this chapter are used to obtain the entropies of the

reactants and products as well as their thermal correction to enthalpies, $\Delta S^{\neq}$ and $\Delta H^{\neq}$ are then easily obtained, and so is the rate constant, as defined in equation 3.32. Once the rate constants have been obtained at different temperatures, the parameters for the Arrhenius (A and E_a) or modified Arrhenius (A, n and E_a) expression may be obtained by a least square fit.

3.3.3 The effect of pressure

A number of gas phase reactions involve an elementary unimolecular step in which the reactant molecule changes into the product ($A \rightarrow P$). Those are generally called "unimolecular" reactions. Such reactions present first-order rate laws (see equation 3.34). The mechanism present both unimolecular and bimolecular steps.

$$\frac{[dP]}{dt} = k[A] \tag{3.34}$$

The problem is that the molecule acquires the necessary energy through collision with another molecule, and a collision is a bimolecular event. How can this result in a first-order rate law. A first successful explanation of this is provided by the mechanism of Lindemann and Hinshelwood [61]. The $A \rightarrow P$ reaction actually begins with the collisional exciation of A to A^*:

$$A + A \rightarrow A^* + A \qquad \frac{d[A^*]}{dt} = k_a[A]^2 \tag{3.35}$$

The energized molecule A^* might lose its excess energy by collision

$$A^* + A \rightarrow A + A \qquad \frac{d[A^*]}{dt} = -k'_a[A][A^*] \tag{3.36}$$

Alternatively, A^* might also continue to form the product P

$$A^* \rightarrow P \qquad \frac{d[A^*]}{dt} = -k_b[A^*] \tag{3.37}$$

The rate of formation of P is given by

$$\frac{d[P]}{dt} = k_b[A^*] \tag{3.38}$$

Considering the steady state approximation for the net rate of formation of A^*, we obtain

$$\frac{d[A^*]}{dt} = k_a[A]^2 - k'_a[A][A^*] - k_b[A^*] \approx 0 \tag{3.39}$$

which leads to

$$[A^*] = \frac{k_a[A]^2}{k_b + k'_a[A]} \tag{3.40}$$

The rate of formation of P then becomes

$$\frac{d[P]}{dt} = k_b[A^*] = k_b \frac{k_a[A]^2}{k_b + k'_a[A]} \tag{3.41}$$

If the collisional deactivation of A^* is much faster than the formation of P, as would be the case in a high pressure environment, we have

$$k_b[A^*] \lll k'_a[A][A^*] \text{ or } k_b \lll k'_a[A] \tag{3.42}$$

We can then neglect k_b and the rate of formation of P becomes

$$\frac{d[P]}{dt} \approx k[A] \text{ with } k = \frac{k_a k_b}{k'_a} \tag{3.43}$$

which is a first-order rate law. In the opposite situation, if the formation of P is very fast compared to the collisional deactivation, the latter becomes the rate limiting step. In this case, we have

$$k_b[A^*] \ggg k'_a[A][A^*] \text{ or } k_b \ggg k'_a[A] \tag{3.44}$$

leading to a bimolecular rate law for the formation of P

$$\frac{d[P]}{dt} \approx k_a[A]^2 \tag{3.45}$$

This mechanism explains the particular pressure dependance of unimolecular reaction by a change of rate limiting step accompanying the changes in pressure.

Chapter 4

Combustion and combustion modeling

This chapter is divided into two sections. The first is dedicated to the description of the fundamental concepts in combustion chemistry. The second provides information about the modeling of combustion processes, such as it is carried out within the university's combustion unit.

4.1 Combustion phenomena

Combustion is a non-spontaneous self-sustained oxidation reaction. Most commonly, the oxidizer is molecular oxygen. The nature of the co-reactant is much more varied. The global combustion equation for a C, H, O, N system is given by equation 4.1.

$$C_xH_yO_zN_w + (x + \frac{y}{4} - \frac{z}{2})O_2 \longrightarrow xCO_2 + \frac{y}{2}H_2O + \frac{w}{2}N_2 \qquad (4.1)$$

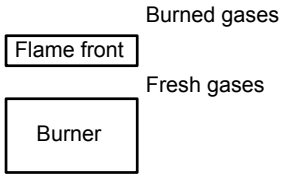

Figure 4.1: Schematic representation of the flame front above a flat flame burner.

4.2 Definitions

This section lists some definitions of concepts that are specific to combustion chemistry.

Equivalence ratio

The equivalence ratio (see equation 4.2) defines whether a flame is rich stoichimetric or lean. A rich flame (Φ >1) has an excess of fuel, and therefore leads to incomplete combustion processes and to the formation of carbonaceous species. A lean flame ($\Phi < 1$) has an excess of oxidizer and therefore allows more complete combustion phenomena.

$$\Phi = \frac{(\frac{\chi_{fuel}}{\chi_{oxidizer}})_{fresh\ \ gases}}{(\frac{\chi_{fuel}}{\chi_{oxidizer}})_{stoichiometry}} \tag{4.2}$$

Flame front

The flame front is the zone in which the combustion process takes place. This front is located between the incoming fresh gases and the burned products (see Figure 4.1). It is a very thin zone at atmospheric pressure and may be widened by working at lower pressure.

4.2.1 Types of flame

Premixed and diffusion flames

We distinguish two types of flames, diffusion flames and premixed ones. In diffusion flames, there is no premixing between the oxidizer and the fuel. This leads to incomplete and therefore to carbonaceous combustion products. Examples of diffusion flames are candles, lighters, and more generally, accidental flames (fire, explosions). In premixed flames, as indicated by the name, there is a premixing of the fuel and oxidizer before the beginning of the combustion process. This premixing allows a more complete combustion and therefore the production of less unburned carbon containing species.

Laminar or turbulent flame.

The difference between those two types of flames is only the nature of the flow of fresh gases. Laminar flames correspond to a laminar flow of fresh gases and turbulent ones to a turbulent flow.

One-dimensional laminar premixed low pressure flames

In the combustion studies carried out at the Universit*é* catholique de Louvain, flames are mostly one dimensional laminar premixed flames burning at low pressures. The laminar and premixed characteristics bring homogeneity to the flame behavior. The low pressure ensures a sufficiently large flame front. Sampling is done at different points of the flame front to analyze the variation in the concentration of the various detectable species.

Temperature profiles can also be established by measuring the temperature at different point of the flame front.

4.3 Combustion modeling

This section describes what a combustion model is composed of, what data is needed, and what equations are solved.

4.3.1 The mechanism

At the heart of the combustion model, there is the mechanism. This mechanism consists in a series of reactions considered to be the most important in the description of the different chemical processes occurring during the combustion process. Commonly, only important reactions are kept to limit the size of the model. For all the reactions included in the mechanisms, one must also know:

- The different gas properties concerning the species present in the mechanism. The properties to be provided to the modeling software (see further) are : the geometry of the molecule (monoatomic, linear, non linear), the Lennard-Jones potential, the Lennard-Jones collision diameter, the dipole moment, the polarizability, and the collision frequency.

- For each compounds in the mechanism, one must provide the heat of formation, the entropy and the heat capacity. This data has to be introduced in the form of the coefficients of the seven coefficient NASA polynomial, which provides a description of the

temperature dependence of the thermodynamic data:

$$\begin{aligned}\frac{C_p}{R} &= a_1 + a_2T + a_3T^2 + a_4T^3 + a_5T^4 \\ \frac{\Delta H_f^\circ}{RT} &= a_1 + \frac{a_2}{2}T + \frac{a_3}{3}T^2 + \frac{a_4}{4}T^3 + \frac{a_5}{5}T^4 + \frac{a_6}{T} \\ \frac{S^\circ}{R} &= a_1 ln(T) + a_2T + \frac{a_3}{2}T^2 + \frac{a_4}{3}T^3 + \frac{a_5}{4}T^4 + a_7\end{aligned}$$

- For all reactions composing the mechanism, one needs to introduce the three parameters A, n, and E_a of the modified Arrhenius expression for the rate constant (see equation 4.3).

$$k = AT^n exp(\frac{-E_a}{RT}) \tag{4.3}$$

This equation is used to account for non-linear behavior of the Arrhenius plot. This effect can be quite important. Those parameters are obtained by a least square fit on the calculated rate constants.

Once all the information is gathered, the model can be introduced in adequate software (COSILAB, CHEMKIN). Equations describing the freely propagating one dimensional premixed laminar flame are solved. Those equations account for mass conservation (equation 4.4), energy conservation (equation 4.5), species conservation (equation 4.6). The perfect gas law is also added to the system (equation 4.7).

$$\dot{M} = \rho\mu A_f \tag{4.4}$$

$$\begin{aligned}&\dot{M}\frac{dT}{dz} - \frac{1}{C_p}\frac{dT}{dz}(\lambda A_f \frac{dT}{dz}) \\ &+\frac{A_f}{C_p}\sum_{k=1}^{K}\rho Y_k V_k C_{p,k}\frac{dT}{dz} \\ &+\frac{A_f}{C_p}\sum_{k=1}^{K}\dot{\omega}_k h_k W_k = 0\end{aligned} \tag{4.5}$$

$$\dot{M}\frac{dY_k}{dz} + \frac{d}{dz}(\rho A_f Y_k V_k) - A_f \dot{\omega_k} W_k = 0 \tag{4.6}$$

$$\rho = \frac{p\bar{W}}{RT} \tag{4.7}$$

The meaning of the different parameters in equations 4.4 to 4.7 are given in Table 4.1. When those equations are solved, one obtains, (among others), the evolution of the mole fraction of any species included in the mechanisms with respect to the distance to the burner and the different pathways of formation of those species, through the net reaction rates.

Table 4.1: Meaning of the different parameters of equations 4.4 to 4.7.

Symbol	Meaning	units
z	distance to the burner	[m]
$\dot{M}$	mass flow rate	[kg s^{-1}m]
T	Temperature	[K]
Y_k	mass fraction of species k	[-]
p	pressure	[Pa]
μ	gas flow rate	[m s^{-1}]
ρ	volume density	[kg m^{-3}]
W_k	molar weight of species k	[kg mol^{-1}]
$\bar{W}$	average molar weight of the mixture	[kg mol^{-1}]
R	gas constant	[J $mol^{-1}K^{-1}$]
λ	thermal conductivity of the mixture	[W $K^{-1}m^{-1}mol^{-1}$]
C_p	Constant pressure heat capacity of the mixture	[J $mol^{-1}K^{-1}$]
$C_{p,k}$	Constant pressure heat capacity of species k	[J $mol^{-1}K^{-1}$]
$\dot{\omega}_k$	net molar production rate of species k per unit of volume	[mol $m^{-3}s^{-1}$]
h_k	specific enthalpy of species k	[J kg^{-1}]
V_k	diffusion rate of species k	[m s^{-1}]
A_f	surface including the flux lines	[m^2]

Part II

Results

Chapter 5

Heats of formation of closed-shell systems

The determination of the heats of formation of closed-shell systems is a major part of this thesis. It allows the evaluation of the method through the comparison with available experimental values (as discussed in the next chapter, such comparisons are harder to make for open-shell systems.). In this chapter, G3B3 energies are used to establish standard heats of formation using the different methodologies described in section 3.2. The results are analyzed and compared to establish the best way to deal with systems for which those heats of formation are inaccurately known or not known at all. Comparison with the test set leads to different types of results:

- First, the standard heats of formation of several small unsaturated cyclic hydrocarbons are redefined, others are just questioned.

- A new type of isodesmic reactions is considered, ring conserving isodesmic reactions. These reactions are used to define the heats of formation of bicyclohexadiene isomers.
- As a result of the analysis of the ring conserving processes, an isodesmicity index is defined and tested.

5.1 Test set

Several methods to determine the heats of formation of closed-shell systems have been presented in section 3.2. All those methods present different advantages and drawbacks. To determine the method to be used and the error we should expect from that method, we introduced a hydrocarbon test set. The G3B3 method coupled with atomization reactions has already been tested on the hydrocarbons contained in the G2/97 test set [43]. Among those hydrocarbons there are only a few large (5-6 carbons) ones, we therefore decided to create our own hydrocarbon test set.

5.1.1 G3B3 energy components

The following sections will discuss the various G3B3 energy components ($\Delta(QCI)$, $\Delta(+)$, $\Delta(2df,p)$ and $\Delta(GTL)$ corrections). The empirical correction is not discussed as its behavior is known by definition. Values of the different energy corrections are provided in the appendix of this chapter (see Table A.1).

$\Delta(QCI)$ corrections: The correlation correction

The $\Delta(QCI)$ corrections accounts for the correlation that has not been accounted for at the MP4SDTQ 6-31G(d) level. As was mentioned in section 2.4.2, a full fourth-order calculation includes between 95 and 98% of the correlation energy. It is therefore not surprising that this correction has the lowest magnitude of the four. On average, this correction brings a stabilization of the energies of 1.27 kcal.mol^{-1}, which only represents 0.45 % of the overall G3B3 stabilization. This small absolute magnitude does not make the $\Delta(QCI)$ correction less important than the others. For example, the energy difference induced between propyne and allene by the $\Delta(QCI)$ is larger than the ones induced by all the other corrections. On the whole test set, no clear tendency can be found, such as a direct dependence of the correction with the number of electrons, bonds or others. Nevertheless, tendencies in sub-groups can be found:

- For linear alkanes, there is a very good correlation between the $\Delta(QCI)$ correction and the number of electrons in the system. This relation is described by equation

$$\Delta(QCI) = -0.054nb(e^-) - 0.33 \qquad R^2 = 0.998 \qquad (5.1)$$

- For cyclic hydrocarbons, alkanes (equation 5.2) or alkenes (equation 5.3), the $\Delta(QCI)$ correction also follows a linear behavior when cycle size is increased.

$$\Delta(QCI) = -0.042nb(e^-) - 0.37 \qquad R^2 = 0.949 \qquad (5.2)$$

$$\Delta(QCI) = -0.047nb(e^-) - 0.26 \qquad R^2 = 0.956 \qquad (5.3)$$

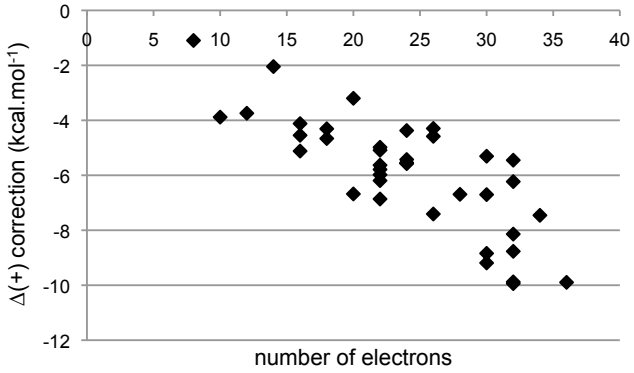

Figure 5.1: Evolution of the $\Delta(+)$ correction with the number of electrons.

- The $\Delta(QCI)$ is positive for two compounds, which are benzene and toluene. The aromatic ring is probably responsible for this situation.

All those observations are however made on very small sub-groups which do not guarantee their validity with increasing system sizes.

$\Delta(+)$ corrections: The diffusion functions correction

The $\Delta(+)$ correction is the second smallest in magnitude. Again, this could be expected, as the use of diffuse functions is known mainly to be useful for the description of weak bonds or ions (see section 2.3.3). This time, the importance of the correction clearly increases with the size of the system, without showing a good correlation coefficient (See Figure 5.1).

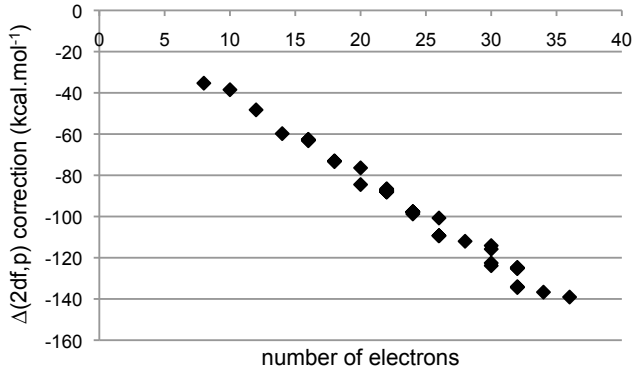

Figure 5.2: Evolution of the $\Delta(2df, p)$ correction with the number of electrons.

$\Delta(2df, p)$ corrections: The polarization functions corrections

The $\Delta(2df, p)$ correction accounts for 32 % of the overall correction. It exhibits a systematic increase of its magnitude with the size of the system (see Figure 5.2). This figure shows, at first glance, a better linear behavior than the equivalent figure for the $\Delta(+)$ (see Figure 5.1). We however must mention that the variation for a given number of electrons is greater for the polarization corrections. The use of polarization functions is known to be useful in the description of spaces having important electron density. As a result, the correction is more important for compounds containing triple bonds or strained patterns.

$\Delta(GTL)$ corrections: Remaining corrections

The $\Delta(GTL)$ correction includes the effects of core electrons as well as those linked to the consideration of separate basis set effects in the two preceding corrections. If this correction is plotted against the number

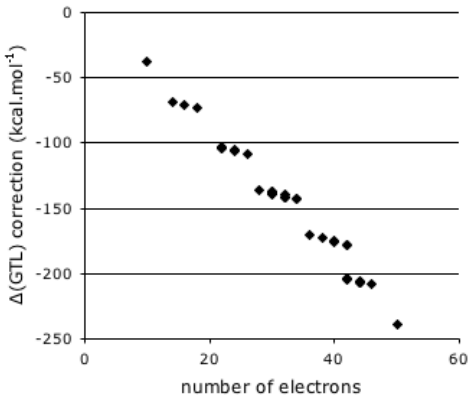

Figure 5.3: Evolution of the Δ (GTL) correction with the number of electrons.

of electrons (see Figure 5.3), one can clearly distinguish the effect of a carbon atom and its core electrons on the magnitude of the correction. The plot is indeed divided into a series of parallel series of points. Within each series, the decrease is linked to the number of hydrogen atom in the system. As shown in Table 5.1, slopes of the linear plots of $\Delta(GTL)$ as a function of the number of hydrogen within a given number of carbon atoms are very similar for two to six-carbons species.

5.1.2 Heats of formation

Results for the 34 hydrocarbons test set are presented in Table 5.2 along with the corresponding experimental data. Unless mentioned otherwise, the experimental value is taken from the Journal of Physical and Chemical Reference Data (JPCRD) [62]. In this table, * indicates a value from Pedley's compilation, ** indicates a value from the NIST Thermochemistry Webbook. The three last lines of that table provide Mean Deviation (MD), Mean Absolute Deviation (MAD, see equation 5.4)

Table 5.1: Slopes of the linear plots of $\Delta(GTL)$ as a function of the number of hydrogen for a given number of carbon atoms, and standard deviation of those slopes.

	slope	s.d.
2 carbons	-1.17	0.02
3 carbons	-1.12	0.14
4 carbons	-1.15	0.11
5 carbons	-1.23	0.13
6 carbons	-1.12	0.16

and Maximum Absolute Deviation (MaxAD). Those deviations are calculated as: experiment-calculated. As methane and two-carbon species are references in the BSR method, average values are calculated on three to seven carbon species to maintain consistency in the method comparisons.

$$MAD = \frac{1}{n}\sum_{1}^{n} |\Delta H_{f,expt.} - \Delta H_{f,calc.}| \tag{5.4}$$

Results from Table 5.2 indicate that AR and BSR both provide accurate data while the use of HyR or CombR yields very poor heats of formations.

Table 5.2: Experimental and calculated standard heats of formation for the test set hydrocarbons (kcal.mol^{-1}). Uncertainties on experimental values are provided when available.

Molecule	Expt	AR	HyR	BSR	CombR
Hydrogen	0	-0.42	-	-	-0.66
Methane	-17.8 ±0.1	-17.89	-	-	-16.81
Ethane	-20.1 ±0.05	-20.09	-20.32	-	-17.68
Ethylene	12.5 ±0.2	12.30	11.65	-	14.95
Acetylene	54.5 ±0.25	54.34	53.27	-	57.23

(Continued on next page)

(Continuing from previous page)

Allene	45.6 ±0.2	44.95	43.56	45.26	49.17
Propyne	44.6 ±0.5	44.08	42.69	44.14	48.30
Cyclopropene	66 ±0.7	68.24	66.84	68.13	72.45
Propene	4.8 ±0.2	4.77	3.79	4.86	8.74
Cyclopropane	12.7 ±0.2	13.44	12.46	13.12	17.42
Propane	-25 ±0.1	-24.97	-25.53	-25.09	-21.24
1-buten-3-yne**	70.4	68.80	66.67	68.97	74.59
1,3-butadiene*	26.3	26.49	24.77	26.69	32.03
1,2-butadiene	38.8 ±0.1	39.55	37.83	39.75	45.09
Methylenecyclopropane	48 ±0.5	46.25	44.53	46.04	51.79
Bicyclobutane	51.9 ±0.2	54.31	52.59	53.69	59.85
Cyclobutene	37.5 ±0.4	39.30	37.58	39.09	44.84
1-butyne*	39.48	39.67	37.96	39.63	45.22
2-butyne	34.7 ±0.2	34.54	32.82	34.49	40.08
cyclobutane	6.8 ±0.2	7.07	5.77	6.65	12.37
(E)-2-butene	-2.9 ±0.2	-2.49	-3.80	-2.51	2.81
(Z)-2-butene	-1.9 ±0.1	-1.04	-2.34	-1.05	4.26
Isobutene	-4 ±0.1	-3.87	-5.17	-3.88	1.43
Butane	-30.2 ±0.1	-29.97	-30.85	-30.19	-24.91
Isobutane	-32.1 ±0.1	-31.92	-32.80	-32.14	-26.86
Cyclopentadiene	32.12	32.59	30.13	32.49	39.69
Spiropentane	44.2 ±0.2	44.55	42.50	43.82	51.41
Cyclopentane	-18.7 ±0.2	-17.59	-19.22	-18.12	-10.96
(Z)-2-Pentene	-6.3 ±0.1	-5.78	-7.41	-5.90	0.84
Pentane	-35 ±0.1	-34.96	-36.18	-35.30	-28.58
2,2-dimethylpropane	-40.1±0.1	-39.94	-41.15	-40.27	-33.56
Benzene	19.8 ±0.1	20.33	17.13	20.34	29.00
bismethylenecyclobutene	80.4	81.22	78.01	81.22	89.89
1,3-cyclohexadiene	25.4 ±0.1	26.09	23.30	25.88	34.52
1,4-cyclohexadiene	25.8 ±0.5	26.17	23.38	25.96	34.59
(E)-1,3,5-hexatriene	40	39.77	36.98	39.97	48.20
(Z)-1,3,5-hexatriene	41	41.35	38.56	41.55	49.78
Cyclohexene	-1.03	-0.69	-3.06	-1.11	7.50

(Continued on next page)

(Continuing from previous page)

Toluene	12.1 ±0.1	11.86	8.33	11.76	21.85
	MD	-0.32	1.49	-0.20	-6.65
	MAD	0.63	1.58	0.55	6.65
	MaxAD	2.41	3.77	2.13	9.75

5.1.3 Atomization and Bond Separation Reactions

Those two methods provide accurate results with BSR giving the best ones. Using both methods provides a MAD below 1 kcal.mol^{-1}. The MD of those two methods indicates a slight tendency to overestimate the heats of formation. In both cases, the MaxAD appears for strained compounds, respectively for bicyclobutane and cyclopropene for AR and BSR. Those methods seem to overestimate the heats of formation of small cyclic patterns. This is further discussed in section 5.2. On the whole test set, the data obtained with those two methods are very similar. It is therefore necessary to determine whether the use of BSR really brings an improvement. This has been evaluated through a bilateral Student test. Results indicate that the two methods do provide different values (details are provided in the appendix; see Table A.4).

5.1.4 Empirical corrections

The empirical correction (Δ(HLC)) has been left out of the discussions in section 5.1.1 because of its well defined behavior. In this section, we examine the effect of this correction on the AR heats of formation. Considering the empirical correction for bond conserving reactions is useless, as, in those cases, the correction is completely canceled in the

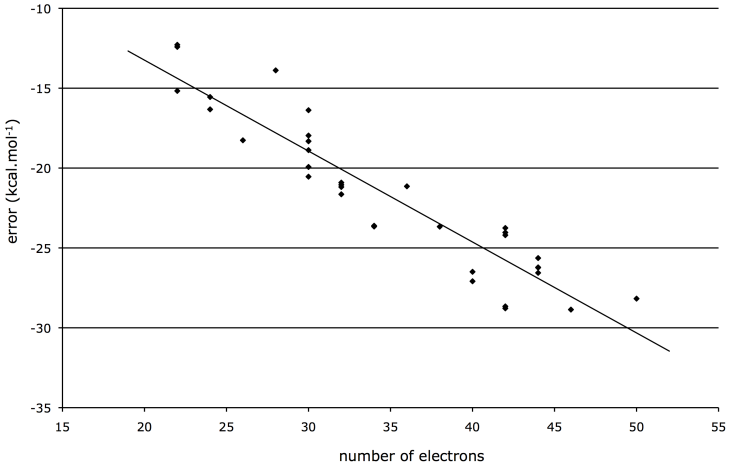

Figure 5.4: Evolution of the error with respect to the number of electrons, using AR and G3B3 energies from which the empirical correction has been removed (R^2=0.86).

calculation of the heat of reaction. The results in Table 5.2 showed that AR and BSR results are very close leading to unexpectedly low improvement from isodesmic reactions. To assess the impact of this empirical correction on the resulting heats of formation, those have been computed using AR and with G3B3 energies from which the empirical corrections has been excluded (details of the results are given in Table A.2 of the appendix of this chapter). Results are quite poor indicating the importance of the empiric correction. The MD and MAD become -21.65 and 21.65 kcal.mol^{-1} respectively. Those two values indicate a systematic overestimation of the data is observed. The error on the compounds can be correlated to the size of the system, in terms of the number electrons (see Figure 5.4).

5.1.5 Isogyric Reactions

Results obtained using HyR are of quite poor quality when the level of theory is taken into consideration. The method clearly underestimates the heats of formation. From a theoretical point of view, the isogyric processes should provide better results than atomization reactions. Observation made on the AR heats of formation indicate that the improvement linked to the use of isogyric reactions is smaller than the one induced by the introduction of the empirical correction. HyR results are however much more accurate than AR results if the empirical correction is excluded, and this is in agreement with expectations.

5.1.6 Combustion reactions

Again, the method provides poor results with a systematic overestimation of the data. The case of combustion reactions is interesting because experimental data exist for the heats of reaction. This allows us to compare, not only the resulting heats of formation, but also to compare the heats of combustion (see Table A.3 in the appendix). Figure 5.5 shows clearly that the error on the heats of formation is already present in the heat of reaction. Those reactions are not isodesmic, the electronic environment are far from being conserved, replacing C-C and C-H bonds by C=O and O-H bonds. Furthermore, those are not even isogyric as the number of paired electrons is not retained due to the triplet oxygen. This might be a cause for such poor results.

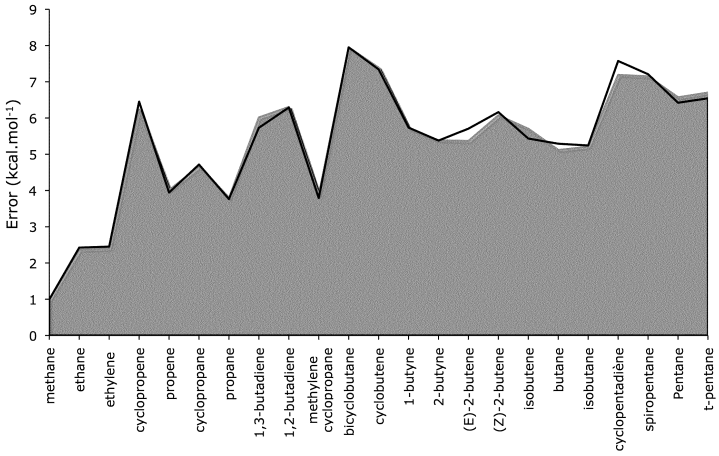

Figure 5.5: Absolute error on the heats of formation (strong black line) and on the heats of reaction (gray surface), in kcal.mol^{-1}.

5.1.7 Effect of reference values

As mentioned earlier, all those methods depend on the values used for the reference heats of formation. Several databases exist and do not systematically provide the same value. In this section, we compare BSR values obtained with different sets of reference values coming from JPCRD [62], Pedleys compilation [63] and the NIST Chemistry Webbook [64] (see Table 5.3). As the NIST database proposes different values for several compounds we choose to use the most recent ones. The values are not compared with experimental data but only to each other through a bilateral Student test. Table A.5 indicates that the results from the use of JPCRD and Pedley reference values do not provide significantly different results, while the use of NIST reference values differs from the two others. The similarity between results obtained with JPCRD and Pedley references probably comes from the compensation of the augmentation of the heat of formation of methane by a variation of the

Table 5.3: Sets of reference values tested (kcal.mol^{-1}). Uncertainties are provided when available.

Molecule	ΔH_f°(JPCRD)	ΔH_f°(Pedley)	ΔH_f°(NIST)
Methane	-17.8 ±0.1	-17.89 ±0.1	-17.89
Ethane	-20.1 ±0.05	-20.24 ±0.1	-20.04 ±0.07
Ethylene	12.5 ±0.2	12.57 ±0.1	12.54
Acetylene	54.5 ±0.25	54.2 ±0.3	54.19 ±0.2

heats of formation of ethane and ethylene. Those variations compensate each other in the determination of reaction heats and therefore lead to results similar to those observed using JPCRD references. This kind of compensation is not observed with the NIST references, chosen as the most recent ones.

5.1.8 Effect of hindered rotations

Hindered rotations are generally considered to have a significant impact on heat capacities and entropies, but not on energies at room temperatures. Their effect on energies is generally accepted as negligible. Indeed, the consideration of the hindered rotation in ethane increases the 298.15 K thermal correction to energy by only 0.052 kcal.mol^{-1} (result obtained using the HinderedRotor keyword in Gaussian03, using the method of Ayala and Schlegel [65]), which is a minor increase. However, in compounds such as cyclopentane, five of those rotors are present on one side of the BSR and none on the other. Considering the hindered rotation in ethane would lower the resulting heat of formation by 0.26 kcal.mol^{-1}, which becomes an important modification. The heats of formation of

the different cyclic system were recalculated using the corrected ethane energy. Results show no improvement in the MD or the MAD. Errors in the small cyclic systems may be due to strain energy which is not conserved in our BSR processes.

5.2 Outliers

The analysis of the test set results indicated several cases for which the error is much greater than the MAD. Those outliers are cyclopropene, cyclobutene, methylenecyclopropane and bicyclo[1,1,0]butane (from now on, simply referred to as bicyclobutane).

5.2.1 Experimental data

The experimental values provided by the different databases can be tracked down to their original measurements. The heat of formation of cyclopropene comes from a combustion calorimetry experiment carried out by Wiberg and coworkers [66]. The heats of formation of the three other outliers also come from combustion calorimetry experiments carried out by Wiberg and Fenoglio [67]. Their work covered a range of cyclic C_4H_6 isomers. Table 5.4 shows the results of Wiberg and Fenoglio's work along with our G3B3/BSR heats of formation. In this table, values for non cyclic systems are from Prosen and coworkers a (see ref. [66] and references therein). All those measurements (both cyclopropene and C_4H_6 isomers) have been carried out using the same procedure and similar calorimeters. The experimental set up was tested on the measurement of the heat of formation of propene, which provided a -491.83 kcal.mol^{-1} heat of combustion leading to a 4.02 kcal.mol^{-1}

Table 5.4: Experimental heats of combustion, and formation for C_4H_6 isomers and G3B3/BSR data (kcal.mol^{-1}).

C_4H_6 Isomer	ΔH°_c	$\Delta H^\circ_{f,exp}$	$\Delta H^\circ_{f,calc}$
1,3-butadiene	-607.16 ±0.18	26.0 ±0.2	26.69
2-butyne	-615.84 ±0.23	34.7 ±0.2	34.49
cyclobutene	-618.60 ±0.36	37.5 ±0.4	39.09
1,2-butadiene	-619.93 ±0.13	38.8 ±0.1	39.75
1-butyne	-620.04 ±0.20	39.5 ±0.2	39.63
methylenecyclopropane	-629.07 ±0.43	48.0 ±0.4	46.04
bicyclobutane	-633.05 ±0.19	59.1 ±0.2	53.69
1-methylcyclopropene	-639.36 ±0.27	58.2 ±0.3	57.55

heat of formation of propene, which is already an underestimation of the data of about 0.8 kcal.mol^{-1}. This comment is valid for both the measures of Wiberg and coworkers, Wiberg and Fenoglio and Prosen and coworkers. We do not wish to mean that old measurements are surely inaccurate, but all those combustion results seem to be the only experimental data for those small cyclic systems. Those were never confirmed by any other experimental measurements and their accuracy has never been tested.

5.2.2 Heat of formation of cyclopropene

Comparison of experimental and theoretical data for the heat of formation of cyclopropene reveals quite important discrepancies. Most commonly used Databases (NIST Chemistry Web-Book , JANAF) provide a 66 ±0.7 kcal.mol^{-1} heat of formation for cyclopropene.

A 66.2 ±0.6 kcal.mol^{-1} heat of formation is also available (Pedleys compilation). All those databases make reference to the work of Wiberg and coworkers, which surprisingly provides a 66.6 ±0.6 kcal.mol^{-1} heat of formation for cyclopropene. This difference is not explained for sure but the value of the heat of formation may be lowered by using more recent data concerning carbon dioxide and water. However, if such procedure is applied on cyclopropene, it should also be applied on the other results of Wiberg and Fenoglio which use the same data. In most cases, it would lead to more important discrepancies between experiment and G3B3 data. It would also lead to a 3.4 kcal.mol^{-1} heat of formation of propene. The heat of formation of cyclopropene has been computed using a wide variety of model chemistries, mainly because it is part of the G2/97 test set [68, 40, 69, 44]. As this compound is one of the most strained monocyclic pattern, it is also included in several studies on ring strain energies [70, 71]. Its computed heat of formation using different high-level model chemistry shows an almost systematic overestimation of about 2 kcal.mol^{-1} when compared to the experimental data (see Table 5.5). Such an error is possible for G2 based model chemistry, as this procedure presents a 1.66 kcal.mol^{-1} MAD on the G2/97 hydrocarbon sub-set (using atomization reactions). This MAD goes down to 1 kcal.mol^{-1} if G3 is used. The issue is not specific to the Gaussian family of model chemistries, several CBS models have also been applied and show similar errors. The range of errors of those CBS methods goes from MADs of 3.59 kcal.mol^{-1} (CBS-4) to 1.08 kcal.mol^{-1} (CBS-QB3). The HL1 and HL2 methods of Miller and Klippenstein [72], which provide a 67.5 kcal.mol^{-1} heat of formation, are claimed to be accurate within a few tenths of a kcal.mol^{-1}. The former is a Gaussian-like approximate of the QCISD(T, full)/6-311++G(3df,2pd) level and the latter an estimate

of the QCISD(T, full) level at the CBS limit. Most of the calculated data lie above the experimental value. Two exceptions appear. First, is the 66.5 kcal.mol^{-1} result from Pan and coworkers [70]. This value is in good agreement with the experimental data. However, in this same work, we note that an underestimation of about 2 kcal.mol^{-1} appears for the two other C_3H_4 isomers. The second exception is the CBS-4 value from Petersson and coworkers [68]. This latter method has a Mean Absolute Deviation (MAD) of 3.59 kcal.mol^{-1} on hydrocarbons with a clear tendency to underestimate (mean deviation from experiment (exp-calc)= 3.14 kcal.mol^{-1}) the heats of formation of the hydrocarbon contained in the test set. When the level of chemistry is quite low, the experimental data falls within the typical error margin of the method. However, when this level of theory is raised, the difference appearing is much greater than the one expected on such a small hydrocarbon.

Results and discussion

The experimental data of Wiberg and coworkers is the only one available and previous discussion has shown reasons to doubt the accuracy of this value. This discussion aims at establishing the value for this heat of formation. In their recent review of bond separation processes, Wheeler and coworkers [58] have indicated that strain could be a source of additional error. Indeed this ring strain is not reproduced in the BSR processes. We therefore choose to use cyclopropane as reference (with a Δ H_f°=12.7 kcal.mol^{-1}) for the determination of the standard heat of formation of cyclopropene.

Table 5.5: Calculated heats of formation of cyclopropene in kcal.mol^{-1}. Experimental value is 66 (JPCRD) or 66.2 (Pedley) or 66.6 (original value) kcal.mol^{-1}.

Reference	Method	$\Delta H^{\circ}_{f,exp}$
Curtiss and coworkers [44]	G2/AR	69.1
	G2MP2/AR	69.7
	G2MP2SVP/AR	67
Notario and coworkers [73]	G2/BSR	67.9
	G2MP2/ BSR	68.1
Curtiss and coworkers [40]	G3/AR	68.4
Miller and Klippenstein [72]	HL1, HL2/HyR	67,5
Pan and coworkers [70]	B3LYP/6-311+G(3df,2dp)/BSR	66.5
Petersson and coworkers [68]	CBS-Q/AR	70.1
	CBS-q/AR	69.6
	CBS-4/AR	65
Petersson and coworkers [69]	CBS-4M/AR	65.4
	CBS-QB3/AR	69.5
	G3(MP2)/AR	67.8
Karton and coworkers [74]	W4.2/AR	67.51

Strain effects The use of cyclopropane aims at conserving the strain in the reference hydrocarbon. This can only be the case if strain in cyclopropane also induces an unexpected error. However we also note that the heat of formation of cyclopropane is not among the outliers as it lies within half a kcal.mol^{-1} of the experimental data. Table 5.2 provides the heats of formation of cyclopropane along with the error on similar compounds: propane (same number of sp^3 carbons) propene (isomer) and butane (same number of bonds). At the BSR level, the error (expt.-calc.) on those heats of formation are -0.42, 0.09, 0.06 and -0.01 kcal.mol^{-1}. It is obvious that the error on cyclopropane is much more important than the others and we may therefore expect an error coming from strain effects, leading to an overestimation of the data. By using cyclopropane as a reference, we can expect the variation in the heat of formation to be an improvement linked to the conservation of strain effects. The heat of formation of cyclopropene obtained by such a process is 67.71 kcal .mol^{-1}. The latter value might still be an overestimate due to remaining strain effects.

Support for the new value If the original value from Wiberg and coworkers is corrected for the error noted on propene, it becomes 67.4 kcal.mol^{-1}, and a better agreement appears between experiment and theory. However, an experimental value, obtained as such is only a small indication. The theoretical value can obtain support from hydrogenation process. We consider the hydrogenation of cyclopropene and 1- and 3-methylcyclopropene (1- and 3-mcp) to the corresponding cyclopropanes. We consider that the heat of hydrogenation should be very similar in cyclopropene and 3-mcp and a lower value is expected for the 1-mcp, from which strain is released through hyperconjugaison.

Table 5.6: Calculated heats of formation and hydrogenation of cyclopropene and substituted cyclopropenes (kcal.mol^{-1}). Standard heat of formation of methylcyclopropane : 5.59 kcal.mol^{-1}.

Compound	$\Delta H^{\circ}_{f,expt.}$	$\Delta H^{\circ}_{f,calc.}$	$\Delta H^{\circ}_{hyd.,expt.}$	$\Delta H^{\circ}_{hyd.,calc.}$
cyclopropene	66 ±0.7	67.71	53.30	55.01
1-mcp	58.2 ±0.3	57.12	52.61	51.53
3-mcp [75]	61.42 ±0.47	60.32	55.92	54.73

Table 5.6 provides the results for the heats of formation and of hydrogenation reactions. It shows that, using experimental heats of formation, the heat of hydrogenation of cyclopropene is closer to that of 1-mcp; the opposite is expected and is provided by the theoretically obtained data. In a recent work, Karton and coworkers have carried out W4.2 calculations on cyclopropene [74]. Using their results and experimental energy corrections provide a heat of formation of 67.51 kcal.mol^{-1}. Energies obtained using Wn families of model chemistry are very accurate. If this value is considered as correct, we may establish that the remaining strain error linked to the inner cycle double bond is of ± 0.2 kcal.mol^{-1}. As a result, the heat of formation of 3-mcp should be lowered by the same value and is believed to be close to 60.12 kcal.mol^{-1}. The value presented in Table 5.6 for 1-mcp is an upper bond and 56.92 kcal.mol^{-1} should be considered as a lower one for this heat of formation.

Conclusions

The heat of formation of cyclopropene has been discussed from both experimental and theoretical points of view. Results indicate that the experimental value is most likely inaccurate and should be replaced by

Table 5.7: Heats of formation (298.15 K) of cyclobutene with different model chemistries (kcal.mol^{-1}).

Reference	Method	$\Delta H^{\circ}_{f,calc.}$
Curtiss and coworkers [44]	G2/AR	40.3
Pan and coworkers [70]	B3LYP/BSR	39.5
Curtiss and coworkers [40]	G3/AR	39.5
Montgomery and coworkers [69]	G3(MP2)/AR	38.8
	CBS-4M/AR	40.2
	CBS-QB3	40.8
Karton and coworkers [76]	W3.2/AR	38.53

a theoretically obtained value. It has also been shown that strain effects are responsible for an overestimation of the data. We consider that the 67.51 kcal.mol^{-1} value of Karton and coworkers should be considered as the reference value for the heat of formation of cyclopropene.

5.2.3 Heat of formation of cyclobutene

As has been observed in the case of cyclopropene, the heat of formation of cyclobutene is also importantly overestimated by our methodologies. Again, the heat of formation of that compound has been computed using a variety of methodologies and again, almost systematic overestimation is noticed (see Table 5.7). The initial idea in this section was to compute the heat of formation of cyclobutene using cyclobutane as reference, as was done with the cyclopropene/cyclopropane couple. An error from strain not being accounted for is expected to be an overestimation; this was confirmed in the previous section. The heat of formation of cyclobu-

tane is underestimated by the BSR method, and only slightly overestimated by the AR method. If strain is responsible for the error on the heat of formation of cyclobutene, it cannot be cancelled by the use of cyclobutane has reference in an isodesmic process. The error using the latter method is not superior to the one that can be expected by looking at the errors on the heats of formation of pentane or butane.

Theoretical support Most model chemistries have shown results about two kcal.mol^{-1} higher than the experimental data. Recently, Karton and coworkers have carried out high level W3.2 calculation on cyclobutene [76]. If their value for the 0 K data is used together with experimental energy corrections, the resulting data is 38.53 kcal.mol^{-1}. This value is 0.56 kcal.mol^{-1} of our data, which is an acceptable error of G3B3 data. Furthermore, it is 1.02 kcal.mol^{-1} over the value of Wiberg and Fenoglio, which is also in agreement with the underestimation observed on propene (0.8 kcal.mol^{-1}) and on cyclopropene (0.91 kcal.mol^{-1}).

The case of cyclobutadiene In our study of the heat of formation of cyclopropene, we could not find a high level theoretical method which could support the experimental data. The case of cyclobutene is different on that point. In their experimental determination of the heat of formation of cyclobutadiene, Fattahi and coworkers [77] have used the experimental heat of formation of cyclobutene. The resulting heat of formation of cyclobutadiene (102.33 kcal.mol^{-1}) is in excellent agreement with W1/AR heat of formation (102.06 kcal.mol^{-1}) obtained in that same work. The value obtained in their work is however provided with a large 4 kcal.mol^{-1} error margin which could hide the error on the heat of formation of cyclobutene.

Conclusion

Several results concerning the heat of formation of cyclobutene have been presented. Despite indications that the experimental data of Wiberg and Fenioglio is probably underestimated, all high level results could not be reconciled. Contrarily to the case of cyclopropene, the origin of the important deviation on this system could not be clearly identified. Despite contradictory results from the experimental work on the determination of the heat of formation of cyclobutadiene, we consider that the W3.2 value of Karton and coworkers should be retained as a new reference heat of formation of cyclobutene with an uncertainty of 0.4 kcal.mol^{-1}.

5.2.4 Heat of formation of methylenecyclopropane

We now focus on methylenecyclopropane. This compound is the only one for which the important deviation from experiment is an underestimation. This compound therefore presents an error which is larger than expected and in the "wrong direction", as we observed a tendency to overestimate data using both AR and BSR. This system also shows another type of strain. One part is linked to forcing a ± 60 degree angle on the sp^2 carbon rather than the typical ± 120 degrees. This time the additional strain added to the cyclopropane pattern comes from an external double bond and cannot be expected to have the same effect as an inner cycle double bond such as presented in cyclopropene. It is quite an issue, as the simplest reference presenting similar strain is methylene cyclopropane itself, which makes it difficult to determine a process conserving such a strain. There are data for methylmethylenecyclopropene and ethylydenecyclopropane from the work of Turner and Goebel [78].

Those values rely on several approximations which make them unusable as references. If we consider increasing isodesmicity, the value for the heat of formation of this system decreases, which increases the difference between theory and experiment. However, none of those isodesmic reactions conserve the strained sp^2 site of methylene cyclopropane. As there are no reliable experimental data, apart from the heat of formation of methylcyclopropane, on methylenecyclopropane or any of its analog it is impossible to determine an isodesmic reaction conserving the problematic pattern and to definitely establish the heat of formation of this compound. In this case, solution would come from a more accurate solution of the Schrödinger equation.

5.2.5 Heat of formation of bicyclobutane

This is the last of the four outliers considered. Again, there is very little experimental data on this system or any of its analog. The heat of formation obtained with AR is the highest deviation for that method and the deviation is under two kcal.mol^{-1} for BSR. Under the hypothesis that the strain in bicyclobutane is responsible for the deviation. We have used cyclopropane as a reference compound for the isodesmic process. The heat of formation obtained is 52.84 kcal.mol^{-1}, which is less than 1 kcal.mol^{-1} over the experimental one. We have shown that strain was responsible for overestimation of the heat of formation of cyclopropane pattern and therefore, this lowering is considered as an improvement. The obtained value is 0.94 kcal.mol^{-1} over the one of Wiberg and Fenoglio which is in good agreement with what is observed for cyclopropene, cyclobutene and propene.

5.2.6 Conclusions

Several compounds in the closed-shell test set showed deviations too important to remain unnoticed and uncommented. The four problematic compounds were discussed. Only for cyclopropene were we able to establish a new heat of formation. The three other cases remain uncertain. The W3.2 value for the heat of formation of cyclobutene is considered as the most accurate available at this time. Concerning the two other outliers, there are too few data on those systems to establish clearly new reference values.

5.3 Benzene isomers

There is a very important number of stable (minima) structures for C_6H_6 isomers [79]. During this work, several of those isomers were encountered in benzene formation mechanisms. Their heats of formation were computed. The first isomer to be investigated is fulvene [80]. This compound is one of the most frequently appearing isomers in benzene formation mechanisms. The next series of isomers to be treated are fused bicyclic compounds. Several of those are also present in benzene formation mechanisms in closed-shell or open-shell forms, the others have been introduce for comparison purposes. As the strain in small cyclic patterns has been shown to be an issue, a Ring Conserving Isodesmic Reaction scheme is developped and used on those systems.

5.3.1 Heat of formation of fulvene

Fulvene, or, 5-methylene-1,3-cyclopentadiene, is one of the many isomers of benzene. Fulvene and its derivatives have already been the subject of a number of studies because of their non alternant structure and their aromatic/antiaromatic character [81, 82, 83]. It is also a major intermediate in benzene formation mechanism in flames [24, 23, 27, 84]. Experimental values published for the heat of formation of fulvene are 53.5 [62] and 53.6 [85, 64] kcal.mol^{-1}. Calculated heats of formation for that particular compound vary greatly, from 48.8 [24] to 56.6 [86] kcal.mol^{-1}. On one hand, nowadays model chemistry provides fairly accurate results. On the other hand, measuring the heat of formation for such a transient molecular species is certainly not an easy task and experimental uncertainty might be important. One should wonder why such a discrepancy appears and what value should be recommended. To try answering such a question, a careful analysis of the published data must be performed. The main objective of this section will be to recommend a reliable heat of formation for fulvene after performing this analysis and carrying out high-level model chemistry, in order to determine an accurate heat of formation.

Methods

In addition to the G3B3 method, a second method is used. The latter is the CBS APNO model of Petersson [46]. This method is more computationally demanding but is expected to provide results with a 0.5 kcal.mol^{-1} accuracy [47, 87]. Those two models have been extensively described in an earlier section.

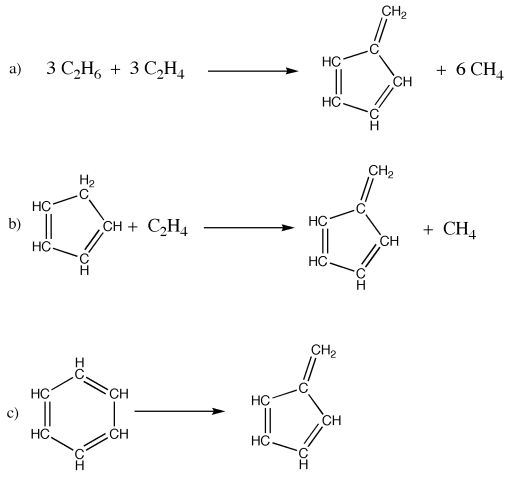

Figure 5.6: Reference isodesmic reactions.

Heat of formation

As the preceding methods provide only a total energy, the latter must be converted into a heat of formation, which can be obtained by using different processes. The first one is the vastly used atomization scheme [88, 89]. As it was shown that in many cases, the use of isodesmic reactions [56] could significantly improve results [90, 91], we also considered such isodesmic processes. Three such reactions are retained in this work. The first reaction is the classical bond separation reaction (Figure 5.6.a). In the second one, more structural similarities are introduced by using cyclopentadiene as a reference (Figure 5.6.b.). Finally, the direct isomerization reaction of benzene to fulvene is used (Figure 5.6.c). With this reaction implying two structurally similar compounds, we hope that the largest part of the error will cancel out. Reference values are taken from Pedleys compilation [63] and give for CH_4, C_2H_6, C_2H_4, C_6H_6, and C_5H_6 respectively -17.89, -20.24, 12.57, 19.80 and 32.12 kcal.mol^{-1}.

Table 5.8: Theoretical heats of formation of fulvene at 298.15 K (kcal.mol^{-1}).

Source	Method	ΔH_f°
Melius Database	1987 BAC-MP4	56.3
Mebel and coworkers	G2(rcc, MP2)	48.8
Miller and Melius	BAC-MP4	52.22
Miller and Klippenstein	HL1	51.44
	HL2	51.34
Bouchoux and coworkers	G2(MP2)	50.91
da Silva and Bozzelli	CBS-QB3	55.3

The latter value is retained as most sources tend to agree on a heat of formation of 32 kcal.mol^{-1} [64, 63, 92].

Results and discussion

Looking at literature, several other theoretically obtained heats of formation can be found for fulvene. These are presented in Table 5.8. The highest value [86] comes from the C. F. Melius database and was obtained using the 1987 BAC-MP4 method, which is nowadays known to give results of relatively poor quality [93]. The lowest value was obtained by Mebel et al. [24] by using a G2-like method. This method has a MAD of 1.28 kcal.mol^{-1} on the atomization energies of the 32 first row G2 test set compounds. This value was obtained using benzene as reference in the isomerization reaction (reaction r.3.). The BAC-MP4 value is printed with an error of 1.74 kcal.mol^{-1} in the Sandia Thermochemical Database [94]. This is the only value that includes the experimental heat of formation in its margin of error. The HL1 and HL2 values of Miller

and Klippenstein [23] are very similar. Those two methods are claimed to be highly accurate, rarely differing by more than 1 kcal.mol^{-1} with a typical deviation of a few tenths of a kcal.mol^{-1}. We have to mention that only the 0 K value are given in the reference (HL1(0 K)=54.7 kcal.mol^{-1}, HL2(0 K)=54.6 kcal.mol^{-1}) and that the 298.15K data was obtained using our calculated enthalpy thermal corrections. The value from Bouchoux and coworkers [95] comes from a G2(MP2) calculation. Such calculations give results with a MAD of 2 kcal.mol^{-1}. Very recently [96] da Silva and Bozzelli published a CBS-QB3 value of 55.3 kcal.mol^{-1} obtained by the atomization scheme. The expected error at this level of theory is known to be around 1 kcal.mol^{-1}. Such deviations from experiment could be the results of the several theoretical approximations (harmonic, incomplete basis sets, electron correlation). It could also come from experimental measurements, considering that the heat of formation is calculated from a hydrogenation reaction and that fulvene is a highly unstable compound [97]. Of all theoretically obtained results, only two propose values for the heat of formation higher than the experimental ones. Among those values (56.3 kcal.mol^{-1}) one comes from a method of low precision and should be rejected. Apart from the CBS-QB3 value, whenever high-level theoretical chemistry is used, the results are lower than the experimental values, and only one includes the experimental value in its typical error range. Our computed atomization results are shown in Table 5.9, for fulvene as well as for the reference compounds. Quite surprisingly, the CBS method does poorly in predicting heats of formation compared to the high accuracy of G3B3 results. As example, the difference between G3B3 and experiment on benzene is 0.54 kcal.mol^{-1} while for CBS it goes up to 2.35 kcal.mol^{-1}, the largest observed difference. The other reference compounds show

Table 5.9: Standard heats of formation computed from the atomization scheme (kcal.mol^{-1}).

Molecule	Expt.	G3B3	CBS-APNO
methane	-17.89 ±0.1	-17.89	-18.90
ethane	-20.24 ±0.1	-20.08	-21.82
ethylene	12.57 ±0.1	12.31	12.14
cyclopentadiene	32.12 ±0.35	32.60	31.06
benzene	19.80 ±0.17	20.34	17.45
fulvene	53.50	51.72	50.66

slightly lower discrepancies. A further analysis of the numbers in Table 5.9 shows that CBS correlates very well to the G3B3 results (equation 5.5) but gives a systematic error of 1.40 kcal.mol^{-1}.

$$\Delta H_f^0(G3B3) = 0.99_9 \Delta H_f^0(CBS) - 1.40_7 \qquad R^2 = 0.999 \qquad (5.5)$$

A similar behavior is found when experimental values are fitted to CBS results.

$$\Delta H_f^0(Exp) = 1.01_5 \Delta H_f^0(CBS) - 1.36_7 \qquad R^2 = 0.999 \qquad (5.6)$$

Finally for fulvene, this analysis suggests that the obtained CBS atomization result is too low and should be corrected for the systematic error. This correction leads to a heat of formation of 52.02 kcal.mol^{-1}. Nevertheless, after this analysis, both G3B3 and CBS are lower than the experiment. Looking further at our selected isodesmic processes, this first proposal could be refined. Table 5.10 reports the reaction energies of the isodesmic processes completed by the heats of formation computed from the latter. Concerning the isodesmicity, the best G3B3

Table 5.10: Heats of isodesmic reactions and resulting standard heats of formation of fulvene (kcal.mol^{-1}).

G3B3	ΔH°_{rxn}	ΔH°_{f}
r.1.	-32.29	52.04
r.2.	-11.08	51.50
r.3.	31.37	51.17
CBS-APNO		
r.1.	-33.72	50.61
r.2.	-11.44	51.13
r.3.	33.21	53.01

result should come from r.3, but, the poor quality of CBS atomization result for benzene leads us to believe this reaction should not be retained and that the best isodesmic result using CBS-APNO method should rather come from reaction r.2. This is confirmed by the similarities between the heats of isodesmic reaction r.2. using both methods. As shown by Table 5.10 those results are close to each other, being respectively equal to 51.50 for r.2. and 51.17 kcal.mol^{-1} for r.3. at G3B3 level, and 51.13 kcal.mol^{-1} at CBS level for r.2.. These latter values are about 0.6 kcal.mol^{-1} under the G3B3 atomization value, which is consistent with our expectations. Whatever the method being used, the best theoretical results remain below the experimental heat of formation of 53.5 kcal.mol^{-1}. As measuring the heat of formation for transient species leads to an experimental uncertainty we recommend retaining theoretically obtained results. As there seems to be a systematic lowering of the value with respect to the increasing structural similarities, and because of the use of the isomerization reaction (r.3.) with accurate G3B3

data, we would retain 51.17 kcal.mol^{-1} as a new value for the heat of formation of fulvene. As all methods give slightly different numbers, the precision of our proposed value may be computed from the root mean square deduced from these data, which gives ± 0.37 kcal.mol^{-1}. Figure 5.7 shows that this value is within the typical error margin of most calculated heats of formation.

Conclusion

In this section, we carried out two high-level model chemistry computations, G3B3 and CBS-APNO, in order to determine the heat of formation of fulvene. We used those energies to calculate the values using an atomization scheme and different isodesmic reactions. Analysis of the results shows that, while G3B3 provides accurate data, the CBS-APNO method does poorly in predicting , as a systematic error is present. Even though the quest of full precision is still open, nowadays most reliable computations tend to a value close to 51.17 ± 0.37 kcal.mol^{-1}, which we will recommend. This value is obtained using G3B3 energies and benzene as reference. The r.m.s. value is deduced from the distribution of our various results and places experiment about 2 kcal.mol^{-1} above this value.

5.3.2 Strained, fused bicyclic isomers

in this section, we determine the heats of formation of highly strained bicyclic benzene isomers. Both bicyclo[2, 2, 0]hexadiene and bicyclo[3, 1, 0]hexadiene are considered. The latter systems are the closed-shell equivalent of several open-shell intermediates in the reactions forming a

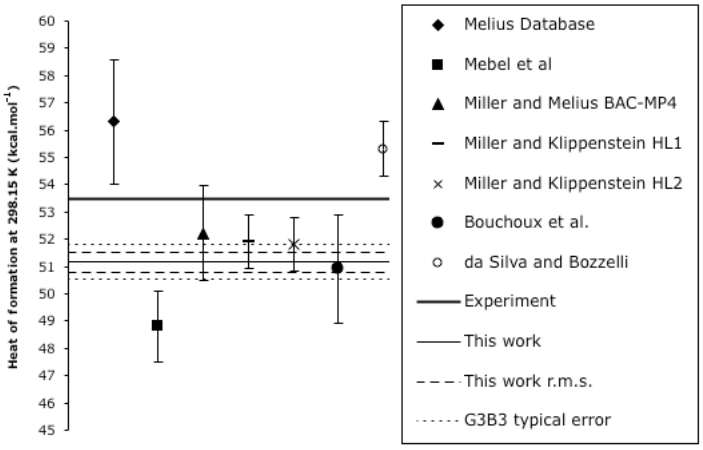

Figure 5.7: Comparison of the different theoretical results. Experimental value is 53.5 kcal.mol^{-1}. Value for this work is 51.17 kcal.mol^{-1}. The G3B3 typical error used is 0.62 kcal.mol^{-1}.

first aromatic ring in hydrocarbon flames. We therefore use a set of cyclic references to assess the performances of Ring Conserving Isodesmic Reactions (RCIR). A similar type of reaction, conserving the benzene pattern have already been used by Sivaramankrishnan and coworkers to account for aromaticity in PAH [98]. We have seen in a previous section that the heats of formation of small cyclic compounds are an issue. The first subsection of this part of the work is therefore devoted to the determination of the cyclic set of reference. The use of such references not only accounts for the ring strain, but also removes the hindered rotation issue presented in section 5.1.8.

RCIR references

The reference set for RCIR is the BSR reference set augmented by 3, 4 and 5-membered cycle references. In the cases of three-membered cy-

cles, two patterns are considered, cyclopropane and cyclopropene. The reference chosen are therefore cyclopropane and cyclopropene with the experimental data for the first and the heat of formation established from Karton and coworker's value in section 5.2.2. References for four membered rings are cyclobutane, cyclobutene and cyclobutadiene. The heat of formation used for cyclobutane and cyclobutadiene are the experimental ones while the value used for cyclobutene is again the Wn value of Karton and coworkers. References for five membered rings are also quite uncertain. The heat of formation of cyclopentadiene is between 31 and 33.4 kcal.mol^{-1} depending on the source. The heat of formation of cyclopentene is between 8.1 and 8.6 , again depending on the source, and finally, the heat of formation of cyclopentane also varies between -18.26 and -18.6 kcal.mol^{-1}. As we have already used the Pedley value for cyclopentadiene in the determination of the heat of formation of fulvene with success, we decide to keep the values from Pedley's compilation for the other five-carbons ring references. All those references account for individual cycle strain. The fusion of the two cycles obviously generate effects that will not be accounted for by those isodesmic processes. As a matter of facts, the reference to be used to describe the strain linked to the fusion of two rings are the system under investigation in the present section. Table 5.11 lists the chosen experimental data for the RCIR test set.

Results

Heats of formation The BSR and RCIR heats of formation of bicyclic compounds are presented in Table 5.12 along with the uncertainty resulting from the combination of the uncertainties on the refer-

Table 5.11: BSR and RCIR reference heats of formation (kcal.mol^{-1}).

Compound	ΔH_f°	uncert.
methane	-17.8	±0.1
ethane	-20.1	±0.05
ethylene	12.5	±0.2
cyclopropane	12.7	±0.2
cyclopropene	67.51	±0.4
cyclobutane	6.8	±0.2
cyclobutene	38.53	±0.4
cyclobutadiene	102.33	±4
cylopentane	-18.26	±0.2
cyclopentene	8.1	±0.33
cyclopentadiene	32.1	±0.36

ence compounds. Reactions used to obtain the RCIR data are given in the appendix of this chapter (see Table A.7). There is only one BSR to be applied to C_6H_6 systems (**1-9**), whatever its structure. This is also the case for the hydrogenation products. A more important number of RCIRs must be used. Those reactions are provided in the appendix (See Table A.7). A student test indicates that the two series of values are significantly different with a tendency of RCIR values to be lower than the BSR ones. The calculated uncertainties on the RCIR values are larger than the ones on BSR data. Not much comparison can be made with other results as there is very few data on those systems. For system **4**, comparison is possible with other theoretical values. There is one estimated value in JPCRD of 87 kcal.mol^{-1}, which is obviously an underestimation. Theoretical works on this system have also been carried

Table 5.12: RCIR and BSR obtained ΔH_f° (kcal.mol^{-1}). Structures of the different compounds are given in Figure 5.9.

Compound	ΔH_{rxn}° (BSR)	ΔH_f° (BSR)	ΔH_{rxn}° (RCIR)	ΔH_f°(RCIR)
1	95.73	162.63	32.69	161.92
2	65.18	132.08	49.99	131.29
3	56.12	123.02	40.93	122.23
4	29.88	96.78	14.69	95.99
5	26.80	93.70	27.99	92.89
6	39.95	106.85	10.02	107.03
7	42.59	109.49	12.66	109.67
8	57.31	124.21	27.37	124.38
9	49.39	116.29	50.58	115.48
10	48.79	83.29	25.35	82.85
11	27.80	62.30	4.36	61.86
12	2.59	37.09	-4.93	35.97
13	39.85	74.35	32.33	73.23
14	43.08	77.58	7.26	77.91
15	-25.45	25.95	-	-
16	-25.52	25.88	-	-
17	28.96	30.66	-2.73	30.97
18	6.57	8.27	-6.83	7.71
19	-19.92	-1.12	-	-
20	-15.79	-29.59	-	-

out and provide data between 94 and 97 kcal.mol^{-1}. Those however, do not consider the conservation of cyclic patterns. The use of RCIR provides a better conservation of errors. The G3B3 procedure (as well as other similar model chemistries) offers the possibility to quantify this conservation. An estimation of the utility of a given correction may be obtained by considering the reaction energy correction. A small absolute value indicates for a given reaction energy correction that the need of correcting for the corresponding effects in the considered isodesmic process is also small because the process already cancels the effects in the calculation of the reaction energy correction. Figure 5.8 shows the average absolute reaction energy correction for the BSR and RCIR processes. This figure clearly indicates the better conservation of errors in the RCIR processes, mainly through the conservation of the Δ(2df,p) correction. The latter correction accounts for the polarization functions by giving more flexibility to the basis set. This flexibility is obviously a very important element in the description of highly strained systems. Table A.8 details the various absolute energy corrections.

Hydrogenation energies The hydrogenation of double and bridging bonds are considered; the latter category leading to a six-carbon monocyclic system (see Figure 5.9).

Discussions

Cyclo[2,2,0]hexadienes We start with the hydrogenation of the bicyclo[2,2,0]hexane systems. The **11** $\rightarrow$ **17** reaction shows an exothermicity similar to that of the cyclobutene$\rightarrow$cyclobutane hydrogenation reaction (-29.73 kcal.mol^{-1}). This is probably mainly because the un-

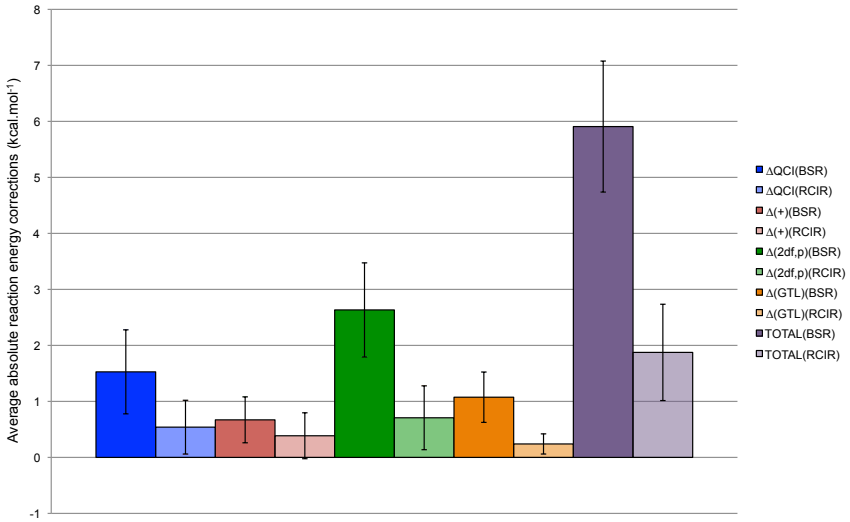

Figure 5.8: Comparison of reaction energy correction in BSR and RCIR. (kcal.mol^{-1}). Dark colors: BSR; light colors: RCIR.

saturation does no causes structural changes much different from the one observed in the monocyclic case. A similar comment can be made on the heat of ring opening hydrogenation, which is only 1.27 kcal.mol^{-1} superior to the saturated case. The hydrogenation of **10** to **17** is much more exothermal. We observe a 19.01 kcal.mol^{-1} raise in the double bond hydrogenation energy and of 22.25 in the ring opening heat. The formation of the double bond is, in this case, accompanied by strong structural changes (see Figure 5.10). First, we consider system **4**, which is the most stable and probably the less strained. The formation of the second double bond decreases by 5.23 kcal.mol^{-1} the heat of double bond hydrogenation. This is more than what can be expected from the formation of a non-conjugative second double bond. The heat of the ring opening reaction is raised by 7.89 kcal.mol^{-1}. System **3** has two non-equivalent double bonds. The hydrogenation of those may be compared to hydrogenation reaction **10** $\rightarrow$ **17** and **11** $\rightarrow$ **17**. The heat hydrogena-

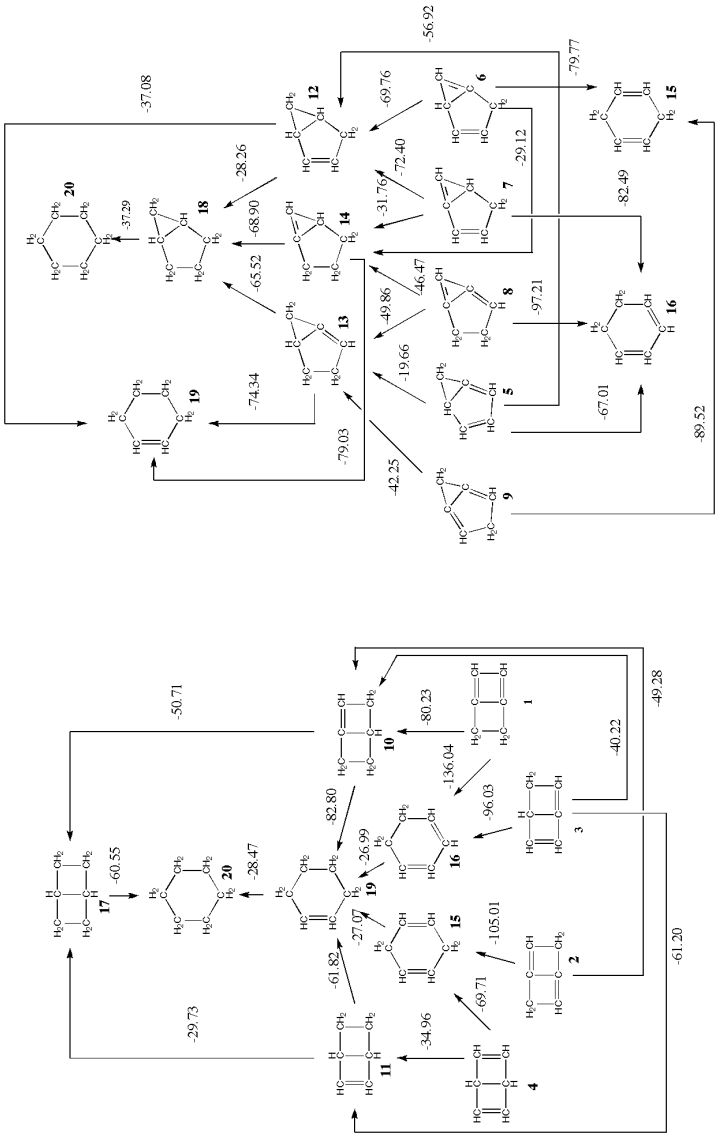

Figure 5.9: Heats of hydrogenation of bicyclo[2,2,0]hexadienes and bicyclo[3,1,0]hexadienes. For monocyclic systems, BSR values are used (kcal.mol^{-1}).

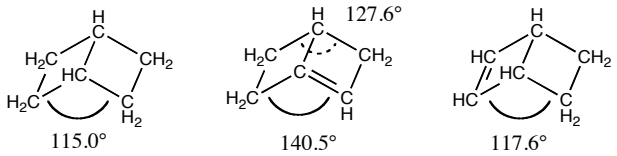

17 **10** **11**

Figure 5.10: Key structural parameters for systems **17**, **10** and **11**.

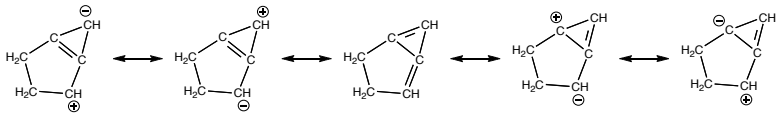

Figure 5.11: Resonance limit forms for system **8**.

tion of the HC=CH bond is about 10 kcal.mol^{-1} inferior (more exothermic) to the one observed in **11** $\rightarrow$ **17** and about 5 kcal.mol^{-1} inferior of the **4** $\rightarrow$ **11** reaction heat, indicating that the difference in position of the second double bond is responsible for a 5 kcal.mol^{-1} destabilization. The heat of hydrogenation of the second double (**3** $\rightarrow$ **11**) bond is 10 kcal.mol^{-1} inferior to that of **10** $\rightarrow$ **17**, and 20 kcal.mol^{-1} inferior to **3** $\rightarrow$ **10**. This difference is only due to the important structural changes, that were already observed to be responsible for a 20 kcal.mol^{-1} destabilization. As represented on Figure 5.9, system **3** could benefit form conjugative stabilization, however, it is not the case as the compound has a structure quite similar to system **10**, and is therefore not planar. The ring opening hydrogenation is more exothermic than for **10** by 13.17 kcal.mol^{-1} and superior to that of **11** by 34.21 kcal.mol^{-1}. The structure of system **2** is planar, therefore, in this case, conjugation is possible. However, the two successive hydrogenation energies are nearly equal, while conjugative effects would lead to a first hydrogenation reaction less exothermic than the second. This is because the conjugative

stabilization is compensated by the further structural changes leading to the planar structure. This compensation of stabilization/destabilization effects also leads to a heat of ring opening of 22.21 kcal.mol^{-1}, which is nearly equal to that of **10**. The last bicyclo[2,2,0]hexadiene (**1**), presents the cyclobutadiene pattern. It is a planar systems and presents an increase of about 30 kcal.mol^{-1} of the exothermicity of the hydrogenation reactions, both the double bond hydrogenation and the ring opening one, when compared to the other planar system (**2**). Compound **1** also presents a conjugative stabilization effect. This difference may be caused by anti aromaticity in the cyclobutadiene pattern. Indeed, the destabilization due to anti isodesmicity has been reported to be around 30-40 kcal.mol^{-1}. Therefore, one could consider that turning **10** into a planar system by the introduction of a second double bond destabilizes the system by an overall 10 kcal.mol^{-1}.

Cyclo[3,1,0]hexadienes We start with the bicyclo[3,1,0]hexane, to evaluate the effect of the introduction of a single double bond. As was observed in the previous section, the heat of hydrogenation of the double bond only importantly varies if this bond involves a bridgehead carbon. In **12**, hydrogenation energy (-28.26 kcal.mol^{-1}) of the double bond is quite close to the hydrogenation energy of cyclopentene to cyclopentane (-26.36 kcal.mol^{-1}). The hydrogenation energy of the ring opening reaction (-37.08 kcal.mol^{-1}) is very close to that of the opening of system **18** to cyclohexane and that of the cyclopopane to propane. Including a bridgehead carbon in the double bond (case of **13** and **14**) increases the exothermicity of the reaction by 35-40 kcal.mol^{-1}, which is almost twice the destabilization observed in **10** in the previous section. Also, it doubles the heat of the ring opening reaction. Again, this is more im-

portant than the increase noted for system **10** in the previous section. Turning to C_6H_6 compounds, we start with system **5**. This system has two double bonds in its five-carbon cycle. The whole system is non planar, but the cyclopentadienyl pattern is, therefore allowing conjugation. The heats of hydrogenation of those bonds are 8.6 kcal.mol^{-1} greater (less exothermic) than their equivalent in **12** or **13**. This is most likely due to the conjugative stabilization. A quite surprising feature is the particularly low energy for reaction **5** $\rightarrow$ **13**. As mentioned, conjugation justifies the difference with reaction **12** $\rightarrow$ **18**, the heat of the former is however 5 kcal.mol^{-1} less exothermic than the heat of hydrogenation of cyclopentadiene, which also shows conjugative stabilization. This is most likely due to destabilization in **13** rather than stabilization in **5**. The heat of ring opening is also lowered but only by 7.33 kcal.mol^{-1}. This is however quite unexpected, as conjugation effect should at least partially be conserved. Compounds **6** and **7** are quite similar. Those two are non planar, preventing conjugation in system **7**. The reactions of hydrogenation of their double bonds are slightly more exothermic than those observed in their bicyclo[3,1,0]hexane counterparts. The two systems differ by the product of the ring opening hydrogenation reactions. The relative agreement with the bicyclohexenes is also observed in their ring opening heat of reaction. System **9** is a planar system, while **5** was non planar. This planar structure may offer complementary stabilization through hyperconjugation. The difference in hydrogenation energies with reaction **13** $\rightarrow$ **18** may therefore be caused by the destabilization linked to the planarization of the structure, to which is added the conjugation in the cyclopentadiene pattern and the addition hyperconjugative stabilization. The sum of all the effects leads to a globally lower heat of double bond hydrogenation. Compound **8** is planar, therefore

presents conjugation effects. In facts, this is the compound presenting the greatest number of resonance limit forms (see Figure 5.11). This conjugative is responsible (at least partially) for the important lowering (19 kcal.mol^{-1}) of the double bond hydrogenation reaction energies observed in the bicyclohexene systems. The heat of ring opening hydrogenation remains quite important. However, as a general observation, the ring opening reaction of the bicyclo[3,1,0]hexadiene are less exothermic than the bicylo[2,2,0]hexadienes.

Conclusion

We have computed the heats of formation of various highly strained C_6H_6 bicyclic isomers. A Ring Conserving Isodesmic Reaction scheme was tested and the results provided were shown to be significantly different from bond separation reaction results. The RCIR heats of formation are lower than the BSR one, and this is in agreement with the observations made in the study of the heat of formation of cyclopropene and cyclobutene.

5.4 Other six-carbon species

The determination of the heats of formation of open-shell systems in chapter to come will require two additional heats of formation for C_6H_6 isomers. The first is the one of bismethylene cyclobutene and the second is the one of 3-acetylcyclobutene. RCIR are used to establish those values.

5.4.1 Heat of formation of bismethylenecyclobutene

The experimental heat of formation of bismethylene cyclobutene is given as 80.4 kcal.mol^{-1} in JPCRD [62]. The value obtained through BSR reaction is 81.22 kcal.mol^{-1}. It is already in reasonable agreement with experimental measurements. We have previously observed that experimental measurements on such systems are not systematically very accurate. Ring conserving isodesmic reactions may be used to evaluate a more accurate value. If the two following processes presented on Figure 5.12 are used, the data obtained is 80.66 and 80.24 kcal.mol^{-1}. Those two values average at 80.45 kcal.mol^{-1} which is very close to the experimental data. We also have to note that the HL1 value of Miller and Klippenstein [23](method which was already accurate on fulvene) on this system, once corrected to 298.15 K is around 80.2 kcal.mol^{-1}. In this case, we suggest that experimental value should be retained for this system.

5.4.2 Heat of formation of 3-acetylcyclobutene

Contrary to the preceding case, there does not seem to exist experimental measurements for this system. The use of RCIR on bismethylenecyclobutene provided accurate values and those reactions are therefore applied to this system also. The reactions used are reactions 3 and 4 of Figure 5.12. The BSR heat of formation is 92.36 kcal.mol^{-1}. The use of the two RCIR processes provide lower data, which are 91.80 and 92.26 kcal.mol^{-1}. The second RCIR provides better conservation of electronic environment but relies on less accurate data.

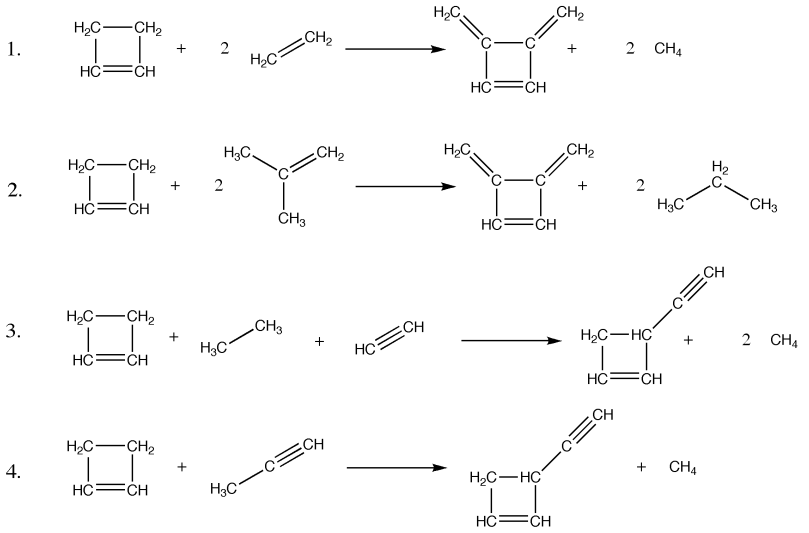

Figure 5.12: RCIR used for the determination of the heats of formation of methylenecyclobutene and 3-acetylcyclobutene.

To account for this, the average of the two values is taken as the heat of formation of this system.

5.4.3 C_6H_8 isomers

Another series of isomers is the methylene cyclopentene and methyl cyclopentadiene systems. Those systems are also potential intermediates in ring formation. For instance, methylcyclopentadiene isomers are the direct product of the addition of the methyl radical on the cyclopentadienyl one [99]. The heats of formation of the various isomers are given in Table 5.13 along with the isodesmic processes used. The notations used are as follows (1): 3-methylene-cyclopentene; (2): 4-methylene-cyclopentene; (3): 5-methyl-cyclopenta-1,3-diene; (4) :1-methyl-cyclopenta-1,3-diene; (5): 2-methyl-cyclopenta-1,3-diene. Heats of formation for (1), (4) and (5) are provided in JPCRD but are estimated values and cannot be

Table 5.13: Heats of formation of the C_6H_8 isomers and the used isodesmic processes (kcal.mol^{-1}).

C_6H_8	ΔH_f°	isodesmic process
(1)	26.13	fulvene+cyclopentene→(1)+cyclopentadiene
(2)	29.89	cyclopentene+ethylene →(2) + methane
(3)	26.24	cyclopentadiene+ethane→(3)+methane
(4)	23.44	cyclopentadiene+propene→(4)+ethylene
(5)	23.08	cyclopentadiene+propene→(5)+ethylene

used as references. The NIST chemistry Webbook lists reference values for (1). The value is 27.6 kcal.mol^{-1}, which is more than 2 kcal.mol^{-1} superior to our value.This experimental data comes from the work of Roth[85], which already showed similar overestimation of the heat of formation of fulvene. Our values for (3) (4) and (5) are globally lower than the CBS-QB3/AR values of Sharma and Green [99], which are respectively (27.1, 23.9 and 24.2 kcal.mol^{-1}. The CBS-QB3 values are obtained through AR. As is shown in section 5.3.2, the conservation of the ring causes a lowering of the heats of formation. This is again observed here.

5.5 Isodesmicity index

Wheeler and coworkers have provided a classification of bond separation processes. This hierarchy is described in section 3.2 of this work. There are some limitations to such a classification:

- It only applies to the bond separation category of isodesmic processes. This ignores pattern conserving processes, such as RCIR used in this work and isomerization processes.
- It does not account for the size of the system studied. For instance isodesmic reactions (as defined by Hehre and coworkers [56]) represent the same level of isodesmicity for propene or hexatriene. It is however clear that electronic environment is better conserved in the former.

This section is an assessment of an isodesmicity index, which is reaction specific. Its application field is therefore larger and it also accounts for the size of the system.

5.5.1 The index

The G3B3 procedure includes several energy corrections. The magnitude of those energy corrections is related to the electronic environment. One may consider that, if electronic environments are similar on both side of the reaction, the energy corrections should cancel in the reaction energy calculation. We define the isodesmicity index ($i.i$) as the sum of absolute reaction energy corrections.

$$i.i. = \sum_{i}^{\Delta E} | \sum_{p}^{prod.} \Delta E_{i,p} - \sum_{r}^{react.} \Delta E_{i,r} | \tag{5.7}$$

Defined as such, the index should show the following behavior:

- Within a given level of bond separation reaction (such as defined by Wheeler and coworkers), the value of the isodesmicity index should increase with the size of the system (keeping its complexity to a similar level).

- Within a given level of isodesmicity, the isodesmicity index should increase with the complexity of the system (keeping its size to a similar level).
- The isodesmicity index should be maximum for atomization reaction and tend to zero as isodesmicity is raised.

This isodesmicity index is tested on a series of compounds for which several different isodesmic reactions could be found.

5.5.2 Results and discussion

Size and complexity

In order to verify the expected behavior of the *i.i.* Values are computed at BSR level (see Table 5.14) for all the compounds in the hydrocarbon test set to which has been added: bicyclobutadiene, cyclopentene and cyclohexane. For alkanes, one can observe the followings:

- In linear alkanes, the *i.i.* increases with the size of the system.
- For a given number of carbon, branching causes an increase of the index.
- For a given number of carbon, cyclization causes an increase of the index.

If alkenes are considered, similar observations can be made:

- Keeping the number of unsaturation constant, increasing the size of the system increases the value of the index.
- If the configuration of a double bond is switched from (E) to (Z), the index increases.

- Closing a cycle increases the index.
- Turning a double bond into a triple bond increases the index.

Exceptions

- The index for propene is smaller than the one for propane despite the higher complexity of propene. However, propene is also smaller. In this case, there might be a conflict between size and complexity.
- Going from cyclopentane to cyclohexane induces a decrease of the index. In this case, the increase in size may be compensated by the decrease in structural strain.

Those comparisons are only made using BSR reactions. The next level in the classification already contains four-carbon references. In the next section, we treat individual cases with isodesmic reactions which do not systematically belong to the established classification.

Examples

Four carbons systems Four carbon systems are the first for which isodesmicity can be increased from the BSR level. Several reactions have been tested for 1,2-butadiene and 1,3 butadiene. Isodesmic reactions tested for 1,2-butadiene are presented on Figure 5.13. Reactions R1, R2 and R5 correspond to levels in the Bond Separation Reaction hierarchy of Wheeler and coworkers. Figure 5.14 presents the *i.i.* of reactions presented on figure 5.13 along with the error on the obtained heats of formation using HF, MP2 and B3LYP with 6-31G(d) basis set. The heats

Table 5.14: Isodesmicity index for the test set compounds with BSR reactions (kcal.mol^{-1}).

compound	*i.i.*	compound	*i.i.*
allene	3.32	butane	1.20
propyne	1.40	isobutane	1.92
cyclopropene	1.98	1,3-cyclopentadiene	3.83
propene	0.52	spiropentane	3.68
cyclopropane	1.83	cyclopentene	2.41
propane	0.63	Cyclopentane	3.12
vinylacetylene	2.26	(Z)-2-Pentene	2.54
1,3-cyclobutadiene	3.62	pentane	1.90
1,3-butadiene	2.03	2,2-dimethylpropane	3.90
1,2-butadine	3.66	cyclohexane	2.93
methylene cyclopropane	2.48	benzene	7.63
bicyclobutane	3.75	bismethylenecyclobutene	7.54
cyclobutene	2.48	1,3-cyclohexadiene	3.41
1-butyne	1.21	1,4-cyclohexadiene	3.87
2-butyne	3.04	(E)-1,3,5-hexatriene	4.24
cyclobutane	2.42	(Z)-1,3,5-hexatriene	4.22
(E)-2-butene	1.15	cyclohexene	2.68
(Z)-2-butene	1.77	toluene	8.26
isobutene	1.40		

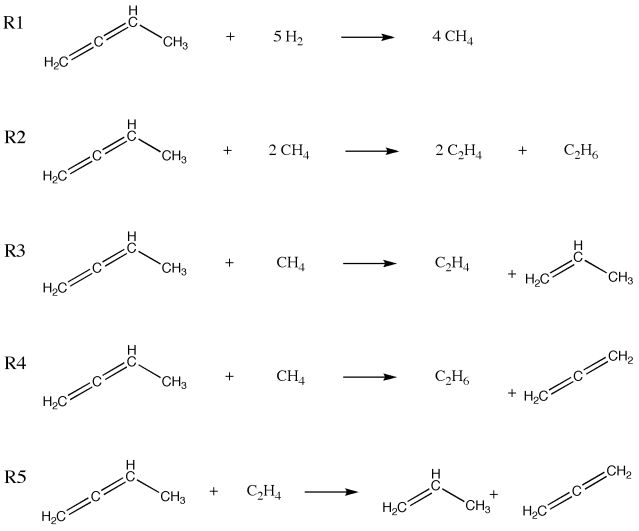

Figure 5.13: Isodesmic reactions tested on 1,2-butadiene.

of formation are calculated at low levels of theory to increase the difference between the results of the various isodesmic processes. At G3B3 level, the error on the reference compound would immediately become an issue. The variation of *i.i* indicates that the cumulenic pattern is to be taken into account if an improvement is desired. The use of propene and acetylene does not provide a much lower *i.i.*. Among the three methods used, B3LYP shows the best behavior with decreasing isodesmicity index. Similar results have been obtained for 1,3-butadiene. The evolution of the index and errors are presented on Figure 5.15. Again, the B3LYP results seems to be in best agreement with the evolution of the index. The MP2 value using R1 presents an unexpectedly low deviation from experiment. The other MP2 values decrease with a decreasing *i.i.* but rather linearly. Those have been obtained using reactions presented on Figure 5.16. As a third example, we consider (E)-2-butene (reactions used are given on Figure 5.18). On Figure 5.17, one notes that the index for the isomerization to the (Z) form presents a higher isodesmicity

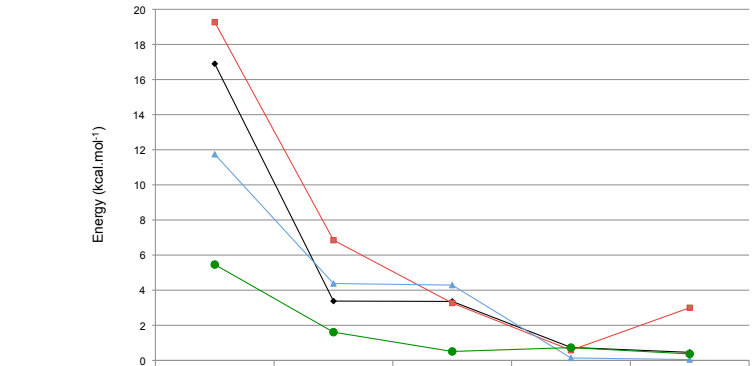

	R1	R2	R3	R4	R5
isodesmicity index	16.9	3.38	3.36	0.74	0.46
MP2 absolute error	19.27	6.85	3.27	0.58	3
B3LYP absolute error	11.74	4.38	4.29	0.14	0.05
HF absolute error	5.46	1.61	0.51	0.73	0.37

Figure 5.14: Isodesmicity index and absolute error on the resulting heat of formation of isodesmic reactions for 1,2-butadiene. Basis set used : 6-31G(d).

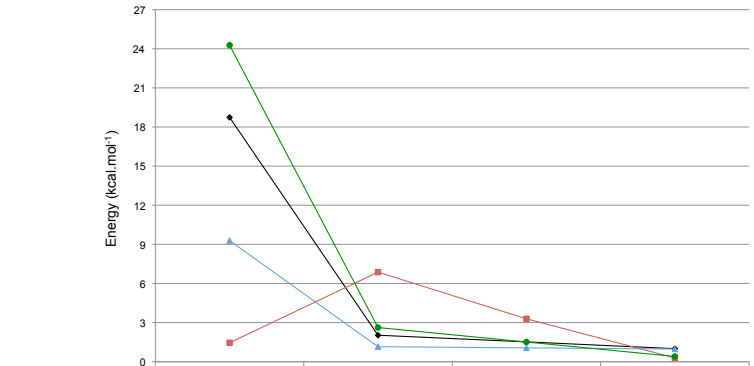

	R1	R2	R3	R4
isodesmicity index	18.74	2.03	1.52	1
MP2 absolute error	1.45	6.87	3.29	0.29
B3LYP absolute error	9.29	1.15	1.06	0.97
HF absolute error	24.27	2.62	1.51	0.4

Figure 5.15: Isodesmicity index and absolute error on the resulting heat of formation of isodesmic reactions for 1,3-butadiene. Basis set used : 6-31G(d).

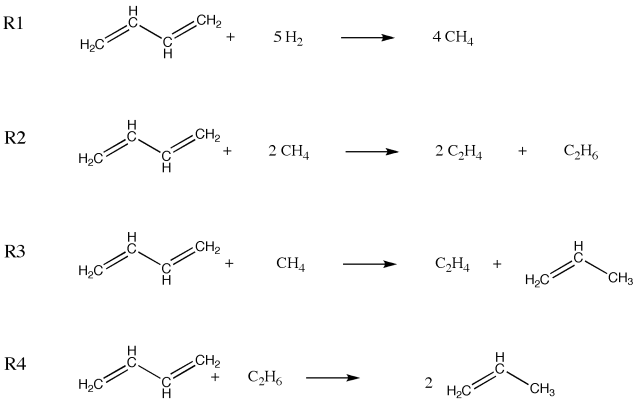

Figure 5.16: Isodesmic reactions tested on 1,3-butadiene.

index than the decomposition into two propenes. This can be explained by the interactions between methyl groups in the (Z) form which do not appear in the (E) one. The (E) form is then closer to the two propenes than to its (Z) counterpart. The error on reaction 4 with MP2 energies corresponds to the use of two propenes as references. A similar increase has been noticed in the case of 1,3-butadiene when two propenes were used. On the overall, there is a relatively poorer agreement between the errors and the index. We however note that in the case of B3LYP and HF, the error quickly becomes very small, which make them more sensitive to the errors on the experimental data of the reference systems.

Larger systems There relatively is small number of isodesmic reactions for small systems, as they quickly become themselves references as the level of isodesmicity is raised. Furthermore, the accuracy of the data for the reference systems decreases as those grow larger and so does the accuracy of the heat of formation of the system under investigation. This makes any comparisons useless, especially at very high level

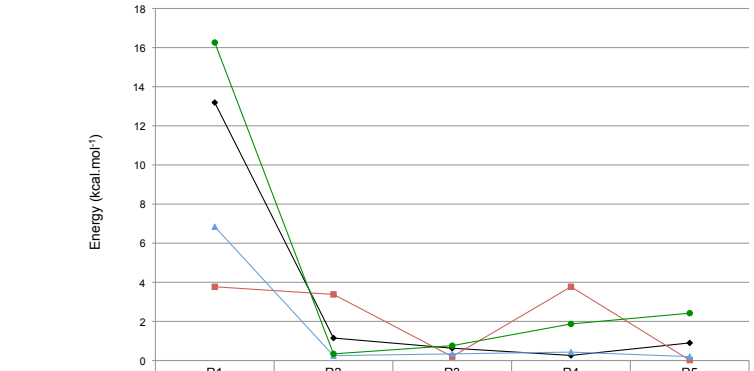

	R1	R2	R3	R4	R5
isodesmicity index	13.19	1.15	0.63	0.26	0.9
MP2 absolute error	3.77	3.38	0.2	3.77	0.02
B3LYP absolute error	6.84	0.25	0.34	0.43	0.2
HF absolute error	16.26	0.34	0.76	1.87	2.42

Figure 5.17: Isodesmicity index and absolute error on the resulting heat of formation of isodesmic reactions for (E)-2-butene. Basis set used : 6-31G(d).

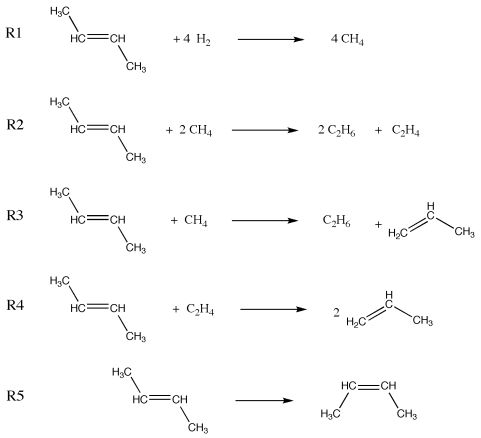

Figure 5.18: Isodesmic reactions tested on (E)-2-butene.

of isodesmicity where variations in the resulting heats of formation are expected to be small. The index is tested on larger systems to confirm its behavior with increasing isodesmicity. Figure 5.19 presents the *i.i.* for the 2-methylhexa-1,3-diene-5-yne, which was the example compound for the description of the bond separation hierarchy. We used the five reactions of the hierarchy along with reactions that were chosen instinctively to lie in-between hierarchy levels. This is confirmed by the index.

Note on fulvene The heat of formation of fulvene has been determined from the best of three isodesmic processes in section 5.3.1. The accuracy of the obtained value has been confirmed *a posteriori* by the W3.2Lite calculations of Karton and coworkers. However, the values of Karton and coworkers is closer to the one obtained with the second best reaction in section 5.3.1. If the index is calculated for those two reactions, we note that the isodesmicity index for the isomerization reaction is higher and therefore, that the isomerization of benzene to fulvene is not the best isodesmic reactions. Two points have to be mentioned. First, the isodesmic reaction conserving the cyclopentadiene pattern also conserves the strain in that system, which is present in fulvene. Second, the $\Delta(QCI)$ correction for aromatic rings was noted to be positive. This could possibly invalidate the index for reaction using aromatic reference.

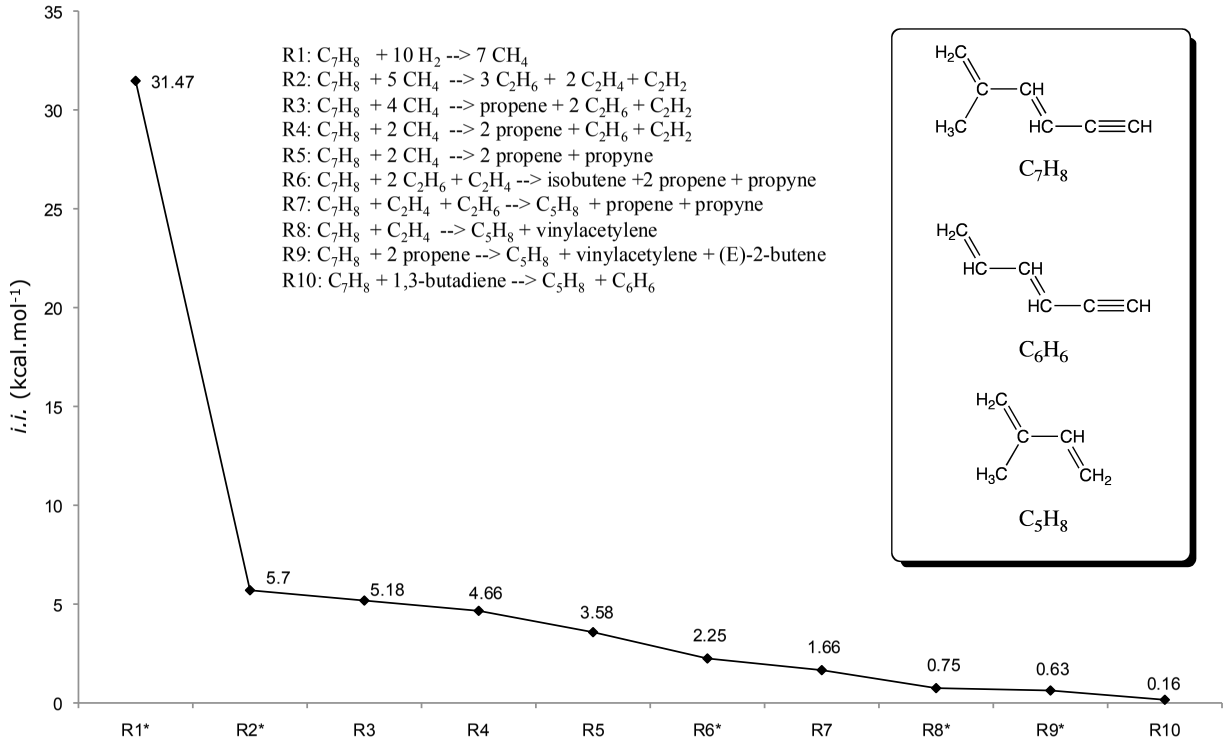

Figure 5.19: Isodesmic index for 2-methyl hexa-1,3-diene-5-yne. Marked(*) reactions indicate level of the bond separation hierarchy.

5.5.3 Conclusions

An isodesmicity index has been defined as the sum of absolute G3B3 reaction energy corrections. This index is reaction-specific and depends on the size and complexity of the system under investigation. As could be expected from such an index, it is maximum for atomization reactions and tends to zero as isodesmicity is raised. This index allows a classification of isodesmic processes. Table A.1 provides the G3B3 data for the hydrocarbons contained in the test set, which may be used for the determination of isodesmicity indices. However, the error on the data obtained does not systematically follow the index' behavior. For large compounds, the extension of isodesmicity also leads to the use of less accurate references. Therefore, the heats of isodesmic reactions probably are accurate, but uncertainties on experimental data become the main sources of errors on the final heat of formation. Finally, to avoid issues linked to positive energy corrections, such as the one appearing in aromatic cycles, one could consider computing the index taking into account energy corrections from HF energies rather than the MP4 6-31G(d) starting point of the G3B3 method.

5.6 Conclusions

The use of G3B3 to determine the heats of formation of closed-shell hydrocarbons has been tested and revealed itself quite accurate. The results are even better if the isodesmic process is well chosen, as has been shown in the case of fulvene. There are however some deficiencies. Indeed, the method does not seem to correctly reproduce the strain situation in highly strained systems. As this issue can be overcome

by the use of ring conserving isodesmic processes, those were only defined for unsubstituted rings. Patterns such as methylenecyclopropane, methylene cyclobutane, bicyclobutane or fusion between cycles remain an issue. The use of isodesmicity indices can help evaluating the best isodesmic process, however the uncertainties on the experimental values may also become the main source of deviation on the final result.

Chapter 6

Heats of formation of open-shell systems

As mentioned in an earlier section, dealing with open-shell systems brings up an additional issue that must be taken into account. This issue is spin contamination. In this chapter, we evaluate the G3B3 heats of formation of several simple open-shell systems using the methods described in section 3.2. As a results of the observations made on the test set, a new method for the determination of heats of formation from Møller-Plesset energies is developed. Finally, the last part is dedicated to the computation of the heats of formation of several radicals appearing as potential intermediates on the reaction mechanisms described in the next chapters.

6.1 Test set

The performances of the methods of determination of heats of formation are evaluated through comparisons with test series of reference heats of formation, such as was done for the closed-shell methodologies.

6.1.1 Reference heats of formation

Reliable experimental values concerning the heats of formation of open-shell systems are scarce. For some, such as the allyl or phenyl radicals, experimental data seem quite well agreed on. For those two systems, we may consider the available experimental data. For others, we choose to use theoretical results of higher accuracy as reference values. Table 6.1 presents the selected heats of formation for our test set.

Two-carbon radicals

As for the BSR method, RBSR needs accurate data for the two-carbon radicals that are used as references. The data for ethyl, vinyl and ethynyl radicals were taken from Burcat's database (update of June 2009). In the case of those systems, the data included in this database comes from the Active Thermochemical Table and should be the most accurate values available. Those are presented in Table 6.1.

C_3H_3 radicals

Four isomers of C_3H_3 radicals are considered (see Figure 6.1). Those are the propyn-1-yl radical , the resonantly stabilized propyn-3-yl radical (from now on called the propargyl radical), the cyclopropen-1-yl

Table 6.1: Reference ΔH_f° for test set open-shell systems (kcal.mol^{-1}). Uncertainties are given when available.

radical	ΔH_f°	radical	ΔH_f°
methyl	35.03 ±0.02	propen-3-yl	40.84 ±0.57
ethynyl	135.7 ±0.076	prop-1-yl	24.02 ±0.5
vinyl	70.60 ±0.4	*n*-C_4H_3	130.27
ethyl	28.61 ±0.16	*i*-C_4H_3	119.11
propyn-1-yl	125.99	*n*-C_4H_5	87.24
propargyl	84.23	*i*-C_4H_5	76.06
cyclopropen-1-yl	125.22	(Z)-C_4H_7-4-yl	32.20
cyclopropen-3-yl	116.30	cyclopentadienyl	64.77 ±1.9
propen-1-yl	65.69	phenyl	81.20 ±0.6
propen-2-yl	61.66	cyclohexadienyl	49.71 ±0.93

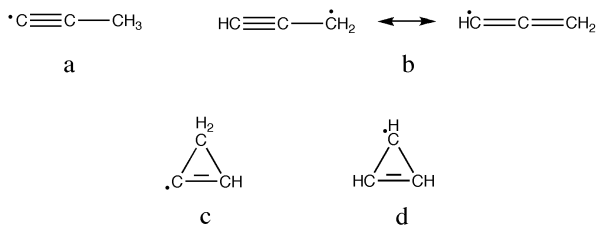

Figure 6.1: Structures of C_3H_3 radicals; a: propyn-1-yl radical, b: propargyl radical, c: cyclopropen-1-yl radical, d: cyclopropen-3-yl radical.

and cyclopropen-3-yl radicals. (See Figure 6.1). An important number of experimental data for the heat of formation of the propargyl radical is available from the literature (see [32] and references therein). Those experimental data range from 79 to 86 kcal.mol^{-1}. Experimental data for the cyclopropenyl radicals are available. However, those were established using the heat of formation of cyclopropene of Wiberg and coworkers and are therefore probably a little overestimated. The C_3H_3 isomers have been the subject of high level calculation, providing the most accurate heats of formation to this date for this series of radicals. The heats of formation at 0 K provided in this work are 126.6, 84.76, 126.28 and 117.36 kcal.mol^{-1} for the propyn-1-yl , propargyl, and the cyclopropen-1-yl and cyclopropen-3-yl radicals respectively. Those have been corrected for temperature effects to obtain data at 298.15 K.

C_3H_5 radicals

Three radicals are considered, the propen-1-yl, propen-2-yl and propen-3-yl (from now on called the allyl radical) radicals. Concerning the allyl radical, the heat of formation has been experimentally measured and is relatively well agreed on. The NIST Chemistry Webbook provides a 40.9 kcal.mol^{-1} value from Tsang's database (1996). Another value is given in Burcat's database an is 39.1 kcal.mol^{-1}. The JPCRD provides a 41 kcal.mol^{-1} value. In their 1996 work, Wenthold and coworkers [100] established a 41.5 kcal.mol^{-1} value and the most recent experimental result from Shuman and coworkers [101] is 40.84 kcal.mol^{-1}. This last value is chosen as reference in this work. Values for other C_3H_5 radicals are much more difficult to find. Values of Wu and Kern [34] provided by Burcat's database are 62.8 and 56.8 kcal.mol^{-1} for the propen-1-yl and

propen-2-yl radicals respectively. The heat of formation of propen-1-yl has been determined using a 33.6 kcal.mol^{-1} heat of reaction for the addition of an hydrogen on propyne. They determined the heat of formation of the propen-2-yl radical by considering the Bond Dissociation Energy (BDE) of ethylene and the heats of formation of propene and of the hydrogen atom. As this method can lead to relatively accurate results, they used 104 kcal.mol^{-1} as BDE of ethylene, which was probably the accepted value at the time. This value is today considered to be around 110.7 kcal.mol^{-1}. Their value is therefore underestimated by about 6 kcal.mol^{-1}. The accuracy of those two values is certainly not guaranteed. Yu and Muckerman [102] carried out CBS extrapolation of UCCSD(T) energies on the c-C_3H_6 + H reaction pathway. From this work, relative enthalpies of the three C_3H_5 radicals may be extracted and therefore, using the 40.84 kcal.mol^{-1} value for the allyl radical, we determine heats of formation of 65.69 and 61.66 kcal.mol^{-1} for propen-1- and propen-2-yl radicals.

C_3H_7 radical

The heat of formation of the C_3H_7 (prop-1-yl) radical is taken to be 24.02 kcal.mol^{-1}. This value comes from JPCRD. Another value exist from the NIST Chemistry Webbook, which is 23.9 kcal.mol^{-1}. The former was chosen as it is also listed in Burcat's database. However, considering this value or the other does not change the results of the comparisons, quantitatively or qualitatively.

C_4H_3 radicals

For those systems, reference values come from a computational study of Wheeler and coworkers [103]. Again, the data is provided at 0 K and must be corrected for temperature effects. The values so obtained are 130.27 and 119.11 kcal.mol^{-1} for *n*- and *i*-C_4H_3 respectively.

C_4H_5 radicals

Again, the reference values come from the work of Wheeler and coworkers [103]. The values, corrected to 298.15 K, are 89.70 and 78.40 kcal.mol^{-1} for *n*- and *i*-C_4H_5 respectively (see Figure 6.2). Some comment has to be made on *i*-C_4H_5, particularly on its structure. The work of Parker and Cooksy [104] indicate that the 1,3-butadien-2-yl structure corresponds to a transition state when single reference methods are used, the closest minimum being the 1,2-butadien-4-yl radical. It is a shallow minimum if multi-configurational methods are used. They also state that this well is so shallow that the configuration probably does not have a sufficiently long lifetime, and therefore, only 1,2-butadien-4-yl is likely to be observable. At the B3LYP 6-31G(d) level, the 1,3-butadien-2-yl structure also is a rotational transition state. Therefore, 1,2-butadiene is used as closed-shell reference in the various hydrogen transfer processes used for determination of the heat of formation of the *i*-C_4H_5 radical.

Cyclopentadienyl radical

The heat of formation of the cyclopentadien-3-yl (from now on called cyclopentadienyl radical) radical has been obtained experimentally at many occasions and the obtained values may vary greatly between 57.84

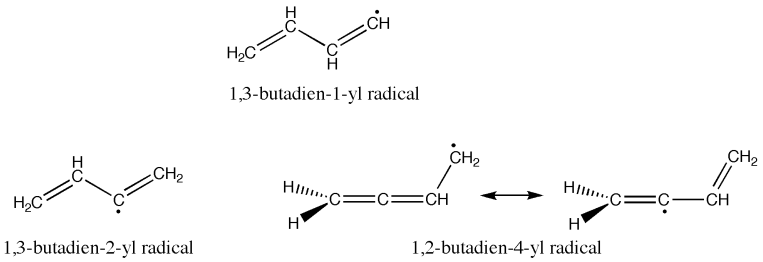

Figure 6.2: Structures of C_4H_5 radicals.

and 65.3 kcal.mol^{-1} (see reference [31] and references therein). The value chosen in this work is the one of Nunes and coworkers [31], which is the most recent experimental result and is also supported by *ab initio* calculations.

The phenyl radical

The heat of formation of the phenyl radical is quite well agreed on. JPCRD [62] provides a 79 $\pm$1 kcal.mol^{-1} value. The NIST Chemistry Webbook provides a 81 $\pm$2 kcal.mol^{-1} data. The most recent experimental data comes from Davico and coworkers [105] and is 81.2 kcal.mol^{-1}. This value is supported by high level calculations from Lau and Ng [106] (CCSD(T, full)/CBS approximation).

Cyclohexadienyl radical

The cyclohexadienyl radical considered in this work is the one obtained by homolytic cleavage of a CH bond invovling a sp^2 carbon of either 1,3- or 1,4-cyclohexadiene. The only value we can find in our common databases (JPCRD, Pedley's compilation, NIST Chemistry Webbook and Burcat's thermodynamic tables) comes from Burcat's table and is

of 47.92 kcal.mol^{-1}. This value cannot be retained as it is taken from the 1984 BAC-MP4 database of C. F. Melius. As already mentioned, this method is now known to provide results of poor accuracy. In recent literature, we found a experimental determination by Gao and coworkers, supported by G3 calculations. We choose to use their 49.71 kcal.mol^{-1} value as heat of formation of this radical [107].

6.1.2 G3B3 energy components

In this section, we review the various energy corrections of the G3B3 procedure, along with the ones of the PG3B3 procedure, which consist in replacing the MPn based corrections by PMPn corrections to account for spin contamination in the basis set corrections of the systems studied. All corrections used in those sections may be found in the appendix of this chapter (See Table B.1).

Δ(QCI) corrections

The $\Delta(QCI)$ corrections of doublet systems is closely related to the spin contamination of the UHF 6-31G(d) wave function. As shown on Figure 6.3 there is a good linear behavior of this correction with respect to the contamination. This behavior is described by equation 6.1. The intercept is non zero due to the part of the correction which is not due to the spin contamination. If Δ(QCI) corrections are compared to those of similar compounds in the closed-shell set, one notes that most of the correction is dedicated to the correction of the spin contamination.

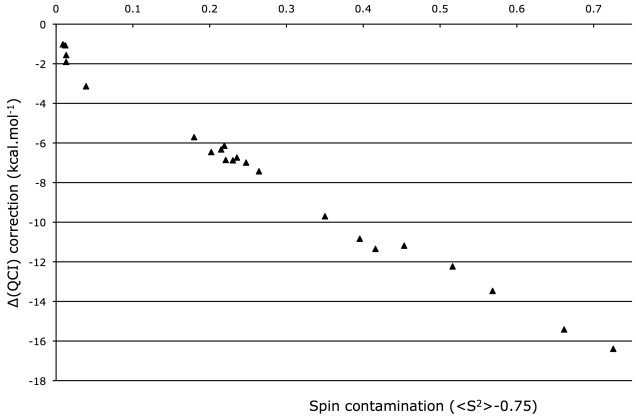

Figure 6.3: Evolution of the $\Delta(QCI)$ correction as a function of the spin contamination.

Note on projected Møller-Plesset energies The difference in energies between spin projected MP4 and MP4 energies have been calculated. As could be expected, those corrections correlate with the magnitude of the spin contamination. However, what is not expected is the non-zero intercept of all correlation straight lines (data concerning the linear regression can be found in Table B.2 in the appendix of this chapter). The intercept is negative, as for the $\Delta(QCI)$ case . This may lead to overcorrection of spin contamination error, and therefore to energies a little lower than they should.

$$\Delta(QCI) = -21.15SC - 1.76 \qquad R^2 = 0.98 \tag{6.1}$$

$\Delta(+)$ corrections

The $\Delta(+)$ correction behaves similarly to what has been observed in the closed-shell G3B3 energy components examination (see Figure 6.4).

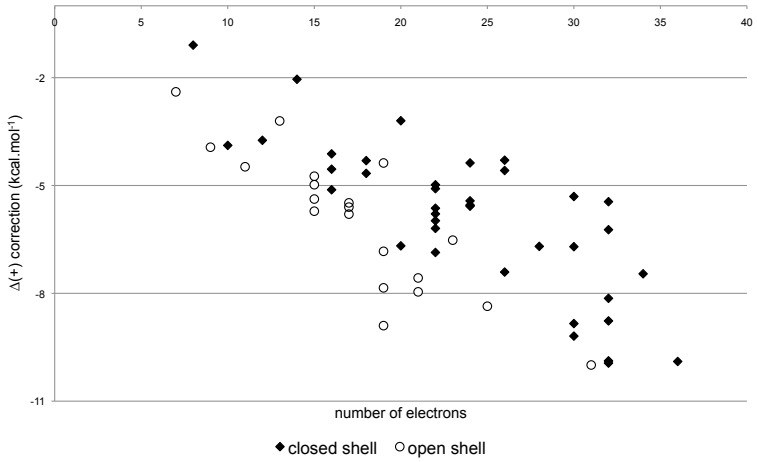

Figure 6.4: Evolution of the $\Delta(+)$ correction with the number of electrons for closed and openshell systems.

There is a clear increase in the correction's importance when the number of electrons is increased, however, still, no good correlation coefficients appear (R^2= 0.64 for the closed-shell series and 0.80 for the open-shell one). There also seems to be a tendency of the $\Delta(+)$ correction to be more important for the open-shell systems. This could be expected, as radicals represent a more diffuse situation (between the closed-shell system and the ion).

Δ(2df,p) corrections

As was observed for closed-shell systems, there is a linear relationship between the magnitude of the $\Delta(2df,p)$ correction and the number of electrons. As can be seen on Figure 6.5, the $\Delta(2df,p)$ corrections of the open-shell systems fit quite well with closed-shell ones. This indicates very little influence of the spin contamination on the magnitude of the correction.

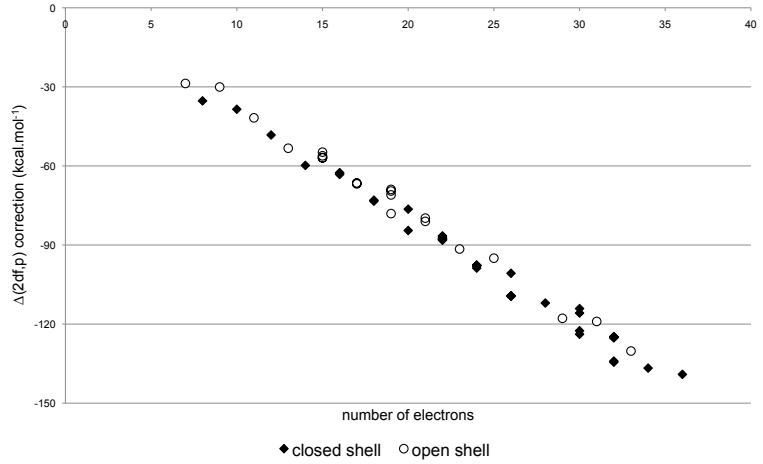

Figure 6.5: Evolution of the $\Delta(2df,p)$ correction with the number of electrons for closed and open-shell systems.

Δ(GTL) corrections

This final correction also behaves as noted in the closed-shell data. The open-shell corrections fit very well with the closed-shell ones (see Figure 6.6). As was noted for the $\Delta(2df,p)$ correction, there is probably very little influence of the spin contamination.

6.1.3 PG3B3 corrections

The PG3B3 corrections are the G3B3 corrections obtained using projected Møller-Plesset energies rather than Møller-Plesset energies. This method can be used to account for spin contamination in the basis set corrections. The use of such corrections yield an average destabilization of 8.08 kcal.mol^{-1} on the overall G3B3 energy. This destabilization is due to the stronger effect of spin contamination on energies obtained with smaller basis sets. For instance the projection of the first four spin

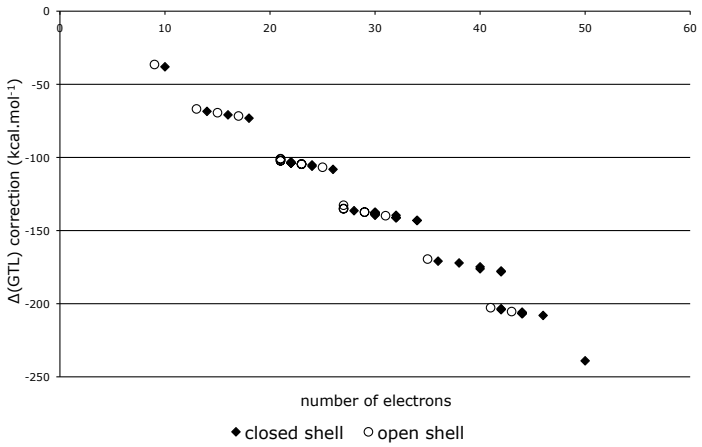

Figure 6.6: Evolution of the $\Delta(GTL)$ correction with the number of electrons for closed and open-shell systems.

contaminants lowers the MP4/6-31G(d) energy more than the MP4/6-31G(2df,p) energy. The result is a decrease of the difference in energy between those two levels, and therefore a decrease of the $\Delta(2df, p)$ correction.

6.1.4 Heats of formation of the test set systems

The three methods to turn raw energies into heats of formation described in section 3.2 have been applied to obtain the heats of formation of the systems included in the test set presented in the previous section. Those methods were combined with G3B3, PG3B3 energies. For comparison purposes, those heats of formation have also been computed using most of the energies contained in the G3B3 procedure, namely: QCISD(T), MP4, PMP4, MP2 and PMP2 with the 6-31G(d) basis set ; MP4, MP2, PMP4, PMP2 with the 6-31+G(d) basis set; and MP4, MP2, PMP4 and PMP2 energies combined with the 6-31G(2df, p) basis set. All those

results are summarized in Table 6.2, which provides the mean deviation and standard deviations from the reference values. A complete list of the obtained values may be found in the appendix.

The RBSR method

Using G3B3 energies, RBSR provides results similar to those of AR reactions. The MD is also much more important than the one observed for hydrogen transfer reaction. However, this method shows the smallest standard deviation. Using PG3B3 energies; RBSR shows the best MD and the best standard deviation. Using the energies included in the G3B3 procedure shows that, again, with all methods, the use of RBSR provides better results in term of MD and standard deviations. This is less systematic if projected energies are used.

Spin contamination One of the expected effect of the RBSR method was a partial cancellation of the spin contamination error. Due to the small variation in the G3B3 results, the heats of formation were calculated at lower levels of theory. As a good correlation may be found between the initial spin contamination and the error for the HTR and AR methods, poor correlation is observed for RBSR. As we expected a partial cancelation, it is not the initial spin contamination that should be looked at, but the reaction spin contamination (see equation 6.2, given for doublet states). In that case, the correlation observed for AR and HTR remains the same, as, in those cases, the initial spin contamination does not differ importantly from the reaction spin contamination.

Table 6.2: Mean deviations (MD), and standard deviations (s.d.) for all the methods tested (kcal.mol^{-1}).

	AR	RBSR	HTR	EXT	MP4	PMP4
G3B3 MD	-0.44	-0.40	0.08	-	-	-
s.d.	1.05	0.91	1.16	-	-	-
PG3B3 MD	-0.06	-0.32	0.45	-	-	-
s.d.	1.16	1.12	1.35	-	-	-
6-31G(d)						
QCISD(T) MD	25.56	0.06	0.08	-	-	-
s.d.	5.94	0.89	1.51	-	-	-
MP4 MD	28.65	3.91	7.24	1.31	2.89	-
s.d.	8.11	4.24	5.10	2.38	5.27	-
MP2 MD	23.75	4.58	9.89	1.51	3.93	-
s.d.	6.52	5.23	6.87	2.76	7.08	-
PMP4 MD	21.35	-1.19	-0.17	-	-	-0.13
s.d.	4.48	0.89	1.45	-	-	1.95
PMP2 MD	13.57	-3.40	-1.07	-	-	-1.08
s.d.	3.15	2.45	1.61	-	-	2.73
6-31+G(d)						
MP4 MD	31.16	4.46	7.62	0.76	2.60	-
s.d.	8.77	4.70	5.22	1.98	5.37	-
MP2 MD	25.86	5.19	10.33	0.99	3.66	-
s.d.	6.85	5.72	6.99	2.39	7.19	-
PMP4 MD	24.79	-0.36	0.64	-	-	-0.22
s.d.	5.61	0.98	1.52	-	-	1.96
PMP2 MD	17.16	-1.99	0.35	-	-	-0.69
s.d.	3.39	1.39	2.43	-	-	3.24
6-31G(2df,p)						
MP4 MD	-13.41	2.94	7.05	0.03	2.15	-
s.d.	10.62	3.95	5.16	1.48	5.33	-
MP2 MD	-18.54	3.84	10.05	0.37	3.43	-
s.d.	10.30	5.16	7.18	2.07	7.41	-
PMP4 MD	-20.12	-2.10	-0.22	-	-	-0.84
s.d.	8.87	1.27	1.55	-	-	1.94
PMP2 MD	-27.84	-4.06	-0.73	-	-	-1.58
s.d.	9.69	2.68	1.82	-	-	2.71

The correlation between the RBSR deviation and the reaction spin contamination is much better.

$$SC_r = \sum_{i}^{products} SC_i - \sum_{j}^{reactants} SC_j \quad with \quad SC_i = \langle S^2 \rangle_i - 0.75 \quad (6.2)$$

A better use of RBSR references: The EXTRAP procedure

In the previous section, we have shown that the spin contamination error on Møller-Plesset heats of formation were linked to reaction spin contamination. The use of a properly contaminated reference may therefore be considered for the determination of a heat of formation. It is however not easy to find, for a given system, another system which has very close spin contamination and a well established heat of formation. As the spin contamination error decreases with the reaction spin contamination, let's consider the following:

- The RBSR references represent a wide range of $\langle S^2 \rangle$ values (C_2H: 1.15; C_2H_3: 0.97 and C_2H_5:0.76).
- If hydrogen transfer reactions using ethane, ethylene and acetylene are considered, three different heats of formation are obtained.
- The error on those three values are correlated to the reaction spin contamination.
- If plotted against the reaction spin contamination, those three values describe a straight line.
- The y-intercept of this plot should provide the heat of formation at the zero reaction spin contamination, therefore removing the spin contamination error from the heat of formation.

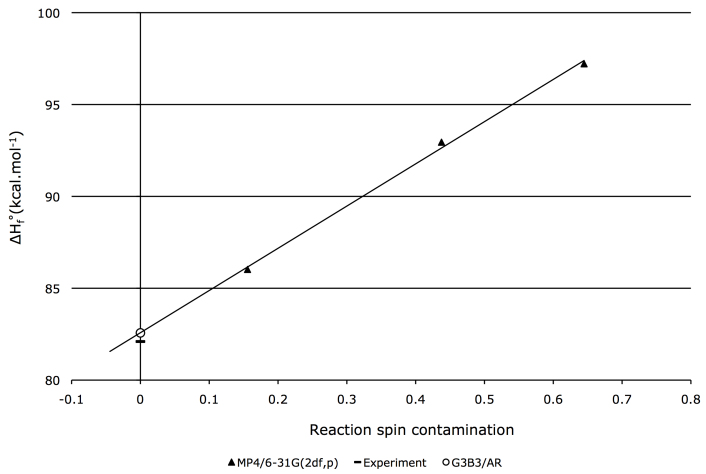

Figure 6.7: Determination of the heat of formation of the phenyl radical by the use of the EXTRAP procedure. Energy: MP4 / 6-31G(2df,p).

Those considerations were tested and the MD and standard deviations are provided under the EXTRAP label in Table 6.2. An example of the application of this procedure is given for the heat of formation of the phenyl radical on Figure 6.7. No QCISD(T) values are provided, as using the latter method does not show the linear behavior of the three heats of formation. This is probably due to the spin contamination correction linked to the configuration interaction treatment. All results of this methods are provided in the appendix (See Tables B.14 and B.14). It comes from Table 6.2 that the EXTRAP methodology provides the best heats of formation if Møller-Plesset energies are used. The results obtained with this method combined with MP4 6-31G(2df,p) are also very close to that obtained with QCISD(T) 6-31G(d). This can be explained. It has been shown that most of the $\Delta(QCI)$ correction is mostly dedicated to the correction of the spin contamination error, the rest of the correction being relatively small.

The EXTRAP methodology extrapolates out the spin contamination error, and the use of a larger basis set provides additional stabilization, leading to similar accuracy, at lower cost. Furthermore, if compared, through a Student test, to G3B3/HTR and PG3B3/HTR results , the MP4 6-31G(2df,p)/EXTRAP method does not provide significantly different results and therefore provides a computationally cheap alternative to the G3B3 procedure.

6.2 Heats of formation of C_6H_5 radicals

The test set allowed to establish that HTR were the most accurate source of heats of formation. However, results using G3B3/HTR and PG3B3/HTR were noted not to be significantly different. No significant differences appeared between those two methods and the EXTRAP methodology established in section 6.1.4. This allows the averaging of values which are of the same accuracy. Therefore, in the next section, we define the heats of formation of C_6H_5 radicals using the three methods. The final heats of formation are taken as the average of the three results.

6.2.1 Cyclic systems

Different C_6H_5 cyclic systems appear in the description of acetylene addition on C_4H_3 radicals (See chapter 7 and reference [28]). In this section, we define their heats of formation. The different cyclic system considered are presented on Figure 6.8. The notations used are those described in section 7.1.2.

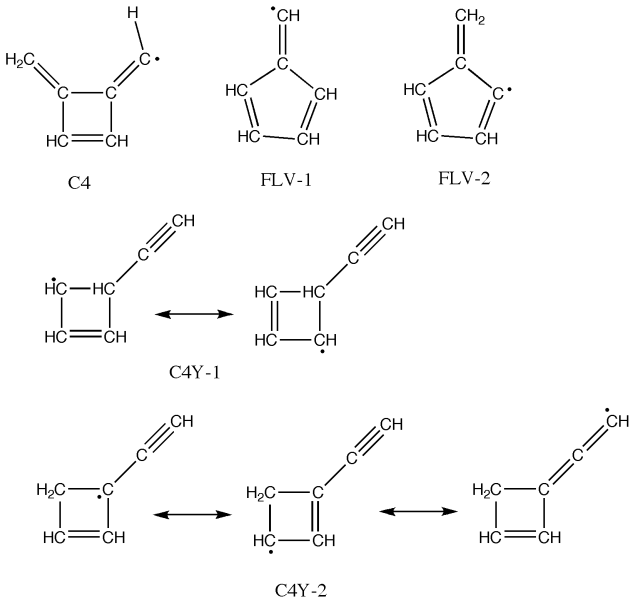

Figure 6.8: Cyclic C_6H_5 radicals considered.

The heats of formation obtained with the three methods for each of those systems are given in Table 6.3 along with the average values, which are our final data.

6.2.2 Linear systems

The direct products of the addition of acetylene on C_4H_3 radicals are divided into two series of systems. The first is the *cis* linear C_6H_5 systems, resulting form the addition of acetylene on *n*-C_4H_3 radicals and the branched system resulting from the addition on the *i*-C_4H_3 radical. The eight radicals for which the heats of formation have been determined are presented on Figure 6.9. As is shown in the description of the isomerization of those different systems, the rotation barriers are not very important, it is therefore necessary to verify whether those rotations should be treated as internal rotors rather than harmonic vibrators.

Table 6.3: Calculated standard heats of formation for the considered cyclic C_6H_5 radicals (kcal.mol^{-1}).

Radical	G3B3/HTR	PG3B3/HTR	EXTRAP	Average	s.d.
FLV − 1	112.02	113.15	112.53	112.57	0.57
FLV − 2	117.26	118.49	119.54	118.43	1.14
C4	141.23	142.66	142.41	142.10	0.76
C4Y − 1	134.30	134.71	135.25	134.76	0.47
C4Y − 2	124.17	125.17	126.44	125.26	1.14

Linear and branched C_6H_5 systems

It has to be determined whether the terminal double bond of these systems are to be considered as internal rotors or vibrators. To do so, two points are examined. First is the rotation barrier, which has to be small if an hindered rotor is present. Secondly, as described by Ayalla and Schlegel [65], a normal vibration mode corresponding to a hindered rotation has unusually large components for the dihedral angles corresponding to the internal rotation. These components are to be close to 100 % if a hindered rotation is to be considered. Table 6.4 provides different information concerning the terminal double bond of the different linear and branched C_6H_5 isomers. The data indicates that for all those systems, the consideration of hindered rotor rather than harmonic oscillator is needed. The heats of formation of the various systems (HTR/G3B3, HTR/PG3B3 and EXTRAP) are provided in Table 6.5.

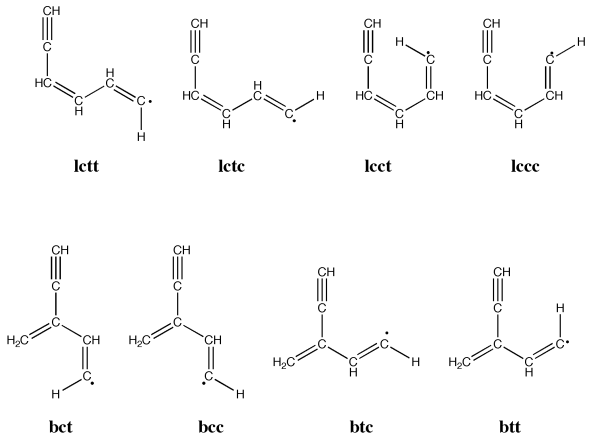

Figure 6.9: Non-cyclic C_6H_5 systems considered. Top: linear isomers; Bottom: branched isomers. Notation used are as described in section 7.1.2.

Table 6.4: Rotor vibrational frequency, percentage of dihedral component of the normal mode and rotation activation barriers (kcal.mol^{-1}) for the C_6H_5 radicals presented on Figure 6.9.

C_6H_5	ν(cm^{-1})	% dihedral	barrier
lctt	129.3	82.7	2.95
lctc	151.8	80.4	3.90
lccc	112.3	80.9	2.20
lcct	79.6	86.6	2.05
bct	78.7	83.8	5.19
btt	138.0	98.7	3.68
bcc	47.0	88.4	1.06
btc	144.0	89.6	3.33

Table 6.5: Calculated standard heats of formation for the C_6H_5 radicals presented on Figure 6.9 (kcal.mol^{-1}).

	G3B3/HTR	PG3B3/HTR	EXTRAP	average	s. d.
lctt	145.49	146.63	145.64	145.92	0.62
lctc	144.68	145.88	145.05	145.21	0.61
lccc	147.62	148.65	147.62	147.96	0.60
lcct	147.98	149.02	147.89	148.30	0.63
bct	147.84	149.04	149.87	148.92	1.02
btt	145.72	147.01	146.94	146.56	0.73
bcc	147.99	149.07	149.15	148.74	0.65
btc	145.82	147.11	147.29	146.74	0.80

6.3 Heats of formation of cyclic C_6H_7 radicals

The system considered in this section are C_6H_7 isomers presenting an unsaturated five membered cycle. Those systems appear not only as the products of hydrogen addition on fulvene [20], but also as a result of acetylene addition on C_4H_5 radicals [27], by the addition of the ethynyl radical on 1-butyne [30], of the methyl radical on the cyclopentadienyl one [99], and probably others. Figure 6.10 shows the structure and resonance forms of the different systems. As one can note, only two of the four systems present an *exo*-C-C bond with no double bond character. This is also reflected on the bond length. (See Table 6.6.) Again, we have to define whether the movement around the *exo* bond should be treated as an internal rotation (hindered or free). The results presented in Table 6.6 indicate that, in the case of C_6H_7C and C_6H_7D, no hindered rotor treatment has to be considered, as the rotation barrier is quite important and the double bond character of the *exo*-C-C bond is clear.

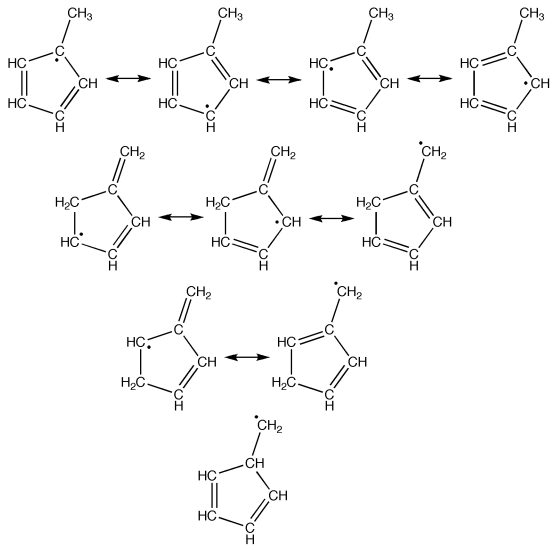

Figure 6.10: Resonance limit forms for C_6H_7 radicals. From top to bottom: C_6H_7B, C_6H_7D, C_6H_7C, C_6H_7A.

Table 6.6: Rotor vibrational frequency, rotation activation barriers (kcal.mol^{-1}) and percentage of dihedral component of the normal mode for the C_6H_7 radicals.

C_6H_7	ν(cm^{-1})	rotation barrier	*exo* C-C bond	% Dihedral
A	117.94	1.32	1.499	90.7
B	78.79	0.18	1.491	88.4
C	333.19	15.40	1.383	19.3
D	178.11	20.34	1.362	18.9

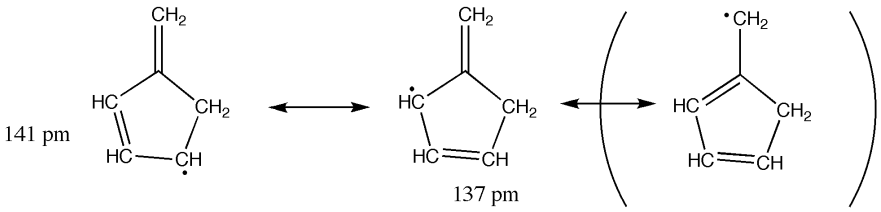

Figure 6.11: Resonance limit forms for radical C_6H_7D.

For C_6H_7A and C_6H_7B, the hindered rotation has to be considered.

6.3.1 Choice of reference closed-shell systems

For radicals C_6H_7C and C_6H_7D, the double bond character of the *exo* C-C bond is clearly defined (see the bond length column in Table 6.6). In the case of C, this uniquely defines the closed-shell system to be used, which is 3-methylene-cyclopentene. In the case of system D, two potential closed-shell system are to be considered, 3-methylene cyclopentene and 4-methylene cyclopentene. The difference comes from the position of the double bond in the five membered ring. The bond length of the two C-C bond concerned by the allylic part of C_6H_7 D (see first and second limit forms on Figure 6.11). Those are not typical single nor double bond lengths. Therefore, the heats of formation using both 3- and 4- methylene cyclopentene were calculated and averaged. The values obtained (see Table 6.6) may be compared to the BAC MP4 values of Melius and coworkers [20] and the CBS-QB3 values of Sharma and Green [99]. Those are given in Table 6.8. As the heats of formation for C_6H_7A and C_6H_7C are quite well agreed on, significant discrepancies appear for C_6H_7B and C_6H_7D. Indeed, the BAC-MP4 values of Melius and coworkers predict C_6H_7D to be more stable than C_6H_7B. Sharma and Green predict the same heat of formation for the two systems.

Table 6.7: Calculated standard heats of formation for the C_6H_7 radicals presented on Figure 6.10 (kcal.mol^{-1}).

C_6H_7	G3B3/HTR	PG3B3/HTR	EXTRAP	average	s. d.
A	76.13	77.23	79.62	77.66	1.79
B	52.88	53.64	53.33	53.28	0.38
C	59.44	60.37	60.12	59.97	0.48
D	54.42	55.26	54.45	54.71	0.48

Our data indicates that C_6H_7B is more stable than C_6H_7D. We have already mentioned that the BAC-MP4 method has poor accuracy. Globally, the CBS-QB3 values are supposed to be of similar accuracy as the G3B3 ones, and should therefore provide similar order of stability. One hypothesis for this difference comes from spin contamination. The wave function of C_6H_7D is more contaminated than the one for C_6H_7B. The CBS-QB3 method contains a correction for spin contamination, which is proportional to the $\langle S^2 \rangle$ value. However, this correction has been established by fitting on reference data for PS, CS and CN radicals. The latter correction might possibly be unadapted for large hydrocarbon radicals. The values obtained in this work are consistent with the number of resonance forms observed on Figure 6.10.

6.4 Heat of formation of bicyclic radicals

The different reaction paths described in the following sections have bicyclic systems as intermediates (see Figure 6.12). Those appear in the hydrogen atom assisted isomerization of fulvene to benzene and in the isomerization of dehydrofulvene radicals to the phenyl radical.

Table 6.8: Calculated standard heats of formation for the C_6H_7 radicals from : this work, Melius and coworker and Sharma and Green ($kcal.mol^{-1}$).

C_6H_7	This work	Melius and coworkers	Sharma and Green
A	77.66	79.83	77.2
B	53.28	54.25	53.3
C	59.97	59.03	59.2
D	54.71	52.58	53.3

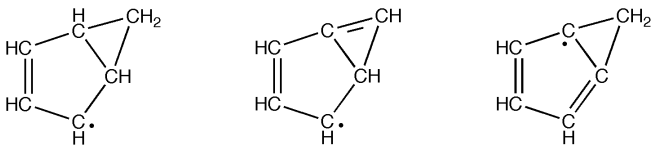

Figure 6.12: Bicyclic radicals considered.

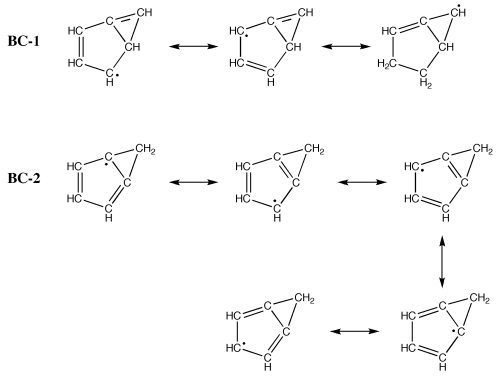

Figure 6.13: Limit forms of the bicyclic C_6H_5 radicals.

6.4.1 Bicyclic C_6H_7 radical.

The bicyclic C_6H_7 presents two equivalent resonance limit forms. The closed-shell system to be used for hydrogen transfer processes is therefore clear. It is bicyclo[3,1,0]cyclohex-2-ene (compound **11** in section 5.3.2). Its RCIR heat of formation is 35.97 kcal.mol^{-1}. The obtained heats of formation are listed in Table 6.9.

6.4.2 Bicyclic C_6H_5 radicals

Two bicyclic C_6H_5 radicals appear on the reaction path from dehydrofulvene radicals to the phenyl radical (see section 7.2). Those present non-equivalent resonance limit forms. This implies that the closed-shell reference for hydrogen transfer reactions have to be chosen according to some criteria. Figure 6.13 presents the limit forms of the two radicals. Structural criteria are used to define which bicyclo[3,1,0]hexadiene must be used as reference in the HTRs for $\mathbf{BC-1}$. Analysis of the latter radical's structure shows the unpaired electron is most likely located in the five membered ring. Indeed, the unsaturated C-C bond length

Table 6.9: Calculated standard heats of formation for the bicyclic radicals (kcal.mol^{-1}).

Radical	G3B3/HTR	PG3B3/HTR	EXTRAP	average	s.d.
BCC6H7	68.05	68.38	67.74	68.06	0.32
BC – 1	139.24	139.81	140.10	139.72	0.44
BC – 2	145.45	146.01	145.88	145.78	0.29

in the three membered cycle is 133 pm, which is very close to a typical double bond. This may be explained by the non planar structure of the bicyclic radical, preventing a good resonance. In this case, the electron is most likely to be found in the five membered cycle, which offers a planar support allowing resonance to take place. The closed-shell system to be used for hydrogen transfer reaction is therefore system **7** from section 5.3.2. The second bicyclic system, **BC – 2** shows significant structural differences. Indeed this system is planar, which was not encountered in the closed-shell bicyclic systems, apart from system **8** and **9** in section 5.3.2. This is probably due to the sp^2 character of both bridge carbons. The bridging C-C bond has a 146 pm length indicating a single bond between two sp^2 carbons, and therefore little contribution of the second and third limit forms (see Figure 6.13). The system to be considered for EXTRAP and HTR is system **9** (also from section 5.3.2). Its RCIR heat of formation is 115.67 kcal.mol^{-1}. Table 6.9 presents the results for all bicyclic radicals of this section. The results show that **BC – 2** is less stable than **BC – 1**. From the number of resonance forms, one could have expected the order of stability to be different. This destabilization of **BC – 2** probably comes from the two unsaturated bridging carbons.

Indeed , in the analysis of RCIR results, it has been observed that unsaturations on bridging carbons significantly destabilize the bicyclic systems.

6.5 Conclusions

The different heats of formation of the system in an established reference set were computed. The data has been computed at G3B3 and PG3B3 levels of theory, and the difference between the methodologies are quite small. To increase the difference between the results, and therefore analyze more closely the effects of the methodologies, the data has been calculated at lower levels of theories. Analysis of those results shows that extrapolation to the zero reaction spin contamination of Møller-Plesset heats of formation can significantly increase the accuracy of the results. In the case of full fourth order MP energies combined with the 6-31G(2df,p) basis set, the results obtained through the extrapolation procedure are not significantly different from the G3B3 and PG3B3 data. The procedure therefore offers a computationally cheap alternative to G3B3 for the determination of the heats of formation of open-shell systems.

Chapter 7

Reactions on the C_6H_5 energy surface

The phenyl radical is one of the possible first aromatic rings, as it can initiate both the HACA, the PAC and the biphenyl pathways of PAH growth. In this section, we examine different cyclization paths on the C_6H_5 energy surface. First, the result of the addition of acetylene on C_4H_3 radicals is extensively discussed. As a logical following of this section's findings, the isomerization of dehydrofulvene radicals to the phenyl radical is studied in a second section. The last part of this chapter consists in establishing global rate constants for the different reactions which are shown to be potentially significant.

7.1 Cycle formation from acetylene addition on C_4H_3 radicals

7.1.1 Introduction

As mentioned in the introduction, it is generally admitted that the formation of a first aromatic ring is a rate-limiting step to the formation of PAH. The formation of that ring is currently believed to be mainly due to the propargyl recombination reaction (R.1), which has been described in detail by Miller and Klippenstein [23]. The contribution of even carbon pathways ((R.2) to (R. 5)) has been and still is subject of debate [25, 26, 108]. One of the main points of discussion has been the energy difference between the *i*- and *n*- isomers of the C_4H_5 and C_4H_3 radicals. The heats of formation of those compounds have been the subject of nu-

$$
\begin{array}{lcll}
C_3H_3 + C_3H_3 & \rightarrow & C_6H_6 \text{ or } C_6H_5 + H & \text{(R.1)} \\
n\text{-}C_4H_5 + C_2H_2 & \rightarrow & C_6H_7 \text{ or } C_6H_6 + H & \text{(R.2)} \\
n\text{-}C_4H_3 + C_2H_2 & \rightarrow & C_6H_5 & \text{(R.3)} \\
i\text{-}C_4H_5 + C_2H_2 & \rightarrow & C_6H_7 \text{ or } C_6H_6 + H & \text{(R.4)} \\
i\text{-}C_4H_3 + C_2H_2 & \rightarrow & C_6H_5 \text{ or } C_6H_4 + H & \text{(R.5)}
\end{array}
$$

merous theoretical studies [103, 104, 109, 110]. All those studies showed, to a different extent, that the resonantly stabilized *i*- forms are thermodynamically more stable than their *n*- counterpart, therefore implying that the equilibrium concentrations of *n*- isomers are too low for (R.2) or (R.3) to significantly contribute to the formation of aromatic cycles. Addition of acetylene on *i*-radicals ((R.4) and (R.5)) was also ruled out for two reasons [108]: The first is the expected high activation energy for the addition step due to the delocalization of the radical site on resonantly stabilized species. The second is the presence of a CH_2 group, which

prevents an easy conversion to a six membered cycle containing six CH carbons. In 2007, Senosiain and Miller [27] provided a theoretical study of reactions (R.2) and (R.4). Rate constants resulting from this work were used to model a series of flames. The conclusions of those tests were that (R.3) contribution to six-membered cycle formation was negligible while (R.4) could be responsible for almost all fulvene formation and for up to 30% of benzene formation in 1,3-butadiene flames. In this work, we consider the formation of cycles from the addition of acetylene on n-C_4H_3 and i-C_4H_3. This study therefore includes the formation of the phenyl radical from (R.3) and (R.5). Formation of the phenyl radical from (R.3) is not expected to be significant for the reasons cited above. This path however remains a phenyl degradation pathway considered in kinetic mechanisms [111, 112]. In their G2M(rcc, MP2) [113] study of the phenyl radical degradation, Madden and coworkers [114] identified ortho-benzyne (o-C_6H_4) as the main degradation product. Decomposition reactions after ring opening were found to be the least significant paths. Those results are based on the consideration that all reactions following the phenyl ring opening, present high energy barriers except for the reverse reaction to form the phenyl radical. For those reasons, Wang and coworkers excluded this path from their phenyl radical decomposition mechanism [115]. In this work we suggest the formation of four- and five-membered rings, which are energetically competitive to (Z)-hex-3-en-1,5-diyne (l-C_6H_4) + H formation and to *ortho*-benzyne (o-C_6H_4) + H, respectively. Much fewer publications have been dedicated to the addition of acetylene on i-C_4H_3. Comparisons are made with the results of Walch,[116] which seems to be the sole work on this reaction. In addition to the reaction included in the work of Walch, we consider the formation of four-membered rings and hydrogen elimination

reactions forming 3-methylene pent-1-en-4yne. In the work of Walch, no polarization functions were included in the geometry optimization step basis set. Polarization functions are nevertheless needed to provide the flexibility required to correctly describe electronic distribution in high electron density spatial volumes, such as double and triple bonds. We therefore introduced such flexibility in our computations, expecting an increase in accuracy. Discussion is divided into four main sections. The first is the description of cycle formation from acetylene addition on n-C_4H_3, which is itself subdivided to describe successively addition steps, conformational changes in the addition products, hydrogen elimination steps, cyclisation steps and, finally, the formation of benzyne cycles from the phenyl radical. The second section concerns the addition of acetylene on i-C_4H_3 and is subdivided in a similar manner. The third section is the description of hydrogen shift reactions, and connects the first two sections. In a final section, conventional transition state theory rate constants for all steps described are given. Those values have been calculated using the *cse*-online infrastructure [117, 118] (http://cse-online.net).

7.1.2 Notations

Applying the official nomenclature rules to the various systems appearing in this work leads to complicated names, which are not well suited for a clear discussion. The names of the various C_6H_5 radicals have been simplified for clarity. A four-letter notation describes each non-cyclic C_6H_5 radical. The first letter defines whether the C_6H_5 radical is linear (l) or branched (b). The second letter (only appearing for linear radicals) indicates whether the central double bond has a cis (c) or

trans (t) configuration. The conformation of the butadienyl pattern of the C_6H_5 radical, transoid (t) or cisoid (c), is given by the third letter. Finally, the fourth letter gives the cis or trans (c or t) configuration of the hydrogen atoms in the HCCH terminal radical site. Using these notations, 1-dehydrohexa-1,3-diene-5-yne; HCCH cis is replaced by the much shorter and explicit notation **lccc**. Two dehydro-fulvene radicals are also encountered. Those are denoted $\mathbf{FLV-1}$ (6-dehydrofulvene) and $\mathbf{FLV-2}$ (1-dehydrofulvene). Their respective structures are provided in Figures 7.2 and 7.4. Also, two acetylenylcyclobutenyl radicals appear on the energy profiles. Those radicals are denoted $\mathbf{C4Y-1}$ and $\mathbf{C4Y-2}$. Finally, the bismethylenecyclobutenyl radical formed from the addition of C_2H_2 on i-C_4H_3 is denoted **C4**.

7.1.3 Spin contamination

Depending on the methodology used, spin contamination may be present. As DFT/B3LYP computations lead to low contamination, Unrestricted Hartree-Fock wave functions present often poor behavior. The C_6H_5 radicals considered in this work present important levels of spin contamination as shown in Tables 7.1 and 7.2 for the various basis sets. The average $\langle S^2 \rangle$ value on all C_6H_5 systems (minima and saddle points) comes out at 1.47 with a standard deviation (s.d.) of 0.18. At DFT level, spin contamination during geometry optimization steps is relatively low, the average $\langle S^2 \rangle$ value is 0.77 with a s.d. of 0.02. It has been shown that DFT performs quite well in obtaining the geometries and frequencies of open-shell systems [119], despite spin contamination, and we are therefore confident in the quality of the obtained structures. Two transition states however present $\langle S^2 \rangle$ values higher than 0.8. Those are entries 20

(0.84) and 39 (0.82) of Tables 7.1 and 7.2. The use of PG3B3 projected results induces a systematic increase of the absolute energies of about 1.26 kcal.mol^{-1} (s.d. =0.28 kcal. mol^{-1}). Looking at the source of this destabilization, one finds it is mainly due to the difference in $\Delta(+)$ corrections which, on average, account for 69% of the overall destabilization. Further, differences in $\Delta(2df,p)$ and $\Delta(GTL)$ corrections are, respectively, responsible for 21 and 10% of the remaining destabilization. Tables 7.1, 7.2 and 7.3 present PG3B3 energies relative to the phenyl radical (with ZPE energy corrections). They are completed by the average $\langle S^2 \rangle$ values obtained, using all basis sets, for UHF wave functions and DFT computations. The use of PG3B3 energies has however no significant effect on the relative energies. The most important deviation is a 0.74 kcal.mol^{-1} relative stabilization for $\mathbf{C4Y-1}$. The reason for these small effects is probably the little variation in spin contamination values with respect to the expansion of the basis set. As those levels of spin contamination remain similar, the errors induced by spin contamination are conserved and cancel each other out in differences when the energy corrections are calculated. The use of PG3B3 corrects the energy for spin contamination. The overall PG3B3 energies are still based on 6-31G(d) UHF wave functions, which are highly contaminated. Equation 7.1 shows that the difference between PMP4 6-31G(d) and MP4 6-31G(d) energies is correlated to the $\langle S^2 \rangle$ values.

$$E[PMP4/6-31G(d)] - E[MP4/6-31G(d)] = -17.02\langle S^2 \rangle + 10.13 \quad R^2 = 0.88 \quad (7.1)$$

This allows partial cancellation of spin contamination errors in relative energies.

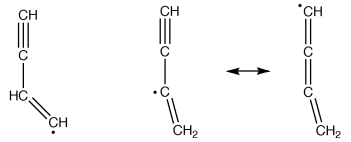

Figure 7.1: C_4H_3 isomers; left: n-C_4H_3; right: limit forms of i-C_4H_3.

Further correction is brought by introduction of the (QCI) correction which is, as shown by equation 7.2, correlated to $\langle S^2 \rangle$ values.

$$\Delta(QCI) = -18.06\langle S^2 \rangle + 10.47; \quad R^2 = 0.79 \tag{7.2}$$

The discussions in the present chapter are based on PG3B3 energies (ZPE excluded). Two C_4H_3 isomers are considered, the n-C_4H_3 and the resonantly stabilized i-C_4H_3 (see Figure 7.1). The relative energies obtained for those two isomers (9.73 kcal.mol^{-1}) are in reasonable agreement with the multi-reference (MRCI) calculations of Miller and Klippenstein[120] (11.70 kcal.mol^1) and with the data of Wheeler and coworkers [103] (11.80 kcal.mol^{-1}), indicating that the PG3B3 method provides good results on such systems.

7.1.4 Cycle formation from n-C_4H_3 +C_2H_2

Cycle formation from n-C_4H_3 + C_2H_2 is considered to proceed through linear C_6H_5 intermediates. The different steps leading to cycles are described in detail in the following subsections. Figure 7.2 presents those different reactions along with the structures and notations of the minima and the relative 0 K (ZPE included) PG3B3 energies of the different stationary points with respect to the energy of the phenyl radical. Those values, along with spin contamination data are provided in Table 7.1. Structures of the transitions states are shown in Figure 7.3.

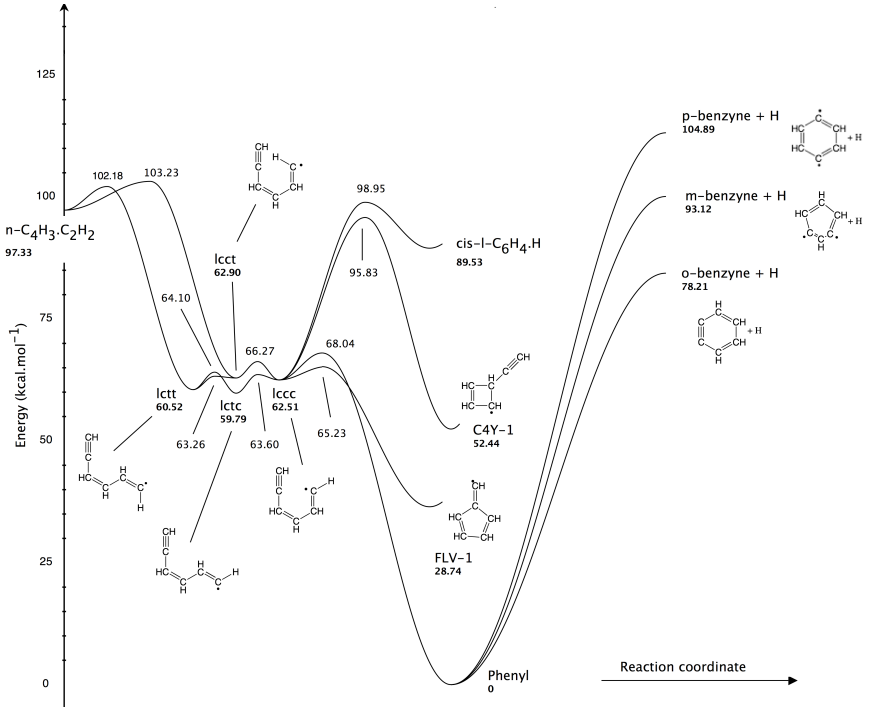

Figure 7.2: PG3B3 potential energy (ZPE) included profile for the formation of cyclic compounds from the addition of acetylene on n-C_4H_3. Energies are given in kcal.mol^{-1} relative to the phenyl radical. For clarity of the figure, hydrogen elimination from **lctc** has been omitted.

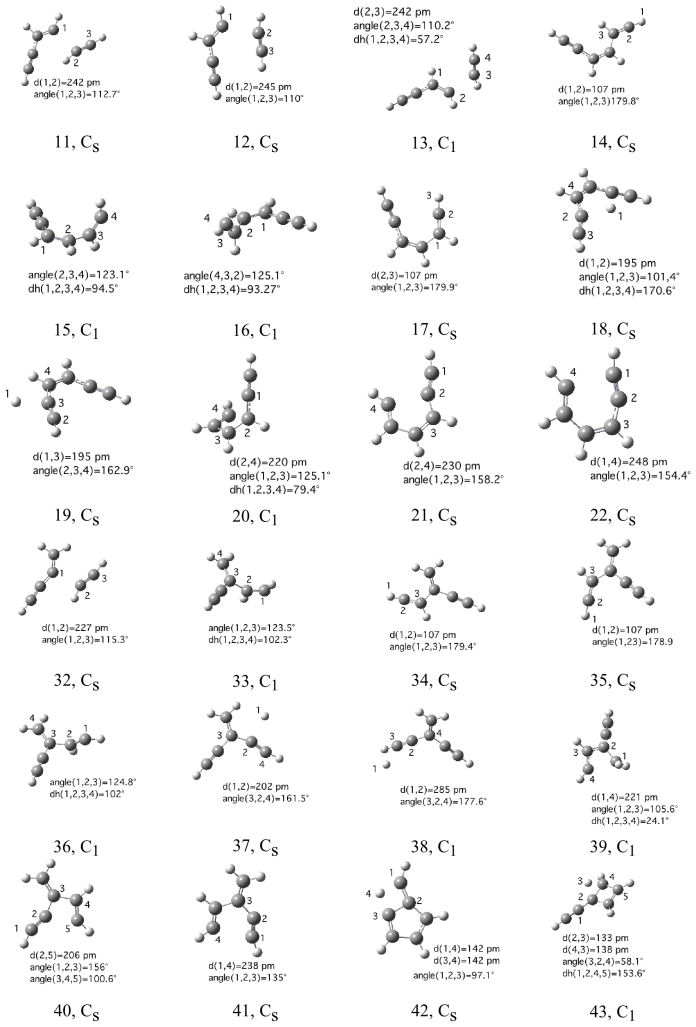

Figure 7.3: Structures of the different transition states located. Numbering corresponds to the entry numbering in Tables 7.1 and 7.2. d indicates a distance in pm, angle, a valence angle and dh a dihedral angle.

Bimolecular step

The addition of acetylene on the *n*-C_4H_3 radical may yield either *cis* or *trans* linear C_6H_5 radicals. This addition only leads to cycle formation if the resulting C_6H_5 has a *cis* configuration. As we are mostly interested in cycle formation, the addition on *n*-C_4H_3 (HCCH *cis*) is the preferred entrance channel. However, competition between the formation of *cis* and *trans* linear C_6H_5 has an influence on the rate of ring formation. For this reason, the formation of *trans* linear C_6H_5 from *n*-C_4H_3 + C_2H_2 was also considered. No further reactions were however considered in that direction. Two transition states, and therefore two entrance channels to the cis linear C_6H_5 region have been found. The first one leads to **lcct**, and shows an activation barrier of 3.62 kcal.mol^{-1}. This is little more than half the barrier proposed by Madden and coworkers (6.70 kcal.mol^{-1}) but relatively close to the one of Walch (4.63 kcal.mol^{-1}). However, this path is not the lowest energy channel. The second entrance channel shows a smaller activation barrier (2.5 kcal.mol^{-1}). This makes it the most probable path to the *cis* linear C_6H_5 sub-region. One transition state leading to compound **ltct** was found (not presented in Figure 7.2 to maintain clarity of the figure). The activation barrier for this step is 3.34 kcal.mol^{-1}. Despite careful analysis of the energy surface, no transition structure leading to **lttt** could be determined. All candidate geometries presented two imaginary frequencies, one corresponding to the C-C bond in formation, the other to the rotation around the latter bond. The pre-reaction van der Waals (vdW) complexes shows low stabilization (1.99 and 1.68 kcal.mol^{-1} for *n*-C_4H_3+C_2H_2 *cis* and *trans* complexes, respectively). Those stabilizations are probably a little underestimated due to spin contamination.

Cis linear C_6H_5.

Four conformers appear in the *cis* linear C_6H_5 (l-C_6H_5) sub-region. Among those four structures, only two are the direct product of acetylene addition on $n-C_4H_3$, **lctt** and **lcct**. Two types of conformational changes are considered in this section: the rotation of the terminal CH group around the axis of the C-C single bond and the *cis-trans* isomerization of the terminal radical site. As could have been expected, the rotations from **lct** conformers to **lcc** ones are endothermic steps. Their energy barriers remain however quite small. Energy barriers for cis-trans isomerization are 4.77 (**lctt** $\rightarrow$ **lctc** reaction) and 4.66 (**lcct** $\rightarrow$ **lccc** reaction) kcal.mol^{-1}. The last value is in relatively good agreement with the data of Walch (5.60 kcal.mol^{-1}) and those of Madden and coworkers (4.90 kcal.mol^{-1}) for the same configurational change. All the barriers in this sub region are below 5 kcal.mol^{-1}. The relative importance of the different barriers in this sub-region will strongly depend on the origin of the C_6H_5 radical. If the chemical activation is important, for example, if the C_6H_5 radicals come from an addition reaction, those barriers will be negligible. If the C_6H_5 originates from $\mathbf{FLV-1}$, the chemical activation of the radical will be similar to the energy barrier, and the reactions will be slower. From those different observations, one may expect that the degradation of the phenyl radical to n-C_4H_3 + C_2H_2 mainly occurs through **lctt** rather than **lcct**, as this last path is globally higher in energy.

Hydrogen elimination steps.

Hydrogen elimination reactions were considered from **lctc** and **lccc**. Efforts to locate transition states connecting the reactants to **lctt** and **lcct** were unsuccessful. Hydrogen elimination activation barrier from **lctc** (45.46 kcal.mol^{-1}) is greater than the one from **lccc** (41.83 kcal.mol^{-1}), probably due to the out of plane torsion in the transition state, imposed by the presence of the triple bond, which increases the energy of the transition state. The barrier for the elimination from **lccc** is very close to that proposed by Madden and coworkers (41.80 kcal.mol^{-1}). Wang and coworkers also considered the reaction and provided a relative energy for the elimination transition state of 97.60 kcal.mol^{-1}. These data include ZPE corrections and the authors do not specify whether this transition states correspond to the elimination from **lctc** or **lccc**. This difference in activation barriers only has a limited effect on the reverse activation barrier due to the difference in stability of **lccc** and **lctc**. Stabilization of the pre-reaction vdW complex in the case of C_6H_4.H (1.67 kcal.mol^{-1}) is similar to the ones observed in n-C_4H_3.C_2H_2 complexes.

Cyclisation steps

Cyclisation is only possible from **lccc**. This system has previously been considered by Madden and coworkers and Huang and coworkers [121] only to close into a six-membered ring. In this work, we consider the formation of four, five and six membered rings. The lowest energy cyclisation step is the formation of $\mathbf{FLV-1}$. The activation barrier for this step (3.17 kcal.mol^{-1}) is even lower than the barrier of the **lccc** $\rightarrow$ **lcct** conformational change.

Table 7.1: PG3B3 (ZPE included) relative energies (kcal.mol^{-1}) and spin contamination values

	n-C_4H_3 + C_2H_2	E(PG3B3)	$\langle S^2 \rangle_{DFT}$	$\langle S^2 \rangle_{UHF}$
1	n-C_4H_3.C_2H_2 (*cis*)	97.33	0.77	1.23
2	n-C_4H_3.C_2H_2 (*trans*)	97.85	0.77	1.23
3	**lctt**	60.52	0.77	1.57
4	**lctc**	59.79	0.77	1.56
5	**lcct**	62.90	0.77	1.59
6	**lccc**	62.51	0.77	1.58
7	**C4Y − 1**	52.44	0.78	0.97
8	**FLV − 1**	28.74	0.77	1.30
9	Phenyl radical	0.00	0.76	1.39
10	l-C_6H_4.H	89.53	0.75	1.43
11	TS(n-C_4H_3 + C_2H_2 *(cis)*→ **lctt**)	102.18	0.78	1.43
12	TS(n-C_4H_3 + C_2H_2 *(cis)*→ **lcct**)	103.23	0.78	1.45
13	TS(n-C_4H_3 + C_2H_2 *(trans)*→ **ltct**)	102.99	0.78	1.43
14	TS(**lctt** → **lctc**)	64.10	0.77	1.56
15	TS(**lctt** → **lcct**)	63.26	0.76	1.35
16	TS(**lctc** → **lccc**)	63.60	0.76	1.36
17	TS(**lcct** → **lccc**)	66.27	0.77	1.57
18	TS(**lctc** → l-C_6H_4 + H)	99.71	0.77	1.60
19	TS(**lccc** → l-C_6H_4 + H)	98.95	0.76	1.62
20	TS(**lccc** → **C4Y − 1**)	95.83	0.84	1.77
21	TS(**lccc** → **FLV − 1**)	65.23	0.78	1.49
22	TS(**lccc** → phenyl radical)	68.04	0.78	1.81

This barrier is also 1.29 kcal.mol^{-1} lower than the one proposed by Walch for this same step. The formation of the phenyl radical is more energy demanding (5.56 kcal.mol^{-1}). In this case, the obtained activation barrier compares quite well with the one of Madden and coworkers (5.60 kcal.mol^{-1}) but is smaller than the ones of Huang and coworkers (7.8 kcal mol^{-1}) and of Walch (7.30 kcal mol^{-1}). One could have expected that the formation of an aromatic ring shows the lowest activation barrier due to the formation of aromatic species. In the case of the formation of the phenyl radical, the length of the C-C bond in formation is 248 pm as compared to 140 pm for the corresponding bond in the phenyl radical. This important difference indicates that aromaticity is probably not installed, even partially, at the transition state. Furthermore, the formation of the phenyl radical requires bending of the triple bond towards the inside of **lccc**, which generates steric hindrance and electronic effects. It is not the case for the formation of the $\mathbf{FLV-1}$. The formation of the four-membered ring presents a 34.30 kcal.mol^{-1} energy barrier. This makes this ring the less probable cycle but its path remains lower in energy than the hydrogen elimination pathways to form *l*-C_6H_4. Considering cycle formation and hydrogen elimination from **lccc**, using the Boltzmann distribution, 69% of **lccc** will form $\mathbf{FLV-1}$ and 31% will form the phenyl radical at 1500 K. Contributions of the two other paths at this temperature are negligible.

Formation of benzyne cycles.

Hydrogen elimination from the phenyl radical has been considered to form *ortho-, para-* or *meta-* benzyne (*o-, p-, m*-C_6H_4). No transition structure or C_6H_4+H VdW complexes could be found for those steps. The results indicate a very flat transition region between the phenyl radical and benzyne compounds + H. This has already been mentioned in previous work for *o*-benzyne [114, 122]. It was also shown that the consideration of a single determinant wave function was inadequate to describe benzynes.[123][124]. The work of Wang and coworkers[115] using the CASSCF(7,7) 6-31G(d) method suggested relative energies of benzyne + H species (76.20, 91.60 and 106.90 kcal.mol^{-1} for *o-, m-* and *p*-benzyne respectively). Those values include ZPE correction and can be compared to our ZPE corrected values for those same compounds, which are 78.22, 93.12 and 115.65 kcal.mol^{-1}.Those energies make the decomposition to *m*-C_6H_4 energetically competitive to the degradation of *l*-C_6H_5 to *l*-C_6H_4 + H. The use of CASSCF MP2 6-31G(d) level of theory also allowed them to determine a reaction barrier for the addition of H on *o*-C_6H_4 which is claimed to be small (the exact data are not provided). From the different elements in their paper, we may estimate this barrier to be between 1 and 2 kcal.mol^{-1}.

7.1.5 Cycle formation from *i*-C_4H_3 + C_2H_2

Similar to the addition on *n*-C_4H_3, the addition on *i*-C_4H_3 is a multi-step process. The various reactions for cycle formation and hydrogen elimination following the addition of acetylene on *i*-C_4H_3 are presented in Figure 7.4 along with the relative energies at 0 K (ZPE included) of

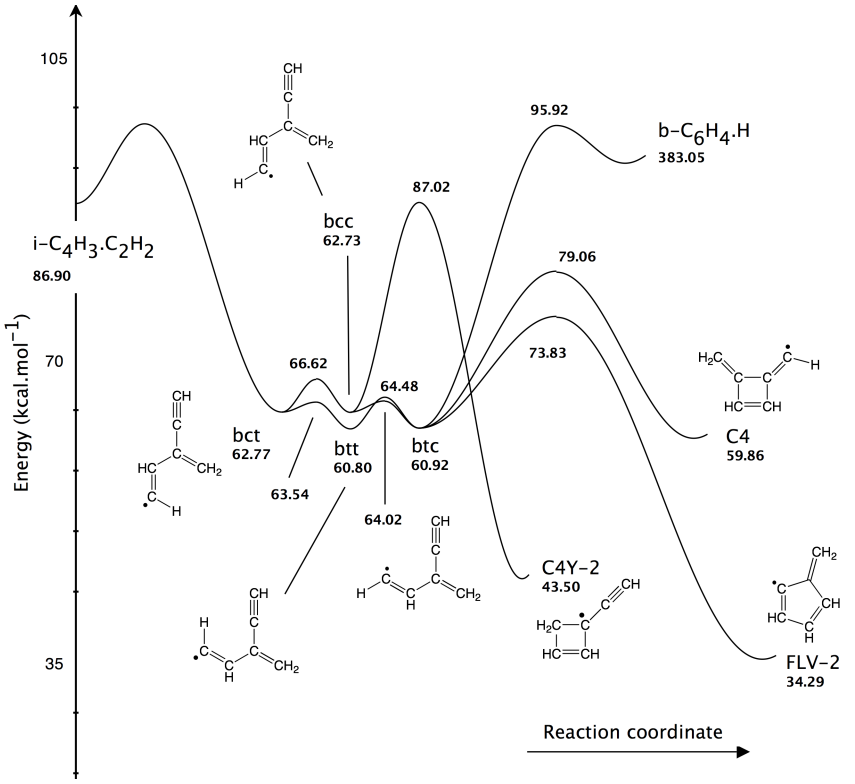

Figure 7.4: Potential energy profile for the formation of cyclic compounds from the addition of acetylene on i-C_4H_3. Energies are given relative to the energy of the phenyl radical. For the clarity of the figure, hydrogen elimination from **bcc** has been omitted.

the minima and transition states. Those values, along with spin contamination data are provided in Table 7.2 The structures of the transition states are given in Figure 7.3.

Bimolecular step.

Similar to the case of the formation of *trans* linear C_6H_5 radicals, only one entrance channel to the b-C_6H_5 sub-region could be found.

This path leads to the formation of **bct**. The search for a transition state leading by addition to **btt**, similar to that proposed by Walch, was unsuccessful. The structure proposed by Walch has two imaginary frequencies at the B3LYP 6-31G(d) level, and does not optimize to a transition state other than the one leading to **bct**. This may be due to a poor description of double and triple bonds in the structure determination, and therefore to poor description of the interaction between the triple bond and the approaching acetylene. As indicated in the Introduction, the activation barrier was previously considered to be too high for the i-C_4H_3 + C_2H_2 reaction to be a significant path for cycle formation. The value proposed by Walch is 10.71 kcal.mol^{-1}, which is more than twice his value for the addition of acetylene on n-C_4H_3. His activation barrier is quite higher than our 6.03 kcal.mol^{-1} activation barrier. In our work the two addition barriers (on i- and n-C_4H_3) are much closer to each other. This significant lowering in activation barrier indicates that the i-C_4H_3 + C_2H_2 path is not as energetically disfavored as previously expected and is in good agreement with the suggestion recently made by Hansen and coworkers [125] that Walch's activation barrier was probably too high. Therefore, the i-C_4H_3 + C_2H_2 reaction may have a more important role in cycle formation than supposed so far. Again, the pre-reaction vdW complex shows low stabilization.

Branched C_6H_5 sub-region.

The conformational changes taken into account in this section are similar to those considered in the l-C_6H_5 sub-region. In this sub-region, every conformational change is subject to a barrier much smaller than any cyclization or decomposition barrier. The barriers for those conformation and configuration changes are similar to those in the l-C_6H_5 sub-region. The barrier for the **btt** $\rightarrow$ **btc** reaction (5.07 kcal mol^{-1}) can be compared to the one proposed by Walch (5.8 kcal mol^{-1}). Hydrogen elimination steps. Similarly to the l-C_6H_5 surface, transition states could only be found for hydrogen elimination from conformers presenting the HCCH cis radical site configuration (**bcc** and **btc**). The barriers for those two elimination reactions are 42.68 and 40.82 kcal.mol^{-1} for elimination from **bcc** and **btt**, respectively. No comparison can be made with other data, as this is, to our knowledge, the first time that those barriers are reported. Stabilization of the vdW C_6H_4.H complex is 1.63 kcal.mol^{-1}, which is very similar to that of the l-C_6H_4.H complex.

Cyclisation steps.

Again, three cycles may be formed, two four-membered and one five-membered cycle. One four-membered ring **C4Y − 2** comes from **bcc** while the two others, **C4** and **FLV − 2** are formed from **btc**. The lowest cyclisation step is here also the fulvenyl radical formation. The formation of **C4Y − 2** and **C4** show activation barriers of 24.61 and 18.84 kcal.mol^{-1}, respectively. This difference may be explained by the fact that a new bond must be formed in **C4Y − 2**, with an sp^2 carbon rather than an sp one. This last cyclisation is however more exothermic

than the formation of **C4** because $\mathbf{C4Y-2}$ is resonantly stabilized and less strained than **C4**. The barrier for the formation of $\mathbf{FLV-2}$ (12.92 kcal.mol^{-1}) is somewhat lower than the value proposed by Walch for that reaction.

Hydrogen shifts

Connection between the two paths (n-C_4H_3 + C_2H_2 and i-C_4H_3 + C_2H_2) has been considered through the isomerization reactions of $\mathbf{C4Y-1}$ and $\mathbf{FLV-1}$ to $\mathbf{C4Y-2}$ and $\mathbf{FLV-2}$. Those two reactions consist in high-energy hydrogen shift but remain lower in energy than the i-C_4H_3 + C_2H_2 entrance transition state. Such reactions open a path from i-C_4H_3 + C_2H_2 to the phenyl radical. The obtained isomerization barrier of $\mathbf{FLV-1}$ to $\mathbf{FLV-2}$ equals 64.28 kcal.mol^{-1}, which is 4.32 kcal.mol^{-1} lower than the one proposed by Walch. The barrier for the $\mathbf{C4Y-1}$ to $\mathbf{C4Y-2}$ reaction is much smaller (46.93 kcal.mol^{-1}) and cannot be compared to any other similar data as, to our knowledge, it has never been described. The transition states of those two hydrogen shifts present high imaginary frequencies ($\mathbf{C4Y-1}\rightarrow\mathbf{C4Y-2}$: 2009 **i** cm^{-1}, $\mathbf{FLV-1}\rightarrow\mathbf{FLV-2}$: 2301 **i** cm^{-1}) implying important tunneling effects should occur. This has been accounted for in rate constant calculations. Such hydrogen shift reactions do open a path, which lies lower in energy than the entrance transition state, from i-C_4H_3 + C_2H_2 to the phenyl radical. The energy barriers of those reactions remain however quite high. In hydrogen rich conditions (rich flames) $\mathbf{FLV-2}$ (and $\mathbf{FLV-1}$) may hydrogenate by recombination with a hydrogen atom or by reaction with H_2. The first reaction is barrierless and we expect the second to have a barrier around 10 kcal.mol^{-1} (C_2H_3 + H_2

Table 7.2: PG3B3 (ZPE included) relative energies (kcal.mol^{-1}) and spin contamination values.

	i-C_4H_3 + C_2H_2	E(PG3B3)	$\langle S^2 \rangle_{DFT}$	$\langle S^2 \rangle_{UHF}$
23	i-C_4H_3.C_2H_2	86.90	0.78	1.46
24	**bcc**	62.73	0.77	1.54
25	**bct**	62.77	0.77	1.49
26	**btt**	60.83	0.77	1.50
27	**btc**	60.92	0.77	1.50
28	**C4Y − 2**	43.50	0.79	1.20
29	**C4**	59.86	0.77	1.63
30	**FLV − 2**	34.29	0.77	1.41
31	b-C_6H_4.H	91.54	0.75	1.33
32	TS(i-C_4H_3 + C_2H_2→ **bct**)	96.10	0.79	1.71
33	TS(**bct** → **btt**)	63.54	0.76	1.36
34	TS(**bct** → **bcc**)	66.62	0.77	1.54
35	TS(**btt** → **btc**)	64.48	0.77	1.49
36	TS(**bcc** → **btc**)	64.02	0.76	1.36
37	TS(**bcc** → b-C_6H_4 + H)	96.36	0.76	1.51
38	TS(**btc** → b-C_6H_4 + H)	95.92	0.76	1.41
39	TS(**bcc** → **C4Y − 2**)	87.02	0.82	1.72
40	TS(btc→ **C4**)	79.06	0.79	1.79
41	TS(btc→ **FLV − 2**)	73.83	0.8	1.55

Table 7.3: PG3B3 (ZPE included) relative energies (kcal.mol^{-1}) and spin contamination values.

	Hydrogen shifts	E(PG3B3)	$\langle S^2 \rangle_{DFT}$	$\langle S^2 \rangle_{UHF}$
42	TS(**FLV − 1 → FLV − 2**)	91.39	0.78	1.51
43	TS(**C4Y − 1 → C4Y − 2**)	96.88	0.76	1.06
	Non-interacting fragments			
44	*n*-C_4H_3 (HCCH cis) + C_2H_2	98.90	0.77	1.24
45	*n*-C_4H_3 (HCCH trans) + C_2H_2	98.88	0.77	1.24
46	*i*-C_4H_3 + C_2H_2	88.16	0.78	1.46
47	*l*-C_6H_4 + Hd	92.18	-	-
48	*b*-C_6H_4 + H	95.94	-	-
49	*o*-C_6H_4 + H	78.21	-	-
50	*m*-C_6H_4 + H	93.12	-	-
51	*p*-C_6H_4 + H	104.89	-	-

C_2H_4 + H; E_a =10.40 kcal.mol^{-1}), phenyl + H_2 C_6H_6 + H; E_a = 8.80 kcal.mol^{-1}) [126]. Formation of a first aromatic ring from *i*-C_4H_3+C_2H_2 may therefore occur through the formation of fulvene and its isomerization according to the different mechanisms available [127].

7.1.6 Rate constants

Conventional transition state theory rate constants have been computed between 300 and 3000 K (with 100 K intervals) and are presented in Table 7.4, under the modified Arrhenius equation form. The data concerning hydrogen shift reactions is provided with Eckart tunneling corrections. Those rate constants have been computed using the PG3B3 energies.

Table 7.4: Rate constants for all the steps appearing in this work. Units for bimolecular rate constants are $cm^3mole^{-1}s^{-1}$ and s^{-1} for unimolecular ones. Hydrogen shift reactions include Eckart tunneling corrections.

	forward			reverse		
reaction	A	n	E_a/R	A	n	E_a/R
n-C_4H_3+C_2H_2→ **lctt**	2.91E-21	2.484	1190.59	3.67E+13	0.627	21847.6
n-C_4H_3+C_2H_2→ **lcct**	1.08E-20	2.489	1752.85	1.26E+14	0.627	21202.1
n-C_4H_3+C_2H_2→ **ltct**	7.43E-21	2.476	1668.28	3.54E+13	0.604	20712.4
lctt → **lcct**	3.85E+12	0.055	1503.81	3.58E+12	0.05	296.138
lcct → **lccc**	6.33E+12	0.178	2017.32	8.02E+12	0.144	2204.39
lctc → **lccc**	4.82E+12	0.053	2097.57	4.42E+12	0.035	707.547
lctt → **lctc**	6.18E+12	0.166	2122.52	7.94E+12	0.146	2491.95
lccc →phenyl radical	1.19E+12	-0.008	2761.28	4.17E+12	0.694	35016
lccc → **FLV − 1**	1.36E+12	0.072	1431.79	9.58E+12	0.432	19001.7
lccc → **C4Y − 1**	1.07E+12	0.158	16844	5.39E+12	0.195	22128.4
lctc →l-C_6H_4 + H	2.75E+11	0.938	20593.9	1.16E-15	1.464	4043.44
lccc →l-C_6H_4 + H	5.63E+11	0.911	18861.2	2.578E-15	1.457	3700.76
i-C_4H_3+C_2H_2→ **bct**	8.82E-22	2.365	3248.84	7.69E+13	0.521	17516.9
bct → **bcc**	1.88E+13	0.179	2285.34	3.55E+02	3.741	5843.51
bct → **btt**	2.66E+12	0.022	658.46	4.16E+12	0.04	1683.17
bcc → **btc**	4.40E+01	3.615	4275	4.33E+12	0.044	1696.48
btt → **btc**	4.16E+12	0.04	1683.17	2.66E+12	0.022	658.46
bcc → **C4Y − 2**	8.09E+11	0.049	12190.9	3.65E+12	0.275	2.22
btc → **FLV − 2**	1.52E+12	0.012	6446.97	3.29E+12	0.5	20444.3
btc → **C4**	2.17E+12	0.092	9226.39	7.17E+12	0.313	10149
bcc →b-C_6H_4+H	1.75E+11	0.887	19306.1	2.021E-15	1.443	3339
btc →b-C_6H_4+H	1.49E+12	0.953	18265.2	6.397E-15	1.482	1308.46
FLV − 1 → **FLV − 2**	1.54E-18	8.755	1.85E+04	7.677E-19	8.855	15650
C4Y − 1 → **C4Y − 2**	2.20E-06	5.227	15507.9	1.481E-06	5.65	19411.9

7.1.7 Conclusions on the surface analysis

In this work, a modified G3B3 method, using spin-projected basis set corrections, has been used to describe the different reactions following the addition of acetylene on C_4H_3 radicals. When possible, energy barriers were compared to previously calculated data. The formation of four- to six-membered rings was considered from the addition of acetylene on n-C_4H_3 and i-C_4H_3 radicals. New addition transition states of lower energies were located for both addition reactions, leading to energy paths globally lower than usually expected. The consideration

of four-membered cycles in addition to the dehydro-fulvene and phenyl ones are shown to be energetically competitive to hydrogen elimination reactions. Two hydrogen shifts reactions are opening pathways from *i*-C_4H_3 + C_2H_2 to the phenyl radical. However, those reactions are not thought to be the main source of 6-membered cycles, at least in rich flames. Spin contamination issues were discussed and comparison with other theoretically obtained data leads to conclude that PG3B3 is a reliable level of theory for the systems concerned. For common steps, good agreement is observed between our work and the one of Madden and coworkers, despite the important spin contamination levels present in our UHF wave functions. This indicates that PG3B3 (and G3B 3) has performance similar to RHF based methods on those systems. This also supports our hypothesis on the spin contamination correction role of the $\Delta(QCI)$ correction. For a number of steps, comparison has been made with the work of Walch. Systematically, the energy barriers presented in this work are found to be lower than those suggested by Walch. Finally, we provide the rate constants for each step considered, computed on the basis of the conventional transition state theory including Eckart tunneling corrections for the hydrogen transfer reactions.

7.2 Isomerization of dehydrofulvene radicals

If the description of the C_6H_5 potential energy surface is limited to what has been presented in the previous section, the isomerization of **FLV − 1** to the phenyl radical can only be considered as going through cycle opening and closing therefore presenting the transition state for **lccc** → phenyl radical as highest energy point on the isomerization path. Similarly, the isomerization of **FLV − 2** to the phenyl radical can also only be

M.1.

M.2.

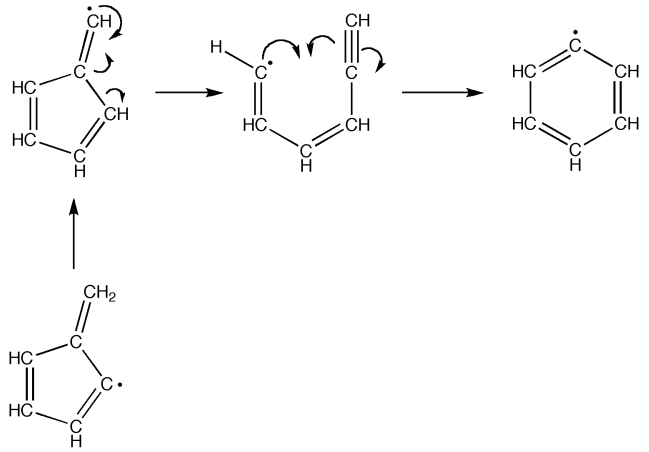

Figure 7.5: Mechanism M.1. and M.2 for isomerization of $\mathbf{FLV-1}$ and $\mathbf{FLV-2}$ to the phenyl radical.

considered to first go through an hydrogen transfer reaction producing $\mathbf{FLV-1}$ followed by the ring opening and closing mechanism (see Figure 7.5). In both cases, the mechanisms involve highly activated steps, which are the ring opening and the hydrogen transfer reactions. In this section, we describe isomerization mechanisms which do not go through an acyclic system. The aim is to study the possibility of a lower energy mechanism for unimolecular isomerization of dehydrofulvene radicals to the phenyl radical.

7.2.1 Results an discussion

Spin contamination

As all other systems on the C_6H_5 energy surfaces, the different stationary points found on the reaction path present important level of UHF spin contamination. On average, the UHF $\langle S^2 \rangle$ value is 1.34 with a 0.14 standard deviation. The $\langle S^2 \rangle$ values for $\mathbf{BC-2}$ are the lowest

observed on the C_6H_5 surface so far (average $\langle S^2 \rangle$=1), Again, the difference between PMP4 6-31G(d) and MP4 6-31G(d) energies is correlated to the extent of the spin contamination by equation 7.3, providing a first cancelation linked to similar spin contamination levels.

$$E(PMP4) - E(MP4) = -16.18\langle S^2 \rangle + 9.06 \quad R^2 = 0.86 \tag{7.3}$$

The magnitude of the Δ (QCI) correction is also correlated to the value of $\langle S^2 \rangle$.

$$\Delta(QCI) = -22.55\langle S^2 \rangle + 16.50 \quad R^2 = 0.94 \tag{7.4}$$

isomerization mechanism

Figure 7.6 shows the PG3B3 energy profile (at 0 K, ZPE included) from the two isomerization mechanisms (from $\mathbf{FLV-1}$ and $\mathbf{FLV-2}$ to the phenyl radical). Those energies are given in kcal.mol^{-1} relative to the energy of the phenyl radical to allow easier comparison with the work of the previous section. Table 7.5 provides relative G3B3 and PG3B3 energies along with the ZPEs. The isomerization of $\mathbf{FLV-1}$ goes through the formation of a resonantly stabilized bicyclic radical ($\mathbf{BC-1}$). The bridge bond of this system is then broken to form the phenyl ring. This mechanism is referred to as M.1.2. isomerization of $\mathbf{FLV-2}$ also involves a resonantly stabilized bicyclic systems ($\mathbf{BC-2}$) which has to undergo intramolecular hydrogen transfer to form $\mathbf{BC-1}$. This mechanism is referred to as M.2.2. Mechanism M.1.2 is analogous to the mechanism of isomerization of 1-methenyl-2,4-cyclopentadiene radical (C_6H_7A in section 6.3) to the cyclohexadienyl radical and also to the mechanism of isomerization of fulvene to benzene [127, 23]. The isomerization of $\mathbf{FLV-2}$ requires an hydrogen transfer reaction, whichever the

Table 7.5: G3B3 and PG3B3 relative energies of the different species appearing on the isomerization mechanism. Energies are given relative to the energy of the phenyl radical (kcal.mol^{-1}).

minima	ZPE	G3B3+ZPE	PG3B3+ZPE
FLV − 1	51.12	28.77	28.74
FLV − 2	51.48	34.22	34.29
BC − 1	50.13	56.10	55.52
BC − 2	50.10	63.08	62.48
Phenyl radical	52.79	0.00	0.00
Transition states			
TS (**FLV − 1** → **BC − 1**)	49.95	58.46	58.30
TS (**FLV − 2** → **BC − 2**)	50.26	74.88	74.63
TS(**BC − 1** → **BC − 2**)	47.51	88.96	89.41
TS(**BC − 1** →Phenyl radical)	49.43	59.95	59.39

considered mechanism. **FLV − 2** can also directly isomerize to **FLV − 1** through hydrogen transfer, and then follow mechanism M.1.2. This path is however higher in energy as the hydrogen transfer step corresponds to the maximum energy point of the M.2. mechanism (See figure 7.6) As indicated on figure 7.6, the isomerization mechanisms of **FLV − 1** and **FLV − 2** through bicyclic intermediates lie lower in energy than M.1. or M.2. respectively. Structures and key geometric parameters of the transition states are given on Figure 7.7. Very little comparison can be made as this mechanism has never been studied (to the best of my knowledge). We can however compare the results with analog mechanisms. Formation of bicyclic systems from fulvene derivatives has already been considered. Energy barriers for the formation of a bicyclic system from fulvene and C_6H_7A are 74.30 and around 7.39 kcal.mol^{-1} respectively. The first is much higher than our barrier due to the out of

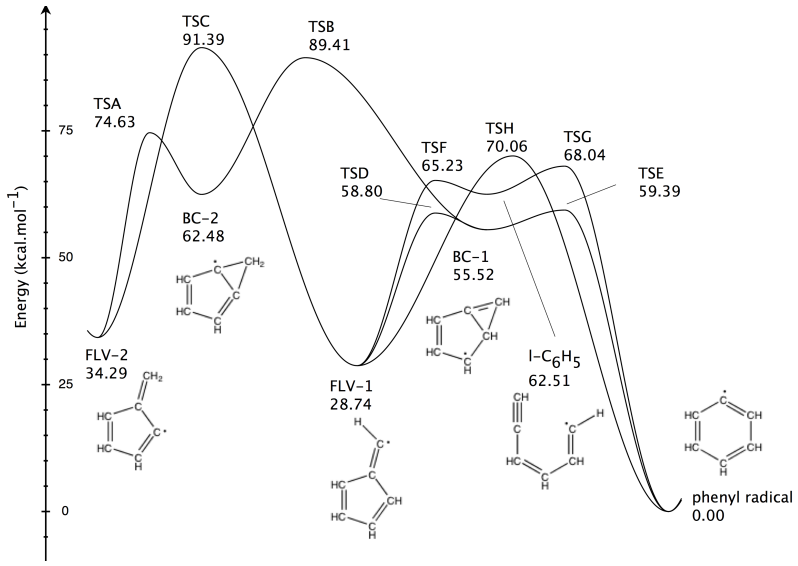

Figure 7.6: Mechanism of isomerization of dehydrofulvene radicals to the phenyl radical. **TSC** corresponds to the 1,3 hydrogen shift from $\mathbf{FLV-2}$ to $\mathbf{FLV-1}$ from the previous sections and **TSF** and **TSG** are also taken from the previous section and presented here for comparison purposes.

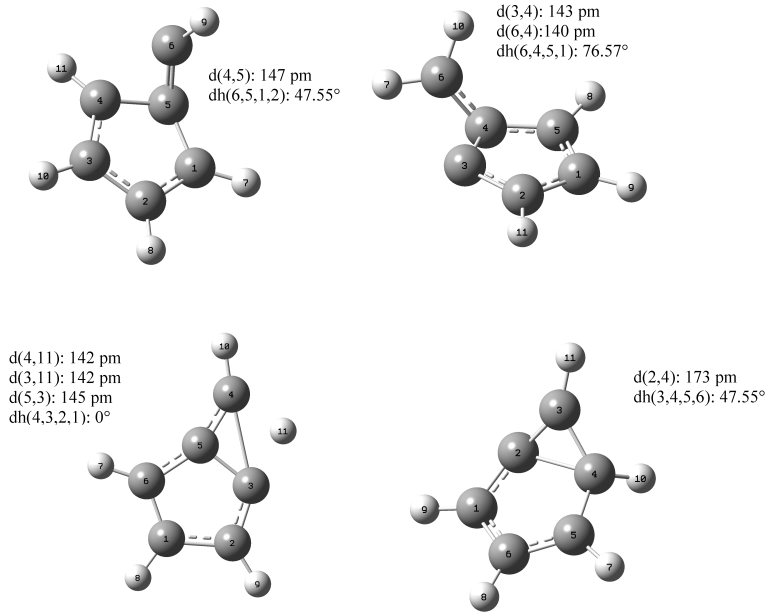

Figure 7.7: Structure of the transition states appearing in the isomerization mechanisms.

plane twisting of the *exo* double bond. The second barrier is lower, as no double bond is twisted, the CH_2 radical site is already out of plane in the reactants geometry. The opening of the bicyclic system to a six-membered ring can also be compared. The barrier for the opening of the C_6H_6 bicyclic to cyclohexadiene carbene is 33.00 kcal.mol^{-1}. The opening of the C_6H_7 bicyclic system is 14.56 kcal.mol^{-1}. Opening of $\mathbf{BC-1}$ to the phenyl radical is much lower (3.86 kcal.mol^{-1}). What comes out of those comparison is that the different mechanisms, while formally very similar, actually differ very importantly from an energetical point of view. Therefore, any rate constant based on analogy should be carefully examined before its use can be considered.

Table 7.6: Arrhenius parameters for the elementary reactions rate constants. Units are s^{-1}.

Reaction	A	n	E_a/R
FLV − 1 → **BC − 1**	4.68E+11	0.444	1.41E+04
BC − 1 → **FLV − 1**	2.16E+12	0.26	7.33E+02
FLV − 2 → **BC − 2**	6.55E+08	1.358	2.57E+04
BC − 2 → **FLV − 2**	1.19E+13	-0.076	6.29E+03
BC − 1 → **BC − 2**	5.51E-04	4.813	1.01E+04
BC − 2 → **BC − 1**	1.45E-03	4.572	7.40E+03
BC − 1 → phenyl radical	1.36E+12	0.367	1.18E+03
Phenyl radical → **BC − 1**	1.47E+11	0.894	2.93E+04
FLV − 1 →phenyl radical	6.07E+12	0.07	3.58E+4
Phenyl radical → **FLV − 1**	3.96E+12	0.38	3.58E+4

Table 7.6 presents the Arrhenius parameters for all elementary steps on the isomerization mechanism.

Single step isomerization of FLV − 1 to the phenyl radical A single step mechanism for the isomerization of **FLV − 1** to the phenyl radical also exists. This corresponds to reaction a.2 on Figure 7.8. Due to the symmetry of the system considered, the difference between the products of the different isomerization mechanisms does not appear clearly. Therefore, Figure 7.8 presents the reaction from a deuterated **FLV − 1**. It then appears that the multistep mechanisms (going through **BC − 1** or *l*-C_6H_5 provide the phenyl radical deuterated in *meta* position with respect to the radical site while the single step mechanism provides a *para* deuteration. The transition state for this single step mechanism is higher than the highest energy points of the two other

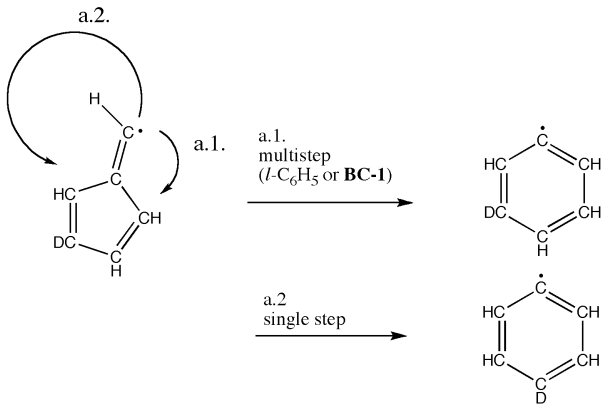

Figure 7.8: Difference between the products of the various isomerization reactions.

mechanisms. Finally, as the latter transition state has only been detected after the completion of the combustion modeling part of this work. This reaction path is therefore not included in the combustion mechanism.

7.3 Determination of global rate constants

The previous sections have described the mechanism in much details. Along with the mechanistic information, transition state theory rate constants have been provided for each elementary reaction. Each step can however not be introduced in the kinetic models. Such a mechanism is indeed over-detailed. A solution would be to completely detail the rest of the mechanism, but this would lead to a huge number of reactions and chemical species. For those reasons the mechanisms have to be simplified in order to determine global rate constant for the reactions. A first simplification is the replacement of the four *l*- or *b*-C_6H_5 radicals by one single system having the averaged properties of the original four. This

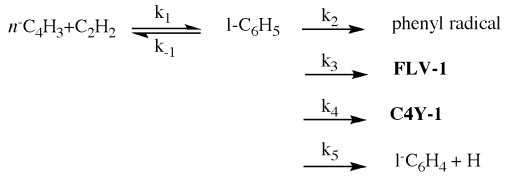

Figure 7.9: Reaction scheme for the determination of the global rate constants for the *n*-C_4H_3+ C_2H_2 reaction.

is done using equilibrium distribution as weighing factor. In the present case, this approximation is not absolutely correct as the activation barrier for the cyclisation of **lccc** to $\mathbf{FLV-1}$ is smaller than the one of $\mathbf{lccc} \rightarrow \mathbf{lcct}$. In this situation, the weighted rate constant $k_{i,weighted}$ for a elementary reaction having a k_i rate constant from a C_6H_5 reactant R_i is given by equation 7.5, in which χ_i is the weight of reactant i in the equilibrium distribution.

$$k_{i,weighted} = \chi_i k_i \tag{7.5}$$

This allows rewriting the mechanism in a more compact way.

7.4 *n*-C_4H_3+ C_2H_2 reaction

The weighted rate constants are used in the scheme presented on Figure 7.9 to obtain the rate constants for the formation of the phenyl radical, $\mathbf{FLV-1}$, $\mathbf{C4Y-1}$ and C_6H_4 + H from the addition of acetylene on the *n*-C_4H_3 radical. In this scheme, quasi-stationarity is considered for the *l*-C_6H_5 radical. The rate of formation of a product i product is given by equation 7.6

$$k_{i,global} = \frac{k_1 k_i}{k_{-1} + k_2 + k_3 + k_4 + k_5} \tag{7.6}$$

Example In order to be clear on how the rate constants are obatined, the methodology is applied to the rate of formation of $\mathbf{FLV-1}$ and details are given. Considering Figure 7.9, the rate of formation of $\mathbf{FLV-1}$ is given by

$$k_{FLV-1} = k_3[l - C_6H_5] \tag{7.7}$$

As only **lccc** can close into a cyclic system, the rate constant k_3 is actually the rate constant of the $\mathbf{lccc \rightarrow FLV-1}$ reaction multiplied by the weight of **lccc** in the equilibrium distribution. Considering quasi stationarity for l-C_6H_5, leads to

$$\frac{d[l - C_6H_5]}{dt} = 0 \tag{7.8}$$

And, if the scheme of Figure 7.9 is considered, this leads to

$$\frac{d[l - C_6H5]}{dt} = k_1[n\text{-}C_4H_3][C_2H_2] - (k_{-1} + k_2 + k_3 + k_4 + k_5) = 0 \tag{7.9}$$

And therefore,

$$k_{FLV-1} = \frac{k_1 k_3}{k_{-1} + k_2 + k_3 + k_4 + k_5} \tag{7.10}$$

Rate constants for the elementary steps were obtained between 300 and 3000 K. The determination of the global rate constants combines those data, leading, in some cases to non-linear Arrhenius plots. For those,

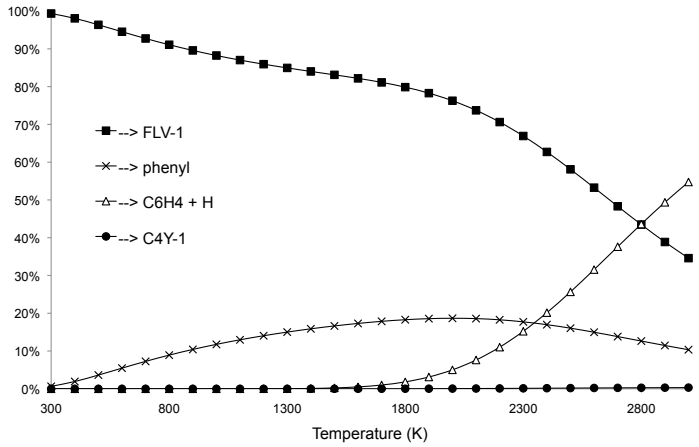

Figure 7.10: Product distribution for the n-C_4H_3+C_2H_2 reaction, according to Figure 7.9.

a single rate expression cannot cover the important temperature domain. For those reasons, the following rate constants were determined between 1000 and 2000 K, which is the temperature domain of interest for combustion processes. As those rate constants may be quite valid for lower temperature, they should not be considered for higher ones, as the non linearity effects principally appears at high temperature. Table 7.7 provides the Arrhenius parameters for all the global rate constants considered in this section. Figure 7.10 presents the reaction product distribution. It clearly shows $\mathbf{FLV-1}$ is the major reaction product, even at very high temperature. It also shows that the proportion of the phenyl radical in the products is at most 20%. The formation of C_6H_4 system becomes important at very high temperature (at temperature $\geqslant$ 1800 K). Finally, there does not seem to be any $\mathbf{C4Y-1}$ formed. Comparison with the rate constants obtained by Madden and coworkers [114] and Westmoreland and coworkers [26] can be made. Those comparisons are carried out in term of Arrhenius plots and are presented

Table 7.7: Arrhenius parameters for the global rate constants for the n-C_4H_3 + C_2H_2 reaction. Units are $cm^3mole^{-1}s^{-1}$.

n-C_4H_3 + C_2H_2	A	n	E_a/R
$\rightarrow$ **FLV − 1**	1.93E+15	-0.82	5460.19
$\rightarrow$ **C4Y − 1**	9.79E+16	-1.24	21577.77
$\rightarrow$ C_6H_4 + H	2.67E+16	-0.33	23529.97
$\rightarrow$ phenyl radical	1.02E+15	-0.84	6703.10

on Figure 7.11. This figure shows that our rate constant is inferior to the two others. The reason is quite simple. The rate constant of Madden and coworkers and of Westmoreland and coworkers have been established using schemes similar to that presented on Figure 7.9; however, not considering the formation of **FLV − 1**. The rate constant of the latter reaction is present in the denominator of equation 7.6, and it lowers all the rate constant obtained. Indeed, if the rate constant of the reaction forming **FLV − 1** is removed from that denominator, the agreement with the data of Westmoreland and coworkers is much better. The value from Madden and coworkers is greater the two others, with an important non linearity.

Cis linear C_6H_4 + H reaction

The addition of an hydrogen atom on linear *cis* C_6H_4 is considered. The most likely products are the phenyl radical and **FLV − 1**. At high temperature, we expect the formation of n-C_4H_3+ C_2H_2 to become significant. The product distribution is given on Figure 7.12 . Due to the similar energy levels of n-C_4H_3+C_2H_2 and C_6H_4 + H, the distribution profiles are very similar to those observed on Figure 7.10.

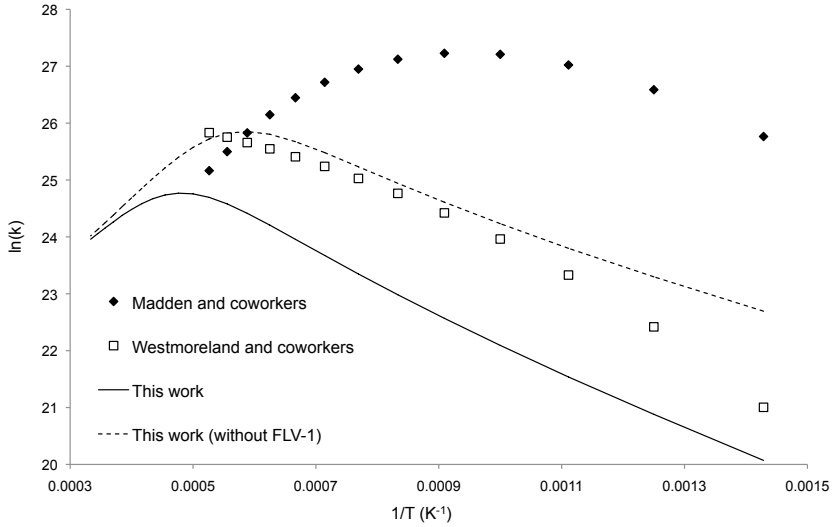

Figure 7.11: Arrhenius plots for the rate constant of the formation of the phenyl radical from the n-C_4H_3 + C_2H_2 reaction.

Table 7.8 presents the Arrhenius parameters for the rate constants considered in this section.

Table 7.8: Arrhenius parameters for the global rate constants for the l-C_6H_4 + H reaction. Units are $cm^3mole^{-1}s^{-1}$.

l-C_6H_4 + H	A	n	E_a/R
$\rightarrow$ **FLV − 1**	3.59E+12	0.53	4354.81
$\rightarrow$ **C4Y − 1**	3.24E+38	-6.66	29679.94
$\rightarrow$ n-C_4H_3 + C_2H_2	3.90E+14	1.12	2403.32
$\rightarrow$ phenyl radical	2.25E+12	0.49	563.35

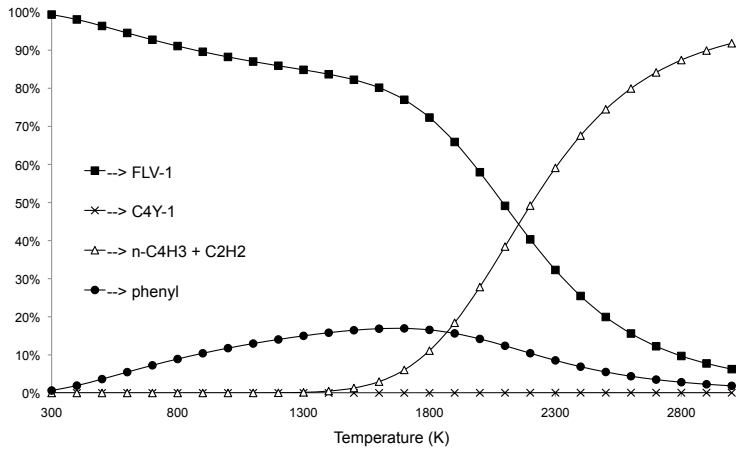

Figure 7.12: Product distribution for the *l*-C_6H_4+H reaction.

7.5 *i*-C_4H_3 + C_2H_2 reaction

The same simplifications have been brought to the mechanism of addition of acetylene on *i*-C_4H_3. Those assumption are more valid in this case as the barriers for the conformational changes are all smaller than the others. The Arrhenius expression for the global rate constants are given in Table 7.9. The *i*-C_4H_3+ C_2H_2 reaction product distribution is shown on Figure 7.13. Due to qualitatively similar energy profiles, the product distribution profile are similar to that of the acetylene addition on *n*-C_4H_3.

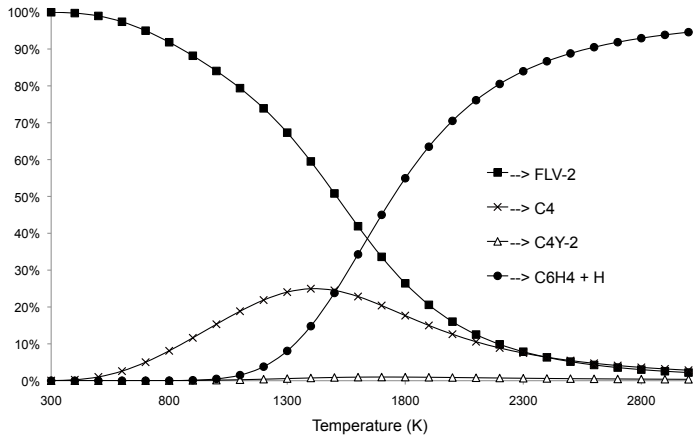

Figure 7.13: Product distribution for the i-C_4H_3 + C_2H_2 reaction.

Table 7.9: Arrhenius parameters for the global rate constants for the i-C_4H_3 + C_2H_2 reaction. Units are $cm^3mole^{-1}s^{-1}$.

	A	n	E_a/R
$\rightarrow$ **FLV − 2**	2.08E+48	-10.89	16881.94
$\rightarrow$ **C4**	2.22E+48	-10.75	19614.28
$\rightarrow$ **C4Y − 2**	9.50E+47	-10.74	23493.87
$\rightarrow$ b-C_6H_4+ H	3.21E+48	-9.96	28854.38

At low temperature, the formation of the dehydrofulvene radical dominates. There is a peak of **C4** (which correspond to the second lowest barrier) at round 20 %. Finally, due to globally higher activation barriers for the cyclisation steps, the formation of b-C_6H_4 + H starts at lower temperatures.

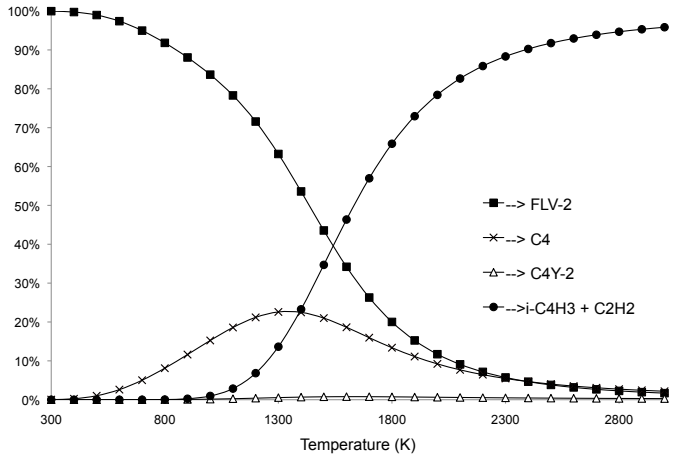

Figure 7.14: Product distribution for the b-C_6H_4 + H reaction.

Table 7.10: Arrhenius parameters for the global rate constants for the b-C_6H_4 + H reaction. Units are $cm^3mole^{-1}s^{-1}$.

b-C_6H_4+ H	A	n	E_a/R
$\rightarrow$ **FLV − 2**	2.50E+54	-11.65	14872.67
$\rightarrow$ **C4**	5.18E+54	-11.59	17716.33
$\rightarrow$ **C4Y − 2**	2.51E+54	-11.59	21616.78
$\rightarrow$ i-C_4H_3 + C_2H_2	5.90E+57	-11.59	27516.87

7.6 *b*-C_6H_4 + H reaction

The Arrhenius expression for the global rate constants are given in Table 7.10. The product distribution of this reaction is given on Figure 7.14. Again, the profile of this distribution is very similar to that observed for the acetylene addition reaction (see Figure 7.13). It is almost identical to that of the addition of acetylene on i-C_4H_3. As was also noted for the other cases, the formation of **C4Y** species is negligible, whatever the temperature.

7.7 Phenyl decomposition to *o*-benzyne +H

7.7.1 Finding a transition structure

The information acquired by the analysis of the potential cyclization paths on the C_6H_5 energy surface may be used to obtain kinetic data; it has been done for almost all elementary steps on this surface. There is however the issue of the formation of *o*-benzyne from the phenyl radical, for which no transition state has been located. To obtain a rate constant on the basis of transition state theory or any post-TST theory, one must have some kind of transition state structure as well as vibrational information.

Methodology

The reaction path is approximated by the C-H bond stretch of the breaking bond. This parameter is scanned from equilibrium geometry of phenyl (1.082 Å) to 3 Å by steps of 0.1 Å while optimizing all other structural parameters. Each of those structure are used to compute PG3B3 energies and generate a PG3B3 scan of the C-H stretch. The thermal correction to Gibbs free energy are obtained at different temperatures (from 300 K to 2500 K by steps of 200 K) to turn the PG3B3 scan into a Gibbs free energy surface. At each temperature, a parabola is fitted on the three highest Gibbs free energies to refine the C-H bond length corresponding to the transition state structure. The C-H bond length is then set at those new value, and the structure is re optimized at the B3LYP 6-31G(d) level. This is followed by other PG3B3 calculations to obtain our temperature dependent transition state structures.

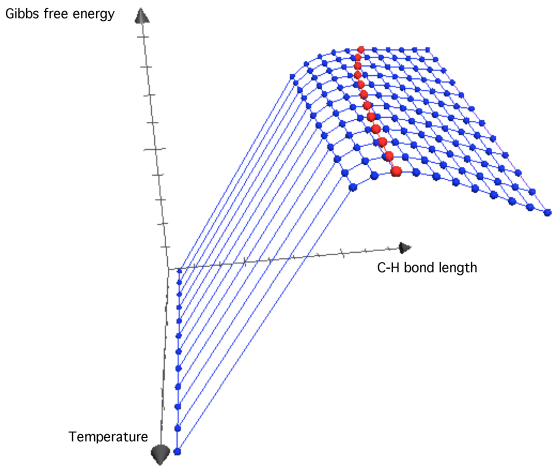

Figure 7.15: Gibbs free energy as a function of the temperature and of the breaking C-H bond length (Å). Red dots represent the maxima of Gibbs free energy.

As can be seen on Figure 7.15 , the C-H bond length at the maximum Gibbs free energy grows smaller as the temperature rises.

Rate constants

The rate constant for the reaction is obtained by applying the classical expression of transition state theory and by using a different transition state at each temperature. The expression of the rate constant obtained from the Arrhenius plot is

$$k = 8.5.10^{+14} exp(\frac{43327.16}{T}) \tag{7.11}$$

No modified Arrhenius expression has to be used in this case as the data presents a good linear behavior.

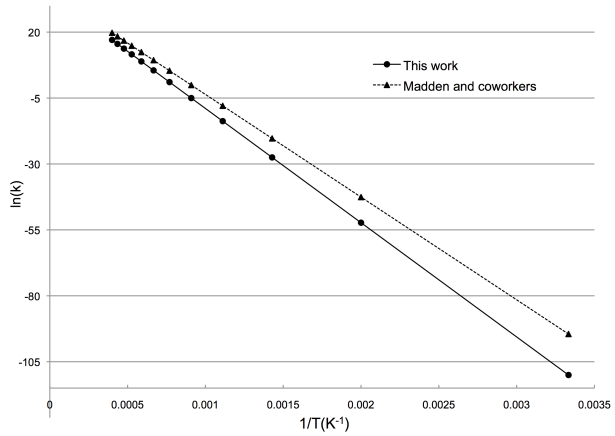

Figure 7.16: Arrhenius plot for the rate constant for the decomposition of the phenyl radical to *o*-benzyne + H.

As shown on Figure 7.16 it can be compared to that obtained by Madden and coworkers. Our rate constant is much lower at low temperature due to the difference in activation energy (8.7 kcal.mol^{-1}).

7.8 Rate constants for the isomerization of dehydrofulvene radicals

The rate of isomerization of $\mathbf{FLV-1}$ to the phenyl radical has been calculated using the scheme shown on Figure 7.17. Quasi stationarity has been considered for $\mathbf{BC-1}$. The rate constant for the hydrogen shift reaction has been added to the denominator to account for the potential competition of the isomerization to $\mathbf{FLV-2}$. The rate for the isomerization of $\mathbf{FLV-1}$ to the phenyl radical can be compared to the rate obtained from the mechanism going through **lccc** (see Figure 7.18). The rate parameters are given in Table 7.11. The reaction through the formation of $\mathbf{BC-1}$ is clearly faster, as could be expected from Figure

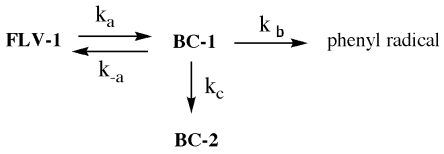

Figure 7.17: Reaction scheme used for the determination of the global rate constant for the isomerization of $\mathbf{FLV-1}$ to the phenyl radical through $\mathbf{BC-1}$.

Table 7.11: Arrhenius parameters for the global rate constants of isomerization to the phenyl radical. Units are s^{-1}.

Mechanism	A	n	E_a/R
through **lccc**	1.16 E+14	0	8150.75
through $\mathbf{BC-1}$	1.17E+13	0	5953.48

7.18. Isomerization of $\mathbf{FLV-2}$ is a little more complex. The rate limiting step is obviously the formation of $\mathbf{BC-1}$. However, once $\mathbf{BC-1}$ is formed, the phenyl radical formation is still in competition with the formation of $\mathbf{FLV-1}$. The rate of formation of $\mathbf{BC-1}$ from $\mathbf{FLV-2}$ is calculated considering a scheme similar to the one presented on Figure 7.17. The rate is then multiplied by the selectivity factor to obtain the rate of isomerization to $\mathbf{FLV-1}$ and to the phenyl radical.

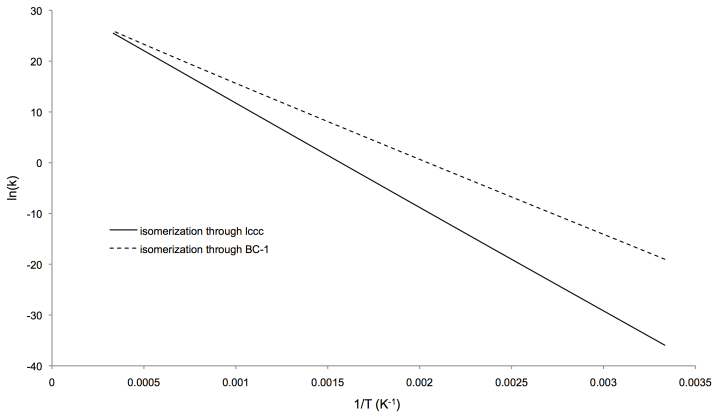

Figure 7.18: Comparison of the two rate constants for the isomerization to the phenyl radical.

Table 7.12: Arrhenius parameters for the global rate constants of isomerization of $\mathbf{FLV-2}$ to the phenyl radical and to $\mathbf{FLV-1}$. Units are s^{-1}.

Mechanism	A	n	E_a/R
to the phenyl radical	5.19 E+13	0	834555.5
to $\mathbf{FLV-1}$	1.95E+14	0	34555.5

The rate data is given in Table 7.12. The comparison between the two rate constants for the isomerization of $\mathbf{FLV-2}$ to $\mathbf{FLV-1}$ shows in this case, a lower rate constant for the isomerization through the bicyclic system.

7.9 Unimolecular fate of the phenyl radical

The different mechanisms that have been presented can be used to redefine the unimolecular fate of the phenyl radical. Considering the formation of $\mathbf{FLV-1}$, *l*-C_6H_4, *n*-C_4H_3+C_2H_2, and *ortho*-benzyne as poten-

tial products. Those paths being considered, the product distribution shows that almost 100 % of the phenyl radical is turned into **FLV − 1**, and this up to over 2000 K. At very high temperatures, the formation of n-C_4H_3+C_2H_2 becomes the second most important path (see Figure 7.19). As the unimolecular fate of **FLV − 1** is the isomerization to the phenyl radical, a loop is generated. Therefore, Figure 7.19 also presents the product distribution if the isomerization to **FLV − 1** is not considered. In that case, the main decomposition pathway is o-benzyne at low temperature and shifts to n-C_4H_3+C_2H_2 as temperature rises. Table 7.13 summarizes the different rate parameters for those rate constants.

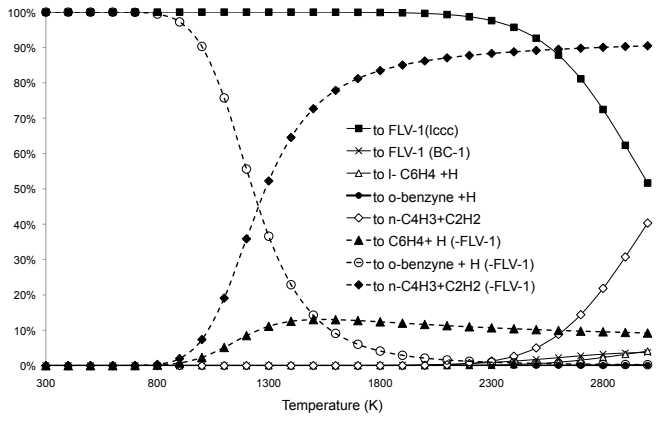

Figure 7.19: Product distribution of the unimolecular transformation of the phenyl radical. Strong lines, product distribution including the isomerization paths to **FLV − 1**. Dashed: product distribution excluding the isomerization paths to **FLV − 1**.

Table 7.13: Arrhenius parameters for the unimolecular reactions involving the phenyl radical. Units are s^{-1}.

phenyl radical	A	n	E_a/R
$\rightarrow$ **FLV − 1** (through **lccc**)	2.01E+15	0	3.58E+07
$\rightarrow$ **FLV − 1** (through **BC − 1**)	2.03E+14	0	3.01E+07
$\rightarrow$ *l*-C_6H_4+ H	9.73E+17	0	5.40E+07
$\rightarrow$ *o*-C_6H_4+ H	8.75E+14	0	4.33E+07
$\rightarrow$ *n*-C_4H_3+C_2H_2	1.67E+19	0	5.57E+07

7.10 Conclusions

In this chapter, we have studied different possible reactions on the C_6H_5 energy surface. Starting by the addition of acetylene on C_4H_3 radicals, we have identified dehydrofulvene radicals as potential intermediates. As a logical following of this, the paths for the isomerization of those radicals to each other and to the phenyl radical were studied. In the case of 6-dehydrofulvene, we have found three possible mechanisms of isomerization to the phenyl radical. As an overall result, we have shown that the lowest energy path form *n*-C_4H_3 + acetylene to the phenyl radical goes through 6-dehydrofulvene and its isomerization to the phenyl radical through a bicyclic intermediate. The rate constants were obtained for all elementary steps identified on the energy surface. This lead to a number of reactions and intermediates that was a little too important to be introduced as such in combustion model. A second part of this chapter was therefore dedicated to the reduction of the number of intermediates and reactions by simplifications of the mechanisms.

Chapter 8

Reactions on the C_6H_7 energy surface

This chapter is focused on the reactions involving fulvene on the C_6H_7 energy surface. Its aim is to examine what becomes of dehydrofulvene radicals once they are hydrogenated. This region of the C_6H_7 energy surface is therefore explored as a continuation of the analysis of the C_6H_5 surface. The first section of this chapter looks at the hydrogenation of dehydrofulvene radicals. The second reviews the products of the addition of an hydrogen atom on fulvene.

8.1 Dehydrofulvene + H_2 reactions

One of the possible ways of turning dehydrofulvene radicals into fulvene in an hydrogen rich environment (such as rich hydrocarbon flames) is to have those radicals react with molecular hydrogen. We therefore consider the hydrogenation of **FLV − 1** and **FLV − 2** to fulvene through

such processes. The reverse reactions, forming **FLV − 1** and **FLV − 2** from fulvene + an hydrogen atom, are also considered. The energies used are again PG3B3 energies. As there are no experimental nor theoretical rate constants available in the literature for those rate constants, we compare our results to rates of model reactions which can, *a priori*, be expected to have similar rate constants. The rate of **FLV − 1** $+H_2$ reaction is compared to that of C_2H_3 + H_2 as those two involve the hydrogenation of a vinyl group. The rate of the **FLV − 2** + H_2 reaction is compared to that of the corresponding reaction involving the phenyl radical. The latter reaction is chosen as it involves a -$\dot{C}$= radical site.

8.1.1 Spin contamination

In the cases encountered before, we considered cancelation of errors through two types of corrections. The first is the relative conservation of the error when spin contamination levels are similar. The second is the spin contamination correction role of the $\Delta(QCI)$ correction. Those two points are conserved for the radical hydrogenation reactions. However, the reverse reactions involves a contaminated transition state and non-contaminated reactants (closed-shell fulvene and atomic hydrogen). The only expected cancelation of spin contamination error comes from the $\Delta(QCI)$ correction. An overestimation of the barrier is therefore to be considered in discussions.

Table 8.1: Modified Arrhenius equation parameters for the **FLV − 1**+ H and **FLV − 2** +H_2 reactions. Units are $cm^3mole^{-1}s^{-1}$.

Reaction	A	n	E_a/R
FLV − 1 + H_2 → Fulvene + H	2.14E+04	2.46	3.46E+03
Fulvene + H→ **FLV − 1** + H_2	3.15E+07	1.96	8.06E+03
FLV − 2 + H_2 → Fulvene + H	1.08E+05	2.43	2.35E+03
Fulvene + H→ **FLV − 2** + H_2	1.63E+08	1.83	9.77E+03

8.1.2 Rate constants for hydrogenation of dehydrofulvene radicals

The coefficients for the modified Arrhenius expression of the rate constants are provided in Table 8.1. As the reactions studied are hydrogen transfer reactions, typically subject to important tunneling effects, Eckart tunneling corrections have been included to the rate constants. Comparison of the rate constant for the hydrogenation of **FLV − 1** with rate constants of hydrogenation of the vinyl radical is shown on Figure 8.1. There is a good agreement between our calculated values and Tsang and Hampton's data [128] at elevated temperatures. As temperature decreases, the agreement between the data also decreases. Between 500 and 1000K, our data is still in good agreement with both Tsang and Hampton values and the values of Knyazev and coworkers [129]. The agreement between the latter two values is not as good. In fact, as temperature decreases, the agreement between experimental data for C_2H_3+ H_2 becomes quite poor. The data from Callear and Smith [130] is higher at low temperature. There seems to be an important difference in the activation energy in this case. The latter being smaller in the results of Callear and Smith. The comparison for the hydrogenation of

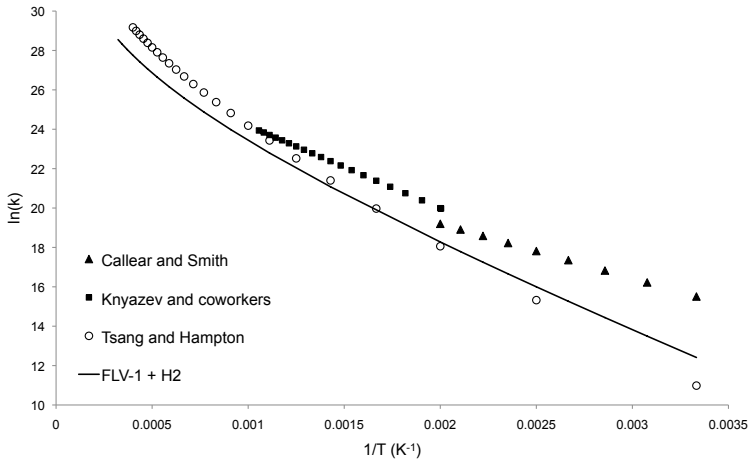

Figure 8.1: Arrhenius plot of the rate constant of the $\mathbf{FLV-1}$ + H_2 reaction (strong line). Marks: Rate constants for the C_2H_3 + H_2 reaction.

$\mathbf{FLV-2}$ shows results not as similar (see Figure 8.2). There seems to be an agreement between theoretical work of Mebel and coworkers [126] and experimental data of Park and coworkers [131] and of Heckmann and coworkers [132] on the rate of hydrogenation of the phenyl radical. The rate constant from the theoretical work of Mebel and coworkers [126] is six time smaller than our results for the hydrogenation of $\mathbf{FLV-2}$ at 1600 K.

8.1.3 Hydrogen abstraction from fulvene

The reverse reactions correspond to the abstraction of an hydrogen atom from the fulvene structure by another hydrogen atom. As mentioned in the spin contamination section, the barrier in that direction may be slightly overestimated due to the non-contaminated character of the reactants. The rate parameters are given in Table 8.1. Again comparison

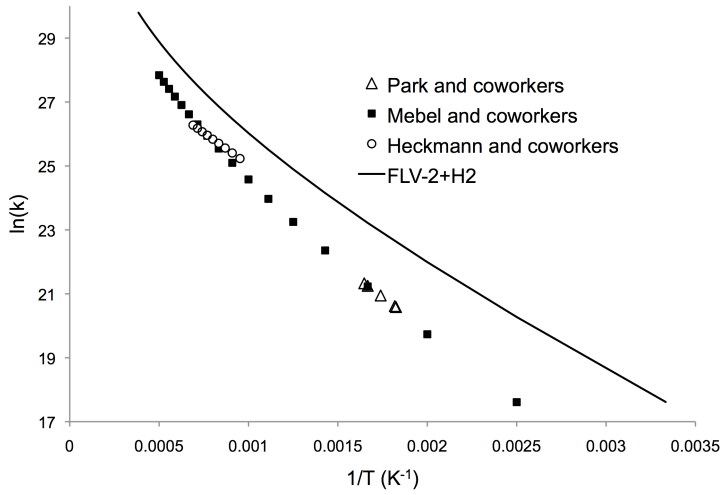

Figure 8.2: Arrhenius plot of the rate constant of the $\mathbf{FLV-2} + H_2$ reaction (strong line). Marks; rate constant for the phenyl radical + H_2 reaction.

can be made with the hydrogen abstraction from ethylene and from benzene. These comparisons are shown on Figures 8.3 and 8.4. The rate of abstraction to form $\mathbf{FLV-1}$ appears to be lower than the equivalent data for the abstraction from ethylene. Artificial lowering due to spin contamination has been mentioned before. However, if such effect was responsible for a decrease of the rate constant, it would be through an overestimated activation barrier. The slopes on Figure 8.3 indicate a relatively good agreement in the activation barrier, except for the data of Warnatz [133]. Spin contamination is not responsible for the difference. It has to be remembered that the comparison are made with rate constants of the corresponding reactions on another reactant. It can therefore not be expected that the rate constants are rigorously identical. Comparison of the rate constant for the reaction forming $\mathbf{FLV-2}$ and the ones forming the phenyl radical is made mostly on

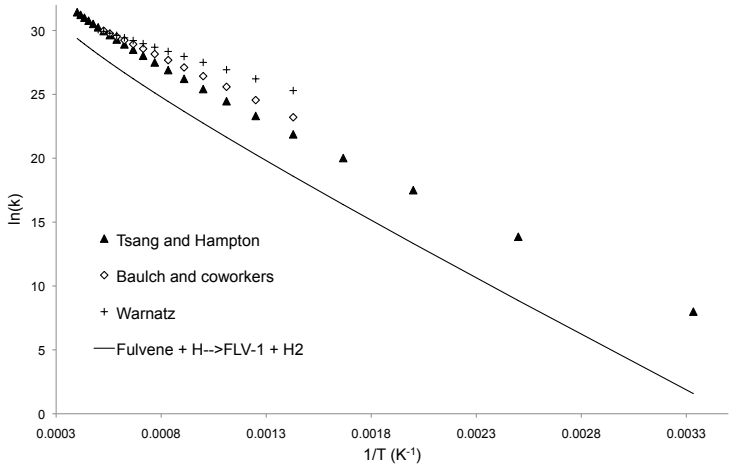

Figure 8.3: Comparison of the rate constant for the abstractions of an hydrogen from fulvene to form $\mathbf{FLV-1}$ and the equivalent reaction on ethylene.

theoretical data. Experimental values are not available, at least in the NIST kinetic database. Again, we note a rate constant globally lower, with deviation in the slope which can become important (see the data of Nicovitch), leading to a potentially overestimated energy barrier.

8.2 Dehydrofulvene + H reactions

In this section, we briefly leave the C_6H_7 energy surface for the C_6H_6 one. If hydrogenation of the dehydrofulvene radicals by molecular hydrogen is considered, it seems consistent to also consider the hydrogenation through recombiniaison of atomic hydrogen. Radical recombination reactions are typically non activated processes. Efforts made to locate transition states for recombination of the dehydrofulvene radicals with an hydrogen atom remained unsuccessful. Maximum free energies of the

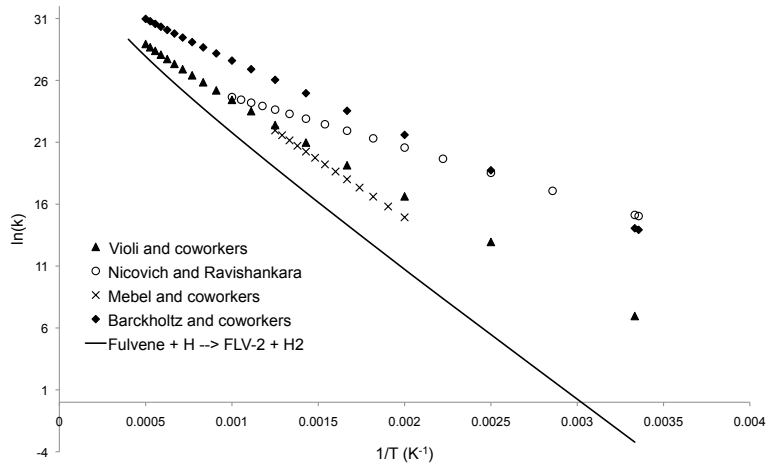

Figure 8.4: Comparison of the rate constant for the abstraction of an hydrogen from fulvene to form $\mathbf{FLV-2}$ and the equivalent reaction on benzene.

Gibbs free energy surface were searched (as was done for the degradation of phenyl to *o*-benzyne) but were not found. The rate constant is approximated by the corresponding data on the vinyl radical. The latter is chosen among the data suggested in the NIST kinetic database [134]. This database lists experimental data measure at 298 K or lower, we therefore choose to use a theoretically obtained value described by equation 8.1.

$$k = 3.8810^{+13} T^{0.2} \quad cm^3 mole^{-1} s^{-1} \tag{8.1}$$

For similar reasons, the rate for the recombination reaction of hydrogen with $\mathbf{FLV-2}$ is taken to be that of the recombination of phenyl with hydrogen (see equation 8.2).

$$k = 9.7910^{+13} T^{0.15} \quad cm^3 mole^{-1} s^{-1} \tag{8.2}$$

8.3 Hydrogen atom assisted isomerization of fulvene to benzene

The hydrogen atom assisted isomerization of fulvene to benzene is the lowest known energy path for such an isomerization. It has been introduced by Melius and coworkers [20]. They used the BAC-MP4 method to describe this mechanism. This method is now known to provide results of poor quality. Inconsistencies have already been observed in the results they presented [135].

8.3.1 Results and discussion

The energies of minima and transition states were obtained as described in the previous sections and are provided in Table 8.2. Figure 8.5 presents the energy profile of the isomerization mechanism, the energies on this figure are given relative to non-interacting benzene + H (-232.558293 hartrees). G3B3, PG3B3 energies and ZPEs are provided in Table 8.2. Rate constants for each elementary reaction have been obtained and are presented in Table 8.3. Structures of the transition states are given in Figure 8.6 along with key structural parameters.

8.3.2 Hydrogen addition on fulvene

The hydrogen atom can attack any of the π bonds of fulvene. From this attack, four C_6H_7 isomers are formed, those are the four systems discussed in section 6.3. Only one transition state has been located and connects the reactants with C_6H_7A, the only C_6H_7 radical showing no

Table 8.2: G3B3 and PG3B3 energies (including ZPE) of the different stationary points, relative to benzene + H (kcal.mol^{-1}).

Stationary point	ZPE	G3B3	PG3B3	$\langle S^2_{DFT} \rangle$	$\langle S^2_{UHF} \rangle$
Fulvene + H	60.71	31.01	31.01	-	-
C_6H_7A	64.14	4.14	5.30	0.75	1.19
C_6H_7B	64.54	-19.08	-18.27	0.77	0.95
C_6H_7C	64.74	-12.13	-11.14	0.79	1.19
C_6H_7D	64.95	-17.09	-16.23	0.79	1.18
BCC6H7	65.68	-2.25	-1.87	0.78	0.96
c-C_6H_7	65.70	-20.98	-20.14	0.79	1.19
benzene+H	59.24	0.00	0.00	-	-
TS(fulvene+H→C_6H_7A)	59.78	34.67	36.11	0.79	1.37
TS(C_6H_7C→C_6H_7D)	62.57	17.23	18.21	0.77	1.09
TS(C_6H_7D→C_6H_7A)	62.08	21.49	22.67	0.76	1.05
TS(C_6H_7A→C_6H_7B)	62.11	26.91	28.66	0.76	1.02
TS(C_6H_7A→BCC6H7)	64.16	11.95	12.69	0.79	1.25
TS(BCC6H7→*c*-C_6H_7)	64.63	6.63	12.69	0.78	1.21
TS(*c*-C_6H_7 →benzene + H)	61.67	6.63	7.75	0.77	1.37

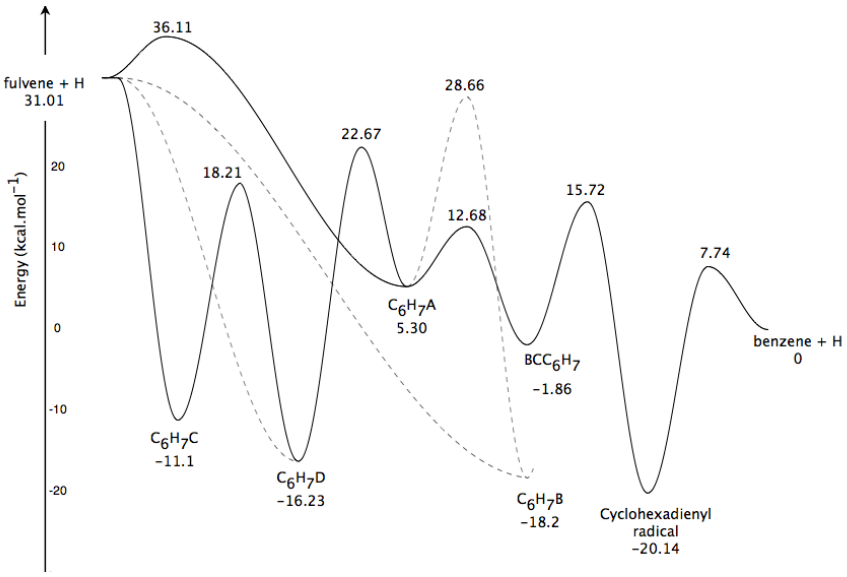

Figure 8.5: PG3B3 (0K, ZPE included) energy profile for the hydrogen assisted fulvene isomerization to benzene mechanism (kcal.mol^{-1}).

resonance. Transition state for the three other paths could not be located due to the very flat transition zone. For those three paths, variational transition state theory was applied using the C-H relaxed energy scans as models for the reaction paths. The Arrhenius plot of the different rate constants for this addition present significant non linear behavior. The modified Arrhenius equation therefore has to be used for a correct reproduction of the temperature dependance of the data. The very little addition barrier, which are already very small, may also be overestimated for the same reason as mentioned in section 8.1.1.

8.3.3 Intramolecular hydrogen transfer reactions

The thermodynamic properties of the different addition products have been discussed in section 6.3. This section concerns the different equilib-

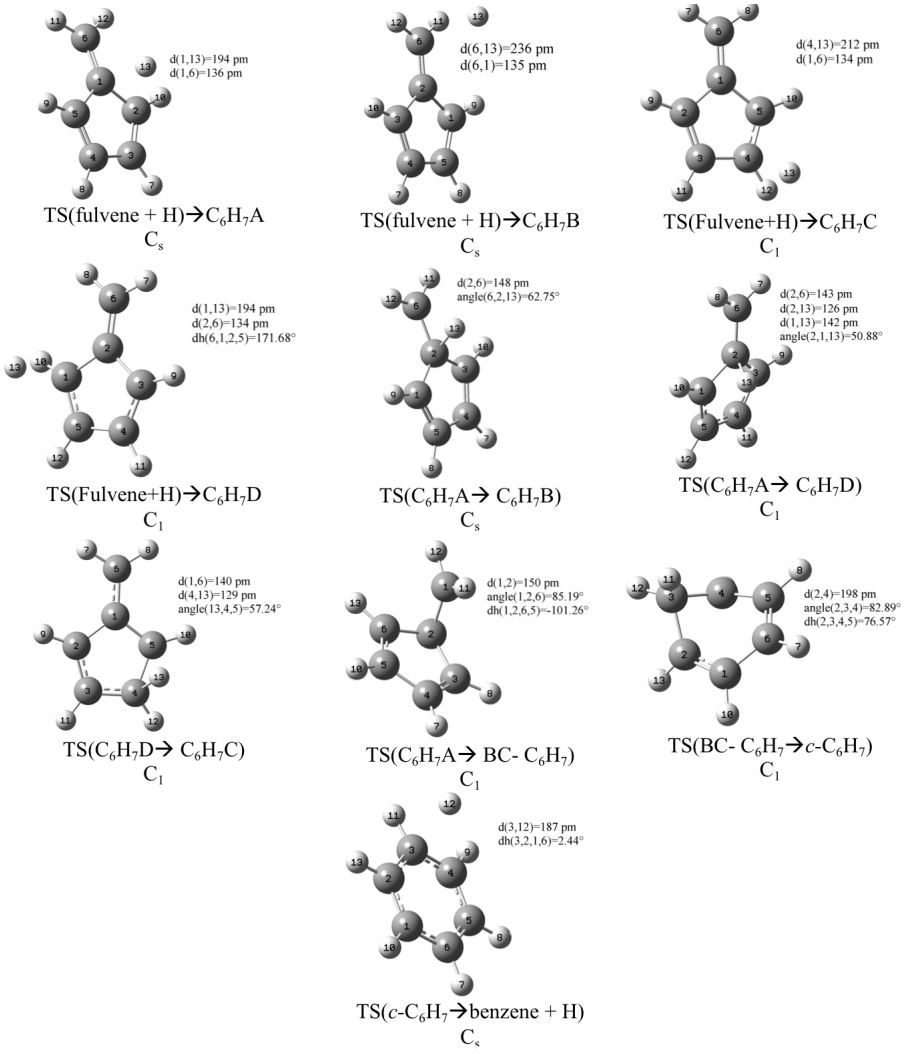

Figure 8.6: Transition states of the hydrogen assisted fulvene isomerization to benzene mechanism, along with key structural parameters. Transition state structures for fulvene + H $\rightarrow$ C_6H_7 B, C and D are taken at 300K.

Table 8.3: Modified Arrhenius equation parameters for the fulvene + H and following reactions. Units are $cm^3mole^{-1}s^{-1}$ for bimolecular reactions and s^{-1} for unimolecular ones.

Reaction	A	n	E_a/R
Fulvene+H→ C_6H_7A	1.15E+14	0.00	3.22E+03
reverse	2.51E+13	0.00	1.65E+04
Fulvene+H→ C_6H_7B	1.70E+12	2.00	2.30E-01
reverse	1.70E+13	0.00	2.59E+04
Fulvene+H→ C_6H_7C	1.15E+11	0.74	1.24E+03
reverse	3.87E+13	0.00	2.32E+04
Fulvene+H→ C_6H_7D	2.51E+12	1.95	3.29E+01
reverse	6.34E+13	0.00	2.66E+04
C_6H_7C→C_6H_7D	2.44E+07	1.63	4.44E+04
reverse	1.99E+07	1.67	4.70E+04
C_6H_7D→C_6H_7A	2.33E+10	0.89	1.89E+04
reverse	1.12E+13	0.00	8.95E+03
C_6H_7A→C_6H_7B	9.75E+12	0.00	1.15E+04
reverse	2.78E+13	0.00	2.26E+04
C_6H_7A→BCC6H7	1.90E+12	0.00	4.17E+03
reverse	7.00E+12	0.22	7.70E+03
BCC6H7→cyclohexadienyl radical	1.47E+14	-0.34	1.37E+04
reverse	2.85E+13	-0.22	2.28E+04
cyclohexadienyl→benzene + H	1.83E+11	0.71	1.43E+04
reverse	4.50E+8	1.45	3.50E+03

ria between those products and the reaction in and out of the region they represent. Hindered rotations had to be considered in the determination of the thermodynamic properties of the minima C_6H_7A and C_6H_7B. It is now necessary to identify the potential rotors in the intramolecular hydrogen transfer transition states.

C_6H_7C to C_6H_7D

This case is probably the easiest one to treat. Indeed, the transition state connects two systems presenting no hindered rotation. Furthermore, this reaction does not involve the double bond. The dihedral components of the vibrator were however verified. It results that only 59.6 % correspond to dihedral angle. There is no need for the treatment of hindered rotations.

C_6H_7D to C_6H_7A

For this reaction also, the dihedral component is quite low (58.1%) indicating that hindered rotation should no be accounted for. This is the less obvious case as we have different situations in the reactants and products.

C_6H_7A to C_6H_7B

This reaction connects two structures for which hindered rotations had to be considered. The dihedral component of the vibrator is only 62%, indicating that no rotor has to be considered. This was unexpected and can be explained, the 90° rotation of the CH_2 group would lead to strong interaction with the hydrogen being transferred.

8.3.4 Formation and degradation of the bicyclic system

The mechanism goes though the formation of a bicyclic system from radical C_6H_7A. This is the step that has been compared to the formation of $\mathbf{BC-1}$ from $\mathbf{FLV-1}$ in the study of the isomerization of dehydrofulvene radicals to the phenyl radical, and shows a much lower activation barrier.

8.3.5 Formation and degradation of the cyclohexadienyl radical.

This is the last step of the isomerization mechanism. Opening of the cycle as been compared to the opening of $\mathbf{BC-1}$. It forms the cyclohexadienyl radical, which forms benzene by restituting an hydrogen atom. The rate constant for the latter reaction can be compared to available rate constants. As can be seen on Figure 8.7, there is a quite good agreement between our rate constant and those of Dean [136] and of Tsang [137], while the experimental data from Nicovich and Ravishankara [138] and from Gao and coworkers [107] are slightly superior. In the case of the reverse reaction, a more important spin contamination effect can be expected. Our value can again be compared to available data. This is shown on Figure 8.8. In this case, we find our data is almost systematically lower than those provided by experiment (Gao [107], Hoyermann (in reference [107]), and Gordon), it is also lower than the review value from Kerr and than the theoretical value of Mebel and coworkers [126]. There is a good agreement with the experimental data of Nicovich and Ravishankara [138].

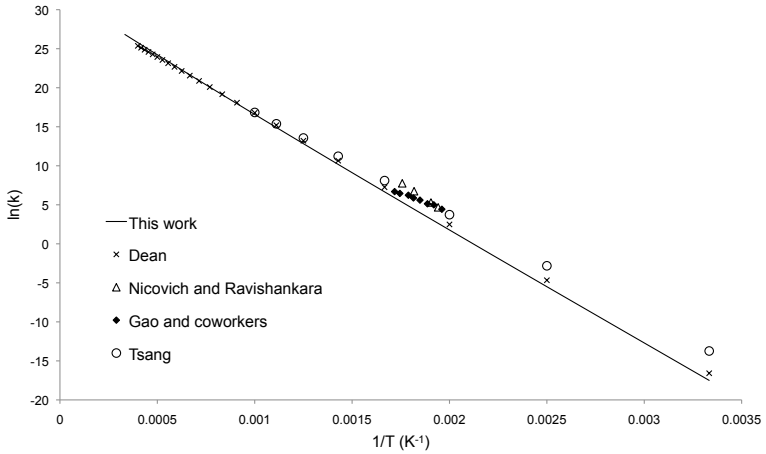

Figure 8.7: Arrhenius plots for the different available rate constants for the cyclohexadienyl radical → benzene + H reaction.

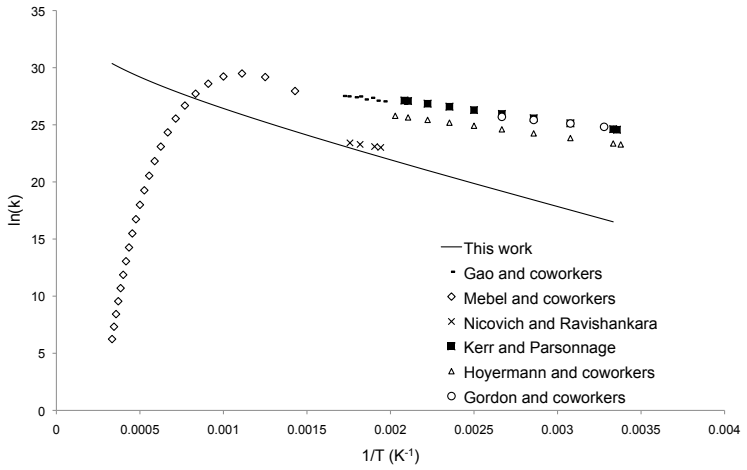

Figure 8.8: Arrhenius plots for the different available rate constants for the benzene + H→ cyclohexadienyl radical reaction.

8.3.6 Global reaction rate

The rate constant for each step of the isomerization mechanisms have been defined. Again, all those steps cannot be included in the combustion model. To simplify the system, the whole mechanism is reduced to addition of hydrogen on fulvene producing the cyclohexadienyl radical. The elimination of an hydrogen atom from the latter completes the mechanism. It is clear that this rate constant is an important simplification of the mechanism. However, including all C_6H_7A, B, C or D as intermediate would lead to inconsistencies in the mechanism.

8.4 Conclusions

The energy surface under investigation in this chapter is the C_6H_7 surface. First we consider the reaction of hydrogenation of the dehydrofulvene radicals identified as potential intermediates in the previous chapter. In a second part, we re-examine the hydrogen atom assisted isomerization of fulvene into benzene. Rate constants are again obtained for every elementary step of the mechanisms. Those rate constants are compared with the available experimental and theoretical values. As was done in the previous, chapter, simplifications are brought to the mechanism for its future introduction in combustion models.

Chapter 9

Introduction in a combustion model

We have now defined rate constants for different reactions and the thermodynamic data for the intermediates involved in those reactions. The final part of this work consists in testing those data in an already existing and validated mechanism. To this end, a sub-mechanism for C_6H_5 species and the reactions for C_6H_7 radicals is introduced in the mechanism of Veronique Dias and coworkers [13] (hereafter noted DIAS mechanism). This mechanism has been developed to model ethylene flames and dimethoxymethane flames. The modified DIAS mechanism to which the sub-mechanism is added is referred to the DIASX mechanism. The experimental data for the test of our sub-mechanism comes from the PhD work of Veronique Dias [139] and are molecular beam mass spectroscopic measurements on a one-dimensional laminar rich ($\phi = 2.5$) ethylene flame. It is not the aim of this section to improve the existing mechanism, but only to evaluate the impact of the sub-mechanism

developed. Suggestions are however made at the end of this chapter. Modeling is carried out with the Cosilab software [140].

9.1 Kinetic mechanism

The mechanism presented in Table 9.1 has been introduced in the DIAS mechanism. In that table, the '= " sign indicates a chemical equilibrium. In this case the reverse rate constant is obtained from the equilibrium constant. In the cases in which a reaction was already present, the latter has been replaced by the new reaction along with the new rate constant. Different mechanisms have been tested. Paths that appeared to have very little to no importance were removed. An example is the isomerization of $\mathbf{FLV-2}$ to $\mathbf{FLV-1}$ or to the phenyl radical. Those were introduced, but appeared to have no influence, principally due to the very small concentration of $\mathbf{FLV-2}$.

9.2 Results

The different results are analyzed at two levels. First, we verify the impact of the sub-mechanism on the simulated mole fraction profiles. the second level is the analysis of the different paths leading to species of interest. In this case, we focus on six-carbon species. As a general observation, the mole fraction profiles of all compounds lighter than six-carbon species do not seem to be much affected by the introduction of our sub-mechanism (see Figures E.1 to E.9 in the appendix of this chapter). Starting at six-carbon species, some effects may be noted and those are discussed in the following sections.

Table 9.1: Kinetic sub-mechanism introduced in the DIAS mechanism. Activation energies are given in cal.mol^{-1}.

Reaction	A	n	E_a
n-C_4H_3+C_2H_2 → C_6H_4+H	2.67E+16	-0.33	4.67E+04
C_6H_4+H → n-C_4H_3+C_2H_2	3.90E+14	1.12	4.77E+04
FLV − 1→ C_6H_4+H	1.00E+15	0.00	7.00E+04
C_6H_4+H → **FLV − 1**	3.59E+12	0.53	8.65E+03
C_6H_5 → C_6H_4+H	9.74E+17	0.00	1.07E+05
C_6H_4+H → C_6H_5	2.25E+12	4.95	1.12E+03
n-C_4H_3+C_2H_2 → C_6H_5	1.02E+015	-0.84	1.33E+04
C_6H_5 → n-C_4H_3+C_2H_2	1.67E+19	0.00	1.11E+05
n-C_4H_3+C_2H_2 → **FLV − 1**	1.93E+15	-0.82	1.08E+04
i-C_4H_3+C_2H_2 → b-C_6H_4+H	3.21 E+48	-9.96	5.73E+04
b-C_6H_4+H →i-C_4H_3+C_2H_2	5.90E+57	-11.59	5.47E+04
i-C_4H_3+C_2H_2 → **FLV − 2**	2.08 E+48	-10.89	3.35E+04
FLV − 2→ b-C_6H_4+H	4.02E+16	0.00	6.19E+04
b-C_6H_4+H → **FLV − 2**	2.50E+54	-11.65	2.95E+04
FLV − 1 → C_6H_5 (through **lccc**)	1.16E+14	0.00	4.10E+04
C_6H_5 → **FLV − 1** (through **lccc**)	2.01E+15	0.00	7.12E+04
FLV − 1 → C_6H_5 (through **BC − 1**)	1.17E+13	0.00	2.99E+04
C_6H_5 → **FLV − 1** (through **BC − 1**)	2.02E+14	0.00	5.98E+04
FLV − 1 = **FLV − 2**	1.54E-18	8.75	3.67E+04
FLV − 1+H = FULVENE	3.88E+13	0.20	0.00
FLV − 2+H = FULVENE	9.79E+13	0.15	0.00
FLV − 1+H_2 = FULVENE+H	2.14E+04	2.45	6.87E+03
FLV − 2+H_2 = FULVENE+H	1.08E+05	2.43	4.67E+03
C_6H_5 = o-benzyne+H	8.75E+14	0.00	8.61E+04
FULVENE+H → CC_6H_7	1.70E+12	2.00	4.60E-01
CC_6H_7 = C_6H_6+H	8.12E+10	0.81	2.78E+04

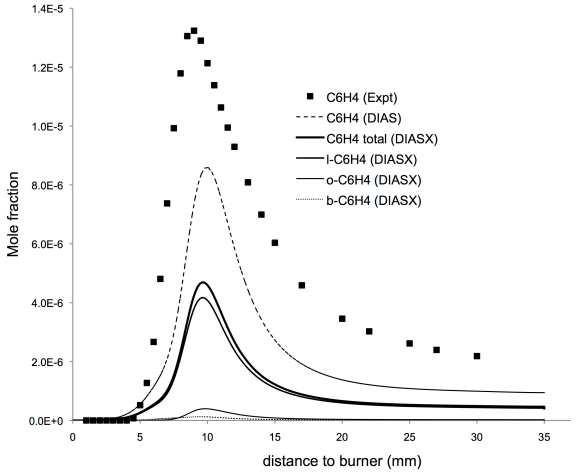

Figure 9.1: Mole fraction profiles for C_6H_4.

C_6H_4 systems.

Starting with the lightest system, we observe a severe decrease of the maximum mole fraction of C_6H_4 (see Figure 9.1), decreasing the agreement with experiment, which was observed for the DIAS mechanism. The C_6H_4 of the DIAS mechanism is only the linear C_6H_4, while the C_6H_4 of DIASX is the sum of l-C_6H_4, b-C_6H_4 and o-benzyne. This is shown on Figure 9.1. Figure 9.2 shows the different formation and consumption pathways for l-C_6H_4 in both mechanisms. Several notable changes appear following the introduction of our sub-mechanism. First of all, we observe that the two main sources (C_3H_2 + C_3H_3 and C_4H_4 + C_2H) of this compound remain the same, and of similar importance. A first change is the formation of n-C_4H_3 and C_2H_2 from C_6H_4, while the latter was formed by n-C_4H_3 + C_2H_2 in the DIAS mechanism. The latter formation path is replaced by the formation of C_6H_4 from the phenyl radical. The most important change is the appearance of $\mathbf{FLV-1}$ as major consumption path (60.39 %). In the initial mechanism, consump-

tion of C_6H_4 only induced the formation of polyynes (via the C_6H_3 radical), it now, in majority, contributes to the formation of cyclic systems, therefore participating to the formation of a first aromatic ring. There also is an overestimation of C_6H_2 mole fraction profiles (see Figure E.5 in the appendix). The formation of this system is mainly due to reactions $C_4H + C_2H_2$ and $C_4H_2 + C_2H$, the contribution of C_6H_4 systems to the total formation of C_6H_2 is almost negligible. The introduction of our sub-mechanism therefore has no significant effect on this issue.

The phenyl radical

The phenyl radical is one of the systems for which we expect changes from the introduction of our sub-mechanism. No experimental mole fraction profile is available, only the modeled mole fraction profiles are therefore presented. As is shown on Figure 9.3 the maximum mole fraction is increased and delayed in DIASX mechanism. Figure 9.4 shows the different paths to and from the phenyl radical. The consequence of the dissociation of the two isomerization mechanisms to $\mathbf{FLV-1}$ appears here. It comes out of the analysis that the phenyl radical is mainly formed (40.74 %) by $\mathbf{FLV-1}$ and is consumed (at 10.72%) in $\mathbf{FLV-1}$. In fact, the phenyl radical is produced from $\mathbf{FLV-1}$ through the isomerization mechanism involving the linear C_6H_5 radical and forms $\mathbf{FLV-1}$ by the mechanism involving the bicyclic system. This new phenyl formation pathway induces a significant reduction of the role of the propargyl radicals recombination reaction (from 20.1 to 7.26 %). The main consumption channel of the phenyl radical is in both cases, the decomposition to n-C_4H_3+C_2H_2 (70.22% in DIAS and 64.59% in

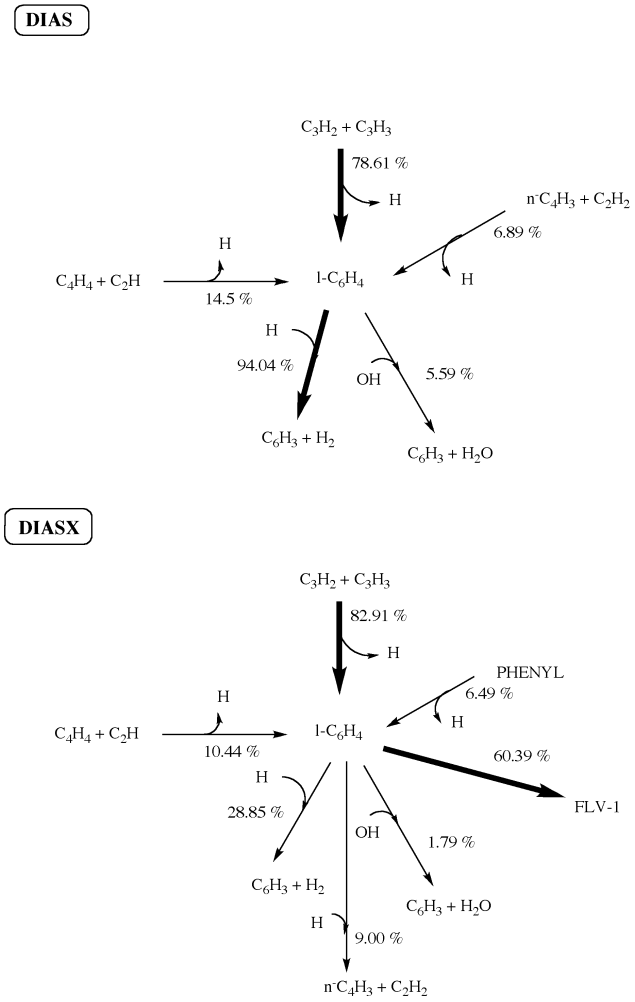

Figure 9.2: Formation and consumption paths of C_6H_4 using DIAS and DIASX mechanisms.

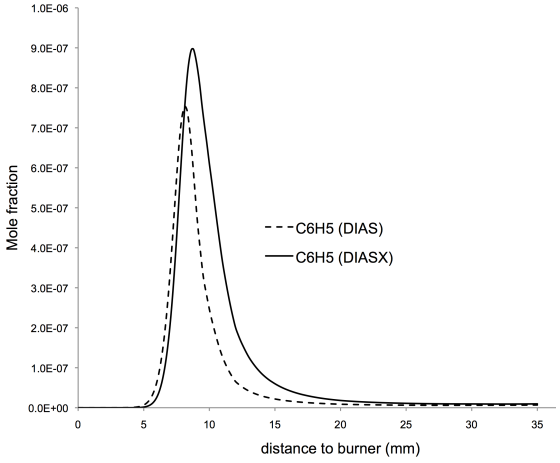

Figure 9.3: Modeled phenyl radical mole fraction profiles using DIAS and DIASX mechanisms.

DIASX). A difference appears in the consumption to C_6H_5O (see Figure 9.4). The importance of this channel is divided by two; this probably has a role in the decrease of the C_6H_6O mole fraction profile (see Figure 9.2). The maximum mole fraction is raised by the introduction of the sub-mechanism, probably because of the formation of cyclic C_6H_5 from linear C_6H_4.

Benzene

In the case of benzene, there is an increase in the maximum mole fraction (see Figure E.7). In this case, this may be viewed as an improvement of the mole fraction profile. Figure 9.5 presents the different reaction to and from benzene. The main source of benzene is FULVENE + H in the case of the DIAS mechanism (63.89%) and cyclohexadienyl in the DIASX one (85.50 %). Those are, in fact the same reactions. Only that we have introduced the cyclohexadienyl radical as an intermediate.

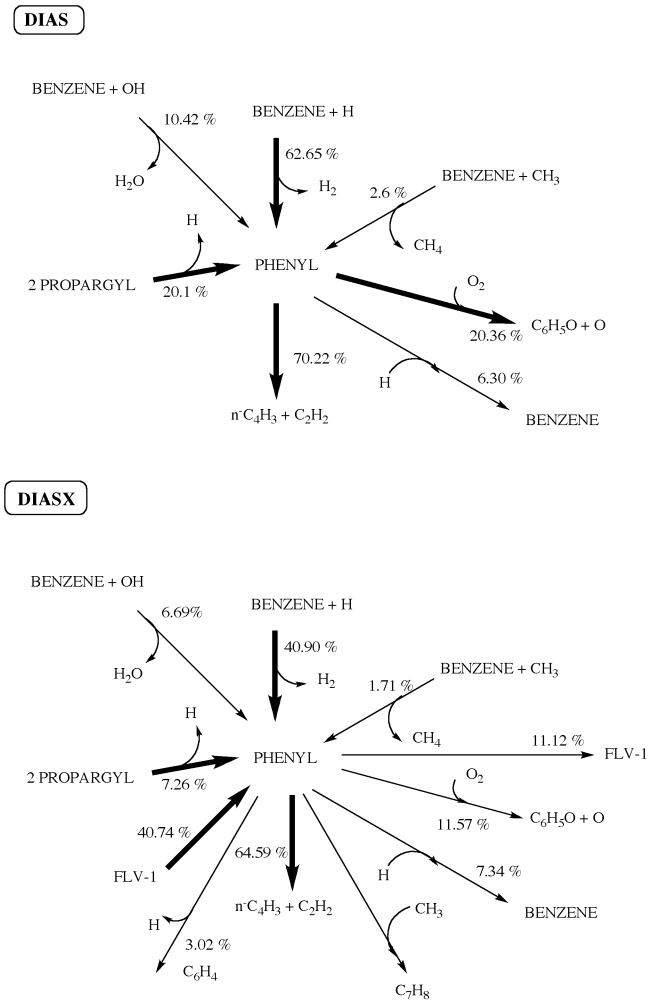

Figure 9.4: Formation and consumption paths of the phenyl radical using DIAS and DIASX mechanisms.

The latter is formed exclusively by the fulvene + H reaction. The increase in the importance of this path is probably due to the increase in the rate constant for the fulvene + H reaction. A notable change is the formation of fulvene from benzene in the DIASX mechanism through the unimolecular isomerization mechanism [127, 23]. As was observed in the case of the formation of the phenyl radical, we now have a loop between benzene and fulvene, with benzene being formed with one mechanism and producing fulvene by another. Another loop appears for benzene and the phenyl radical, as in both mechanisms, benzene is produced by the phenyl + H recombination reaction and produces the phenyl radical by reaction with H, OH or CH_3.

Fulvene and dehydrofulvene radicals

The modeled mole fraction profile indicates a severe decrease of the maximum mole fraction of fulvene. Indeed, the maximum mole fraction in the DIAS mechanism is around 3.2 10^{-6}, while using DIASX, this mole fraction goes down to around 6 10^{-11}. Again, this is probably mainly due to the increase in the fulvene + H reaction rate constant. This is a change which may not be really significant, as it is not surprising to see a highly unstable intermediate react rapidly. In the DIAS mechanism, two reactions account for 100% of fulvene formation. Those are *i*-C_4H_3 + C_2H_3 (55.94%) and the recombination of propargyl radicals (40.97 %). The fulvene so formed reacts in two ways to form benzene (See Figure 9.6) There is a third formation path in the DIASX mechanism. Indeed the unimolecular isomerization to benzene mechanism is now a source of fulvene (14.05 %). The exit channel, providing the cyclohexadienyl radical and therefore benzene + H is responsible for 100%

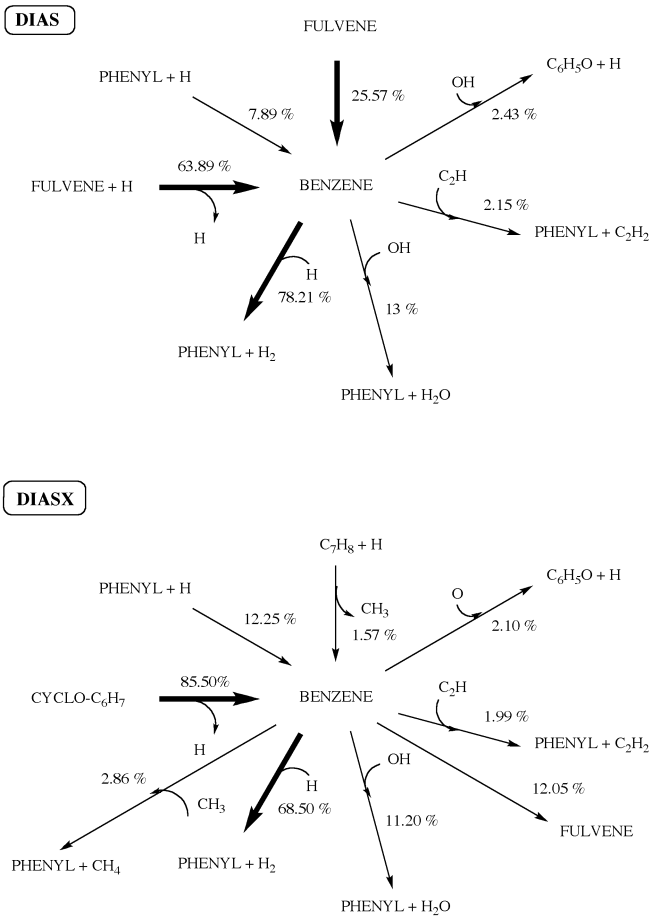

Figure 9.5: Formation and consumption paths of benzene using DIAS and DIASX mechanisms.

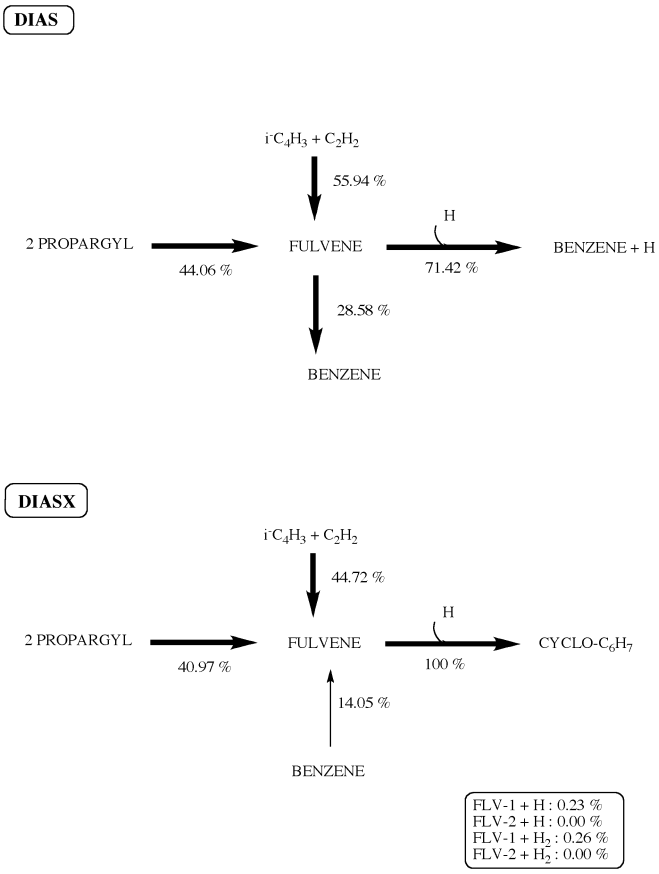

Figure 9.6: Formation and consumption paths of fulvene using DIAS and DIASX mechanisms.

of fulvene consumption. Formation of fulvene from hydrogenation of dehydrofulvene radicals is negligible. Concentrations of those compounds are too small. Figure 9.7 shows the different formation and consumption pathways of the dehydrofulvene radicals considered. **FLV − 1** is mainly formed through the addition of an hydrogen atom on the linear *cis*-C_6H_4. The second most important source is the phenyl radical which isomerises to **FLV − 1** through **BC − 1**. Finally, the addition of acetylene on *n*-C_4H_3 is responsible for the rest of the formation of this compound. **FLV − 1** is consumed in phenyl radical through the **lccc** system (97.85 %) and into **FLV − 2** (1.82 %). The latter reaction is also the main source of **FLV − 2** (78.33%). Addition of acetylene on *i*-C_4H_3 is responsible for the remaining 21.67 %. **FLV − 2** decomposes to *b*-C_6H_4 only. The latter reaction is responsible for 100% of the formation of *b*-C_6H_4, which itself decomposes to *i*-C_4H_3+ C_2H_2, creating again, a loop in the system.

Phenol

Phenol (C_6H_6O in the mechanisms and Figure E.8) is one of the systems for which the agreement with experiment decreases. In the DIAS mechanism, the formation of this system is solely due to the C_6H_5O + H reaction. In the DIASX mechanism the formation of this system is, in majority due to the C_6H_6 + OH → C_6H_6O + H reaction (87.1 %), the rest being formed by C_6H_5O + H. The addition of our submechanism also induces an important decrease in the maximum C_6H_5O mole fraction (see Figure 9.8) , which explains the loss in importance of the C_6H_5O + H reaction.

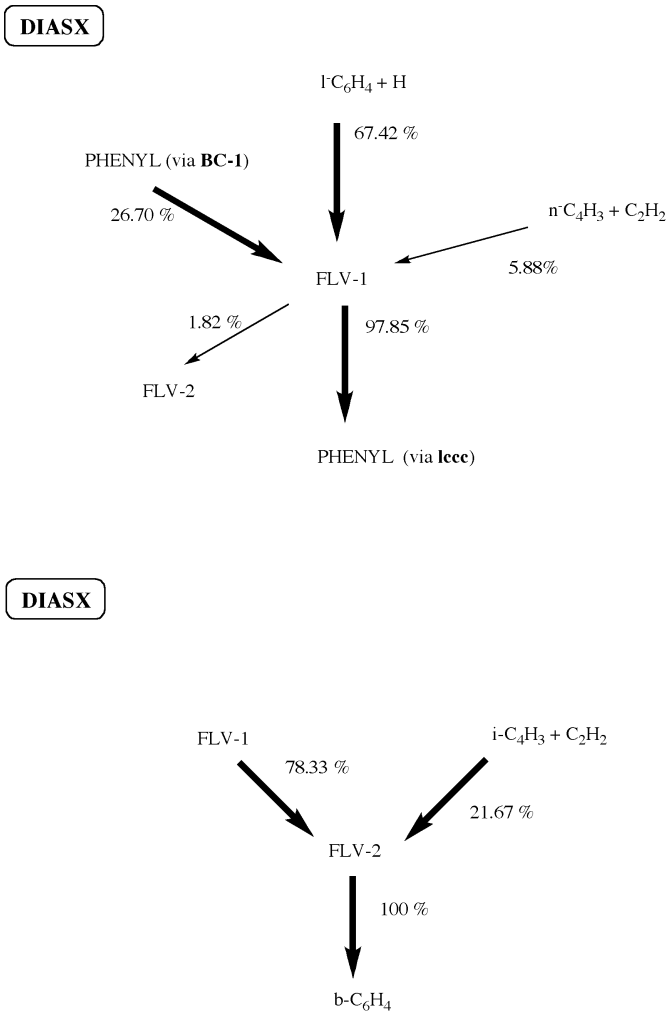

Figure 9.7: Formation and consumption paths of the dehydrofulvene radicals using DIASX mechanism.

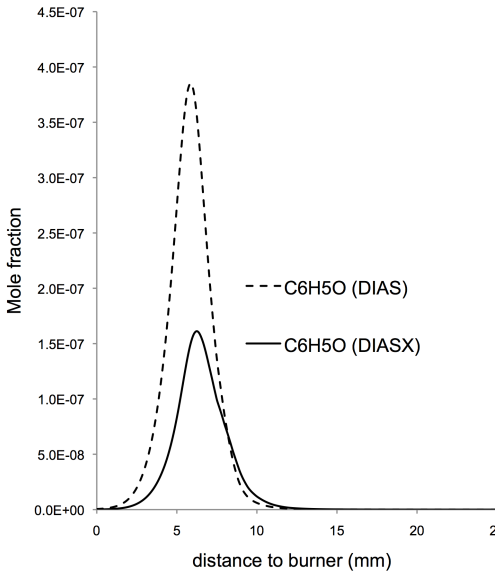

Figure 9.8: C_6H_5O radical mole fraction profiles using DIAS and DIASX mechanisms.

The decrease in the mole fraction maximum is probably due to the decrease of the importance of the $C_6H_5 + O_2 \rightarrow C_6H_5O + O$ reaction (see Figure 9.4).

Phenylacetylene and phenylethylene

Phenylacetylene (C_8H_6) and phenylethylene (C_8H_8) are the last two profiles for which a significant variation is observed (See Figures E.6 and E.8) . Those are obviously linked by C_8H_7 and there is much chance that the explanation for those two changes are common to the two cases. In comparing results from the two mechanisms, not much changes, apart the formation pathways for C_8H_8 (see Figure 9.9). Similarly to what is observed for phenol, there is an important loss of importance of the path involving the phenyl radical, because of the addition of reaction paths

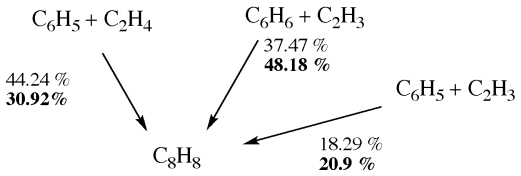

Figure 9.9: Formation paths to phenylethylene using the DIAS (normal) and DIASX (bold) mechanisms.

for the latter. Again, this leads to an increased importance of a path involving benzene.

9.3 Discussion

The introduction of the sub mechanism in a more global combustion model induces changes in the mole fraction profiles of several species, and in their formation and consumption pathways. In some cases, the changes induce a reduction of the agreement between experimental and modeled mole fraction profiles. This can be viewed as a decrease in the quality of the modeled results, but the different observations made showed no unrealistically high or low mole fraction profile nor formation or degradation paths. An hypothesis is the incompleteness of the initial reaction mechanism. The different reactions missing in the mechanism cancel each other out and remove the errors. By introducing our sub- mechanism, we have disturbed this balance and created a more important disagreement with the experimental results. This does not invalidate our results, but rather indicates that, if the new mechanism is to be included in the global model, even more reactions have to be included.

9.3.1 Suggestions

Again, the reaction path cannot be described fully, as was done in the energy surfaces studies. However, to improve the mechanism, some actions could be taken.

Adding details

Without fully describing every detail of the reaction mechanisms, describing in more details the different paths could allow some improvement. For instance, C_6H_7A appeared as an important intermediate for the isomerization of fulvene to benzene. It was not included in the submechanism to avoid inconsistencies. This intermediate also appears as an intermediate in the formation of fulvene + H (or benzene + H) from n-C_4H_5 + C_2H_2 [27] (reaction not included in the mechanism). If one wants to introduce a new intermediate, one also has to introduce a set of reactions concerning this intermediate. The n-C_4H_5+ C_2H_2 should therefore be detailed to allow the detailing of the fulvene + H isomerization. So should the i-C_4H_5 + C_2H_2 reaction (which also produces fulvene + H or benzene + H) as the C_6H_7C system appears as potential intermediate. Furthermore, the reaction of methyl with cyclopentadiene also generates C_6H_7 systems and should be added. Those are examples of reactions which should be detailed, but such a detailing would imply using data from different works and highly modifying the DIAS mechanism. This is out of the scope of this work.

Adding reactions

The introduction of our sub-mechanism highlighted incompleteness in the description of the C_6H_4 species in the DIAS mechanism. Indeed an important number of isomeric forms (see Figure 9.10) of C_6H_4 can be drawn (some more likely to occur than others). All those systems have different reacting properties. For instance, the main C_6H_4 producing reaction on Figure 9.2 (C_3H_2 + C_3H_3 → C_6H_4 + H) can obviously produce both the (E) and (Z) forms of hexa-1,5-diyne-3-ene, while only the (Z) form of the latter can form a cyclic system through reaction with atomic hydrogen. The second source of C_6H_4 is the addition of C_2H on vinylacetylene. This reaction can provide a wide variety of C_6H_4 (see Figure 9.11). Among those we find (E) and (Z) form of hexa-1,5-diyne-3-ene, and the methylenepenta-1,4-diyne. The latter can form a cyclic system by addition of an hydrogen atom ($\mathbf{FLV-2}$), but will not participate in the formation of C_6H_2, at least not through direct hydrogen elimination. From this it seems quite clear that considering only one C_6H_4 system in the model is too simple. However, there does not seem to be extensive thermodynamic nor kinetic data on the subject. Some other reactions seem to be missing. Indeed, the reaction *i*-C_4H_3 + C_2H_2 → $\mathbf{FLV-2}$ finds itself in competition with the reaction of *i*-C_4H_3 + C_2H_3 → fulvene, while the reaction *n*-C_4H_3 + C_2H_2 → $\mathbf{FLV-1}$ is not in competition with the *n*-C_4H_3 + C_2H_3 → benzene.

9.4 Conclusions

The different rate constants and thermochemical information that were obtained in the previous parts of this thesis have been introduced in a

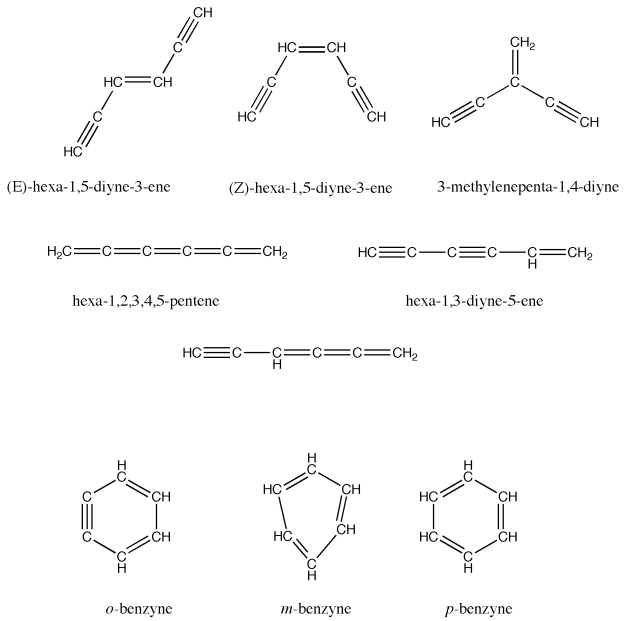

Figure 9.10: Possible C_6H_4 isomers (among others).

combustion model (DIAS) to obtain the modified DIAX model. The results were compared to the experimental measurements, and to the DIAS model. Those comparisons were made at two different levels. First, the resulting mole fraction profiles were examined, second, the different paths of formation and consumption of the different intermediates were analyzed. Only small effects were noticed for compounds having less than six carbons. In terms of mole fraction profiles, important changes were noted for C_6H_4 and phenol. In term of reaction paths, loops were created due to the introduction of two isomerization paths between the phenyl radical and 6-dehydrofulvene. Finally, this analysis also allowed to establish what looks like important deficiencies in the treatment of C_6H_4 species in the DIAS mechanism. Those deficiencies may be partially, or totally responsible for the problems encountered with the description of C_6H_2 system by this model.

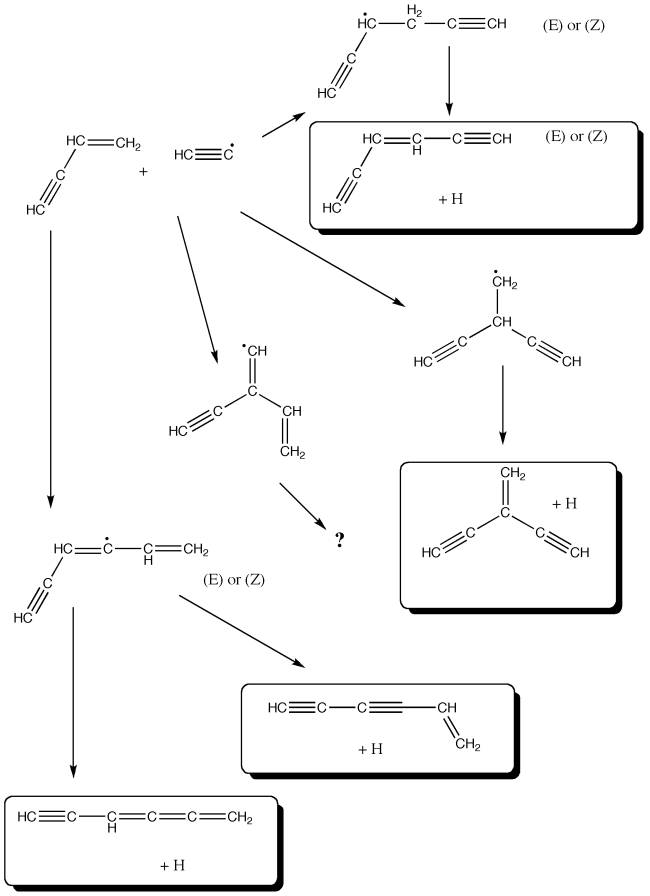

Figure 9.11: Hypothetical paths for the C_4H_4 + C_2H reaction.

Chapter 10

Growth of a second and third aromatic cycle

The mechanisms analyzed so far concerned the formation of a first aromatic ring. The mechanisms of isomerization of **FLV − 1** to the phenyl radical that have been determined can also be applied to the growth of a second and a third aromatic cycle. Figure 10.1 shows the ring closing steps that may be encountered in PAH growth mechanisms such as the HACA or biphenyl paths (see introduction). Those are the steps that

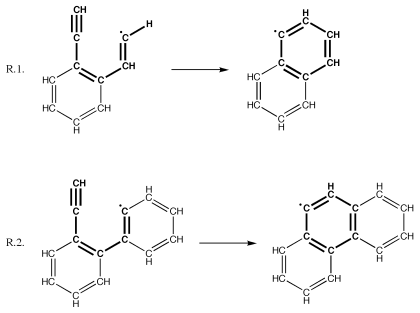

Figure 10.1: Ring closing steps reconsidered in this chapter.

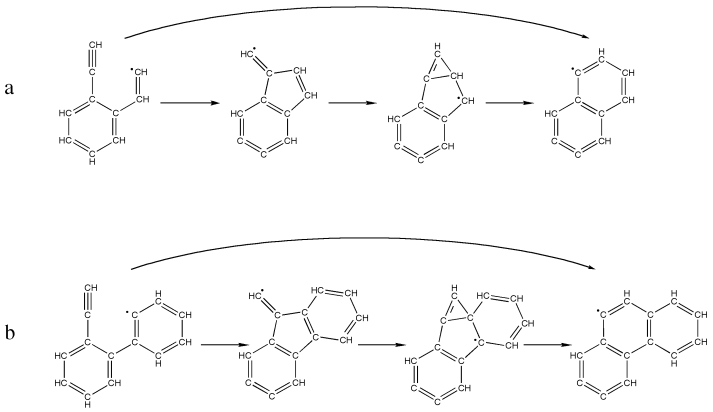

Figure 10.2: Hypothetical paths forming the naphtyl radical (a) and the phenantryl radical (b).

are reconsidered in this chapter. As highlighted on Figure 10.1, the reactants present the l-C_6H_5 pattern. We can therefore imagine that the energy barrier to form a five carbon ring, analogue to $\mathbf{FLV-1}$ from those reactants is lower than that of the direct formation of a six carbon ring, as indicated in chapter 7. Considering this, we may start with two hypothetical mechanisms for lower energy paths for the formation of second and third aromatic rings (See Figure 10.2.a and 10.2.b). Those mechanisms are studied in this chapter in order to be confirmed.

10.1 Energies and rate constants

In this thesis, most of the calculations have been carried out at the G3B3 (or PG3B3) level. In the present case, the size of the systems is too important for such calculations. Density functional theory is then used to describe those reactions. Two different functionals are used, the first is the B3LYP functional and the second is the Boese Martin for Kinetics functional (BMK)[141], which has been optimized for thermo-

chemical kinetic calculations. Those two functionals are used with the 6-311++G(2df,p) basis set. The scale factor used for the frequencies is the one established for the 6-311+G(2df,p) basis set (B3LYP:0.9686 ; BMK: 0.95554) by Merrick and coworkers [142]. It is not the exact scale factor for the basis set used, however, the very little variation in scale factor between 6-311+G(3df,3pd) (B3LYP: 0.9672, BMK: 0.9540) basis set and the 6-311++G(3df,3pd) (B3LYP: 0.9673, BMK: 0.9541) leads us to believe that the 6-311+G(2df,p) scale factor is very close to that of the 6-311++G(2df,p) one. The BMK results are the ones used for the calculation of rate constants. The nature of the different stationary points located is verified by checking their number of imaginary frequencies (0: minimum; 1 first-order saddle point, transition state). For all transition states, internal reaction coordinates calculations were carried out to ensure their connectivity to the reactants and products. The rate constants were again obtained by the transition state theory.

10.2 Formation of a second aromatic ring

10.2.1 The mechanisms

The different energies (B3LYP and BMK) of the different stationary points located are given in Table 10.1. Those are accompanied by the scaled ZPEs. The energy profile with the structure of the different intermediates is given on Figure 10.3. According to Figure 10.3, the formation of the second aromatic ring from **M1** can occur through direct ring closing (**M1**-**TS1**-**M5**), from now on called mechanism MECA-1)), which corresponds to the formation of phenyl by closing the **lccc** system (see chapter 7). This reaction has a barrier of 5.35 and 4.74 kcal.mol^{-1}

Table 10.1: Energies relative to **M1** for the different systems appearing on Figure 10.3 (kcal.mol^{-1}).

	ZPE(B3LYP)	E(B3LYP)	ZPE(BMK)	BMK
M1	77.68	0.00	77.30	0.00
M2	80.01	-31.56	79.34	-36.63
M3	80.02	-31.46	79.51	-36.35
M4	79.12	0.92	78.00	-5.46
M5	81.45	-53.91	80.87	-58.18
M6	81.36	-53.99	80.74	-58.48
TS1	77.70	4.74	77.23	5.35
TS2	77.26	2.83	76.63	3.37
TS3	78.99	-28.59	78.46	-33.03
TS4	78.58	3.04	77.73	-4.31
TS5	78.43	4.48	77.66	-2.23
TS6	77.98	14.37	77.28	7.40
TS7	78.65	16.32	78.14	9.00
TS8	78.82	13.87	78.21	6.79

for BMK and B3LYP respectively. Those barrier are in good agreement with that observed for the closing of **lccc** (5.53 kcal.mol^{-1}). In Figure 10.3, strong lines indicate de BMK data, dashed lines, the B3LYP data, and the frame presents the energy profiles for the concerted paths. In this last cases, the B3LYP curves are not shown to maintain the clarity of the figure. As could be expected, there also is a multistep mechanism analogue to that observed for the isomerization of $\mathbf{FLV-1}$, this time going through a tricyclic intermediate (**M4**, analogue to $\mathbf{BC-1}$). This mechanism is referred to as MECA-2. However, the result of the five carbon ring closing reaction is **M2**, an intermediate which cannot be considered as a starting point for the multistep mechanism. The latter intermediate has to undergo an intramolecular hydrogen switch to form **M3** for the multistep mechanism to be initiated. The formation of the tricyclic system (**M4**) from **M3** has a barrier of 32.04 and 31.63 kcal.mol^{-1} for BMK and B3LYP respectively. Those are a little higher than that observed for the formation of $\mathbf{BC-1}$ from $\mathbf{FLV-1}$ (30.17 kcal.mol^{-1}), but remain in excellent agreement. The ring reopening shows a small barrier (3.23 and 3.55 kcal.mol^{-1} for BMK and B3LYP) which is again in good agreement with the data observed for the $\mathbf{FLV-1}$ isomerization (3.87 kcal.mol^{-1}). **M2** and **M3** are also the starting point for single step isomerization to **M5** or **M6**. The transition states **TS7** and **TS8** connecting **M3** to **M6** and **M2** to **M5** are the bicyclic equivalents of the transition state of the single step isomerization mechanism of $\mathbf{FLV-1}$ to the phenyl radical. The radical system **M3** therefore shows the exact same behavior as $\mathbf{FLV-1}$. In this bicyclic system, the difference between the products of the two different isomerization mechanisms appears more clearly.

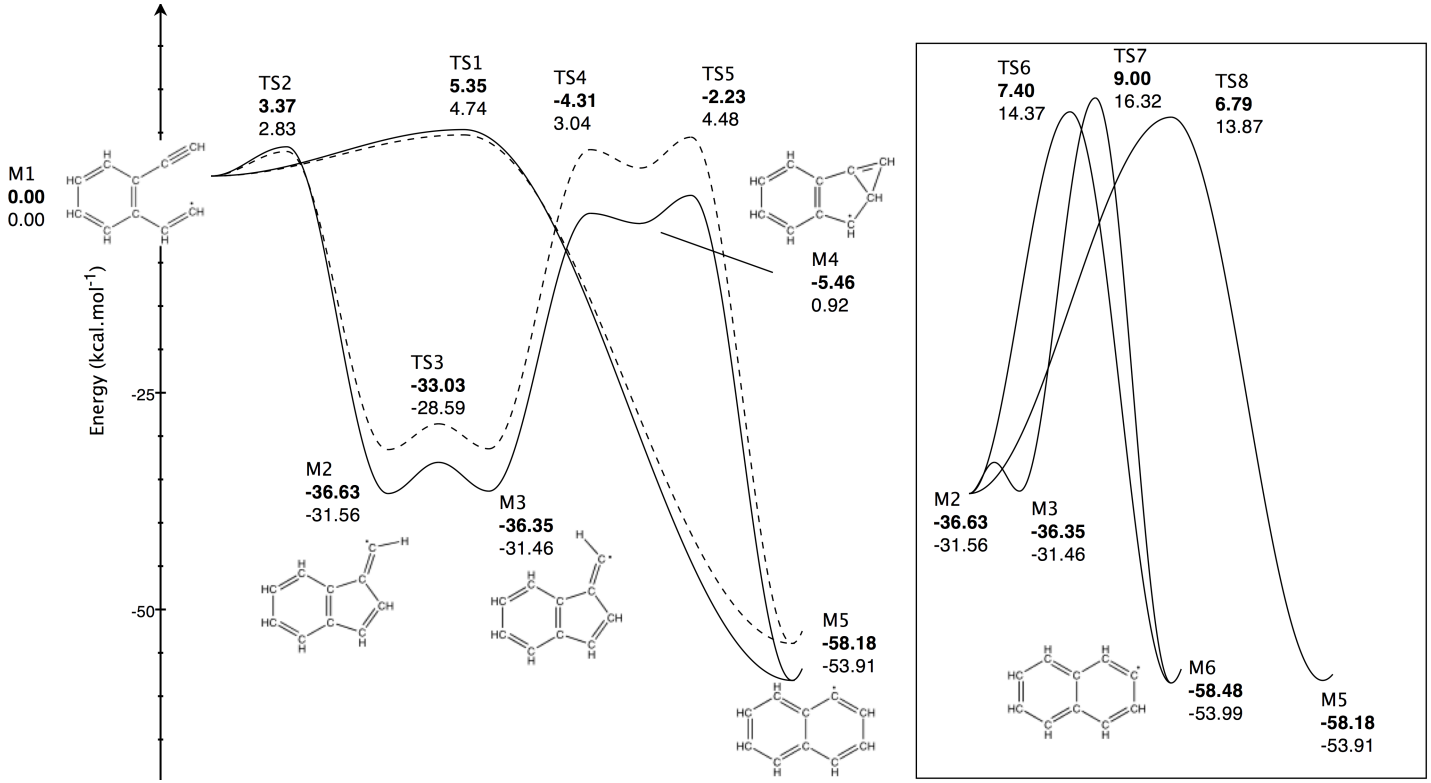

Figure 10.3: Energy profiles for the alternative ring formation paths, Bold curves: BMK profile, dashed curves: B3LYP profiles.

The multi-step mechanism (MECA-2) leads to the 1-naphtyl radical while the single step path leads to the formation of the 2-naphtyl radical. The reaction going through **TS6**, connecting **M2** to **M6** has no equivalent in the monocyclic case. At first, a transition state for the formation of a tricyclic system (similar to **M4**, but with the three carbon cycle on the side of the aromatic ring) was searched. All attempts to locate this transition state provided **M2**, **M6**, **TS6** or **TS8**. This can be explained. The intermediate **M4** is a quite shallow well. In attempting to form its equivalent on the aromatic side, the aromaticity is broken, which leads to further destabilization and to the disappearance of the well. This analysis confirms the hypothetical mechanism suggested on Figure 10.2.a (with an additional hydrogen switch reaction) and also provides additional reaction paths

Effect of the functional

Figure 10.3 provides the B3LYP and BMK data for the steps included in the mechanisms. The main observation is that the use of BMK favors the alternative pathways going through **M2** and **M3**, both the multistep and concerted path. Indeed, there is a good agreement between the ring closing barrier obtained by B3LYP and BMK, but the exothermicity of these reaction is greater using the latter functional. Consecutively, the rest of the profile is also lowered. Using B3LYP, there only is 0.26 kcal.mol^{-1} energy difference between **TS5** and **TS1**, in this condition, the maximum energy levels of the direct ring closing mechanism and of the multistep mechanism are basically equal. Using BMK, the energy difference between those two points is 7.49 kcal.mol^{-1}, which is much closer to what is observed in the monocyclic systems (8.65 kcal.mol^{-1}).

Also, the barriers for the concerted path are systematically lowered by about 2.4 kcal.mol^{-1} if BMK is used. The only reaction which can be compared to the monocyclic case is the reaction from **M2** to **M5** through **TS8**, all other concerted steps may suffer from important interference from the aromatic cycle. The activation barrier is 45.43 and 43.41 kcal.mol^{-1} using B3LYP and BMK respectively. This last value is much closer to the monocyclic data (41.32 kcal.mol^{-1}). **TS8** is, with both functional, the lowest energy transition state for concerted reactions, however, using BMK it is only about 1.5 kcal.mol^{-1} higher then **TS1** while using B3LYP, it lays over 9.5 kcal.mol^{-1} higher.

10.2.2 Rate constants

Table 10.2 provides the rate parameters for the elementary reactions as well as the global rate constants.

Global rate constant

The global rate constants for the isomerization of **M3** to **M5** and the reverse reaction (k_{45} and k_{-45}) are obtained by considering quasi stationarity for **M4**. The rate expression for those reactions are given by equations 10.1 and 10.2.

$$k_{45} = \frac{k_4 k_5}{k_{-4} + k_5} \tag{10.1}$$

$$k_{-45} = \frac{k_{-4} k_{-5}}{k_{-4} + k_5} \tag{10.2}$$

The rate data obtained shows that the reactant (**M1**) closes in **M2** rather than directly into **M5**. At the highest temperature, only 27% of reactants closes directly into **M5**. The mechanisms as presented offer

Table 10.2: Arrhenius parameters for the rate constants of the reactions presented in the previous section. Units are s^{-1}.

	reaction	A	n	E_a/R
k_1	**M1** − **TS1** − **M5**	1.43E+12	0.00	2.66E+03
k_{-1}	**M5** − **TS1** − **M1**	2.02E+13	0.43	3.29E+04
k_2	**M1** − **TS2** − **M2**	1.15E+12	0.16	1.730.02
k_{-2}	**M2** − **TS2** − **M1**	2.92E+13	0.28	2.09E+04
k_3	**M2** − **TS3** − **M3**	2.03E+13	0.00	2.23E+03
k_{-3}	**M3** − **TS3** − **M2**	2.35E+13	0.00	2.14E+03
k_4	**M3** − **TS4** − **M4**	5.81E+12	0.13	1.65E+04
k_{-4}	**M4** − **TS4** − **M3**	8.26E+12	0.00	7.67E+02
k_5	**M4** − **TS5** − **M5**	8.58E+12	0.00	1.81E+03
k_{-5}	**M5** − **TS5** − **M4**	6.26E+12	0.34	2.88E+04
k_6	**M2** − **TS6** − **M6**	6.51E+12	0.00	2.26E+04
k_{-6}	**M6** − **TS6** − **M2**	6.55E+12	0.00	3.39E+04
k_7	**M3** − **TS7** − **M6**	7.76E+12	0.05	2.32E+04
k_{-7}	**M6** − **TS7** − **M3**	1.01E+13	0.23	3.46E+04
k_8	**M2** − **TS8** − **M5**	6.37E+12	0.00	2.21E+04
k_{-8}	**M5** − **TS8** − **M2**	5.54E+12	0.00	3.32E+04
k_{45}	**M3** → **M4** → **M5**	9.14E+12	0.00	1.74E+04
k_{-45}	**M5** → **M4** → **M3**	5.05E+13	0.00	2.89E+04

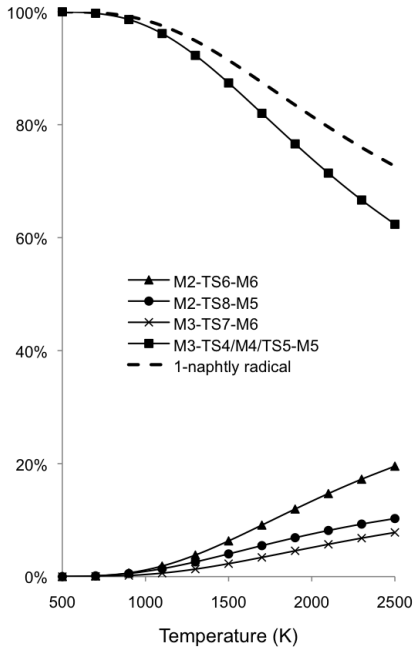

Figure 10.4: Importance of the different path of naphtyl radical formation from **M2** and **M3**. Dashed line: proportion of 1-naphtyl radical.

different possibilities for the formation of naphtyl radicals from **M2** or **M4**. Figure 10.4 shows the importance of the different naphtyl radical production paths from **M2** or **M3**. According to this figure, it is quite clear that most of the naphtyl is formed from the multistep mechanism involving the tricyclic system **M4**. It also shows formation of 2-naphtyl radical as important as 10 % from 1500K and about 20% around 1700 K. The formation of 2-naphtyl radical permits considering the further growth of the PAH into anthracene, which cannot be done from 1-naphtyl without considering hydrogen shift reactions.

10.3 Formation of a third aromatic ring

As a final application, the different mechanisms are applied to evaluate their role in the formation of phenantrene from biphenyl. The mechanism is presented on Figure 10.6. In this case, the presence of the two aromatic cycles on the sides of the $\mathbf{FLV-1}$ pattern exclusively lead to concerted mechanisms. This was observed on the ring-side of **M2** and **M3** in the previous section. In this case, due to the symmetry of phenantrene, only one product is possible, 9-phenantrenyl (See **B3** on Figure 10.4). In more details, the direct closing reaction to **B3** provides 9-phenantrenyl, as does the concerted path going through **TSN**. The concerted path going through **TSM** rather produces 10-phenantrenyl. In this particular case, 9- and 10- phenantrenyl are not distinguishable, again, as was noted in the case of the phenyl radical, any substitution breaking the symmetry of the system would provide different products. The relative energies of all stationary points located are given in Table 10.3. In terms of energy barriers, the ring closing reactions are again in good agreement with previous observations. The ring closing reactions energy barriers indicate, again, that the formation of the five-carbon ring is favored over the formation of the six-carbon one. There is however a recent result from Raj and coworkers [143], showing that steric hindrance appear if the size of the PAH increases (see Figure 10.5). This effect raises the barrier for the formation of a five-membered ring, making the six member cycle the most likely ring. This shows that the expected mechanism presented on Figure 10.2.b is invalid as no tricyclic intermediate could be located. We note that using B3LYP, the energy barrier for the direct formation of phenantrenyl is very small. We also note that the formation of the dehydro-fulvene pattern is more exother-

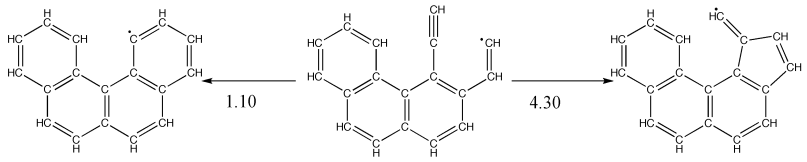

Figure 10.5: Energy barriers (kcal.mol^{-1}) obtained at the B3LYP 6-311++G(d,p) level by Raj and coworkers.

Table 10.3: Energies and ZPE of the different stationary points located on the surface (kcal.mol^{-1}).

	ZPE(B3LYP)	E(B3LYP)	ZPE(BMK)	BMK
B1	107.38	0.00	106.48	0.00
B2	108.71	-35.03	107.89	-39.30
B3	109.88	-49.38	109.16	-53.26
TSK	106.73	0.98	106.04	2.14
TSL	107.03	5.79	106.26	6.63
TSM	106.74	14.37	105.81	8.24
TSN	107.45	16.30	106.48	9.47

mic in this case, while the overall aromatic ring presents reaction energy smaller than the ones observed for the formation of a first and second ring.

Effect of the functional

It again appears that the use of BMK favors the alternative paths by lowering their maximum energy points. Again, the activation barriers for the concerted mechanisms are lowered by about 2.5 kcal.mol^{-1} compared to the B3LYP barriers.

Table 10.4: Arrhenius parameters for the rate constants of the reactions presented in the previous section. Units are s^{-1}.

	reaction	*A*	*n*	*Ea/R*
k_L	**B1 − TSL − B3**	2.26E+12	0	3.09E+03
k_{-L}	**B3 − TSL − B1**	8.06E+14	0	3.10E+04
k_K	**B1 − TSK − B2**	2.28E+12	0	1.22E+03
k_{-K}	**B2 − TSK − B1**	1.93E+14	0	2.17E+04
k_M	**B2 − TSM − B3**	2.27E+13	0	2.45E+04
k_{-M}	**B3 − TSM − B2**	9.54E+13	0	3.20E+04
k_N	**B2 − TSN − B3**	1.26E+13	0	2.50E+04
k_{-N}	**B3 − TSN − B2**	5.31E+13	0	3.24E+04
k_{KM}	**B1 − B2 − TSM − B3**	2.54E+11	0	4.03E+03
k_{-KM}	**B3 − TSM − B2 − B1**	9.04E+13	0	3.19E+04
k_{KN}	**B1 − B2 − TSN − B3**	1.41E+11	0	4.44E+03
k_{-KN}	**B3 − TSN − B2 − B1**	5.03E+13	0	3.24E+04

Compared to the equivalent reactions in the formation of the naphtyl radicals, the energy barriers are raised by 3.4 and 4.1 kcal.mol^{-1} for reactions going through **TSN/TS7** and **TSM/TS6** respectively.

10.3.1 Rate constants

The three parameters of the Modified Arrhenius expression of the rate constant for all elementary reactions are provided in Table 10.4 along with calculated global rate constants. All those rate constants present very linear Arrhenius plots, leading to a zero value for parameter *n*. The latter have been computed using steady state approximation for **B2**. The expression of those rate constants are given by equations 10.3 to 10.6.

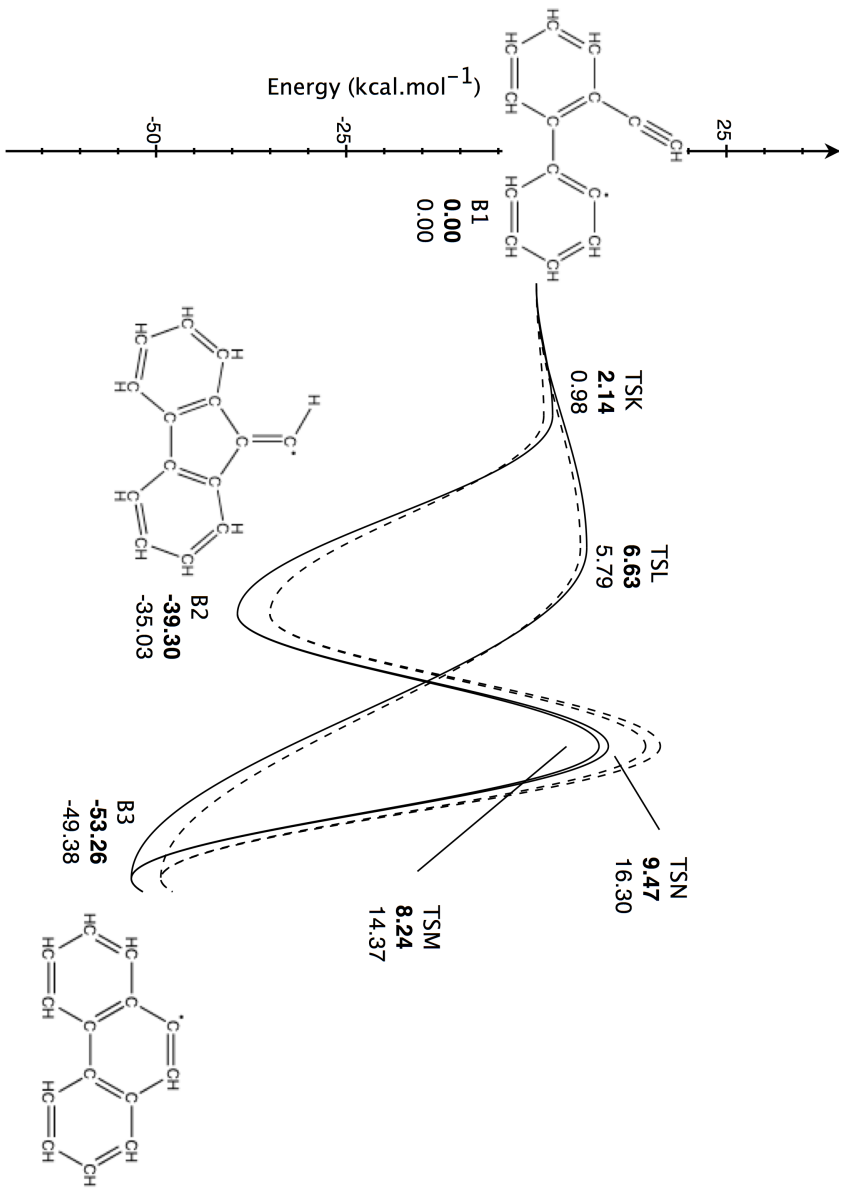

Figure 10.6: Energy profile for the formation of a third aromatic ring, Bold curves: BMK profile, dashed curves: B3LYP profiles.

$$k_{KM} = \frac{k_K k_M}{k_{-K} + k_M + k_N} \tag{10.3}$$

$$k_{KM} = \frac{k_{-K} k_{-M}}{k_{-K} + k_M + k_N} \tag{10.4}$$

$$k_{KN} = \frac{k_K k_N}{k_{-K} + k_M + k_N} \tag{10.5}$$

$$k_{-KN} = \frac{k_{-K} k_{-N}}{k_{-K} + k_M + k_N} \tag{10.6}$$

The product distribution obtained with those rate constants reveals that there is at most (2500 K) 7% of 10 phenantrenyl formed. At this temperature, 9-phenantrenyl is mainly formed by the direct closing path (90%). Therefore, in this case, there does not seem to be an alternative faster reaction path for the closing of the third cycle. As comparison point, Figure 10.7 shows the rate constant for the direct ring closing reactions (**M1** to **M5**, and **B1** to **B3**) obtained in this work, and in the different works of Kislov and coworkers [16, 144]. There is a very good agreement between our values for the formation of **M5** from **M1** and the G3 value of Kislov and coworkers [16]. Those values are also in good agreement with our rate data for reaction **B1** to **B3**. The rate constants for the latter reaction from Kislov and coworkers [144] are quite higher than ours. Their value is obtained at B3LYP 6-31(d) level, we therefore believe our values to be more accurate.

10.4 Conclusions

In this work, we have defined new mechanisms for the isomerization of dehydro-fulvene radicals to the phenyl radical. In combinaison with literature data, these mechanisms provide the lowest energy path from *i*-

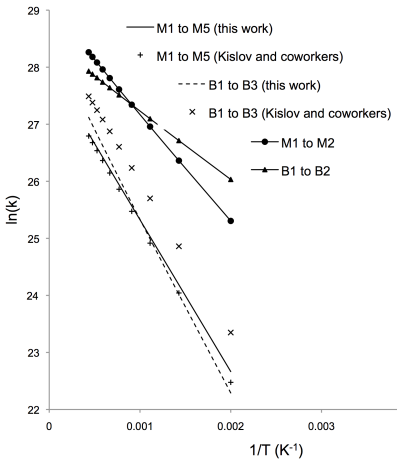

Figure 10.7: Comparison of the different ring closing rate constant for the growth of PAH.

or *n*- C_4H_3 + acetylene to the phenyl radical. Those mechanisms were applied to the formation of additional aromatic rings to assess their impact on the growth of PAH. The tests included the formation of naphtyl radical and of phenantrenyl radicals. Main results for the formation of naphtyl radicals include a faster ring closing process and a new product distribution including the formation of 2-naphtyl radical. Application to the formation of phenantrenyl radical from a biphenylic system showed no faster path than the usually considered direct ring closing reaction, due to the presence of the aromatic ring, preventing the formation of a stable intermediate. As a general comment, the mechanisms presented offer faster and new significant path for the closing of additional aromatic ring on free edges of PAH. This path goes through a dehydromethyleneinedene radical. This, again, emphasizes the importance of fulvene-like intermediates in PAH formation mechanisms.

Chapter 11

Conclusions and perspectives

11.1 Conclusions

11.1.1 Heats of formation

The standard heats of formation of closed and open-shell systems have been calculated using the G3B3 theory. This model chemistry contains single point calculations using quite accurate quantum chemistry methods (such as QCISD(T)) and extended basis sets. Comparisons have been made with experimental and theoretical values. Those comparisons lead to several observations among which:

- The G3B3 procedure does not correctly reproduce the ring strain in small cyclic systems. In order to treat larger systems containing small cyclic pattern, a Ring Conserving Isodesmic Reaction method has been developed and tested. Furthermore, the exper-

imental data concerning small cyclic systems is scarce and seems inaccurate. This issue should also be considered.

- If very unstable systems are dealt with (such as fulvene), it seems that the experimental value tends to be less accurate than the results from high-level *ab initio* calculations.
- The use of G3B3 energies with thoughtfully chosen isodesmic process provide results of quite high accuracy. It is not clear, that , in the case of relatively small closed-shell systems, increasing the level of theory to really expensive calculations (Weizmann methods and others) is absolutely necessary. This is good news, calculations using those methods on much larger systems are not widely available.
- In order to define a way to choose the best possible isodesmic reaction, an isodesmicity index has been defined.

The standard heats of formation of open-shell systems have also been obtained and compared to a set of reference data. On the overall, the deviations in the case of the open-shell systems are larger than the one observed for closed-shell ones. Detailed analysis of the G3B3 energy component showed that the QCISD(T) calculation probably accounts for most of the spin contamination error, leading to small influence of the spin contamination in the resulting G3B3 energies. If large systems have to be studied, a procedure leading to the removal of the spin contamination error from the Møller-Plesset heats of formation has been developed. Comparison showed that the procedure has an accuracy similar to that of the G3B3 and PG3B3 energy.

On the whole, if an adequate isodesmic process is chosen, it is not obvious that the use of a level of chemistry as high as G3B3 is necessary for such small systems to reach sub-kcal.mol^{-1} accuracy.

11.1.2 Energy surfaces and rate constants

As far as the formation of a first ring is concerned, two energy surfaces were analyzed to locate transition states and intermediates significant to the formation of a first aromatic ring. The main part of the attention was focused on the reaction of addition of acetylene on C_4H_3 radicals. Cycle formation from those reactions were considered, and showed the potential importance of dehydrofulvene radicals in the formation of cycle from this path. As a consequence, the isomerization of those radicals to the phenyl radical has also been analyzed in details. The hydrogenation of the dehydrofulvene radical (through hydrogen abstraction from H_2) leads us to the C_6H_7 energy surface. The part of the surface studied corresponds mainly to the hydrogen assisted isomerization of fulvene to benzene. For each step of the reaction mechanisms identified on each surface, transition state theory rate constant have been calculated. For practical use, those rate constant were recombined in order to establish a reduced mechanism with global rate constants. Comparisons were made with data from the literature. In a final chapter, the mechanisms studied on the C_6H_5 energy surface were used to describe the growth of a second and third ring. They have been shown to be applicable to the growth on a PAH free edge, and faster than the usually considered direct ring closing reaction.

11.1.3 Combustion modeling

The mechanisms established in the analysis of the energy surfaces have been simplified in order to be introduced in combustion modeling software. A sub-mechanism has been established and tested. It appeared that, this sub-mechanism did not lead to major changes to the overall agreement between experimental and modeled mole fraction profiles. However, for six carbon species, it importantly modified the different pathways from and to the different intermediates. This confirms the potential role of 6-dehydrofulvene as intermediate in ring formation mechanism. This shows the impact of the sub-mechanism and allowed to identify sub systems to be studied (C_6H_4 sub system).

11.2 Perspectives

11.2.1 Isodesmicity index

The development of the isodesmicity index should be further carried out. It would be interesting to verify whether an index such as defined in this thesis can be defined at lower level of chemistry. If this is the case, the index should be tested on much larger systems, which allow more possibilities of isodesmic processes. Furthermore, the index, as defined in this work presented a converging behavior. Further studies could show a similar behavior of the error, leading to possibilities of extrapolation of the heats of formation.

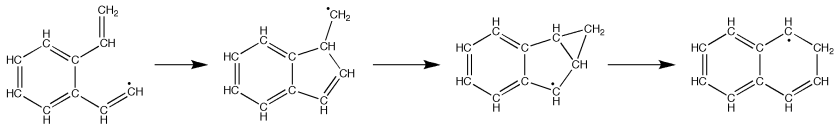

Figure 11.1: Potential path for PAH growth, using the *n*-C_4H_5+C_2H_2→ C_6H_7 path of cyclohexadienyl radical formation.

11.2.2 Extrapolation methodology.

An extrapolation method to remove spin contamination in MøllerPlesset heats of formation has been developed. It was shown that using the 6-31G(2df,p) basis set provides data of accuracy similar to that of G3B3 and PG3B3 methods. Tests could be carried out using this method and correlation consistent basis sets to consider a double extrapolation procedure, the first extrapolating out the spin contamination error, and the second extrapolating the value to the complete basis set limit.

11.2.3 Rate constant

In this work, the rate constants were obtained by conventional transition state theory. This method does not account for pressure effects. The consideration of such effects may lead to improvement, particularly for the type of flames studied in the former combustion unit of the Université catholique de Louvain. The reactivity model to this end exists (RRKM theory) and softwares are available to carry out the calculations (Chemrate, Variflex and others). As far as mechanisms are concerned, there are many possible connections between C_6H_5, C_6H_6 and C_6H_7 surfaces, the different possibilities should be considered. However, it has to be mentioned that most of the reactions included in existing mechanism do not include pressure effects.

11.2.4 Reaction mechanisms

Formation and decomposition of the C_6H_4 isomers

Among results, the incompleteness of the description of the fate of the various C_6H_4 systems was noted. Hypothesis for the formation mechanism from the C_2H + C_4H_4 reaction has been proposed. However, it remains to be confirmed. Furthermore, a closer look should also be taken on other formation and degradation pathways to ensure a correct reproduction of the experimental fraction profiles of those isomers by the model.

Growth of PAH

In the last chapter of this thesis, we have shown that the mechanism of formation of a first ring can be applied to the formation of additional rings. We have shown that the formation of an additional cycle rather goes through a fulvenyl-like radical. In their recent work, da Silva and Bozzelli have used the fulvene to benzene isomerization mechanism to describe the formation of indene from the addition of acetylene on fulveneallene [145]. From available literature, it also seems realistic that a similar work can be carried out by considering the ring formation on the C_6H_7 energy surface, which also indicates a lower energy path going through five carbon cycles (see Figure 11.1).

Appendix A

Heats of formation of closed shell systems

Table A.1: G3B3 energy corrections for the systems in the closed shell test set (kcal.mol^{-1}).

System	Δ(QCI)	Δ(+)	Δ (2df,p)	Δ(GTL)	Δ(total)
methane	-0.74	-1.09	-35.32	-38.03	-92.15
ethane	-1.12	-2.04	-59.79	-73.15	-165.80
ethylene	-1.46	-3.74	-48.26	-70.89	-149.80
acetylene	-0.39	-3.88	-38.49	-68.48	-132.46
allene	-1.57	-5.12	-62.55	-103.66	-206.83
propyne	-0.34	-4.55	-63.23	-104.00	-206.05
cyclopropene	-0.95	-4.12	-62.81	-103.01	-204.82
propene	-1.61	-4.66	-72.99	-106.01	-223.45
cyclopropane	-1.05	-4.31	-73.38	-105.12	-222.03
propane	-1.45	-3.20	-84.50	-108.14	-239.70
vinylacetylene	-0.57	-6.68	-76.40	-136.43	-262.49
1,3-butadiene	-1.98	-6.86	-86.55	-138.77	-280.82
1,2-butadiene	-1.73	-6.19	-86.99	-138.51	-280.08

(continued on next page)

(continuing)

methylenecyclopropane	-1.32	-5.98	-87.38	-137.78	-279.12
bicyclobutane	-0.66	-5.63	-88.16	-137.41	-278.52
cyclobutene	-1.42	-5.09	-87.47	-137.70	-278.34
1-butyne	-0.56	-5.79	-87.95	-138.79	-279.75
2-butyne	-0.26	-4.98	-87.95	-139.53	-279.38
cyclobutane	-1.48	-4.37	-98.76	-139.55	-295.06
(E)-2-butene	-1.75	-5.43	-97.64	-141.14	-296.87
(Z)-2-butene	-1.07	-5.54	-97.70	-141.11	-296.32
isobutene	-1.72	-5.58	-97.99	-141.15	-297.34
butane	-1.76	-4.30	-109.26	-143.19	-313.66
isobutane	-1.70	-4.58	-109.40	-142.95	-313.78
cyclopentadiene	-1.10	-7.41	-100.73	-170.89	-335.27
spiropentane	-0.99	-6.69	-112.01	-172.14	-351.22
Cyclopentane	-1.60	-5.31	-123.85	-174.82	-369.21
Z-2-Pentene	-1.16	-6.70	-122.55	-176.14	-370.18
Pentane	-2.07	-5.45	-134.03	-178.19	-387.61
2,2-dimethylpropane	-1.85	-6.23	-134.45	-177.60	-388.01
Benzene	0.29	-8.84	-114.11	-204.11	-390.41
bismethylenecyclobutene	-1.45	-9.19	-115.81	-203.42	-393.51
1,3-cyclohexadiene	-1.68	-8.77	-125.12	-205.75	-409.19
1,4-cyclohexadiene	-1.82	-8.14	-125.17	-206.53	-409.53
(E)-1,3,5-hexatriene	-2.25	-9.88	-124.76	-206.75	-411.50
(Z)-1,3,5-hextriene	-2.26	-9.94	-124.87	-206.82	-411.77
cyclohexene	-1.84	-7.46	-136.70	-208.01	-426.12
toluene	0.33	-9.90	-139.08	-239.05	-464.05

Table A.2: G3B3 heats of formation using AR and no empirical corrections (kcal.mol^{-1}).

Compound	ΔH_f°	deviation	Compound	ΔH_f°	deviation
allene	57.88	-12.28	isobutene	16.91	-20.91
propyne	57.02	-12.42	butane	-6.54	-23.66
cyclopropene	81.17	-15.17	isobutane	-8.49	-23.61
propene	20.35	-15.55	cyclopentadiene	53.26	-21.14
cyclopropane	29.03	-16.33	spiropentane	67.87	-23.67
propane	-6.74	-18.26	Cyclopentane	8.39	-27.09
vinylacetylene	84.28	-13.88	Z-2-Pentene	20.19	-26.49
1,3-butadiene	44.62	-18.32	Pentane	-6.34	-28.66
1,2-butadiene	57.68	-18.88	2,2-dimethylpropane	-11.32	-28.78
methylenecyclopropane	64.38	-16.38	Benzene	43.55	-23.75
bicyclobutane	72.44	-20.54	bismethylenecyclobutene	104.43	-24.03
cyclobutene	57.43	-19.93	1,3-cyclohexadiene	51.96	-26.56
1-butyne	57.80	-18.32	1,4-cyclohexadiene	52.03	-26.23
2-butyne	52.67	-17.97	e 1,3,5-hexatriene	65.63	-25.63
cyclobutane	27.85	-21.05	z 1,3,5-hextriene	67.22	-26.22
(E)-2-butene	18.28	-21.18	cyclohexene	27.83	-28.86
(Z)-2-butene	19.74	-21.64	toluene	40.27	-28.17

Table A.3: Computed and experimental heats of combustion (kcal.mol^{-1}).

	calc.	expt. $_{liquid}$	expt.$_{gaseous}$
methane	-192.84	-212.88	-191.85
ethane	-343.82	-373.01	-341.47
ethylene	-318.65	-337.29	-316.26
cyclopropene	-470.20	-485.00	-463.97
propene	-464.29	-491.83	-460.29
cyclopropane	-472.97	-499.85	-468.31
propane	-492.11	-530.39	-488.33
1,3 butadiene	-581.63	-607.16	-575.62
1,2 butadiene	-594.69	-619.93	-588.39
methylenecyclopropane	-601.39	-629.07	-597.53
bicyclobutane	-609.45	-633.05	-601.51
cyclobutene	-594.44	-618.60	-587.06
1-butyne	-594.82	-620.64	-589.10
2-butyne	-589.68	-615.84	-584.30
E-2-butene	-610.21	-646.90	-604.84
Z-2-butene	-611.66	-647.65	-605.59
isobutene	-608.83	-645.19	-603.13
butane	-640.29	-687.75	-635.18
isobutane	-638.34	-685.71	-633.14
cyclopentadiene	-683.34	-707.70	-676.16
spiropentane	-752.86	-787.77	-745.71
Pentane	-788.47	-844.99	-781.90
2,2-dimethylpropane	-783.49	-839.88	-776.79

Table A.4: Results of the Student test for the comparison of AR and BSR values heats of formation; x=average difference, s: standard deviation, d. o. f= number of degrees of freedom.

	AR-BSR
x	0.12
s	0.24
t_{calc}	2.97
d. o. f.	33
t(bi, 95%, 33 d.o.f)	2.03

Table A.5: Results of the Student test for comparisons of the different sets of BSR reference values; x=average difference, s: standard deviation, d. o. f= number of degrees of freedom.

	JANAF-Pedley	JANAF-NIST	Pedley-NIST
x	0.04	-0.49	-0.52
s	0.22	0.31	0.29
t_{calc}	0.96	9.60	10 .95
d. o. f.		33	
t(bi, 95%, 33 d.o.f)		2.03	

Table A.6: Results of the comparison of the Student test for the comparison of RCIR and BSR heats of formation for bicyclic compounds; x=average difference, s: standard deviation, d. o. f= number of degrees of freedom.

	BSR-RCIR
x	0.99
s	0.44
t_{calc}	8.80
d. o. f.	15
t(bi, 95%, 15 d.o.f)	2.14

Table A.7: BSR and RCIR reactions used to obtain the heats of formation of the fused bicyclic benzene isomers and their hydrogenation products in section 5.3.2.

Compounds	BSR
C_6H_6	5 C_2H_6 + 2 C_2H_4 → C_6H_6 + 8 CH_4
C_6H_8	6 C_2H_6 + C_2H_4 → C_6H_6 + 8 CH_4
C_6H_{10}	7 C_2H_6 → C_6H_6 + 8 CH_4
	RCIR
C_6H_6 (**1**, **2**, **3**)	2 cyclobutene → C_6H_6 + C_2H_6
C_6H_6 (**4**)	Cyclobutadiene + cyclobutane → C_6H_6 + C_2H_6
C_6H_6 (**5**, **9**)	Cyclopentadiene + cyclopropane→ C_6H_6 + C_2H_6
C_6H_6 (**6**, **7**, **8**)	Cyclopentene + cyclopropene→ C_6H_6 + C_2H_6
C_6H_8 (**10**, **11**)	Cyclobutene + cyclobutane→C_6H_8 + C_2H_6
C_6H_8 (**12**, **13**)	Cyclopentene + cyclopropane→ C_6H_8 + C_2H_6
C_6H_8 (**14**)	Cyclopentane + cyclopropene→ C_6H_8 + C_2H_6
C_6H_{10} (**17**)	Cyclopentane + cyclopropane→ C_6H_{10} + C_2H_6
C_6H_{10} (**18**)	Cyclopentane + cyclopropane→ C_6H_{10} + C_2H_6

Table A.8: Reaction energy correction for BSR and RCIR (kcal.mol^{-1}).

BSR	ΔΔ (QCI)	ΔΔ (+)	ΔΔ (2df,p)	ΔΔ (GTL)
1	0.70	0.84	-4.34	1.69
2	1.73	1.03	-3.90	1.33
3	1.71	-0.06	-2.51	1.66
4	1.71	0.48	-2.66	1.08
5	3.37	-0.90	-2.15	0.75
6	2.09	0.13	-2.12	0.59
7	2.13	0.18	-2.14	0.75
8	2.20	0.66	-4.06	0.62
9	2.38	0.26	-3.47	0.67
10	1.21	-0.73	-2.64	1.70
11	1.01	-0.23	-2.78	1.36
12	1.24	-0.91	-1.72	0.52
13	1.15	-1.12	-2.01	1.12
14	1.57	-0.39	-2.22	0.79
17	0.32	-0.99	-2.64	1.62
18	0.77	-1.41	-1.61	0.55
RCIR	ΔΔ (QCI)	ΔΔ (+)	ΔΔ (2df,p)	ΔΔ (GTL)
1	0.94	0.47	-1.51	0.37
2	0.08	0.31	-1.11	0.30
3	0.07	-0.78	0.28	0.63
4	0.06	-0.24	0.12	0.06
5	1.76	-0.18	-0.77	0.36
6	0.85	-0.40	-0.07	0.02
7	0.89	-0.35	-0.08	0.18
8	0.96	0.13	-2.01	0.05
9	1.14	-0.27	-1.42	0.10
10	0.31	-0.52	-0.38	0.28
11	0.11	-0.02	-0.52	-0.06
12	0.45	0.45	-0.64	-0.19
13	0.35	0.24	-0.92	0.41
14	0.77	0.97	-1.13	0.08
17	0.18	0.15	-0.90	-0.20
18	0.33	0.60	-0.17	-0.41

Appendix B

Heat of formation of open-shell systems

Table B.1: Values for the different G3B3 energy corrections of the open-shell test set (kcal.mol^{-1}).

Radical	$\Delta(QCI)$	$\Delta(+)$	$\Delta(2df,p)$	$\Delta(GTL)$
methyl	-1.07	-2.39	-28.71	-36.45
ethenyl	-11.35	-3.93	-30.05	-66.83
vinyl	-6.87	-4.48	-41.75	-69.41
ethyl	-1.56	-3.20	-53.28	-71.66
propyn-1-yl	-10.83	-4.74	-54.78	-102.20
propyn-3-yl	-6.99	-5.71	-56.97	-102.37
cyclopropen-1-yl	-5.70	-5.38	-56.16	-100.83
cyclopropen-3-yl	-1.02	-4.98	-56.85	-101.19
propen-1-yl	-6.86	-5.60	-66.51	-104.39
propen-2-yl	-6.46	-5.48	-66.54	-104.61
propen-3-yl	-6.14	-5.80	-66.80	-104.66
prop-1-yl	-1.91	-4.37	-78.08	-106.69
n-C_4H3	-12.23	-7.85	-69.52	-134.92
i-C_4H3	-16.39	-6.83	-71.00	-135.15
n-C_4H_5	-13.47	-7.96	-79.80	-137.39
i-C_4H_5	-9.70	-7.57	-81.03	-137.34
(Z)-C_4H_7-4-yl	-6.33	-6.52	-91.53	-139.82
Cyclopentadienyl	-7.43	-8.36	-95.00	-169.47
phenyl	-15.42	-9.99	-106.99	-202.73
cyclohexadienyl	-11.19	-9.24	-119.00	-205.36

Table B.2: Data for the linear regressions correlating PMP4-MP4 energies to the spin contamination. (kcal.mol^{-1}).

	slope	s.d.	y-intercept	s.d.
6-31G(d)	-21.53	0.91	-1.03	0.32
6-31+G(d)	-21.59	0.88	-0.95	0.29
6-31G(2df,p)	-21.52	0.88	-1.03	0.30

Table B.3: AR standard heats of formation using 6-31G(d) basis set energies (kcal.mol^{-1}).

Radical	QCISD(T)	MP4	MP2	PMP4	PMP2
propyn-1-yl	144.37	150.84	146.97	141.96	134.88
propyn-3-yl	107.47	110.10	106.43	103.07	96.45
cyclopropen-1-yl	145.04	146.39	141.08	142.45	136.43
cyclopropen-3-yl	137.81	134.46	126.66	134.64	127.38
propen-1-yl	84.68	87.17	86.02	82.38	80.50
propen-2-yl	81.39	83.49	82.40	78.98	77.18
propen-3-yl	61.90	63.68	62.57	57.59	54.77
prop-1-yl	45.08	42.62	42.87	42.51	43.12
n-C_4H_3	158.56	164.98	157.58	154.80	143.39
i-C_4H_3	150.36	160.94	155.77	144.26	128.37
n-C_4H_5	114.41	122.06	118.37	111.40	103.74
i-C_4H_5	104.24	108.13	104.54	99.15	92.05
(Z)-C_4H_7-4-yl	59.50	60.01	57.96	53.99	50.79
Cyclopentadienyl	95.33	95.49	85.34	89.42	77.11
phenyl	116.93	123.63	110.79	110.96	90.83
cyclohexadienyl	86.40	88.87	79.17	78.53	64.68

Table B.4: AR standard heats of formation using 6-31+G(d) basis set energies (kcal.mol^{-1}).

Radical	MP4	MP2	PMP4	PMP2
propyn-1-yl	153.31	149.08	145.24	138.02
propyn-3-yl	111.59	107.43	105.46	98.60
cyclopropen-1-yl	148.22	142.55	144.81	138.44
cyclopropen-3-yl	136.69	128.56	137.18	129.58
propen-1-yl	88.78	87.42	84.76	82.75
propen-2-yl	85.21	83.88	81.47	79.51
propen-3-yl	65.09	63.75	59.74	56.75
prop-1-yl	45.46	45.67	45.72	46.31
n-C_4H_3	166.75	158.71	157.78	146.29
i-C_4H_3	163.72	158.10	148.14	132.49
n-C_4H_5	123.71	119.66	114.17	106.54
i-C_4H_5	110.17	106.14	102.32	95.09
(Z)-C_4H_7-4-yl	63.10	60.85	58.17	54.54
Cyclopentadienyl	99.14	88.20	94.23	81.37
phenyl	128.05	114.40	116.92	101.89
cyclohexadienyl	94.04	83.79	84.98	70.86

Table B.5: AR standard heats of formation using 6-31G(2df, p) basis set energies (kcal.mol^{-1}).

Radical	MP4	MP2	PMP4	PMP2
propyn-1-yl	122.80	118.68	114.46	107.39
propyn-3-yl	79.87	75.86	73.35	66.65
cyclopropen-1-yl	116.97	110.98	113.45	106.96
cyclopropen-3-yl	104.35	95.86	104.82	97.05
propen-1-yl	47.40	46.73	43.15	42.00
propen-2-yl	43.68	43.02	39.73	38.61
propen-3-yl	23.61	23.14	17.89	15.87
prop-1-yl	-8.72	-7.15	-8.50	-6.35
n-C_4H_3	131.12	122.70	121.64	109.67
i-C_4H_3	125.59	119.76	109.65	93.61
n-C_4H_5	77.91	74.18	67.92	60.62
i-C_4H_5	62.75	58.96	54.50	47.59
(Z)-C_4H_7-4-yl	4.14	2.84	-1.12	-3.57
Cyclopentadienyl	45.05	33.72	39.58	26.47
phenyl	70.11	55.70	58.25	37.01
cyclohexadienyl	23.34	12.83	13.77	-0.45

Table B.6: RSBSR standard heats of formation using G3B3 and PG3B3 energies (kcal.mol^{-1}).

Radical	H G3B3	H PG3B3
propyn-1-yl	125.52	125.47
propyn-3-yl	83.42	83.79
cyclopropen-1-yl	124.85	124.76
cyclopropen-3-yl	116.36	116.22
propen-1-yl	63.67	63.66
propen-2-yl	59.97	60.31
propen-3-yl	40.01	40.48
prop-1-yl	23.91	23.91
n-C_4H_3	130.09	130.44
i-C_4H_3	120.05	120.53
n-C_4H_5	87.16	87.53
i-C_4H_5	75.36	76.32
(Z)-C_4H_7-4-yl	32.38	33.37
Cyclopentadienyl	62.81	63.54
phenyl	82.53	78.23
cyclohexadienyl	50.00	50.82

Table B.7: RBSR standard heats of formation using 6-31G(d) basis set energies (kcal.mol^{-1}).

Radical	QCI	MP4	MP2	PMP4	PMP2
propyn-1-yl	125.89	124.99	124.86	125.41	125.46
propyn-3-yl	84.15	86.74	88.12	82.28	80.91
cyclopropen-1-yl	124.74	126.02	126.21	124.65	124.32
cyclopropen-3-yl	116.70	115.78	113.88	116.08	114.36
propen-1-yl	64.00	63.59	63.48	63.81	63.74
propen-2-yl	60.22	61.91	62.27	59.97	59.81
propen-3-yl	40.68	44.54	45.28	38.58	37.24
prop-1-yl	24.38	24.34	24.30	24.35	24.31
n-C_4H_3	129.79	135.10	136.95	129.70	128.00
i-C_4H_3	120.22	132.19	136.67	117.85	111.50
n-C_4H_5	87.68	93.17	93.65	87.29	84.26
i-C_4H_5	76.26	82.96	84.37	73.88	71.09
(Z)-C_4H_7-4-yl	33.12	36.78	37.59	30.65	29.63
Cyclopentadienyl	63.97	68.36	68.25	61.95	58.70
phenyl	82.33	91.49	91.41	80.71	72.61
cyclohexadienyl	51.39	59.15	60.48	48.24	44.14

Table B.8: RBSR standard heats of formation using 6-31+G(d) basis set energies (kcal.mol^{-1}).

Radical	MP4	MP2	PMP4	PMP2
propyn-1-yl	125.13	125.03	125.58	125.67
propyn-3-yl	87.58	88.94	83.44	82.24
cyclopropen-1-yl	126.14	126.28	124.72	124.31
cyclopropen-3-yl	116.51	114.65	116.75	115.04
propen-1-yl	63.42	63.34	63.62	63.57
propen-2-yl	62.06	62.48	60.31	60.25
propen-3-yl	44.59	45.45	38.99	37.83
prop-1-yl	24.12	24.09	24.13	24.10
n-C_4H_3	135.47	137.27	130.39	129.10
i-C_4H_3	133.79	138.46	119.85	114.34
n-C_4H_5	93.29	93.99	87.62	85.12
i-C_4H_5	83.89	85.53	75.44	73.20
(Z)-C_4H_7-4-yl	37.06	38.02	31.53	30.43
Cyclopentadienyl	69.31	69.10	63.45	60.34
phenyl	93.24	93.33	83.06	81.00
cyclohexadienyl	60.17	61.65	49.81	46.14

Table B.9: RBSR standard heats of formation using 6-31G(2df, p) basis set energies (kcal.mol^{-1}).

Radical	MP4	MP2	PMP4	PMP2
propyn-1-yl	124.73	124.58	125.12	125.14
propyn-3-yl	85.34	86.92	80.96	79.82
cyclopropen-1-yl	125.25	125.42	123.86	123.51
cyclopropen-3-yl	114.32	112.51	114.57	112.92
propen-1-yl	63.31	63.15	63.55	63.43
propen-2-yl	61.59	61.97	59.77	59.67
propen-3-yl	43.96	45.05	38.01	36.99
prop-1-yl	24.02	23.95	24.02	23.96
n-C_4H_3	134.99	136.99	129.66	128.22
i-C_4H_3	130.60	135.70	116.44	110.92
n-C_4H_5	92.53	93.35	86.68	84.05
i-C_4H_5	81.10	82.90	72.28	69.99
(Z)-C_4H_7-4-yl	35.96	37.04	30.14	29.09
Cyclopentadienyl	66.16	66.35	59.78	56.83
phenyl	90.25	90.85	79.48	72.04
cyclohexadienyl	57.42	59.24	46.58	42.95

Table B.10: HTR standard heats of formation using G3B3 and PG3B3 energies (kcal.mol^{-1}).

Radical	H G3B3	H PG3B3
propyn-1-yl	124.45	125.97
propyn-3-yl	84.50	85.18
cyclopropen-1-yl	124.90	125.12
cyclopropen-3-yl	116.57	116.39
propen-1-yl	64.14	64.78
propen-2-yl	60.59	61.23
propen-3-yl	40.78	41.21
prop-1-yl	24.83	24.80
n-C_4H_3	131.65	132.65
i-C_4H_3	121.76	122.54
n-C_4H_5	87.30	88.32
i-C_4H_5	75.23	76.16
(Z)-C_4H_7-4-yl	32.82	33.77
Cyclopentadienyl	63.25	63.94
phenyl	82.67	78.68
cyclohexadienyl	50.27	51.05

Table B.11: HTR standard heats of formation using 6-31G(d) basis set energies (kcal.mol^{-1}).

Radical	QCI	MP4	MP2	PMP4	PMP2
propyn-1-yl	122.16	132.33	135.86	123.53	123.42
propyn-3-yl	84.90	90.60	92.96	83.65	82.65
cyclopropen-1-yl	124.22	128.65	130.95	124.78	125.96
cyclopropen-3-yl	116.54	116.28	116.09	116.53	116.47
propen-1-yl	63.87	68.79	70.05	64.07	64.18
propen-2-yl	60.45	64.97	66.30	60.54	60.73
propen-3-yl	41.27	45.47	46.77	39.45	38.62
prop-1-yl	25.04	25.17	25.47	25.12	25.38
n-C_4H_3	131.32	142.66	146.35	132.32	131.28
i-C_4H_3	122.12	137.61	143.54	120.77	115.26
n-C_4H_5	87.15	98.32	100.76	87.50	85.24
i-C_4H_5	76.38	84.03	86.41	74.89	73.04
(Z)-C_4H_7-4-yl	33.38	37.63	39.28	31.45	31.23
Cyclopentadienyl	63.95	69.95	72.87	63.49	63.23
phenyl	82.20	97.58	105.03	84.30	83.12
cyclohexadienyl	50.82	60.37	64.05	49.42	47.60

Table B.12: HTR standard heats of formation using 6-31+G(d) basis set energies (kcal.mol^{-1}).

Radical	MP4	MP2	PMP4	PMP2
propyn-1-yl	133.43	136.92	125.04	125.10
propyn-3-yl	91.02	93.32	84.57	83.73
cyclopropen-1-yl	128.69	131.04	124.95	126.17
cyclopropen-3-yl	116.72	116.60	116.88	116.86
propen-1-yl	69.15	70.54	64.80	65.12
propen-2-yl	65.45	66.88	61.38	61.75
propen-3-yl	45.63	47.05	39.96	39.29
prop-1-yl	25.29	25.62	25.22	25.50
n-C_4H_3	142.79	146.44	133.16	132.61
i-C_4H_3	138.76	144.82	122.51	117.81
n-C_4H_5	98.52	101.23	88.30	86.70
i-C_4H_5	83.95	86.41	75.42	73.95
(Z)-C_4H_7-4-yl	37.83	39.57	32.23	31.85
Cyclopentadienyl	70.30	73.15	64.36	64.27
phenyl	97.73	105.21	85.24	89.99
cyclohexadienyl	61.20	65.06	50.78	49.42

Table B.13: HTR standard heats of formation using 6-31G(2df, p) basis set energies (kcal.mol^{-1}).

Radical	MP4	MP2	PMP4	PMP2
propyn-1-yl	134.18	138.01	125.57	125.83
propyn-3-yl	89.92	92.63	83.13	82.53
cyclopropen-1-yl	128.70	130.97	124.90	126.07
cyclopropen-3-yl	115.64	115.41	115.83	115.72
propen-1-yl	68.66	70.11	64.14	64.50
propen-2-yl	64.81	66.27	60.58	60.98
propen-3-yl	45.05	46.69	39.05	38.54
prop-1-yl	24.98	25.23	24.93	25.14
n-C_4H_3	142.94	147.02	132.85	132.36
i-C_4H_3	136.42	143.07	119.85	115.30
n-C_4H_5	98.46	101.52	87.85	86.33
i-C_4H_5	83.39	86.19	74.51	73.19
(Z)-C_4H_7-4-yl	37.14	39.11	31.27	31.07
Cyclopentadienyl	69.07	72.39	62.64	62.77
phenyl	98.10	106.51	84.93	84.71
cyclohexadienyl	59.89	64.12	49.00	47.73

Table B.14: EXTRAP standard heats of formation using MP4 energies (kcal.mol^{-1}).

Radical	MP4 6-31G(d)	MP4 6-31+G(d)	MP4 6-31G(2df,p)
propyn-1-yl	125.41	125.40	125.84
propyn-3-yl	85.85	85.63	84.47
cyclopropen-1-yl	124.88	124.33	124.63
cyclopropen-3-yl	115.01	115.29	114.76
propen-1-yl	64.42	64.22	63.83
propen-2-yl	60.87	60.85	60.35
propen-3-yl	41.12	40.62	40.06
prop-1-yl	23.84	23.81	24.03
n-C_4H_3	133.97	132.82	132.33
i-C_4H_3	125.87	124.86	121.64
n-C_4H_5	88.87	87.54	86.83
i-C_4H_5	77.77	76.80	76.01
(Z)-C_4H_7-4-yl	33.34	32.87	32.24
Cyclopentadienyl	64.94	64.64	63.21
phenyl	86.77	85.18	84.45
cyclohexadienyl	52.60	51.80	50.35

Table B.15: EXTRAP standard heats of formation using MP2 energies (kcal.mol^{-1}).

Radical	MP2 6-31G(d)	MP2 6-31+G(d)	MP2 6-31G(2df,p)
propyn-1-yl	125.97	125.88	126.44
propyn-3-yl	86.40	86.12	85.23
cyclopropen-1-yl	125.91	125.34	125.58
cyclopropen-3-yl	114.88	115.15	114.61
propen-1-yl	64.08	64.02	63.61
propen-2-yl	60.75	60.83	60.30
propen-3-yl	40.84	40.40	39.97
prop-1-yl	24.16	24.10	24.33
n-C_4H_3	133.76	132.59	132.18
i-C_4H_3	126.25	125.26	122.22
n-C_4H_5	86.99	85.91	85.19
i-C_4H_5	77.54	76.66	76.01
(Z)-C_4H_7-4-yl	33.45	33.00	32.52
Cyclopentadienyl	65.93	65.58	64.41
phenyl	89.18	87.63	87.27
cyclohexadienyl	52.62	51.93	50.60

Appendix C

Reactions on the C_6H_5 energy surface

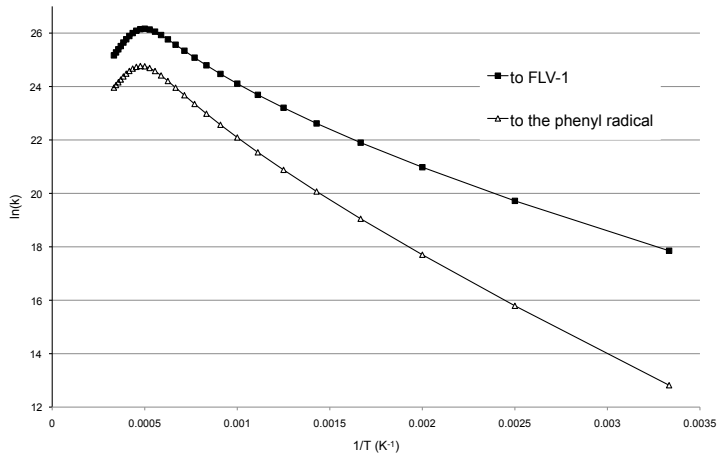

Figure C.1: Arrhenius plot for the n-C_4H_3 + C_2H_2 → **FLV − 1** and n-C_4H_3 + C_2H_2 → phenyl radical global reaction rate constants.

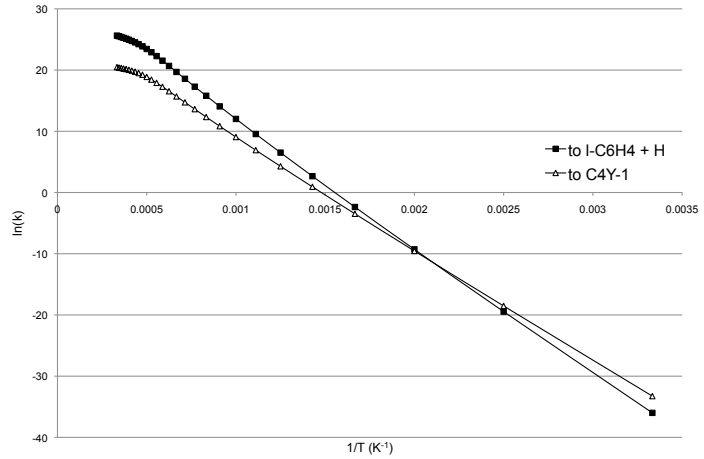

Figure C.2: Arrhenius plot for the n-C_4H_3 + C_2H_2 → l-C_6H_4 + H and n-C_4H_3 + C_2H_2 → **C4Y − 1** global reaction rate constants.

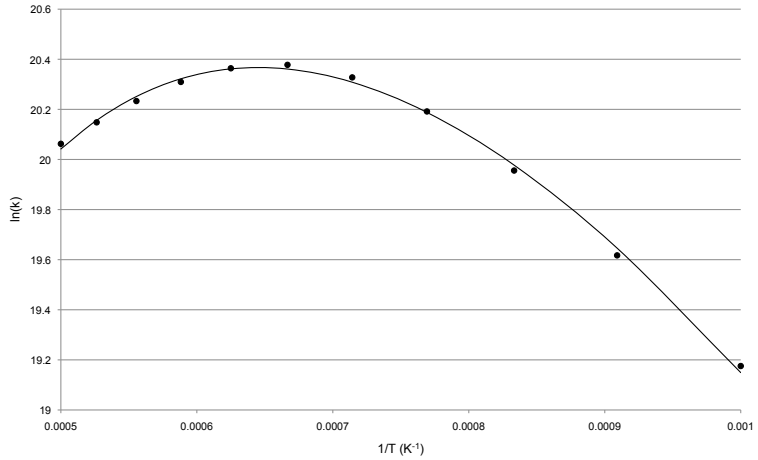

Figure C.3: Arrhenius plot for the i-C_4H_3 + C_2H_2 $\rightarrow$ **FLV − 2** global reaction rate constant.

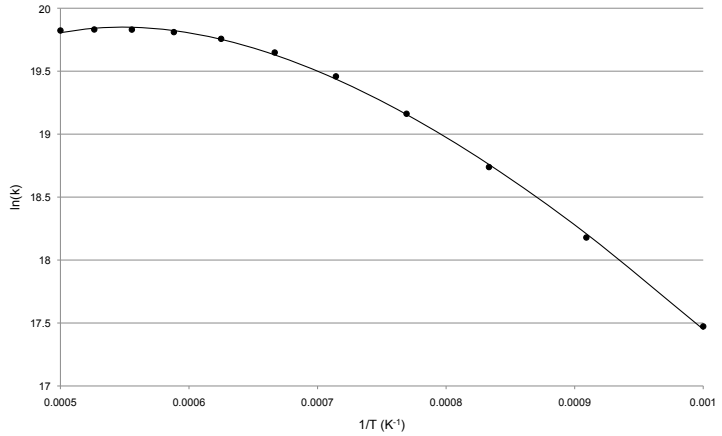

Figure C.4: Arrhenius plot for the i-C_4H_3 + C_2H_2 $\rightarrow$ **C4** global reaction rate constant.

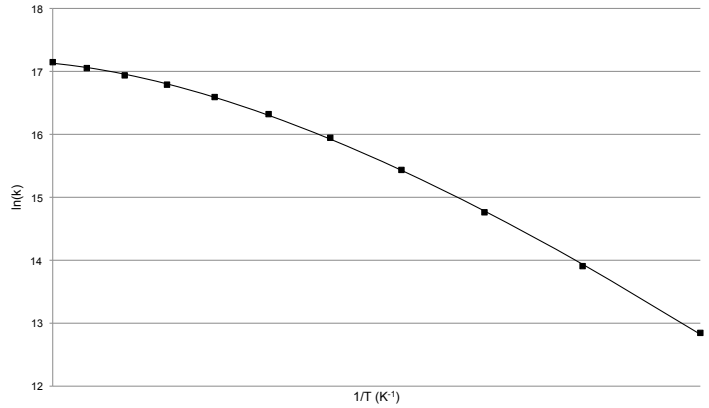

Figure C.5: Arrhenius plot for the i-C_4H_3 + C_2H_2 → **C4Y − 2** global reaction rate constant.

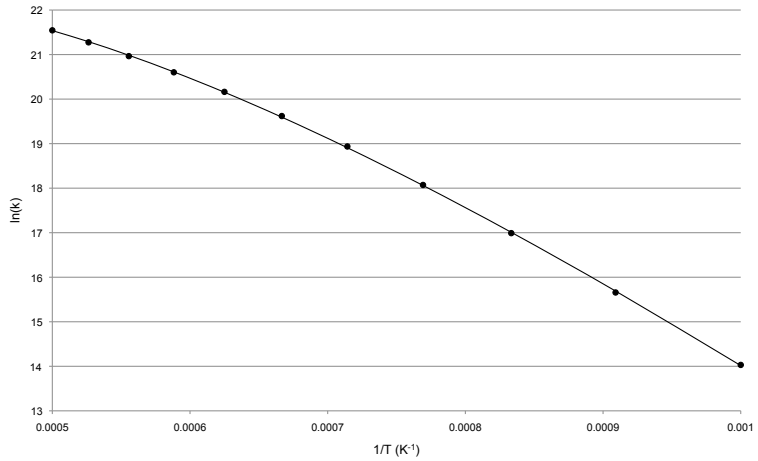

Figure C.6: Arrhenius plot for the i-C_4H_3 + C_2H_2 → b-C_6H_4 + H global reaction rate constant.

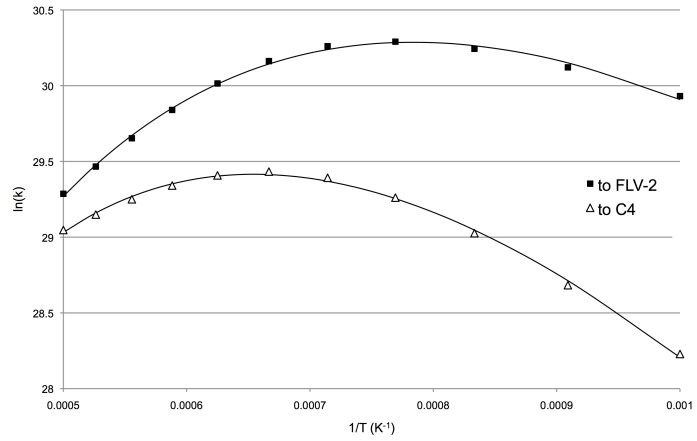

Figure C.7: Arrhenius plot for the *b*-C_6H_4 + H $\rightarrow$ **FLV − 2** and *b*-C_6H_4 $\rightarrow$ **C4** global reaction rate constants.

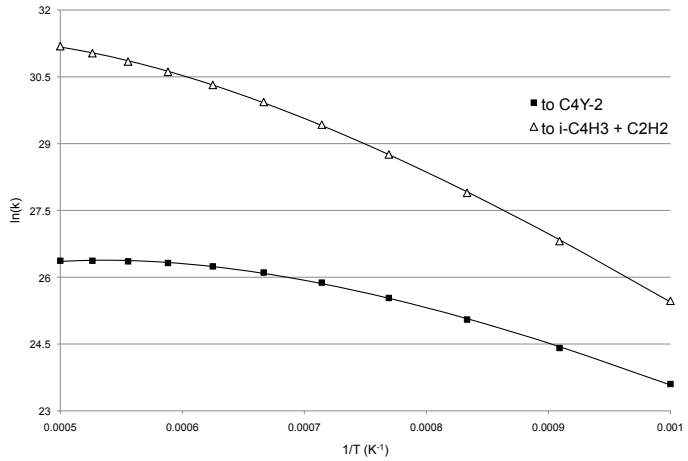

Figure C.8: Arrhenius plot for the *b*-C_6H_4 + H $\rightarrow$ **C4Y − 2** and *b*-C_6H_4 $\rightarrow$ *i*-C_4H_3 + C_2H_2 global reaction rate constants.

Appendix D

Reactions on the C_6H_7 energy surface

Table D.1: $\langle S^2 \rangle$ values for the different stationary points on the fulvene + H $\rightarrow$ benzene +H isomerization mechanism.

	B3LYP	6-31G(d)	6-31+G(d)	6-31g(2df,p)	GTL		average
C_6H_7A	0.75	1.22	1.17	1.21	1.16	1.19	
C_6H_7B	0.77	0.97	0.94	0.96	0.94	0.95	
C_6H_7C	0.79	1.21	1.18	1.20	1.17	1.19	
C_6H_7D	0.79	1.19	1.17	1.19	1.16	1.18	
BCC6H7	0.78	0.97	0.96	0.97	0.96	0.96	
Cyclohexadienyl	0.79	1.20	1.18	1.20	1.17	1.19	
TS (fulvene+H$\rightarrow$ C_6H_7A	0.79	1.41	1.35	1.40	1.34	1.37	
TS($C_6H_7C\rightarrow C_6H_7D$)	0.77	1.10	1.08	1.10	1.07	1.09	
TS($C_6H_7D\rightarrow C_6H_7A$)	0.76	1.07	1.03	1.06	1.02	1.05	
TS($C_6H_7A\rightarrow C_6H_7B$)	0.76	1.05	1.00	1.04	0.97	1.02	
TS($C_6H_7A\rightarrow$BCC6H7)	0.79	1.27	1.24	1.26	1.24	1.25	
TS(BCC6H7$\rightarrow$ c-C_6H_7)	0.78	1.23	1.20	1.22	1.19	1.21	
TS(c-C_6H_7 $\rightarrow$benzene + H)	0.77	1.39	1.35	1.39	1.35	1.37	

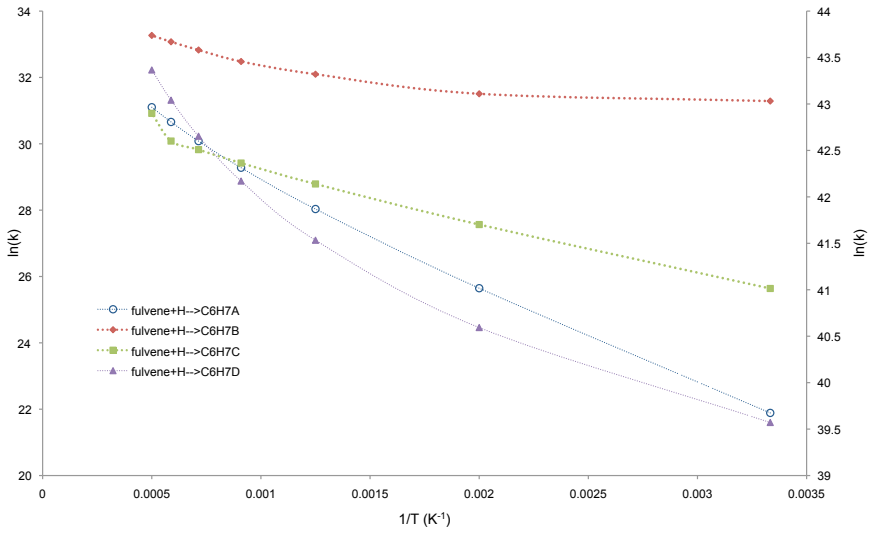

Figure D.1: Arrhenius plots rate constants for the reactions of addition of an hydrogen atom on fulvene. Secondary axis (right) only concerns the reaction forming C_6H_7D.

Appendix E

Combustion modeling

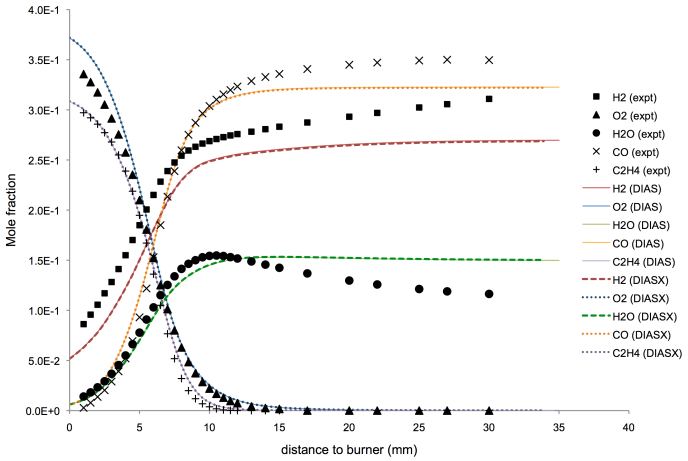

Figure E.1: Mole fraction profiles for H_2, O_2, H_2O, CO, C_2H_4.

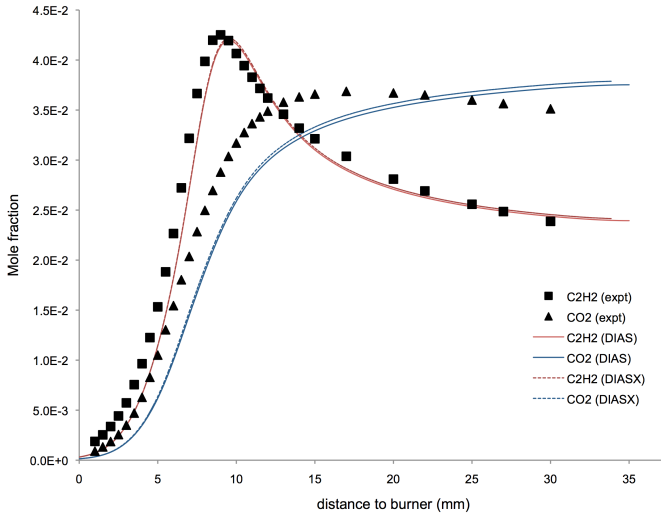

Figure E.2: Mole fraction profiles for C_2H_2 and CO_2.

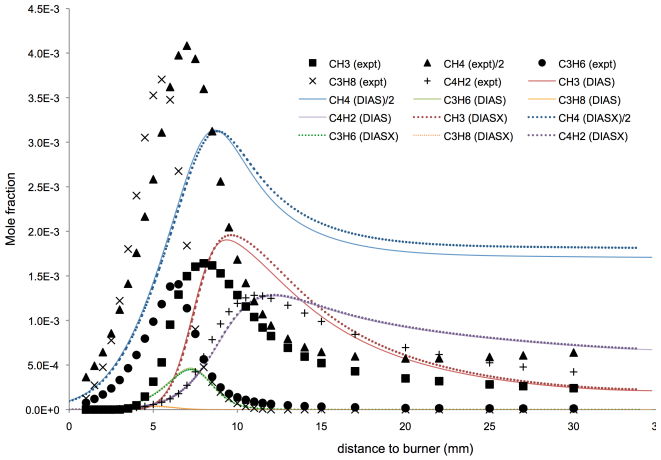

Figure E.3: Mole fraction profiles for CH_3, CH_4 (divided by two for clarity of the figure), C_3H_6, C_3H_8 and C_4H_2.

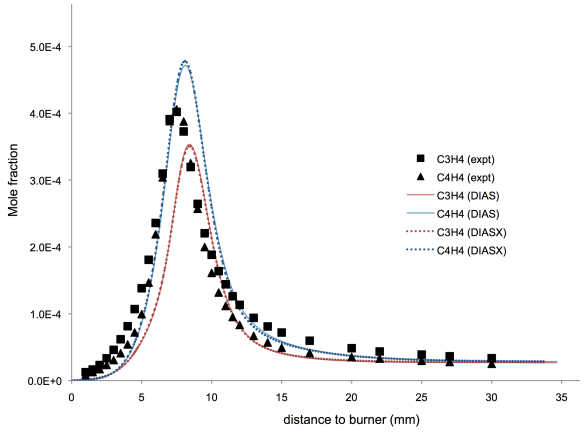

Figure E.4: Mole fraction profiles for C_3H_4 (sum of allene and propyne mole fraction) and C_4H_4 (vinylacetylene).

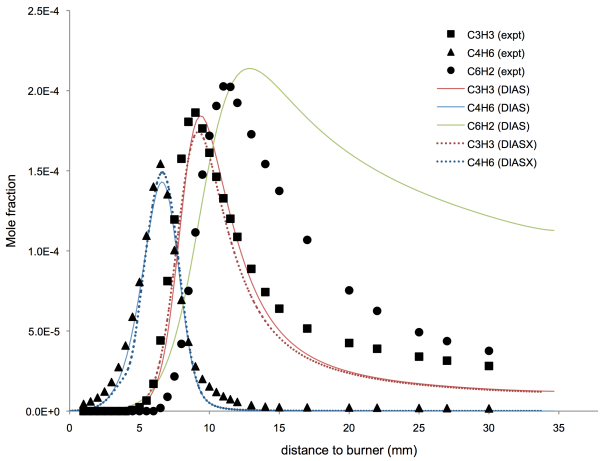

Figure E.5: Mole fraction profiles for C_3H_3, C_4H_6, C_6H_2.

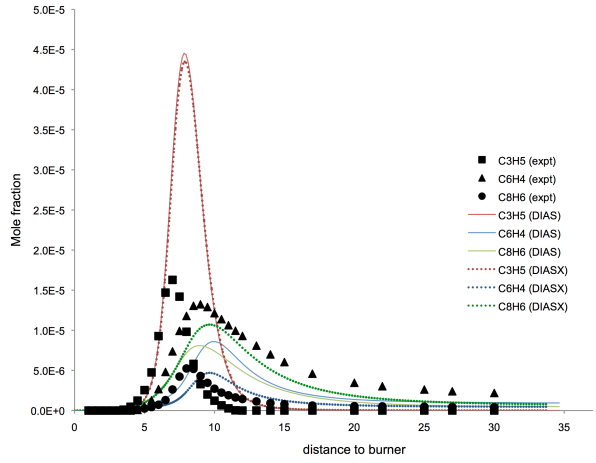

Figure E.6: Mole fraction profiles for C_3H_5, C_6H_4 and C_8H_6.

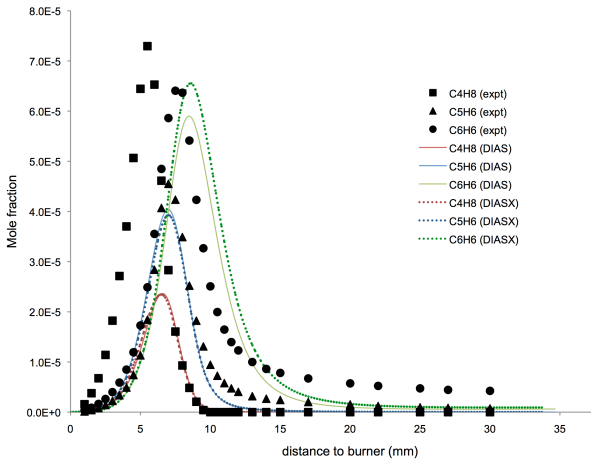

Figure E.7: Mole fraction profiles for C_4H_8, C_5H_6, C_6H_6 (benzene).

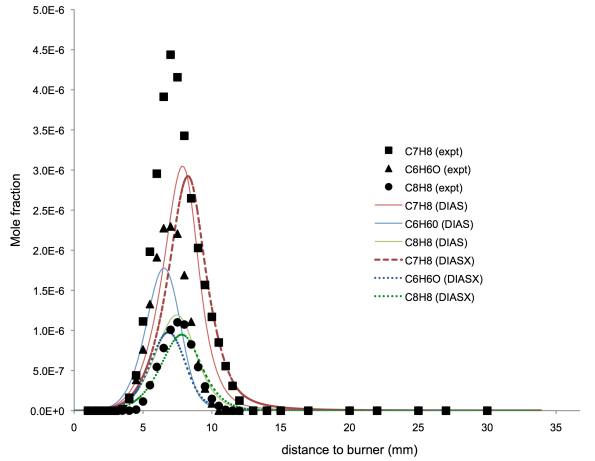

Figure E.8: Mole fraction profiles for C_7H_8, C_6H_6O (phenol) and C_8H_8.

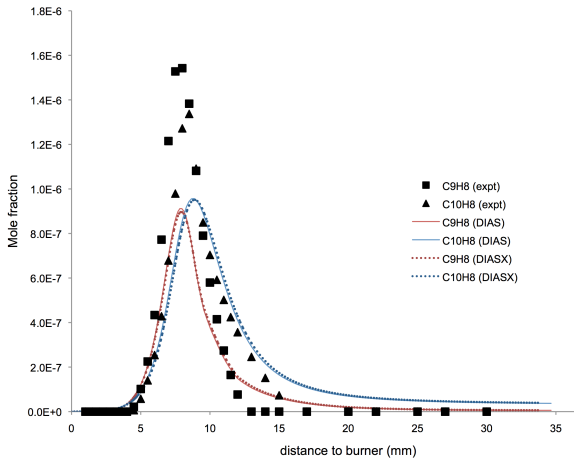

Figure E.9: Mole fraction profiles for C_9H_8 and $C_{10}H_8$.

Bibliography

[1] I. M. Kennedy. The health effects of combustion-generated aerosols. *Proceedings of the Combustion Institute*, 31:2757–2770, 2007.

[2] C.A. Pope III, R.T. Burnett, G.D. Thurston, M.J. Thun, E.E. Calle, D. Krewski, and J.J. Godleski. Cardiovascular mortality and long-term exposure to particulate air pollution: epidemiological evidence of general pathophysiological pathways of disease. *Circulation*, 109:71, 2004.

[3] J. Heinrich. Non-allergic respiratory morbidity improved along with a decline of traditional air pollution levels: a review. *European Respiratory Journal*, 21:64S–69S, 2003.

[4] Professor Alfred Bernard. Toxicologie humaine et animale AGRO 2750.

[5] A. D. Clarke and K. J. Noone. Soot in the Arctic snowpack: A cause for perturbations in radiative transfer. *Atmospheric Environment*, 41:64–72, 2007.

[6] World Climate Report (www.worldclimatereport.com). Is soot, not CO_2, to blame for the loss of Arctic ice?, 2005.

[7] W.L. Chameides and M. Bergin. Climate Change: Enhanced: Soot Takes Center Stage. *Science*, 297:2214–2215, 2002.

[8] V. Detilleux and J. Vandooren. Molecular Beam Mass Spectrometry Analysis of Pah Production Pathways in $C_6H_6/O_2/Ar$ and $C_6H_6/C_2H_2/O_2/Ar$ Flames. *Combustion Science and Technology*, 180:1347–1369, 2008.

[9] V. Detilleux and J. Vandooren. Experimental study and kinetic modeling of benzene oxidation in one-dimensional laminar premixed low-pressure flames. *Combustion, Explosion, and Shock Waves*, 45:392–403, 2009.

[10] V. Detilleux and J. Vandooren. Experimental and Kinetic Modeling Evidences of a C7H6 Pathway in a Rich Toluene Flame. *The Journal of Physical Chemistry A*, 113:8971–8978, 2009.

[11] N. Leplat, A. Seydi, and J. Vandooren. An experimental study of the structure of a stoichiometric ethanol/oxygen/argon flame. *Combustion Science and Technology*, 180:519–532, 2008.

[12] N. Leplat and J. Vandooren. Experimental investigation and numerical simulation of the structure of $CH_3CHO/O_2/Ar$ flames at different equivalence ratios. *Combustion Science and Technology*, 182:436–448, 2010.

[13] V. Dias, X. Lories, and J. Vandooren. Lean and Rich Premixed Dimethoxymethane/Oxygen/Argon Flames: Experimental and Modeling. *Combustion Science and Technology*, 182:350–364, 2010.

[14] V. Dias, C. Renard, and J. Vandooren. Modeling of Rich Premixed $C_2H_4/O_2/Ar$ and C_2H_4/Dimethoxymethane$/O_2/Ar$

Flames. *Zeitschrift für Physikalische Chemie*, 223:565–577, 2009.

[15] C. Duynslaegher, H. Jeanmart, and J. Vandooren. Flame structure studies of premixed ammonia/hydrogen/oxygen/argon flames: Experimental and numerical investigation. *Proceedings of the Combustion Institute*, 32:1277–1284, 2009.

[16] V. V. Kislov, N. I. Islamova, A. M. Kolker, S. H. Lin, and A. M. Mebel. Hydrogen Abstraction Acetylene Addition and Diels- Alder Mechanisms of PAH Formation: A Detailed Study Using First Principles Calculations. *Journal of Chemical Theory and Computation*, 1:908–924, 2005.

[17] A. M. Mebel, V. V. Kislov, and R. I. Kaiser. Photoinduced mechanism of formation and growth of polycyclic aromatic hydrocarbons in low-temperature environments via successive ethynyl radical additions. *Journal of the American Chemical Society*, 130:13618–13629, 2008.

[18] M. Frenklach and H. Wang. Detailed modeling of soot particle nucleation and growth. *Symposium (International) on Combustion*, 23:1559–1566, 1991.

[19] M. Frenklach, D. W. Clary, W. C. Gardiner Jr, and S. E. Stein. Effect of fuel structure on pathways to soot. *Symposium (International) on Combustion*, 21:1067–1076, 1988.

[20] C. F. Melius, M. E. Colvin, N. M. Marinov, W. J. Pitz, and S. M. Senkan. Reaction Mechanisms in Aromatic Hydrocarbon Formation Involving the C_5H_5 Cyclopentadienyl Moiety. *Proccedings of the Combustion Institute*, 1:685–692, 1996.

[21] A. M. Mebel and V. V. Kislov. Can the C_5H_5+ C_5H_5→$C_{10}H_{10}$→$C_{10}H_9$+ H/$C_{10}H_8$+ H_2 Reaction Produce Naphthalene? An *Ab Initio*/RRKM Study. *The Journal of Physical Chemistry A*, 113:9825–9833, 2009.

[22] B. Shukla, A. Susa, A. Miyoshi, and M. Koshi. Role of phenyl radicals in the growth of polycyclic aromatic hydrocarbons. *Journal of Physical Chemistry A*, 112:2362–2369, 2008.

[23] J. A. Miller and S. J. Klippenstein. The Recombination of Propargyl Radicals and Other Reactions on a C_6H_6 Potential. *The Journal of Physical Chemistry A*, 107:7783–7799, 2003.

[24] A. M. Mebel, S. H. Lin, X. M. Yang, and Y. T. Lee. Theoretical Study on the Mechanism of the Dissociation of Benzene. The C_5H_3+ CH_3 Product Channel. *The Journal of Physical Chemistry A*, 101:6781–6789, 1997.

[25] J. A. Cole, J. D. Bittner, J. P. Longwell, and J. B. Howard. Formation mechanisms of aromatic compounds in aliphatic flames. *Combustion and Flame*, 56:51–70, 1984.

[26] P. R. Westmoreland, A. M. Dean, J. B. Howard, and J. P. Longwell. Forming benzene in flames by chemically activated isomerization. *The Journal of Physical Chemistry*, 93:8171–8180, 1989.

[27] J. P. Senosiain and J. A. Miller. The reaction of n- and i-c_4h_5 radicals with acetylene. *The Journal of Physical Chemistry A*, 111:3740–3747, 2007.

[28] X. Lories, J. Vandooren, and D. Peeters. Cycle formation from acetylene addition on C_4H_3 radicals. *Physical Chemistry Chemical Physics*, 12:3762–3771, 2010.

[29] F. Zhang, B. Jones, P. Maksyutenko, R. I. Kaiser, C. Chin, V. V. Kislov, and A. M. Mebel. Formation of the Phenyl Radical [C_6H_5(X (2) A (1))] under Single Collision Conditions: A Crossed Molecular Beam and *ab initio* Study. *Journal of the American Chemical Society*, 132:2672–2683, 2010.

[30] S. Soorkia, A. J. Trevitt, T. M. Selby, D. L. Osborn, C. A. Taatjes, K. R. Wilson, and S. R. Leone. Reaction of the C_2 H Radical with 1-Butyne (C_4H_6): Low-Temperature Kinetics and Isomer-Specific Product Detection. *The Journal of Physical Chemistry. A*, 114:3340–3354, 2010.

[31] P. M. Nunes, F. Agapito, B. J. C. Cabral, R. M. B. dos Santos, and J. A. M. Simoes. Enthalpy of formation of the cyclopentadienyl radical: Photoacoustic calorimetry and *ab initio* studies. *Journal of Physical Chemistry A*, 110:5130–5134, 2006.

[32] S. E. Wheeler, K. A. Robertson, W. D. Allen, H. F. Schaefer, Y. J. Bomble, and J. F. Stanton. Thermochemistry of key soot formation intermediates: C_3H_3 isomers. *The Journal of Physical Chemistry A*, 111:3819–3830, 2007.

[33] N. Cohen and S. W. Benson. Estimation of heats of formation of organic compounds by additivity methods. *Chemical Reviews*, 93:2419–2438, 1993.

[34] C. H. Wu and R. D. Kern. Shock-tube study of allene pyrolysis. *Journal of Physical Chemistry*, 91:6291–6296, 1987.

[35] Frank Jensen. *Introduction to Computational Chemistry.* John Wiley and Sons, second edition, 2007.

[36] Per-Olof Widmark. *European Summerschool in Quantum Chemistry, books I to III.* Lund University, 2005.

[37] J. A. Pople, M. Head-Gordon, and K. Raghavachari. Quadratic configuration interaction. A general technique for determining electron correlation energies. *The Journal of Chemical Physics*, 87:5968–5975, 1987.

[38] J. A. Pople, M. Head-Gordon, D. J. Fox, K. Raghavachari, and L. A. Curtiss. Gaussian-1 theory: A general procedurefor prediction of molecular energies. *The Journal of Chemical Physics*, 90:5622–5629, 1989.

[39] L. A. Curtiss, K. Raghavachari, G. W. Trucks, and J. A. Pople. Gaussian-2 theory for molecular energies of first and second-row compounds. *The Journal of Chemical Physics*, 94:7221–7230, 1991.

[40] L. A. Curtiss, K. Raghavachari, P. C. Redfern, V. Rassolov, and J. A. Pople. Gaussian-3 (G3) theory for molecules containing first and second-row atoms. *The Journal of Chemical Physics*, 109:7764–7776, 1998.

[41] L. A. Curtiss, P. C. Redfern, and K. Raghavachari. Gaussian-4 theory. *The Journal of Chemical Physics*, 126:084108, 2007.

[42] L. A. Curtiss, P. C. Redfern, and K. Raghavachari. Gaussian-4 theory using reduced order perturbation theory. *The Journal of Chemical Physics*, 127:124105, 2007.

[43] A. G. Baboul, L. A. Curtiss, Redfern P. C., and K. Raghavachari. Gaussian-3 theory using density functional geometry and zero-

point energies. *The Journal of Chemical Physics*, 110:7650–7657, 1999.

[44] L. A. Curtiss, K. Raghavachari, P. C. Redfern, and J. A. Pople. Assessment of Gaussian-2 and density functional theories for the computation of enthalpies of formation. *The Journal of Chemical Physics*, 106:1063–1079, 1997.

[45] J. A. Montgomery Jr, M. J. Frisch, J. W. Ochterski, and G. A. Petersson. A complete basis set model chemistry. VI. Use of density functional geometries and frequencies. *The Journal of Chemical Physics*, 110:2822, 1999.

[46] J. A. Montgomery Jr, J. W. Ochterski, and G. A. Petersson. A complete basis set model chemistry. IV. An improved atomic pair natural orbital method. *The Journal of Chemical Physics*, 101:5900, 1994.

[47] J. M. L. Martin and G. de Oliveira. Towards standard methods for benchmark quality *ab initio* thermochemistryw1 and w2 theory. *The Journal of Chemical Physics*, 111:1843–1856, 1999.

[48] A. D. Boese, M. Oren, O. Atasoylu, J. M. L. Martin, M. Kállay, and J. Gauss. W3 theory: Robust computational thermochemistry in the kJ/mol accuracy range. *The Journal of chemical Physics*, 120:4129, 2004.

[49] A. Karton, E. Rabinovich, J. M. L. Martin, and B. Ruscic. W4 theory for computational thermochemistry: In pursuit of confident sub-kJ/mol predictions. *The Journal of Chemical Physics*, 125:144108, 2006.

[50] C. Peng, P. Y. Ayala, H. B. Schlegel, and M. J. Frisch. Using redundant internal coordinates to optimize equilibrium geometries and transition states. *Journal of Computational Chemistry*, 17, 1996.

[51] C. Peng and H. B. Schlegel. Combining synchronous transit and quasi-Newton methods to find transition states. *Israel Journal of chemistry*, 33:449–454, 1993.

[52] C. Gonzalez and H. B. Schlegel. An improved algorithm for reaction path following. *The Journal of Chemical Physics*, 90:2154–2161, 1989.

[53] C. Gonzalez and H. B. Schlegel. Reaction path following in mass-weighted internal coordinates. *The Journal of Physical Chemistry*, 94:5523–5527, 1990.

[54] K. S. Pitzer and W. D. Gwinn. Energy levels and thermodynamic functions for molecules with internal rotation I. Rigid frame with attached tops. *The Journal of Chemical Physics*, 10:428–440, 1942.

[55] J. W. Ochterski. Thermochemistry in Gaussian. *Gaussian Technical Support Information*, 2006.

[56] W. J. Hehre, R. Ditchfield, L. Radom, and J. A. Pople. Molecular orbital theory of the electronic structure of organic compounds. V. Molecular theory of bond separation. *Journal of the American Chemical Society*, 92:4796–4801, 1970.

[57] P. George, M. Trachtman, C. W. Bock, and A. M. Brett. Homodesmotic reactions for the assessment of stabilization energies in benzenoid and other conjugated cyclic hydrocarbons. *Journal*

of the Chemical Society, Perkin Transactions 2, 1976:1222–1227, 1976.

[58] S. E. Wheeler, K. N. Houk, P. R. Schleyer, and W. D. Allen. A Hierarchy of Homodesmotic Reactions for Thermochemistry. *Journal of the American Chemical Society*, 131:2547–2560, 2009.

[59] D. J. Henry and L. Radom. Theoretical Thermochemistry of Radicals. *Understanding chemical reactivity*, 22:161–198, 2001.

[60] A. G. Vandeputte, M. K. Sabbe, M. F. Reyniers, V. Van Speybroeck, M. Waroquier, and G. B. Marin. Theoretical study of the thermodynamics and kinetics of hydrogen abstractions from hydrocarbons. *Journal of Physical Chemistry A*, 111:11771–11786, 2007.

[61] P. Atkins and J. De Paula. *Atkins' Physical Chemistry*. Oxford University Press, seventh edition, 2002.

[62] S. G. Lias, J. E. Bartmess, J. F. Liebman, J. L. Holmes, R. D. Levin, and W. G. Mallard. The Journal of Physical and Chemical Reference Data, 17, 1988.

[63] J. B. Pedley, R. D. Naylor, and S. P. Kirby. *Thermochemical Data of Organic Compounds*. Chapman and Hall, second edition, 1986.

[64] H. Y. Afeefy, J. F. Liebman, and S. E. Stein. Neutral Thermochemistry data, NIST Standard Reference Database http://webbook.nist.gov.

[65] P.Y. Ayala and H.B. Schlegel. Identification and treatment of internal rotation in normal mode vibrational analysis. *The Journal of Chemical Physics*, 108:2314–2325, 1998.

[66] K. B. Wiberg, W. J. Bartley, and F. P. Lossing. On the Strain Energy in Cyclopropene and the Heat of Formation of the $C_3H_3^+$ Ion. *Journal of the American Chemical Society*, 84:3980–3981, 1962.

[67] K. B. Wiberg and R. A. Fenoglio. Heats of formation of C_4H_6 hydrocarbons. *Journal of the American Chemical Society*, 90:3395–3397, 1968.

[68] G. A. Petersson, D. K. Malick, W. G. Wilson, J. W. Ochterski, J. A. Montgomery Jr, and M. J. Frisch. Calibration and comparison of the Gaussian-2, complete basis set, and density functional methods for computational thermochemistry. *The Journal of Chemical Physics*, 109:10570–10579, 1998.

[69] J. A. Montgomery Jr, M. J. Frisch, J. W. Ochterski, and G. A. Petersson. A complete basis set model chemistry. VII. Use of the minimum population localization method. *The Journal of Chemical Physics*, 112:6532–6542, 2000.

[70] J. W. Pan, D. W. Rogers, and F. J. McLafferty. Density functional calculations of enthalpies of hydrogenation, isomerization, and formation of small cyclic hydrocarbons. *Journal of Molecular Structure(Theochem)*, 468:59–66, 1999.

[71] J. P. Senosiain, J. H. Han, C. B. Musgrave, and D. M. Golden. Use of quantum methods for a consistent approach to combustion modelling: Hydrocarbon bond dissociation energies. *Faraday Discussions*, 119:173–189, 2002.

[72] J. A. Miller and S. J. Klippenstein. From the Multiple-Well Master Equation to Phenomenological Rate Coefficients: Reactions on

a C_3H_4 Potential Energy Surface. *The Journal of Physical Chemistry A*, 107:2680–2692, 2003.

[73] R. Notario, O. Castano, J. L. M. Abboud, R. Gomperts, L. M. Frutos, and R. Palmeiro. Organic Thermochemistry at High *ab initio* Levels. 1. A G2 (MP2) and G2 Study of Cyclic Saturated and Unsaturated Hydrocarbons (Including Aromatics). *Journal of Organic Chemistry*, 64:9011–9014, 1999.

[74] A. Karton, A. Tarnopolsky, J.F. Lamre, G. C. Schatz, and J. M. L. Martin. Highly Accurate First-Principles Benchmark Data Sets for the Parametrization and Validation of Density Functional and Other Approximate Methods. Derivation of a Robust, Generally Applicable, Double-Hybrid Functional for Thermochemistry and Thermochemical Kinetics. *The Journal of Physical Chemistry A*, 112:12868–12886, 2008.

[75] J. W. Keister, T. Baer, M. Evans, C. Y. Ng, and C. W. Hsu. Methyl Loss Kinetics of Energy-Selected 1, 3-Butadiene and Methylcyclopropene Cations. *The Journal of Physical Chemistry A*, 101:1866–1872, 1997.

[76] A. Karton, I. Kaminker, and J. L. M. Martin. Economical Post-CCSD (T) Computational Thermochemistry Protocol and Applications to Some Aromatic Compounds. *The Journal of Physical Chemistry A*, 113:7610–7620, 2009.

[77] A. Fattahi, L. Lis, Z. Tian, and S. R. Kass. The heat of formation of cyclobutadiene. *Angewandte Chemie*, 118:5106–5110, 2006.

[78] R. B. Turner, P. Goebel, B. J. Mallon, F. A. Doering, W. von E., J. F. Cobburn Jr, and M. Pomerantz. Heats of Hydrogenation.

VIII. Compounds with Three- and Four-Membered Rings. *Journal of the American Chemical Society*, 90:4315–4322, 1968.

[79] T. C. Dinadayalane, U. D. Priyakumar, and G. N. Sastry. Exploration of C_6H_6 potential energy surface: A computational effort to unravel the relative stabilities and synthetic feasibility of new benzene isomers. *The Journal of Physical Chemistry A*, 108:11433–11448, 2004.

[80] X. Lories, J. Vandooren, and D. Peeters. Theoretical calculation of the heat of formation of fulvene. *Chemical Physics Letters*, 452:29–32, 2008.

[81] H. Möllerstedt, M. C. Piqueras, R. Crespo, and H. Ottosson. Fulvenes, fulvalene, and azulene: Are they aromatic chameleons ? *Journal of the American Chemical Society*, 126:13938–13939, 2004.

[82] T. M. Krygowski and M. K. Cyrańnski. Structural aspects of aromaticity. *Chemical Review*, 101:1385, 2001.

[83] A. P. Scott, I Agranat, P. U. Biedermann, N. V. Riggs, and L. Radom. Fulvalenes, fulvenes and related molecules, an ab initio study. *Journal of Organic Chemistry*, 62:2026–2038, 1997.

[84] C. F. Melius, J. A. Miller, and E. M. Evleth. Unimolecular reaction mechanisms involving C_3H_4, C_4H_4, and C_6H_6 hydrocarbon species. *Symposium (International) on Combustion*, 24:621– 628, 1992.

[85] W. R. Roth, O. Adamczak, R. Breukmann, H.-W. Lennartz, and R Boes. Die Berechnung von Resonanzenergien; das MM2ERW-Kraftfeld. *Chemische Berichte*, 100:2499–2521, 1991.

[86] A. Burcat. Alexander Burcats Ideal Gas Thermochemical Database, http://garfield.chem.elte.hu/Burcat/BURCAT.THR, 2003.

[87] Y.-S. Cheung, C.-K. Wong, and W.-K. Li. *Ab initio* calculations of the heats of formation for $(CH)_6$ isomers. *Journal of Molecular Structure (Theochem)*, 454:17–24, 1998.

[88] R. J. Berry, D. R. F. Burgess Jr., M. R. Nyden, M. R. Zachariah, and M. Schwartz. Halon thermochemistry: *Ab initio* calculation of the enthalpies of formation of fluoromethanes. *The Journal of Physical Chemistry*, 99:17145–17150, 1995.

[89] L. A. Curtiss, K. Raghavachari, P. W. Deutsch, and J. A. Pople. Theoretical study of Si_2H_n (n= 0–6) and $Si_2H_n^+$ (n= 0–7): Appearance potentials, ionization potentials, and enthalpies of formation. *The Journal of Chemical Physics*, 95:2433–2441, 1991.

[90] A. Nicolaides and L. Radom. An evaluation of the performance of G2, G2 (MP2) and G2 (MP2, SVP) theories for heats of formation and heats of reaction in the case of large hydrocarbons. *Molecular Physics*, 88:759–766, 1996.

[91] K. Raghavachari, B. B. Stefanov, and L. A. Curtiss. Accurate thermochemistry for larger molecules: Gaussian-2 theory with bond separation energies. *The Journal of Chemical Physics*, 106:6764–6767, 1997.

[92] J.D. Cox and G. Pilcher. *Thermochemistry of organic and organometallic compounds*. Academic Press London, 1970.

[93] A. Burcat and B. Ruscic. Third millennium ideal gas and condensed phase thermochemical database for combustion with up-

dates from active thermochemical tables. *Aerospace Engineering, and Argonne National Laboratory*, 2005.

[94] M. D. Allendorf. Sandia national laboratories Gas phase database. http://www.sandia.gov/HiTempThermo/mp4search.html.

[95] G. Bouchoux, M. T. Nguyen, and J. Y. Salpin. Condensation reactions between 1, 3-butadiene radical cation and acetylene in the gas phase. *The Journal of Physical Chemistry A*, 104:5778–5786, 2000.

[96] G. da Silva and J. W. Bozzelli. Quantum chemical study of the thermal decomposition of *o*-quinone methide(6-methylene-2, 4-cyclohexadien-1-one). *The Journal of Physical Chemistry A*, 111:7987–7994, 2007.

[97] J. E. Kent and J. Jones. A one step synthesis of fulvene. *Australian Journal of Chemistry*, 23:1059–1062, 1970.

[98] R. Sivaramankrishnan, R. S. Tranter, and K. Brezinsky. Ring Conserved Isodesmic Reactions: A New Method for Estimating the Heats of Formation of Aromatics and PAHs. *The Journal of Physical Chemistry A*, 109:1621–1628, 2005.

[99] S. Sharma and W. H. Green. Computed rate coefficients and product yields for $cC_5H_5+ CH_3 \rightarrow$ products. *The Journal of Physical Chemistry A*, 113:8871–8882, 2009.

[100] P. G. Wenthold, M. L. Polak, and W. C. Lineberger. Photoelectron spectroscopy of the allyl and 2-methylallyl anions. *The Journal of Physical Chemistry*, 100:6920–6926, 1996.

[101] N. S. Shuman, W. R. Stevens, K. Lower, and T. Baer. Heat of Formation of the Allyl Ion by TPEPICO Spectroscopy. *The Journal of Physical Chemistry A*, 113:10710–10716, 2009.

[102] H. G. Yu and J. T. Muckerman. Exploring the multiple reaction pathways for the H+ cyc-C_3H_6 reaction. *The Journal of Physical Chemistry A*, 108:10844–10849, 2004.

[103] S. E. Wheeler, W. D. Allen, and H. F. Schaefer III. Thermochemistry of disputed soot formation intermediates C_4H_3 and C_4H_5. *The Journal of Chemical Physics*, 121:8800–8813, 2004.

[104] C. L. Parker and A. L. Cooksy. *Ab Initio* study of the 1,3-butadienylradical isomers. *The Journal of Physical Chemistry A*, 102:6186–6190, 1998.

[105] G. E. Davico, V. M. Bierbaum, C. H. DePuy, G. B. Ellison, and R. R. Squires. The CH Bond Energy of Benzene. *Journal of the American Chemical Society*, 117:2590–2599, 1995.

[106] K. C. Lau and C. Y. Ng. Accurate *ab initio* predictions of ionization energies and heats of formation for the 2-propyl, phenyl, and benzyl radicals. *The Journal of Chemical Physics*, 124:044323, 2006.

[107] Y. Gao, N. J. DeYonker, E. C. Garrett, A. K. Wilson, T. R. Cundari, and P. Marshall. Enthalpy of Formation of the Cyclohexadienyl Radical and the C- H Bond Enthalpy of 1, 4-Cyclohexadiene: An Experimental and Computational Re-Evaluation. *The Journal of Physical Chemistry. A*, 113:6955–6963, 2009.

[108] J. A. Miller and C. F. Melius. Kinetic and thermodynamic issues in the formation of aromatic compounds in flames of aliphatic fuels.

Combustion and flame, 91:21–39, 1992.

[109] C. L. Parker and A. L. Cooksy. *Ab Initio* Study of the Most Stable C_4H_5 Isomers. *Journal of Physical Chemistry A*, 103:2160–2169, 1999.

[110] X. Krokidis, N. W. Moriarty, W. A. Lester Jr, and M. Frenklach. A quantum Monte Carlo study of energy differences in C_4H_3 and C_4H_5 isomers. *International Journal of Chemical Kinetics*, 33:808–820, 2001.

[111] N. M. Marinov, W. J. Pitz, C. K. Westbrook, A. M. Vincitore, M. J. Castaldi, S. M. Senkan, and C. F. Melius. Aromatic and polycyclic aromatic hydrocarbon formation in a laminar premixed n-butane flame. *Combustion and flame*, 114:192–213, 1998.

[112] H. Richter and J. B. Howard. Formation and consumption of single-ring aromatic hydrocarbons and their precursors in premixed acetylene, ethylene and benzene flames. *Physical Chemistry Chemical Physics*, 4:2038–2055, 2002.

[113] A. M. Mebel, K. Morokuma, and M. C. Lin. Modification of the Gaussian-2 theoretical model: The use of coupled-cluster energies, density-functional geometries, and frequencies. *The Journal of Chemical Physics*, 103:7414–7421, 1995.

[114] L. K. Madden, L. V. Moskaleva, S. Kristyan, and M. C. Lin. *Ab initio* MO study of the unimolecular decomposition of the phenyl radical. *The Journal of Physical Chemistry A*, 101:6790–6797, 1997.

[115] H. Wang, A. Laskin, N. W. Moriarty, and M. Frenklach. On unimolecular decomposition of phenyl radical. *Proceedings of the*

Combustion Institute, 28:1545–1556, 2000.

[116] S. P. Walch. Characterization of the minimum energy paths for the ring closure reactions of ch with acetylene. *The Journal of Chemical Physics*, 103:8544–8547, 1995.

[117] T. N. Truong, M. Nayak, H. H. Huynh, T. Cook, P. Mahajan, L. T. T. Tran, J. Bharath, S. Jain, H. B. Pham, C. Boonyasiriwat, et al. Computational Science and Engineering Online (CSE-Online): a cyber-infrastructure for scientific computing. *Journal of Chemical Information and Modeling*, 46(3):971–984, 2006.

[118] Thanh N. Truong (project director). Computational Science and Engeneering Online, http://cse-online.net.

[119] E. F. C. Byrd, C. D. Sherrill, and M. Head-Gordon. The theoretical prediction of molecular radical species: a systematic study of equilibrium geometries and harmonic vibrational frequencies. *The Journal of Physical Chemistry A*, 105:9736–9747, 2001.

[120] S. J. Klippenstein and J. A. Miller. The addition of hydrogen atoms to diacetylene and the heats of formation of *i*-C_4H_3 and *n*-C_4H_3. *The Journal of Physical Chemistry A*, 109:4285–4295, 2005.

[121] J. H. Huang, K. L. Han, W. Q. Deng, and G. Z. He. Theoretical studies of the decyclization/cyclization of the C_6H_5 radical. *Chemical Physics Letters*, 273:205–210, 1997.

[122] W. Q. Deng, K. L. Han, J. P. Zhan, and G. Z. He. *Ab initio* and RRKM calculations of *o*-benzyne pyrolysis. *Chemical Physics Letters*, 288:33–36, 1998.

[123] T. D. Crawford, E. Kraka, J. F. Stanton, and D. Cremer. Problematic *p*-benzyne: Orbital instabilities, biradical character, and broken symmetry. *The Journal of Chemical Physics*, 114:10638–10650, 2001.

[124] S. G. Wierschke, J. J. Nash, and R. R. Squires. Multiconfigurational SCF and correlation-consistent CI study of the structures, stabilities, and singlet-triplet splittings of *o-, m-,* and *p*-benzyne. *Journal of the American Chemical Society*, pages 11958–11967, 1993.

[125] N. Hansen, S. J. Klippenstein, C. A. Taatjes, J. A. Miller, J. Wang, T. A. Cool, B. Yang, R. Yang, L. Wei, C. Huang, et al. Identification and chemistry of C_4H_3 and C_4H_5 isomers in fuel-rich flames. *The Journal of Physical Chemistry A*, 110:3670–3678, 2006.

[126] A. M. Mebel, M. C. Lin, T. Yu, and K. Morokuma. Theoretical study of potential energy surface and thermal rate constants for the C_6H_5+ H_2 and C_6H_6+ H reactions. *The Journal of Physical Chemistry A*, 101:3189–3196, 1997.

[127] L. K. Madden, A. M. Mebel, and M. C. Lin. Theoretical study of the thermal isomerization of fulvene to benzene. *Journal of Physical Organic Chemistry*, 9:801–810, 1996.

[128] W. Tsang and R. F. Hampson. Chemical kinetic data base for combustion chemistry. Part I. Methane and related compounds. *Journal of Physical and Chemical Reference Data*, 15:1087, 1986.

[129] V. D. Knyazev, A. Bencsura, S. I. Stoliarov, and I. R. Slagle. Kinetics of the C_2H_3+ H_2→H+ C_2H_4 and CH_3+ H_2→ H+ CH_4 Reactions. *Journal of Physical Chemistry*, 100:11346–11354, 1996.

[130] A. B. Callear and B. Smith. Addition of atomic hydrogen to acetylene. Chain reactions of the vinyl radical. *Chemical Physics Letters*, 105:119–122, 1984.

[131] J. Park, I. V. Dyakov, and M. C. Lin. FTIR and Mass-Spectrometric Measurements of the Rate Constant for the C_6H_5+ H_2 Reaction. *The Journal of Physical Chemistry A*, 101:8839–8843, 1997.

[132] E. Heckmann, H. Hippler, and J. Troe. High-temperature reactions and thermodynamic properties of phenyl radicals. *Symposium (international) on combustion*, pages 543–550, 1996.

[133] J. Warnatz. *Combustion Chemistry*. Springer-Verlag, New York, 1984.

[134] Manion J. A., R. E. Huie, R. D. Levin, D. R. Burgess Jr., V. L. Orkin, W. Tsang, W. S. McGivern, J. W. Hudgens, V. D. Knyazev, D. B. Atkinson, E. Chai, A. M. Tereza, C.-Y. Lin, T. C. Allison, W. G. Mallard, F. Westley, J. T. Herron, R. F. Hampson, and D. H. Frizzell. NIST Chemical Kinetics Database, NIST Standard Reference Database 17, Version 7.0 (Web Version), Release 1.4.3, Data version 2008.12, National Institute of Standards and Technology, Gaithersburg, Maryland, 20899-8320. Web address: http://kinetics.nist.gov/.

[135] X. Lories, J. Vandooren, and D. Peeters. Theoretical Study of the C_6H_7 Energy Surface. *Proceedings of the fourth European Combustion Meeting*, 2009.

[136] A. M. Dean. Predictions of pressure and temperature effects upon radical addition and recombination reactions. *The Journal of*

Physical Chemistry, 89:4600–4608, 1985.

[137] W. Tsang. Thermodynamic and kinetic properties of the cyclohexadienyl radical. *The Journal of Physical Chemistry*, 90:1152–1155, 1986.

[138] J. M. Nicovich and A. R. Ravishankara. Reaction of hydrogen atom with benzene. Kinetics and mechanism. *The Journal of Physical Chemistry*, 88:2534–2541, 1984.

[139] V. Dias. *Etude de la formation des précurseurs des suies dans les flammes riches prémélangée d'éthylène*. PhD thesis, Université catholique de Louvain, Belgium, 2003.

[140] Rotexo GmbH & Co. COSILAB. The Combustion Simulation Laboratory (Version 2.1), 2007.

[141] A. D. Boese and J. M. L. Martin. Development of density functionals for thermochemical kinetics. *The Journal of Chemical Physics*, 121:3405–3416, 2004.

[142] J. P. Merrick, D. Moran, and L. Radom. An evaluation of harmonic vibrational frequency scale factors. *The Journal of Physical Chemistry A*, 111:11683–11700, 2007.

[143] A. Raj, P. L. W. Man, T. S. Totton, M. Sander, R. A. Shirley, and M. Kraft. New polycyclic aromatic hydrocarbon (PAH) surface processes to improve the model prediction of the composition of combustion-generated PAHs and soot. *Carbon*, 48:319–332, 2010.

[144] V. V. Kislov, A. M. Mebel, and S. H. Lin. Ab Initio and DFT study of the formation mechanisms of polycyclic aromatic hydrocarbons:

the phenanthrene synthesis from biphenyl and naphthalene. *Journal of Physical Chemistry A*, 106(25):6171–6182, 2002.

[145] G. da Silva and J. W. Bozzelli. Indene Formation from Alkylated Aromatics: Kinetics and Products of the Fulvenallene+ Acetylene Reaction. *The Journal of Physical Chemistry A*, 113:8971–8978, 2009.